The Evaluation of RGD-Peptide Modified Poly(lactic acid-*co*-lysine) as a Resorbable, Interactive Biomaterial

by

Alonzo David Cook

B.S. Chemical Engineering
Brigham Young University, 1989

M. S. Chemical Engineering
Brigham Young University, 1991

Submitted to the Department of Chemical Engineering
in partial fulfillment of the requirements for the degree of

Doctor of Philosophy in Chemical Engineering

at the

MASSACHUSETTS INSTITUTE OF TECHNOLOGY
February 1996

© Massachusetts Institute of Technology 1996
All rights reserved

Signature of Author.....
Department of Chemical Engineering
February 2, 1996

Certified by.....
Professor Robert Langer
Thesis Supervisor

Accepted by.....
Professor Robert E. Cohen
Chairman, Committee for Graduate Students

MASSACHUSETTS INSTITUTE
OF TECHNOLOGY

MAR 2 2 1996

ARCHIVES

LIBRARIES

The Evaluation of RGD-Peptide Modified Poly(lactic acid-*co*-lysine) as a Resorbable, Interactive Biomaterial

by

Alonzo David Cook

Submitted to the Department of Chemical Engineering on February 2, 1996, in partial fulfillment of the requirements for the degree of Doctor of Philosophy in Chemical Engineering

Abstract

The lack of donor organs has limited the extent to which organ transplantations can be performed. Tissue engineering, in which dissociated cells supported on resorbable polymer scaffolds are transplanted, is an alternative strategy that is being developed. As the polymers degrade, the cells synthesize and excrete extracellular matrix proteins, which are then remodeled into tissues. The objective of this research was to control cell behavior by incorporating synthetic cell adhesive peptides into the scaffold materials. Incorporation of the peptides was made possible by copolymerizing lysine with lactic acid. The ε-amino group of lysine provided functional sites to which Arginine-Glycine-Aspartic Acid (RGD) peptides were attached. This thesis comprises an evaluation of the interactive properties of RGD-peptide modified samples of poly(lactic acid-*co*-lysine) (PLAL). The evaluation consisted of synthesizing and characterizing the material at each stage of its development, which included monomer synthesis, copolymerization, deprotection, processing, peptide attachment and interaction with cells. Both bulk property characterization and surface characterization studies were conducted, with a focus on the latter as a means to interpret the observed changes in cell behavior. Bulk attachment chemistry was performed using 1,1'-carbonyldiimidazole (CDI). Surface attachment chemistry was performed using 1,ethyl-3-(3-dimethylaminopropyl) carbodiimide (EDC). Amino groups were measured using colorimetric assays and X-ray Photoelectron Spectroscopy (XPS). Peptides were measured by incorporating ^{125}Iodine as a radioactive marker or ^{127}Iodine as a distinct elemental marker for use with XPS. Typical samples contained on

the order of 1 nmol/cm^2 of amino groups and 10 pmol/cm^2 of peptides. After incubating bovine aortic endothelial cells for 4 hours on surfaces with RGD-containing peptides, the mean spread cell area increased to 405 ± 29 μm^2 compared to 116 ± 11 μm^2 on Poly(lactic acid), 87 ± 4 μm^2 on PLAL and 105 ± 4 μm^2 on surfaces with RDG-containing (control) peptides. Mathematical models of cell adhesion and cell spreading were used to confirm that the experimentally observed results correlated with predicted cell responses. The significance of this work is that the first interactive, resorbable biomaterial was developed. The use of this material to control cell behavior was demonstrated.

Thesis Supervisor: Robert Langer
Title: Kenneth J. Germeshausen Professor of Chemical and Biomedical Engineering
Department of Chemical Engineering, MIT

To

Amy, Analisa and Christina

Acknowledgments

Many individuals contributed to the successful completion of this project. I first wish to thank Bob Langer for giving me the opportunity to work in his lab, and for setting such high standards for scientific experimentation. I thank my Thesis Committee members: Linda Cima, Don Ingber, and Jay Vacanti for their advice, vision, enthusiasm, and interest in the success of this project. Many thanks are extended to Pam Brown for her patience, fortitude, and willingness to repeat instructions time and time again. I thank Denise Barrera for providing the groundwork for this project and teaching me how to synthesize and analyze the lysine-containing monomer. Jeff Hrkach very ably assisted with the polymer synthesis, deprotection, and peptide attachment reactions. Scott Cannizzaro also assisted in performing peptide attachment reactions.

Many thanks are extended to Richard Cook, Mike Kelley, Heather LeBlanc, John Augliera, and Suzanne Wright of the MIT Biopolymers Laboratory, for synthesis of the peptides, conducting amino acid analysis and for helpful discussions.

I especially wish to thank the UROP students who worked tirelessly to conduct experiments and analyze the data: Nicholas Gao, Yichin Liu, Eric Dong, Susan Dusenbery, Ketaki Patel, Anand Raghunathan, Marlo Kemp, Utpal Pajvani, and Ivette Johnson.

I thank Mike Frongillo for his assistance in the attainment of scanning electon micrographs and John Martin for help in operating the SIMSLAB system at MIT. I am grateful to Ted Tsomides, who assisted in radiolabeling and purifying the ^{125}I-labeled peptides. I thank Professor Buddy Ratner and his staff at the University of Washington in Seattle: Deborah Leach-Scampavia, Steve Golledge, and Natalie Winblade, who helped with the XPS and Static SIMS studies.

I thank my collaborators at the Roswell Park Cancer Institute in Buffalo, New York, Dr. Wesley Hicks and Leon Hall III for their interest in developing additional applications for this material.

Helpful suggestions were received along the way from Noah Lotan, Dave Mooney, Joyce Wong, Matt Nugent, Professor Paul Laibinis, Professor Joe Gardella, Professor Doug Lauffenburger, Prasad Shastri, Yuan Lu, and Christine Schmidt.

I wish also to thank my office mates, Mark Johnson, Samir Mitragotri, and Guillermo Ameer for their friendship and occassional diversionary conversations.

I thank my family for their support and encouragement, and especially my brother Blaine for his timely assistance toward the end of this project. Most of all, I wish to acknowledge the love and support of my wife, Amy. Thank you for allowing me this opportunity.

This work was funded by Advanced Tissue Sciences (La Jolla, CA), the National Institutes of Health (MIT Biotechnology Training Grant No. GM08334-06), the National Science Foundation (NSF Grant No. BCS-9202311), and the Massachusetts Institute of Technology.

Contents

Abstract 3
Acknowledgments 7
Contents 9
List of Figures 13
List of Tables 15
1. Introduction 17
1.1 Overview 17
1.2 Objectives 18
1.3 Outline of the Thesis 21
1.4 References 23
2. Background 25
2.1 Introduction 25
2.1.1 History of Biomaterials/Artificial Organs 26
2.1.2 History of Organ Transplantation 28
2.2 History of Tissue Engineering 28
2.3 Development of PLAL + RGD 30
2.3.1 Selection of Scaffold Materials 30
2.3.2 Integrins 31
2.3.3 Extracellular Matrix 32
2.3.4 Fibronectin 32
2.3.5 RGD Peptides 33
2.4 Prospective Uses for PLAL + RGD 34
2.4.1 Engineered Blood Vessels 35
2.4.2 Engineered Tracheal Linings 36
2.5 References 37
3. Sample Preparation 43
3.1 Monomer Synthesis 43
3.1.1 Reactions 44
3.1.2 NMR Results 47
3.1.3 FTIR Results 47
3.1.4 DSC Results 51
3.1.5 Elemental Analysis Results 52
3.2 Polymerization & Deprotection 53
3.3 Processing Methods 56

3.3.1 Solvent Casting 58
3.3.2 Spraying 61
3.3.3 Melt/Quench 63
3.3.4 Annealing 63
3.3.5 Blending 64
3.4 Bulk Characterization 64
3.4.1 Lysine and Peptide Contents from AAA 64
3.4.2 Degradation Kinetics 69
3.4.3 Thermal Transitions and Crystallinity 70
3.4.4 Density determination 71
3.4.5 Molecular Weight 71
3.5 References 72
3A Monomer Synthesis Protocol 73
3B Polymerization and Deprotection Protocols 82
4. Peptide Attachment 85
4.1 Bulk-Attachment 85
4.2 Surface-Attachment 85
4.2.1 Evaluation of Surface Attachment Chemistries 87
4.2.2 Materials and Methods 89
4.2.3 Results 93
4.2.4 Discussion 105
4.3 Comparison of Bulk and Surface Attachment Chemistries 106
4.4 References 108
5. Surface Characterization 109
5.1 Introduction 109
5.1.1 Methods to perform surface analysis 111
5.1.2 Sensitivity Analysis of Surface Analysis Techniques 113
5.2 Measurement of Surface Amino Group Densities 118
5.2.1 Colorimetric Methods 120
5.2.2 XPS 130
5.3 Measurement of Surface Peptide Densities 136
5.3.1 Materials and Methods 136
5.3.2 Peptide detected when attached by surface chemistry 138
5.3.3 Peptide detected when attached by bulk chemistry 140
5.3.4 Peptide Stability/Cold Stage Studies 141
5.3.5 Discussion 141

5.4 Contact Angles 142
5.4.1 Materials and Methods 142
5.4.2 Results 143
5.5 Secondary Ion Mass Spectroscopy 153
5.5.1 Background 153
5.5.2 Materials and Methods 155
5.5.3 Results 155
5.5.4 Summary 160
5.5.5 Discussion 164
5.6 References 165
5A Determination of Lysine and Peptide Surface Densities from XPS.. 168
5B Derivation of Surface Energy Equations 174
6. Cell Interactions 177
6.1 Introduction 177
6.1.1 Cell Adhesion Assays 177
6.1.2 Cell Detachment Assays 178
6.1.3 Spreading Assays 179
6.2 Adhesion & Spreading Experiments 179
6.2.1 Materials and Methods 179
6.2.2 Results 180
6.2.3 Discussion 190
6.3 Viability Experiments 191
6.3.1 Materials and Methods 191
6.3.2 Results 192
6.3.3 Discussion 194
6.4 Theoretical Predictions 195
6.4.1 Point Attachment Model 196
6.4.2 Spreading Model 209
6.5 References 216
6A Cell Spreading Protocol 219
7. Conclusions 221
7.1 Summary 221
7.1.1 X-ray Photoelectron Spectroscopy 225
7.1.2 Contact Angles 225
7.1.3 Colorimetric Dyes 226
7.1.4 Radiolabeled Peptides 226

7.1.5 Scanning Electron Microscopy 226
7.1.6 Cell Spreading Assays 227
7.2 Future Directions 227
7.3 References 230

List of Figures

2.1 Schematic of Fibronectin 33
2.2 RGD 34
3.1 Poly(lactic acid-*co*-lysine) 44
3.2 Monomer Synthesis Scheme 46
3.3 ^{1}H NMR Spectra 48
3.4 Sample FTIR Results 50
3.5 DSC Results 51
3.6 Copolymerization Scheme 54
3.7 Copolymerization Optimization 57
3.8 Top & Bottom of Solvent-cast PLA 60
3.9 Cross-sections of Polymer films 62
3.10 Bulk Lysine Content of PLAL+GRGDY-I_2:PLA Blends 67
3.11 Bulk Peptide Content of PLAL+GRGDY-I_2:PLA Blends 67
3.12 Degradation Results 69
3.13 Crystallinity of Blends 71
4.1 Reaction Scheme for Bulk Peptide Attachment 86
4.2 EDC/Sulfo-NHS Reaction Scheme 90
4.3 HPLC Separation of Radiolabeled Peptide Fractions 94
4.4 Micro-BCA Standard Curve for Radioiodination 96
4.5 Micro-BCA Standard Curve of BSA vs. GRGDY-I_2 peptide 96
4.6 Comparison of Radioiodination Results 97
4.7 Optimization of Reaction Conditions 99
4.8 Effect of Time on Peptide Attachments 101
4.9 Effect of pH on Peptide Attachment 103
4.10 Effect of Input Concentration on Peptide Attachment 104
5.1 Scheme for Surface Analysis of Biomaterials 110
5.2 Relative Sensitivities of the Detection Methods 114
5.3 Sulfo-SDTB Colorimetric Assay Reaction Scheme 121
5.4 Typical Standard Curve 122
5.5 Representative Results of Sulfo-SDTB Assay 124
5.6 Average Results of PLAL Blends with 100,000 MW PLA 124
5.7 PLAL vs. Protected PLAL Blends 125
5.8 Pentafluorobenzaldehyde 134

5.9 Bulk Peptide Density Results 140
5.10 Effect of Soaking in PBS on the Contact Angle of PLA 144
5.11 Effect of Soaking in Water on the Contact Angle of PLA 146
5.12 Surface Energy 148
5.13 Contact Angle Hysteresis 149
5.14 The Effect of Peptides on the Wettability of PLA 152
5.15 Positive and Negative SIMS spectra of PLA 154
5.16 Positive Static SIMS Spectra of PLAL+GRGDY on Silicon 156
5.17 Negative Static SIMS Spectra of PLAL+GRGDY on Silicon 156
5.18 Negative Static SIMS Spectra of PLAL+GRGDY on Gold 157
5.19 Static SIMS Spectra of PLA: Top Surface 158
5.20 Static SIMS Spectra of PLA: Bottom Surface 158
5.21 Static SIMS Spectra of PLAL 159
5.22 Static SIMS Spectra of GRGDY 159
5.23 Static SIMS Spectra of GRGDY-I_2 160
5.24 Static SIMS Spectra of PLAL + GRGDY-I_2 160
6.1 BAE Cell Behavior on PLA and PLAL+GRGDY 182
6.2 Comparison of Spread Cell Area on PLA and PLAL + GRGDY 183
6.3 Spreading Measurements on 40% Blends 184
6.4 Spreading of BAE cells on RGD vs. Polymer Controls 189
6.5 Spreading of BAE cells on PS and PS with Serum 189
6.6 Live/Dead® Assay Results 194
6.7 Point Attachment Model 197
6.8 Typical Results of the Point Attachment Model 203
6.9 Receptor Number vs. Bond Dissociation 204
6.10 Sample Calculation Plot of log R_T vs. log κ 207
6.11 Stages of Cell Spreading 210
6.12 Forces on Bonds for Uniform Stress and Peeling Model 213
6.13 Effect of Shear Stress on Bonds Required 215

List of Tables

1.1 Objectives 19
1.2 Contributions 19
3.1 Typical Batch Conversions 45
3.2 Lysine-Containing Monomer (LCM) Synthesis Results 45
3.3 Analysis of ^{1}H NMR Spectra 49
3.4 FTIR Analysis 49
3.5 Melting Temperature Results 52
3.6 Elemental Analysis Results 53
3.7 Copolymerization Results 55
3.8 Deprotection Results 55
3.9 Copolymerization Optimization Results 57
3.10 Casting Results 59
3.11 Bulk Lysine Content of PLAL:PLA Blends 66
3.12 Bulk Peptide Content of PLAL+GRGDY-I_2:PLA Blends 68
3.13 Crystallinity of Blends 70
4.1 Bulk Peptide Attachment Results 87
4.2 Surface Attachment Reagents 88
4.3 Surface Attachments using Trace-labeled ^{125}I-GRGDY 91
4.4 Optimization of Reaction Conditions 98
4.5 Effect of Time on Peptide Attachment 100
4.6 Effect of pH on Peptide Attachment 102
4.7 Effect of Input Concentration on Peptide Attachment 104
4.8 Comparison of Bulk and Surface Attachment Methods 107
5.1 Methods for Characterizing PLAL & Bound Peptides 111
5.2 Sensitivity Data 113
5.3 Summary of Sulfo-SDTB Experiments 123
5.4 Statistical Analysis of Sulfo-SDTB Results 126
5.5 Analysis of Slopes 128
5.6 Comparison of Expected and Measured NH_2 Concentrations 129
5.7 XPS Results 131
5.8 Evidence for Species Segregation 132
5.9 Evidence for Species Segregation: Follow-up Study 132
5.10 Effect of Soaking 133

5.11 The Use of PFBA to Detect Lysine 134
5.12 The Effect of Soaking 135
5.13 Species in PLAL + GRGDY-I_2 samples 138
5.14 The use of Iodine-labeled peptides 139
5.15 Effect of soaking on PLA 144
5.16 Effect of soaking on PLA 145
5.17 Surface Energy of PLAL films 147
5.18 Summary of Contact Angle Hysteresis 151
5.19 Effect of Lysine and Peptides on Surface Wettability 152
5.20 Summary of Static SIMS Data for PLA on various substrates 161
5.21 Static SIMS results for PLAL, GRGDY and GRGDY-I_2 162
5.22 Comparison of Dry and Soaked Samples 163
6.1 Results of Spreading Experiments 181
6.2 Spreading of BAE cells on 40% blends 188
6.3 Statistical Analysis of 4 hr. Spreading Data 190
6.4 Statistical Analysis of Slopes from Spreading Experiments 191
6.5 Live/Dead® Assay Results 193
6.6 Dimensionless Parameters 201
6.7 Parameter Values 205
6.8 Asymptotic Limits 206
6.9 Determination of α 207
6.10 Effect of Increasing Ligand Density 208
6.11 High Affinity Asymptotes 209
6.12 Regression Slope for Spreading model 210
6.13 Parameters for Spreading model 212
6.14 Number of Bonds Required 214
7.1 Characterization Questions and Techniques 224

Chapter 1

Introduction

1.1 Overview

The development of routine surgical techniques to transplant tissues and organs, while being unquestionably one of the greatest medical accomplishments of all time, has led to one of the largest contemporary medical crises: the lack of a sufficient quantity of donor tissues and organs for all patients who could benefit from an organ or tissue transplant. Due to the scarcity of replacement organs and tissues, a new technology, referred to herein as tissue engineering, has been conceived. The goal of this technology is to create new tissues from cultured cells, which can be isolated, purified, stored indefinitely, are more plentiful than tissues or organs, and are often more robust in an *in vitro* environment than whole tissues or organs. The implication of this technology is that a much greater number of patients could be treated for ailments resulting from loss of tissue or organ function (1-2).

The underlying concept of tissue engineering is that cells have an inherent capability to organize into tissues and organs if given the proper environment of mechanical and chemical signals. The basic assumption of this technology is that cells cultured in an environment which closely mimics the native environment will develop into tissues which resemble natural tissues (3).

The approach which our research group has pursued to test the concept of tissue engineering has been to transplant cells supported on extracellular matrix analogs made from resorbable polymers (1-3). The materials currently under investigation include poly(glycolic acid) (PGA), poly(lactic acid) (PLA), and copolymers and blends of PGA and PLA. Commercially, these materials have been marketed as resorbable sutures and meshes. The main function of these materials is to provide mechanical support for cells during transplantation. As temporary scaffolds, the polymers provide mechanical signals to regulate the shape of the final tissue products. As the polymers degrade, the mechanical support for cells is furnished by extracellular matrix proteins which the cells synthesize, excrete, and organize. After sufficient time *in vitro*, the cells are then

placed into an *in vivo* environment, where further remodeling is expected to take place.

To gain additional control over the process of tissue regeneration, we have proposed to modulate cell behavior by the introduction of chemical signals into the polymer scaffolds. In addition to mechanical support, the polymer scaffolds would also provide chemical signals, thus bringing the scaffolds one step closer to the extracellular matrix proteins found in the native environment. The strategy which we have pursued to accomplish this goal has been to incorporate into the polymer peptide fragments of natural extracellular matrix proteins which are known to interact with cells. To accomplish this, a new copolymer was created: Poly(lactic acid-*co*-lysine) (PLAL). Covalent coupling of peptides to the ε-amino groups of the lysine side-chains of the copolymer provides stability, uniformity and control of the number of peptides within the scaffolds. In essence, we have created a modified version of PLA which has two additional entities of major interest: NH_2 funtionalities and cell adhesion peptides.

1.2 Objectives

The goal of this research was to develop techniques to make the required engineering measurements of the modifications that were created by the introduction of lysine and peptides into PLA. At the start of the research described herein, the monomer synthesis, copolymerization, deprotection and bulk peptide attachment reactions had been developed (4-6). Only one polymer processing method had been developed and attempts to detect peptides on the surface of the samples had not been successful. One of the objectives of this thesis was to conduct extensive product development studies to explore the properties, limitations and capabilities of this new biomaterial. One of the underlying guidelines was to focus on making measurements where the interaction between the biomaterial and the cells takes place--at the cell-surface interface. More specifically, it was desired to create and analyze the surface features of intact scaffolds with acceptable mechanical properties to support cells during transplantation, rather than to coat thin layers of this material onto glass or another substrate and investigate the properties of the resulting surface treatment. Table 1.1 specifies the research objectives. The measurements which were desired were the surface density of NH_2 functionalities, both the number present and the number available for reaction with peptides, and the surface density of peptides, both the number present and the number available for

interaction with cells. Another objective of this research was the development of methods to measure and correlate the interactions of cells with the immobilized peptides.

Table 1.1
Objectives

1. Process PLAL into scaffolds
2. Develop methods to measure NH_2 surface densities
3. Optimize a surface attachment chemistry
4. Develop methods to measure peptide surface densities
5. Develop methods to measure cell interactions
6. Correlate peptide densities with cell interactions

As this research progressed, a series of technical challenges were overcome by developing innovative approaches to apply existing technologies to this system. This thesis describes the methods which were developed to accomplish the aims of the research. In summary, some of the contributions which are described in the thesis are listed in Table 1.2

Table 1.2
Contributions

1. Optimization of polymer processing using blends
2. Development of colorimetric methods to measure NH_2 densities
3. Optimization of a surface attachment chemistry
4. Modification of the peptide to include ^{127}I for detection by XPS
5. Measurement of surface stability of the peptides by Cold-Stage XPS
6. Measurement of surface wettability using contact angles
7. Measurement of cell interactions

Due to limitations in the achievable molecular weights of large batches of PLAL, it was necessary to process the samples by blending high molecular weight PLA with the PLAL. The effect of this processing step was determined by creating samples ranging in PLAL content from 10 to 50%. This also provided a way to control the amino group and peptide surface densities.

Optimization of the water-soluble carbodiimide (EDC) surface attachment chemistry was accomplished using alkylamine-derivitized polystyrene beads and ^{125}I-radiolabeled peptides.

Sensitive surface analytical techniques were used to distinguish the surface densities of amino groups and peptides. For the amino groups, colorimetric methods were used. For the peptides, non-radioactive iodine was used as a distinct elemental marker that could be detected by X-ray Photoelectron Spectroscopy (XPS).

The stability of the peptides on the surfaces of both bulk-attached and surface-attached samples was determined in degradation studies using cold-stage XPS. It was found that samples maintained sufficient surface densities of peptides to promote cell interactions for up to one month after continuous exposure to hydrolytic conditions.

The wettability of samples containing PLAL and bulk-attached peptides was found to be the same as control samples of pure PLA, signifying that the incorporation of peptides did not change the hydrophobic nature of the polymer. It can also be concluded that the observed effects of the peptides on cell spreading can be attributed to the peptides and not to changes in surface wettability.

The interaction of cells was measured by tracing the areas of individual cells from scanning electron microscope images, and reporting the distribution of cell sizes on the various surfaces.

The main value of this work is that it demonstrates the possibility of controlling cell functions by incorporating cell adhesive peptides into the polymer scaffolds. As one example of this concept, this thesis demonstrates the feasibility of using PLAL with covalently attached Arginine-Glycine-Aspartic Acid (RGD)-containing peptides to control the spreading behavior of bovine aortic endothelial (BAE) cells. Other peptides, drugs and proteins (*i.e.*, growth factors, pharmaceutical agents, insulin) could be attached in similar fashion to this material to promote a variety of responses. Because of its degradative nature, this biomaterial may prove useful in the field of tissue engineering.

1.3 Outline of the Thesis

The history of biomaterials is often characterized as having three stages of development. The first stage consisted of adapting existing materials for medical use. The second stage consisted of making the materials "inert" by surface treatments or by altering the bulk properties. The third (present and future) stage has consisted of rationally designing biomaterials to accomplish specific functions. Chapter 2 treats the history of biomaterials and the development of artificial organs. Also included in Chapter 2 are descriptions of the history of whole organ transplantation and tissue engineering or cell transplantation. The development of poly(lactic acid-*co*-lysine) and some of the proposed uses for this material are also reviewed.

Chapter 3 discusses the methods used to create samples for testing and the results of bulk characterization studies performed on these samples. In order to optimize the samples which were created, a number of sample preparation challenges were overcome. Several methods to prepare samples were explored, each of which is described, along with the nature of the products they produced. The majority of the samples were created by solvent-casting blends of PLAL+GRGDY bulk-attached peptides with PLA. This technique yielded the most reproducible samples and maximized the use of the peptide.

The methods of peptide attachment are described in Chapter 4. The bulk attachment chemistry had been optimized previously, so it is simply summarized herein. The surface attachment method had not been successfully developed previously, so the description of the optimization of this method is more extensive.

Chapter 5 describes the surface characterization studies which were performed. As with any chemical entity, there are two ways to measure it, as the number present, and as the number that are reactive (the number which are reactive presumably being lower than the number present). Methods were developed to measure the number and reactivity of amino groups as well as the number and the interactive capability of the peptides. XPS was used to determine the number of amino groups. Colorimetric methods were developed to measure the reactivity of the amino groups. Peptides were measured by incorporating a distinct element into the peptides, purifying the peptides and then measuring the attached peptides. Surface-attached peptides were measured by ^{125}I-radiolabeled peptides, and also by XPS to detect non-radioactive ^{127}I. Bulk attached peptides exposed on the surface were measured by using non-

radioactive iodine ^{127}I. The levels of peptide that have been reported to be necesssary for the promotion of cell adhesion and spreading are on the order of 1-10 fmol/cm^2 (7). In all cases, the densities of peptides present on the samples created for these studies were significantly higher than the minimally required peptide densities. Contact angle measurements were also conducted, and the results are presented in Chapter 5.

In Chapter 6 are reported the results of experiments designed to measure the extent of interaction of cells with RGD-containing peptides attached to PLAL. The conclusion that was found was that cells, in the absence of serum, remain round on I LA, PLAL, and PLAL+GRDGY, but on RGD-containing surfaces they spread, presumably by specific integrin-ligand interactions. Measurements of spread cell area were made using computerized image analysis of images of cells acquired by scanning electron microscopy. As a way to correlate the results of the cell interaction studies, the mathematical models that have been developed to explain the processes of cell adhesion and spreading were explored. The parameters for two mathematical models were collected, one describing adhesion, the other describing spreading. Each of the models supports the experimental observations of adhesion and spreading on surfaces containing densities of cell adhesion peptides above 100 fmol/cm^2.

This thesis describes the details of the development of the concepts behind the use of rationally designed biomaterials in the field of tissue engineering. Specifically, the methods to make the measurements and the characterization results which support the hypothesis that a modified, resorbable scaffold can be created by incorporating peptides into PLA are reported. A summary of these concepts and the data are included in Chapter 7, along with suggestions for future directions of research.

1.4 References

1. Vacanti, J.P., "Beyond transplantation", *Arch. of Surg.*, **123** (May): 545-549, (1988).

2. Vacanti, J.P., Morse, M. A., Saltzman, W. M., Domb, A. J., Perez-Atayde, A., Langer, R., "Selective cell transplantation using bioabsorbable artificial polymers as matrices", *J. Ped. Surg.*, **23** (1): 3-9, (1988).

3. Langer, R., Vacanti, J. P., "Tissue engineering", *Science*, **260**: 920-926 (1993).

4. Barrera, D.A., Zylstra, E., Lansbury, P. T., Langer, R., "Synthesis and RGD peptide modification of a new biodegradable copolymer: poly(lactic acid-*co*-lysine)", *J. Amer. Chem. Soc.*, **115** : 11010-11011, (1993).

5. Barrera, D.A., Zylstra, E., Lansbury, P. T., Langer, R., "Copolymerization and degradation of poly(lactic acid-*co*-lysine)", *Macromol.*, **28**(2): 425-432 (1995).

6. Barrera, D.A., "Synthesis and characterization of a novel biodegradable polymer-poly(lactic acid-*co*-lysine)", Ph.D. Thesis, MIT (1993)

7. Massia, S.P., Hubbell, J. A., "RGD spacing of 440 nm is sufficient for integrin $\alpha_v\beta_3$-mediated fibroblast spreading and 140 nm for focal contact and stress fiber formation", *J. Cell Biol.*, **114** (5): 1089-1100, (1991).

Chapter 2

Background

2.1 Introduction

The development and use of artificial organs, medical devices and prostheses has been very successful in recent years. Much of the success has been due to the use of synthetic polymeric biomaterials, such as polyurethanes (artificial heart), polysiloxanes (catheters), poly(hydroxyethylmethacrylate) (contact lenses), and expanded polytetrafluoroethylene (vascular grafts). The one common characteristic of these polymers is their remarkable "biocompatibility": *i.e.*, they elicit only minimal harmful interactions with living cells. Nevertheless, long-term use of these polymers is often hampered by the harmful interactions that do occur when these materials are implanted into the body for extended periods of time. Many investigators have attempted to elucidate and minimize the polymer-cell interactions by creating "inert" implants. The universal finding, however, is that there really is no material that is entirely inert (1). The very presence of any material in the tissue bed alters the microenvironment of host cells in the local vicinity and results in abnormal remodeling (2).

Recognizing that any foreign material will influence the surrounding tissue, an alternative strategy used in designing biomaterials is the development of materials that are designed to have favorable interactions with cells. These materials have been proposed as being useful for studying cell behavior *in vitro* and as scaffolds for cell transplantation, a proposed alternative to organ transplantation.

Alternatives such as cell tansplantation are needed because every year thousands of Americans who are candidates for organ transplantation die due to the lack of available donor organs. For example, at the end of 1990, there were over 21,000 people on the United Network for Organ Sharing waiting list, but only 15,000 organs were donated during the year (3). In addition, there are millions of Americans who suffer tissue loss (*e.g.*: burn victims) every year. The total national health care cost for patients who suffer from organ or tissue deficiencies exceeds 400 billion dollars per year (4). One proposed solution to this problem is to transplant dissociated cells supported on a biodegradable

polymer matrix. The synthetic matrix is needed in order to provide the cells with initial mechanical support and stimulation for neomorphogenesis.

This chapter outlines the history of biomaterials, as used in the development of artificial organs, biomedical implants, and prostheses. The development of the field of organ transplantation is also reviewed as well as the pertinent background on the identification of RGD sequences as the functional cell-adhesion promoting entity within fibronectin and other molecules. The concepts leading up to the development of PLAL and prospective uses for PLAL are also reviewed.

2.1.1 History of Biomaterials/ Artificial Organs

Humans have always searched for ways to aid the body's own healing mechanisms and replace lost parts. One very dramatic example of the success that has been achieved in designing artificial organs occurred in 1982 when a total artificial heart was permanently implanted into Barney Clark (5). Synthetic devices have permeated our health care system to the point that virtually every human in technologically-advanced societies will host a biomaterial sometime during their life, whether it be contact lenses, sutures, a catheter, dental implants, joint replacements, or an artificial organ. A look at past attempts to duplicate the function of living tissues and organs is relevant to our study.

The first evidence of the use of artificial devices to replace normal functions in humans extends back to the ancient Egyptians, who fitted their mummies with artificial limbs and eye inlays. Although there is no evidence that similar prostheses were used by the living, these devices did have the well-defined purpose of assisting the deceased in functioning in the next world (6). A Roman artificial leg, which served to replace the loss of bipedal locomotion, was found in Italy and is believed to date from about 300 B.C. It consisted of a central wooden core with a coating of bronze sheets and was attached to the stump by a leather skirt (6). Eyeglasses have existed since 1350 A.D., and iron hands were used in the 16th century (6). The iron hands could be manipulated into a flexed position by a good hand and then locked in place. From these and other examples, it is observed that the first challenge in developing an artificial device is defining its specific purpose, because no synthetic device can replace all of the functions of its biological counterpart.

As new technology became available, alternative solutions became possible. For example, the optical principle underlying the development of the

contact lenses can be traced to the work of Leonardo da Vinci, but it wasn't until Wichterle discovered the biocompatibility of poly(hydroxyethylmethacrylate) that the wide-spread commercilaization of contact lenses became possible (7). In the last 50 years, considerable progress has been made towards replacing lost function of such complex organs such as the kidney, heart and liver. The first artificial organ was a dialysis machine developed by Willem Kolff in the Netherlands during World War II (8). The use of this device on September 11, 1945 marked the first successful and life-saving substitution of the function of a failing vital internal organ by an artificial device. Several different types of devices have been used to replace or supplement the pumping action of the heart, including the heart-lung machine, intra-aortic balloon pumps, left ventricular assist devices, intravascular oxygenators, extracorporeal membrane oxygenation systems, and the artificial heart (9, 10). Several approaches to treat liver failure have been developed, including charcoal hemoperfusion, hemodialysis using a variety of membranes to selectively remove water-soluble toxins and lipophilic toxins simultaneously, and hollow fiber bioreactors containing adult mammalian hepatocytes (11-13). In each of these systems, the patient must be hospitalized or hooked up to large equipment which limits the patient's mobility. To fully replicate the lost function of such organs as the heart, kidney or liver, the challenge is to develop systems which operate so they are "forgettable" by the patient.

Essentially all of the tissues in the body are vascularized, and it is essential for survival that the tissues receive sufficient nutrients and gas exchange by being in close apposition to a blood supply. Large diameter vascular grafts have been in use since 1953 (14) but small diameter vascular grafts continue to pose a challenge for designers. Considerable effort continues to be made in engineering materials and devices that will not cause thrombosis even when formed into tubes less than 5 mm in diameter (15, 16). The main biomaterials in use for vascular grafts are dacron and expanded PTFE. An alternative strategy is to transplant autologous veins from one location within the body to another. The saphenous vein and the internal mammary artery are two of the vessels which are commonly used. The development of strategies to control the ingrowth of blood vessels into tissues is essential to the success of tissue engineering and provides the motivation for our experimental efforts to provide understanding and strategies for controlling the behavior of vascular endothelial cells.

The lessons learned from prior artificial organ research include deciding on a specific function to replace, anticipating major changes in the design as new technology becomes available, and designing the device to be forgettable. In the development of biomaterials for use in artificial organ design, there have been three stages of development. The first materials were those which were already commercially available and were adapted by physicians for use in medical applications. The observation that certain adverse reactions occurred with certain materials led to an effort to passivate materials in order to prevent foreign body reactions. The final stage of biomaterial development is the rational design of materials to accomplish a specific purpose.

2.1.2 History of Organ Transplantation

Another fascinating medical procedure is the transplantation of organs and tissues from one human to another. Accounts have been found of autologous transplants of human tissue as early as 600 B.C., when Hindu surgeons are known to have reconstructed noses by taking skin flaps from arms (6). The science of organ transplantation has developed in parallel with the creation of artificial organs, with most of the successes also occurring in the twentieth century. The first attempt to transplant an organ of any kind was a kidney transplant that was performed in 1950 (6). The first transplant of a human liver was performed in March of 1963 (6), and the first transplant of a human heart was performed by Dr. Christiaan Barnard in South Africa on December 3, 1967 (17). Today, the transplantation of major organs has become widely practiced.

Immunosuppressive drugs such as Cyclosporin A and FK-506 are essential in sustaining the current success of transplantation therapy. (18). This has been necessary to prevent the rejection of transplanted organs (6).

2.2 History of Tissue Engineering

In most cases, direct transplants are more successful than artificial devices, so it is preferable to use a transplanted organ instead of an artificial organ. The use of transplanted organs is limited, however, by the availability of donor organs. Due to the regenerative capacity of most cell types, a new approach has been proposed to transplant a fraction of the donor organ on a synthetic scaffold or encapsulated in a polymeric material. This would enable one donor organ to serve several recipients. Names for this technology are tissue engineering (19-

22), cell transplantation (23-27), hybrid artificial cells (28, 29), and hybrid artificial organs (30-32).

One of the first hybrid artificial organs to be developed was artificial dermis, which is composed of parenchymal epidermal and dermal cells seeded onto a collagen-based matrix made from type IV collagen and chondroitin 6-sulfate (33, 34). In essence, this device is an extracellular matrix analog which acts as an insoluble growth factor, functioning as a transient basal lamina during morphogenesis of skin. Clinical trials (35-37) have demonstrated that the copolymer of collagen and chondroitin 6-sulfate interrupts the formation of a myofibroblast network over the scale of the wound (33). This prevents large scale contraction of the new epidermis.

Another hybrid artificial organ that is being developed is the artificial pancreas, which consists of islets of langerhans enveloped in a synthetic polymer capsule (38). The successful development of such a device is hampered by the lack of a proper membrane and the relative fragility of pancreatic cells. Islets of langerhans, the insulin producing cells of the pancreas, are very sensitive to oxygen concentrations. The membrane surrounding them must allow sufficient oxygen to reach the cells, but prevent any cells of the immune system from entering the capsule.

Several attempts have been made to create hybrid artificial blood vessels that are lined on the interior with endothelial cells (16, 22). Wildevuur has developed an artificial blood vessel from biodegradable polyurethane, which allows smooth muscle cells to grow into the structure and endothelial cells to line the inside of the graft. A complete neo-artery was regenerated within six weeks, resembling a normal artery (40). Wildevuur also replaced an esophagus with a compliant, biodegradable graft seeded with smooth muscle cells and observed that a neo-esophagus regenerated and adapted to the configuration of a normal food bolus (40). In addition, a tracheal prosthesis with the proper material characteristics formed a complete ciliated neo-epithelial lining which protected the material from airborne contamination (40).

There have been numerous attempts to create a hybrid artificial liver (19). Early attempts consisted of injecting dissociated hepatocytes into the spleen, where it was thought that the natural extracellular matrix of the spleen would provide a framework on which the cells would re-associate and begin to regenerate into a functional liver mass (24, 41-43). Hepatocyte transplantation is a conceptually appealing alternative to liver transplantation in two cases: For

patients with hepatic enzyme defects, and for patients with acute fulminant hepatic failure whose liver, after temporary metabolic support, may regain function as regeneration occurs. It could also be used as a partial support system while a recipient is awaiting the availability of an organ (39). In one study it was found that human liver cells remained viable up to 5 months when injected into immunocompromised rats (27). Extracorporeal bioreactors containing pig (30), rabbit (44), or rat hepatocytes (45-47) have been proposed. A collagen sandwich system for culturing hepatocytes *in vitro* has been developed to provide long-term hepatocyte culture and hepatocyte cryopreservation (48). It has been proposed that this system could be used as an artificial liver. Attachment of hepatocytes to microcarrier beads, and encapsulated cells have also been attempted. The main limitation of these approaches is that the isolated cells lose viability due to a lack of oxygen and other nutrients.

2.3 The development of PLAL + RGD

One of the factors which needed to be resolved before tissue engineering could progress was the selection of materials to be used for the scaffolds. The materials had to be biocompatible in that they could not provoke connective tissue responses, they needed to be capable of being fabricated into porous 3-D devices with a high surface area/volume ratio and needed to have sufficient strength to prevent collapse. Since it is known that cells must be attached to survive for a prolonged time, the material needed to be an adhesive substrate for the transplanted cells, allow for retention of differentiated function by the cells, and possibly for cell growth.

Many materials have been proposed for use in constructing biodegradable synthetic scaffolds, such as collagen (34), polyorthoesters (49), polyurethane (40) polyanhydrides (50), poly(lactic acid) (51) and poly(glycolic acid) (52).

2.3.1 Selection of Scaffold Materials

Our group has been investigating ways to create hybrid artificial organs and tissues for the past decade. Studies have been done in rats with hepatocytes (53), chondrocytes (21, 54), and enterocytes (55). In support of this work, cell studies have been done on surfaces coated with extracellular matrix components (56, 57), and on the development of implantation devices (58, 59). In early work, bioabsorbable materials were used to prevent long-term fibrotic and immune responses. Eventually, all of the synthetic material was removed from the area

by natural mechanisms since the polymers degrade by hydrolysis to produce natural molecules. The first materials used were polyanhydrides, polyglactin and polyorthoesters. Results showed that cells remained viable for longer on the polyglactin (PGA 910) fibers than on the other materials (23, 60).

In later studies, polylactic acid (PLA) and polyglycolic acid (PGA) were chosen since they have been approved by the FDA for human use, are resorbable, and degrade by hydrolysis into nontoxic components (61). Using a 50:50 blend of PLA and PGA 85:15 (PLGA) to seed hepatocytes, it was found that differentiated liver cells with proper function survived up to 6 months *in vivo* (61). However, the performance of these materials left much to be desired. For example, the PLGA blends, which were composed of very small diameter fibers, compressed under pressure and the curvature of the fibers was too great for cells to adhere and spread. After 3 or 4 days, hepatocytes detached from the PLGA due to cell-cell tensions that overcame the cell-substratum tension. It was suggested that sponge-like, highly porous structures may work better than PLGA fibers (61).

The results of this experimental work demonstrated the need to develop new scaffold materials which could promote interactions of cells with the biomaterial. The strategy that was adapted was to incorporate synthetic cell adhesion peptides that were being reported to increase cell adhesion and spreading into the polymer scaffolds (64, 70-74). Poly(lactic acid) was chosen as the base material due to its good mechanical properties and processing capabilities.

2.3.2 *Integrins*

It has long been accepted that cells of all kinds have membrane receptors in their membranes that allow specific covalent bonds to form with other cells and with physical substrates. For example, Obrink demonstrated in 1977 that rat and chicken hepatocytes prefer to adhere to similar cells, supposedly because they possess adhesion sites that are specific for cell-cell adhesion (62). However, the chemical nature of these cell membrane receptors has only recently been characterized. For example, in 1985 Knudsen reported the isolation of a glycoprotein complex involved in chick embryo cell adhesion to a substrate (63). Localization studies showed that a monoclonal antibody co-aligned with stress fibers adjacent to vinculin-rich focal contact sites. Thus, the glycoprotein complex was in a location consistent with its proposed involvement in adhesion. Also in 1985, Pytela isolated a 140 kd glycoprotein imbedded in the membrane of

cells which acted as a cell surface receptor for the RGD sequence (64). This protein was inserted into a lipid bilayer of liposomes which then adhered to RGD and fibronectin surfaces. It is now recognized that integrins are heterodimers consisting of noncovalently associated α and β subunits. Recent reviews on integrins are available (65, 66). Three major integrin groups can be distinguished by the β subunit: the β_1 group consists of six complexes that are predominantly involved in cell-matrix adhesion and are expressed by most cell types; the β_2 group has three complexes which mediate cell-cell adhesion exclusively in leukocytes; the β_3 group consists of cell-matrix adhesion receptors. Endothelial cells are known to express all six of the β_1 group integrins, the $\alpha_v\beta_3$ integrins and integrins containing the β_5 subunit. In the native environment, cells interact with their natural extracellular matrix (ECM) through integrins. The internal cytoskeleton of a cell is attached to integrin proteins which are dimeric and cross the cell membrane. Many integrins have affinity for the RGD segment of fibronectin, vitronectin, von Willebrand factor and many other proteins.

Although they are important, integrins are not the only molecules involved in cellular adhesion to surfaces. A complete adhesive interaction requires that several surface molecules, including glycoprotein complexes, proteoglycans, and glycolipids all come together in the proper molecular configuration (67).

2.3.3 *Extracellular Matrix*

The extracellular matrix is a dynamic structure. It serves as a major conduit for cell traffic and assures pattern integrity (68). It also provides mechanical support, determines cell orientation, controls cell growth, maintains cell differentiation, provides a scaffold for orderly tissue renewal, establishes a microenvironment, and stores and presents soluble regulatory molecules (69). The major components of the ECM are structural glycoproteins such as collagens, elastin, laminin, and fibronectin. Collagen provides the structural support, while fibronectin provides attachment sites for epithelial cell adhesion.

2.3.4 *Fibronectin*

The central function of fibronectin is in the adhesion of cells to the extracellular matrix, but cells do not adhere passively to fibronectin--it is a complex process. There are multiple sites for interaction of cells within fibronectin (see Figure 2.1). Fibronectin contains binding sites for cells and for

collagen, the main component of the ECM. A RGD site and a second site within the cell-binding domain are both required for effective adhesion, assembly of microfilament bundles, full spreading, cytoskeletal organization, focal contact formation, and migration (66). The REDV segment purportedly interacts preferentially with integrins on the surface of endothelial cells and , but not smooth muscle cells, fibroblasts and platelets (70).

Figure 2.1
Schematic of Fibronectin

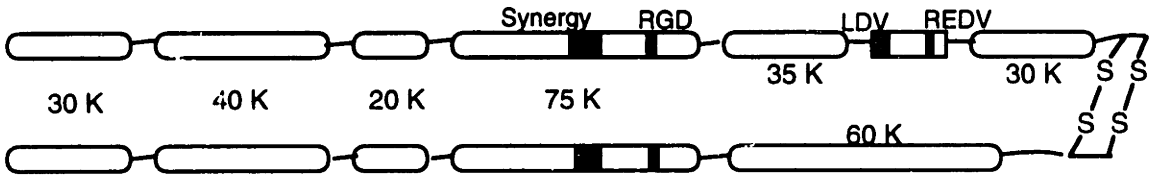

Figure 2.1: Fibronectin is a 450 K (kilodalton) protein which contains two Arginine-Glycine-Aspartic Acid (RGD) sequences, along with several other cell-adhesive peptide binding sites (*e.g.*, Synergy, LDV and REDV). This schematic illustrates the various subunits of fibronectin. Adapted from reference (75).

2.3.5 RGD Peptides

Pierschbacher and Ruoslahti used enzyme techniques to reduce the cell-binding domain of fibronectin to the RGD segment (71), and showed that most of the cell adhesion activity of fibronectin can be attributed to this tripeptide. Due to the popularity of this tripeptide sequence, RGD-containing peptides were chosen as model cell adhesion peptides in our studies. These peptides have been shown to be effective analogs of the extracellular matrix (72-74). The chemical structure of the RGD peptide sequence is shown in Figure 2.2. Other proteins, such as vitronectin, von Willebrand factor, fibrinogen and thrombospondin also contain RGD peptide sequences. The isolated peptide fragments from these proteins differ in the amino acid sequences surrounding RGD.

Figure 2.2
RGD

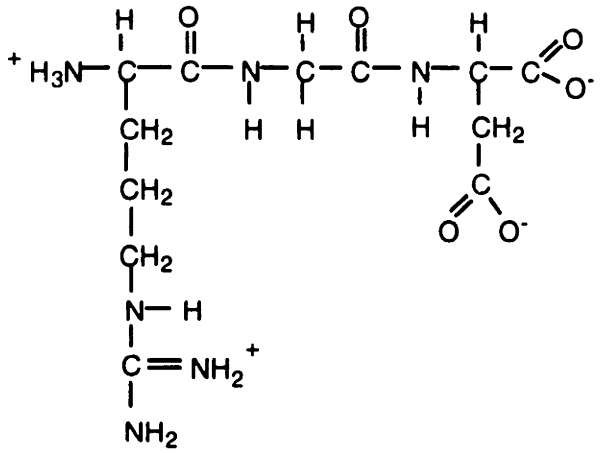

Figure 2.2: The chemical structure of Arginine-Glycine-Aspartic Acid (RGD).

2.4 Prospective Uses for PLAL + RGD

The attachment of RGD-containing peptides to PLA was accomplished by creating a new copolymer system which incorporated lysine into the polymer backbone, thus creating poly(lactic acid-*co*-lysine). The ε-amino group of the lysine was used to covalently link RGD-containing peptides to the copolymer. The experience which we have gained so far with PLAL has shown that it is a potentially useful biomaterial. Because it can be blended with PLA, it can potentially be used in any application for which PLA is now used. The types of structures that can be formed include, but are not limited to: films, fibers, meshes, porous sponges, and tubes. Due to the availability of functional groups which can be used to attach biologically active entities such as cell-adhesion peptides, the use of PLAL:PLA blends has the advantage of promoting interaction with cells. Blends formed into various structures, designed to support cells such as chondrocytes, endothelial, epithelial, smooth muscle, or hepatocytes could produce engineered tissues. This section describes two potential uses for this copolymer-peptide system, as scaffolds for tissue engineered blood vessels and as scaffolds for tissue engineered tracheal linings.

2.4.1 *Engineered blood vessels*

In order to effectively engineer a blood vessel, the following criteria must be satisfied:

1. The engineered vessel must be sturdy, yet compliant.
2. Interactions between the endothelial cells and the smooth muscle cells must be established.
3. The endothelial layer must be uniform and completely intact.
4. The endothelial cells must be able to quickly repair any defects that occur
5. The polymer support should either be totally degraded or degraded sufficiently that it will not disturb the natural reorganization of the cells within the engineered tissue.
6. The endothelial cells must be in the proper differentiated mode, excreting factors which aid in their natural incorporation into the vasculature.

The cells within the vessels of the vasculature are exposed to many potentially harmful substances and forces. The exposure of the cells to fluid forces during formation of the engineered tissue is expected to be essential to the development of the properties the vessels need to function properly.

Two approaches could be conceptualized. The first would consist of attaching endothelial cells onto PLAL+RGD polymer films in a flat format, then rolling the films up into a device for incubation with smooth muscle cells on the outside of the tube and the exposure of the endothelial cells on the inside of the tube to a flow stream. The second approach could be the formation of the polymer into tubes, then exposing the tubes to cells in a static system. Once the cells have adhered, then the tubes could be exposed to a flow stream.

One way to make an endothelialized tube of smooth muscle cells using PLAL:PLA blends with RGD-containing peptides as a temporary basement membrane may be to make the smooth muscle tube first, then add the endothelial cells. It may occur that the endothelial cells interact directly with the smooth muscle cells, but in the absence of an initial basement membrane, the interaction may not be entirely characteristic of the natural tissue. If it is found that the PLAL:PLA film is too thick, the next alternative could be a mesh made from fibers extruded from mixtures of PLAL and PLA.

2.4.2 *Engineered tracheal linings*

The goal of studying the interaction of normal respiratory epithelial (NRE) cells with PLAL is the creation of an epithelial lining for a trachea composed of an engineered cartilage tube and the epithelial lining. The criteria which must be satisfied with regards to engineering a functional trachea include:

1. The epithelial cells must attach, spread and proliferate on the PLAL until they form an intact layer.
2. The epithelial cells must become ciliated.
3. The epithelial cells must be able to repair any defects that occur.
4. The epithelial cells must interact with the underlying cartilage tube as the polymer degrades and disappears.
5. The degradation of the PLAL must not interfere with the formation of the engineered tissue.

One of the variables which needs to be examined is the rate of degradation of the material and how the cells behave at various stages during degradation. The current status of the trachea engineering project is the ability to form cartilage tubes *in vivo*. In order for the engineered trachea to successfully function, it is felt that an epithelial lining is necessary to prevent infections from airborne microorganisms. One could use cartilage tubes as an initial support for the PLAL liners with attached respiratory epithelial cells. The trachea project may be easier than the blood vessel project because the need for exposure to blood is eliminated during seeding of the NRE cells. The protocol could be as follows:

Insert a spiral PLA tube seeded with cartilage cells into the animal. Over the course of a few days, this tube will form into cartilage. If the tube is formed in the neck of the animal, the tube will become vascularized. During cartilage tube formation, make a liner seeded with epithelial cells *in vitro*. Bring the cells to air-interface so they become ciliated. Insert the liner into the tube during the operation to move the engineered tube into proper position to replace the natural trachea. The intact epithelia supported on the basement membrane analog will protect the cartilage from infection.

2.5 *References*

1. Ratner, B.D., "New ideas in biomaterials science--a path to engineered biomaterials", *JBMR*, **27** : 837-850, (1993).

2. Spector, M., Cease, C., Tong-Li, X., "The local tissue response to biomaterials", *Crit. Rev. Biocomp.*, **5** (3): 269-295, (1989).

3. Evans, R.W., "Executive summary: The national cooperative transplantation study", (1991)

4. Langer, R., Vacanti, J. P., "Tissue engineering", *Science*, **260**: 920-926 (1993).

5. DeVries, W.C., Anderson, J. L., Joyce, L. D., Anderson, F. L., Hammond, E. H., Jarvik, R. K., Kolff, W. J., "Clinical use of the artificial heart", *N. Engl. J. Med.*, **310** (5): 273-278, (1984).

6. Roth, C.A., Lenfant, C., "Implants, transplants, and other parts of the medicine of the future", *Ann. Biomed. Engin.*, **18** : 337-346, (1990).

7. Tighe, B.J., "Hydrogels as contact lens materials", Hydrogels in Medicine and Pharmacy, Vol. III: Properties and Applications, Peppas, N.A., ed., CRC Press, Florida, (1987)

8. Kolff, W.J., "First clinical experience with the artificial kidney", *Ann. Intern. Med.*, **62** (3): 608-619, (1965).

9. Bernstein, B.J., "The misguided quest for the artificial heart", *Tech. Rev.*, (Nov/Dec): pp. 12-19 & 62-63, (1984).

10. Pennington, D.G., "Circulatory support at the turn of the decade: a clinician's view", *ASAIO Trans.*, **36** : M126-M131, (1990).

11. Silk, D.B.A., Williams, R., "Treatment of fulminant hepatic failure by charcoal haemoperfusion and polyacrilonitroile haemodialysis", Artificial Kidney, Artificial Liver, and Artificial Cells, Chang, T.M.S., ed., Plenum Press, New York, (1978)

12. Jauregui, H.O., Muller, T. E., "Long-term cultures of adult mammalian hepatocytes in hollow fibers as the cellular component of extracorporeal (hybrid) liver assist devices", *Artif. Organs*, **16** (2): 209-212, (1992).

13. Konstantin, P., Chang, J., Otto, V., Brunner, G., "Artificial liver", *Artif. Organs*, **16** (3): 235-242, (1992).

14. Clark, M., Copeland, J. B., Shapiro, D., Abramson, P., Hager, M., Sandza, R., "An incredible affair of the heart", *Newsweek*, **100** (24): 70-74,79, (1982).

15. Connolly, R.J., Anderson, J. M., Kambic, H. E., Greisler, H., Merrill, E. W., "Small diameter vascular prostheses", *Trans. ASAIO*, **34** : 1043-1046, (1988).

16. Greisler, H.P., Dennis, J. W., Endean, E. D., Ellinger, J., Buttle, K. F., Kim, D. U., "Derivation of neointima in vascular grafts", *Circ.*, **78** (suppl I): I6-I12, (1988).

17. "An unexpected difficulty: Details of heart transplant reported", *JAMA*, **202** (12): 23-24, (1968).

18. Cooper, D.K.C., "Experimental development and early clinical experience", Heart Transplantation: The Present Results of Orthotopic and Heterotopic Heart Transplantation, Cooper, D.K.C., Lanza, R. P., ed., MTP Press, Ltd., Lancaster, (1984)

19. Cima, L.G., Vacanti, J. P., Vacanti, C., Ingber, D., Mooney, D., Langer, R., "Tissue engineering by cell transplantation using degradable polymer substrates", *J. Biomech. Eng.*, **113** (May): 143-151, (1991).

20. Yarmush, M.L., Toner, M., Dunn, J. C. Y., Rotem, A., Hubel, A., Tompkins, R. G., "Hepatic tissue engineering: development of critical technologies", *Ann. N. Y. Acad. Sci.*, **665** : 238-252, (1992).

21. Vacanti, C.A., Langer, R., Schloo, B., Vacanti, J. P., "Synthetic polymers seeded with chondrocytes provide a template for new cartilage formation", *Plastic and Reconst. Surg.*, **88** (5): 753-759, (1991).

22. Hubbell, J.A., Massia, S. P., Drumheller, P. D., "Surface-grafted cell-binding peptides in tissue engineering of the vascular graft", *Ann. N. Y. Acad. Sci.*, **665** : 253-258, (1992).

23. Vacanti, J.P., Morse, M. A., Saltzman, W. M., Domb, A. J., Perez-Atayde, A., Langer, R., "Selective cell transplantation using bioabsorbable artificial polymers as matrices", *J. Ped. Surg.*, **23** (1): 3-9, (1988).

24. Ricordi, C., Flye, M. W., Lacy, P. E., "Renal subcapsular transplantation of clusters of hepatocytes in conjunction with pancreatic islets", *Transplant.*, **45** (6): 1148-1151, (1988).

25. Aebischer, P., Winn, S. R., Tresco, P. A., Jaeger, C. B., Greene, L. A., "Transplantation of polymer encapsulated neurotransmitter secreting cells: Effect of the encapsulation technique", *Trans. ASME*, **113** (May): 178-183, (1991).

26. Asonuma, K., Gilbert, J. C., Stein, J. E., Takeda, T., Vacanti, J. P., "Quantitation of transplanted hepatic mass necessary to cure the Gunn rat model of hyperbilirubinemia", *J. Ped. Surg.*, **27** (3): 298-301, (1992).

27. Moscioni, A.D., Chowdhury, J. R., Barbour, R., Brown, L. L., Chowhdury, N. R., Competiello, L. S., Lahiri, P., Demetriou, A. A., "Human liver cell transplantation: prolonged function in athymic-Gunn and athymic-analbuminemic hybrid rats", *Gastroent.*, **96** : 1546-1551, (1989).

28. Chang, T.M.S., "Hybrid artificial cells: microencapsulation of living cells", *ASAIO J.*, **38** (2): 128-130, (1992).

29. Chang, T.M.S., "Artificial cells: 35 years", *Artif. Organs*, **16** (1): 8-12, (1992).

30. Uchino, J., Matsue, H., Takahashi, M., Nakajima, Y., Matsushita, M., Hamada, T., Hashimura, E., "A hybrid artificial liver system: function of cultured monolayer pig hepatocytes in plasma from hepatic failure patients", *ASAIO Trans.*, **37** : M337-M338, (1991).

31. Colton, C.K., Weinless, N. L., "A theoretical model for insulin secretion rate in a hybrid artificial pancreas", Artificial Organs, Andrade, J.D., Brophy, J. J., Detmer, D. E., Kim, S. W., Normann, R. A., Olsen, D. B., Stephen, R. L., ed., VCH Publishers, Inc., New York, (1987)

32. Matsuda, T., Kondo, A., Makino, K., Akutsu, T., "Development of a novel artificial matrix with cell adhesion peptides for cell culture and artificial and hybrid organs", *ASAIO Trans.*, **35** : 677-679, (1989).

33. Murphy, G.F., Orgill, D. P., Yannas, I. V., "Partial dermal regeneration is induced by biodegradable collagen-glycosaminoglycan grafts", *Lab. Invest.*, **63** (3): 305-313, (1990).

34. Yannas, I.V., Lee, E., Orgill, D. P., Skrabut, E. M., Murphy, G. F., "Synthesis and characterization of a model extracellular matrix that induces partial regeneration of adult mammalian skin", *Proc. Natl. Acad. Sci. USA*, **86** : 933-937, (1989).

35. Heimbach, D., Luterman, A., Burke, J., Cram, A., Herndon, D., Hunt, J., Jordan, M., McManus, W., Solem, L., Warden, G., Zawacki, B., "Artificial dermis for major burns. A multi-center randomized clinical trial", *Ann. Surg.*, **208** (3): 313-320, (1988).

36. Michaeli, D., McPherson, M., "Immunologic study of artificial skin used in the treatment of thermal injuries", *J. Burn Care Rehabil.*, **11** (1): 21-26, (1990).

37. Stern, R., McPherson, M., Longaker, M. T., "Histologic study of artificial skin used in the treatment of full-thickness thermal injury", *J. Burn Care Rehabil.*, **11** : 7-13, (1990).

38. Colton, C.K., Avgoustiniatos, E. S., "Bioengineering in development of the hybrid artificial pancreas", *Trans. ASME*, **113** : 152-170, (1991).

39. Bumgardner, G.L., Fasola, C., Sutherland, D. E. R., "Prospects for hepatocyte transplantation", *Hepatology*, **8** (5): 1158-1161, (1988).

40. Wildevuur, C.R.H., van der Lei, B., "Artificially induced biological organs: a new concept", Artificial Organs, Andrade, J.D., Brophy, J. J., Detmer, D. E., Kim, S. W., Normann, R. A., Olsen, D. B., Stephen, R. L., ed., VCH Publishers, Inc., New York, (1987)

41. Jaffe, V., Darby, H., Selden, C., Hodgson, H. J. F., "The growth of transplanted liver cells within the pancreas", *Transplant.*, **45** (2): 497-498, (1988).

42. Mito, M., Ebata, H., Kusano, M., Onishi, T., Saito, T., Sakamoto, S., "Morphology and function of isolated hepatocytes transplanted into rat spleen", *Transplant.*, **28** (6): 499-505, (1979).

43. te Velde, A.A., Bosman, D. K., Oldenburg, J., Sala, M., Maas, M. A. W., Chamuleau, R. A. F. M., "Three different hepatocyte transplantation techniques for enzyme deficiency disease and acute hepatic failure", *Artif. Organs*, **16** (5): 522-526, (1992).

44. Matthew, H.W.T., Salley, S. O., Peterson, W. D. Jr., Deshmukh, D. R., Mukhopadhyay, A., Klein, M. D., "Microencapsulated hepatocytes: prospects for extracorporeal liver support", *ASAIO Trans.*, **37** : M328-M330, (1991).

45. Sun, A.M., O'Shea, G. M., Cai, Z., Shi, Z., Darquy, S., Carpenter, R. C., "Microencapsulation of living cells as bioartificial organs", Artificial Organs, Andrade, J.D., Brophy, J. J., Detmer, D. E., Kim, S. W., Normann, R. A., Olsen, D. B., Stephen, R. L., ed., VCH Publishers, Inc., New York, (1987)

46. Wong, H., Chang, T. M. S., "Bioartificial liver: implanted artificial cells microencapsulated living hepatocytes increases survival of liver failure rats", *Inter. J. Art. Org.*, **9** (5): 335-336, (1986).

47. Chang, T.M.S., "Biotechnological and medical applications based on immobilization of hepatocytes, microorganisms, or enzyme systems by microencapsulation in artificial cells", *Ann. N. Y. Acad. of Sci.*, 613: 109-115, (1990).

48. Dunn, J.C.Y., Yarmush, M. L., Koebe, H. G., Tompkins, R. G., "Hepatocyte function and extracellular matrix geometry: long-term culture in a sandwich configuration", *FASEB J.*, **3** : 174-177, (1989).

49. Saltzman, W.M., Parkhurst, M. R., Parsons-Wingerter, P., Zhu, W-H., "Three-dimensional cell cultures mimic tissues", *Ann. N. Y. Acad. Sci.*, **665** : 259-273, (1992).

50. Lucas, P.A., Laurencin, C., Syftestad, G. T., Domb, A., Goldberg, V. M., Caplan, A. I., Langer, R., "Ectopic induction of cartilage and bone by water-soluble proteins

from bovine bone using a polyanhydride delivery vehicle", *J. Biomed. Mat. Res.*, **24** : 901-911, (1990).

51. Agrawal, C.M., Haas, K. F., Leopold, D. A., Clark, H. G., "Evaluation of poly(L-lactic acid) as a material for intravascular polymeric stents", *Biomat.*, **13** (3): 176-182, (1992).

52. Therin, M., Christel, P., Li, S., Garreau, H., Vert, M., "*In vivo* degradation of massive poly(α-hydroxy acids): validation of *in vitro* findings", *Biomat.*, **13** (9): 594-600, (1992).

53. Cima, L.G., Ingber, D. E., Vacanti, J. P., Langer, R., "Hepatocyte culture on biodegradable polymeric substrates", *Biotech. and Bioeng.*, **38** : 145-158, (1991).

54. Freed, L.E., Marquis, J. C., Nohria, A., Emmanual, J., Mikos, A. G., Langer, R., "Neocartilage formation *in vitro* and *in vivo* using cells cultured on synthetic biodegradable polymers", *J. Biomed. Mat. Res.*, **27** : 11-23, (1993).

55. Organ, G.M., Mooney, D. J., Hansen, L. K., Schloo, B., Vacanti, J. P., "Enterocyte transplantation using cell-polymer devices to create intestinal epithelial-lined tubes", *Transplant. Proc.*, **25** (1): 993-1001, (1993).

56. Mooney, D., Hansen, L., Vacanti, J., Langer, R., Farmer, S., Ingber, D., "Switching from differentiation to growth in hepatocytes: control by extracellular matrix", *J. Cell Phys.*, 151: 497-505, (1992).

57. Mooney, D.J., Langer, R., Hansen, L. K., Vacanti, J. P., Ingber, D. E., "Induction of hepatocyte differentiation by the extracellular matrix and an RGD-containing synthetic peptide", in Tissue Inducing Biomaterials, Materials Research Society Symposium Proceedings, Cima, L. G, Eyal, R. S., eds., **252**: 199 (1992).

58. Wald, H.L., Sarakinos, G., Lyman, M. D., Mikos, A. G., Vacanti, J. P., Langer, R., "Cell seeding in porous transplantation devices", *Biomaterials*, **14** (4): 270-278 (1993).

59. Wintermantel, E., Cima, L., Schloo, B., Langer, R., "Angiopolarity: A new design parameter for cell transplantation devices and its application to degradable systems", *ASAIO Trans..*, **37**: M334-M336 (1991).

60. Vacanti, J.P., "Beyond transplantation", *Arch. of Surg.*, **123** (May): 545-549, (1988).

61. Cima, L.G., Langer, R., Vacanti, J. P., "Polymers for tissue and organ culture", *J. Bioact. and Compat. Poly.*, **6** : 232-240, (1991).

62. Obrink, B., Kulhenschmidt, M. S., Roseman, S., "Adhesive specificity of juvenile rat and chicken liver cells and membranes", *Proc. Natl. Acad. Sci. USA*, **74** (3): 1077-1081, (1977).

63. Knudsen, K.A., Horwitz, A. F., Buck, C. A., "A monoclonal antibody identifies a glycoprotein complex involved in cell-substratum adhesion", *Exp. Cell Res.*, **157** : 218-226, (1985).

64. Pytela, R., Pierschbacher, M. D., Ruoslahti, E., "Identification and isolation of a 140 kd cell surface glycoprotein with properties expected of a fibronectin receptor", *Cell*, **40** : 191-198, (1985).

65. Albelda, S.M., Buck, C. A., "Integrins and other cell adhesion molecules", *FASEB J.*, **4** : 2868-2880, (1990).

66. Hynes, R.O., "Cellular adhesion and cell surface receptors", Fibronectins, Rich, A., ed., Springer-Verley, New York, (1990)

67. Buck, C.A., Horwitz, A. F., "Cell surface receptors for extracellular matrix molecules", *Ann. Rev. Cell Biol.*, **3** : 179-205, (1987).

68. Ingber, D.E., Folkman, J., "Mechanochemical switching between growth and differentiation during fibroblast growth factor-stimulated angiogenesis *in vitro*: role of extracellular matrix", *J. Cell Biol.*, **109** : 317-330, (1989).

69. Ingber, D.E., Folkman, J., "How does extracellular matrix control capillary morphogenesis?", *Cell*, **58** : 803-805, (1989).

70. Massia, S.P., Hubbell, J. A., "Vascular endothelial cell adhesion and spreading promoted by the peptide REDV of the IIICS region of plasma fibronectin is mediated by integrin $\alpha_4\beta_1$", *J. Biol. Chem.*, **267** (20): 14019-14026, (1992).

71. Pierschbacher, M.D., Ruoslahti, E., "Cell attachment activity of fibronectin can be duplicated by small synthetic fragments of the molecule", *Nature*, **309** : 30-33, (1984).

72. Massia, S.P., Hubbell, J. A., "Covalent surface immobilization of Arg-Gly-Asp- and Tyr-Ile-Gly-Ser-Arg- containing peptides to obtain well-defined cell-adhesive substrates", *Anal. Biochem.*, **187** : 292-301, (1990).

73. Massia, S.P., Hubbell, J. A., "Covalently attached GRGD on polymer surfaces promotes biospecific adhesion of mammaliam cells", *Ann. N. Y. Acad. Sci.*, **589** : 261-270, (1990).

74. Massia, S.P., Hubbell, J. A., "RGD spacing of 440 nm is sufficient for integrin $\alpha_v\beta_3$-mediated fibroblast spreading and 140 nm for focal contact and stress fiber formation", *J. Cell Biol.*, **114** (5): 1089-1100, (1991).

75. Yamada, K.M., "Fibronectin and other cell interactive glycoproteins", Cell Biology of the Extracellular Matrix, 2nd edition, Ed. Elizabeth D. Hay, Plenum Press, New York, N.Y., 111-146 (1991).

Chapter 3

Sample Preparation

The preparation of samples for testing required the following steps: synthesis of the lysine-containing monomer, copolymerization, deprotection, polymer processing, and peptide attachment. At each stage of preparation, characterization of the products was performed to ensure the quality of the samples. This chapter describes the results of the characterization studies which were performed. It also describes the various polymer processing techniques which were explored with a general description of the properties of the resulting samples as prepared by each method.

A major goal of this research was to elucidate the relative importance of the various sample preparation steps on the characteristics of the surfaces that were created. Prior to the initiation of the studies described herein, many batches of monomer were synthesized and these batches were fully characterized (1). Similarly, the copolymerization and deprotection reactions were already extensively studied (2). The focus of the studies described below involved the study of peptide attachment reactions, processing steps, sterilization techniques and cell interaction experiments. The majority of the samples which were investigated were thin solvent-cast disks made from blends of PLA with random PLAL copolymers composed of approximately 98-99% lactic acid and 1-2% lysine as determined by ^{1}H-NMR (see Figure 3.1).

3.1 Monomer synthesis

The monomer was synthesized by reacting purified bromo-substituted D-alanine with thionyl chloride to produce 2-bromopropionyl chloride. This was then purified, combined with ε-amino-protected-lysine and cyclized to form a closed ring 3,3',6,6'-tetrasubstituted-2,5-morpholinedione. Figure 3.2 depicts the scheme which was followed. The reactions and results of the characterization of each batch of monomer are described in more detail in the subsections below.

Figure 3.1
Poly(lactic acid-co-lysine)

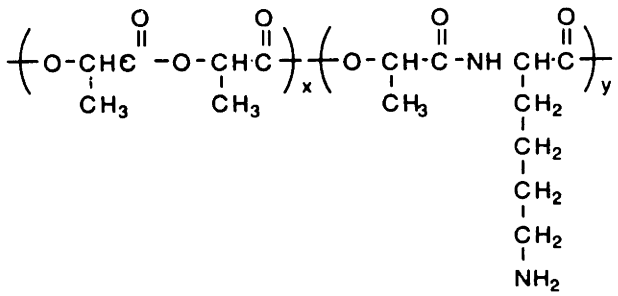

Figure 3.1: The chemical structure of Poly(lactic acid-*co*-lysine)
x = number of lactide units incorporated (contains two lactic acid units) Typically: 96-98%
y = number of lysine-containing monomer units incorporated (contains one lactic acid unit and one lysine unit) Typically: 2-4%
Overall, there are 98-99% lactic acid units and 1-2% lysine in a typical sample of PLAL.

3.1.1 Reactions

Eleven batches of monomer were completed. The reactions that were conducted were the following:

1. D-Alanine (**1**, M.W. = 89.1 g/mol) was converted to bromo-substituted D-Alanine (**2**, M.W. = 153 g/mol).
2. Bromo-substituted D-Alanine (**2**) was converted to D-α-bromopropionyl chloride (**3**, M.W. = 171.4 g/mol).
3. D-α-bromopropionyl chloride (**3**) was combined with N-ε-CBZ-L-Lysine (**4**, M.W. = 280.3 g/mol) to produce (2-bromo-1-oxopropyl)-[(phenyl methoxy) carbonyl]-L-Lysine (**5**, M.W. = 415.3 g/mol)
4. (2-bromo-1-oxopropyl)-[(phenyl methoxy) carbonyl]-L-Lysine (**5**) was closed into a ring structure: phenylmethyl ester-[4-(6-methyl-2,5-dioxo-3-morpholinyl)butyl carbamic acid (**6**, M.W. = 334.4 g/mol).

The products from reactions 1 and 2 were purified by distillation. The product from reaction 4 was purified by silica gel chromatography. A complete protocol for synthesizing the monomer is included in Appendix 3A. In a typical batch the following results were obtained (see Table 3.1):

Table 3.1
Typical Batch Conversions

Reaction	Amount of Reagent (g)	Amount of Product (g)	Conversion
1a.	50	46	54%
1b.	50	54	63%
2.	95	16	15%
3&4.	13.8	3	9%

Table 3.1: Monomer synthesis reaction conversions were assessed at three stages during synthesis, after reaction 1 (which was repeated in 2 batches, 1a and 1b), after reaction 2, and following the final purification after reactions 3 and 4. See text for a discussion of the reaction steps.

Each batch was characterized by ^{1}H NMR, FTIR, DSC and Elemental Analysis. Each batch was also tested for silicon grease contamination. Batch designations and yields are shown in Table 3.2. The yield from each batch ranged from 2 to 7 g, averaging about 4 g per batch. In batches 3-8, the product was divided into fractions A and B depending on the observed presence of impurities from thin layer chromatography. Fraction A was designated as the fraction of highest purity in all cases.

Table 3.2
Lysine-Containing Monomer (LCM) Synthesis Results

Batch #	Date Completed	Designation*	Yield (g)
LCM1	8/31/92	LC1.095	7.2
LCM2	6/2/93	LC1.145	2.1
LCM3	11/3/93	LC1.216	5.8
LCM4	11/29/93	LC1.245	3.1
LCM5	12/20/93	LC1.276	2.8
LCM6	1/31/94	LC2.011	4.0
LCM7	2/17/94	LC2.020	2.6
LCM8	3/1/94	LC2.034	1.5
LCM9	7/1/94	ED1.094	0.5
LCM10	7/6/94	ED1.099	0.5
LCM11	7/11/94	ED1.105	0.9
			31.0

Table 3.2: *This designation refers to the volume and notebook pages of the lab notebooks in which the synthesis was recorded (LC = Lon Cook, ED = Eric Dong).

Figure 3.2
Monomer Synthesis Scheme

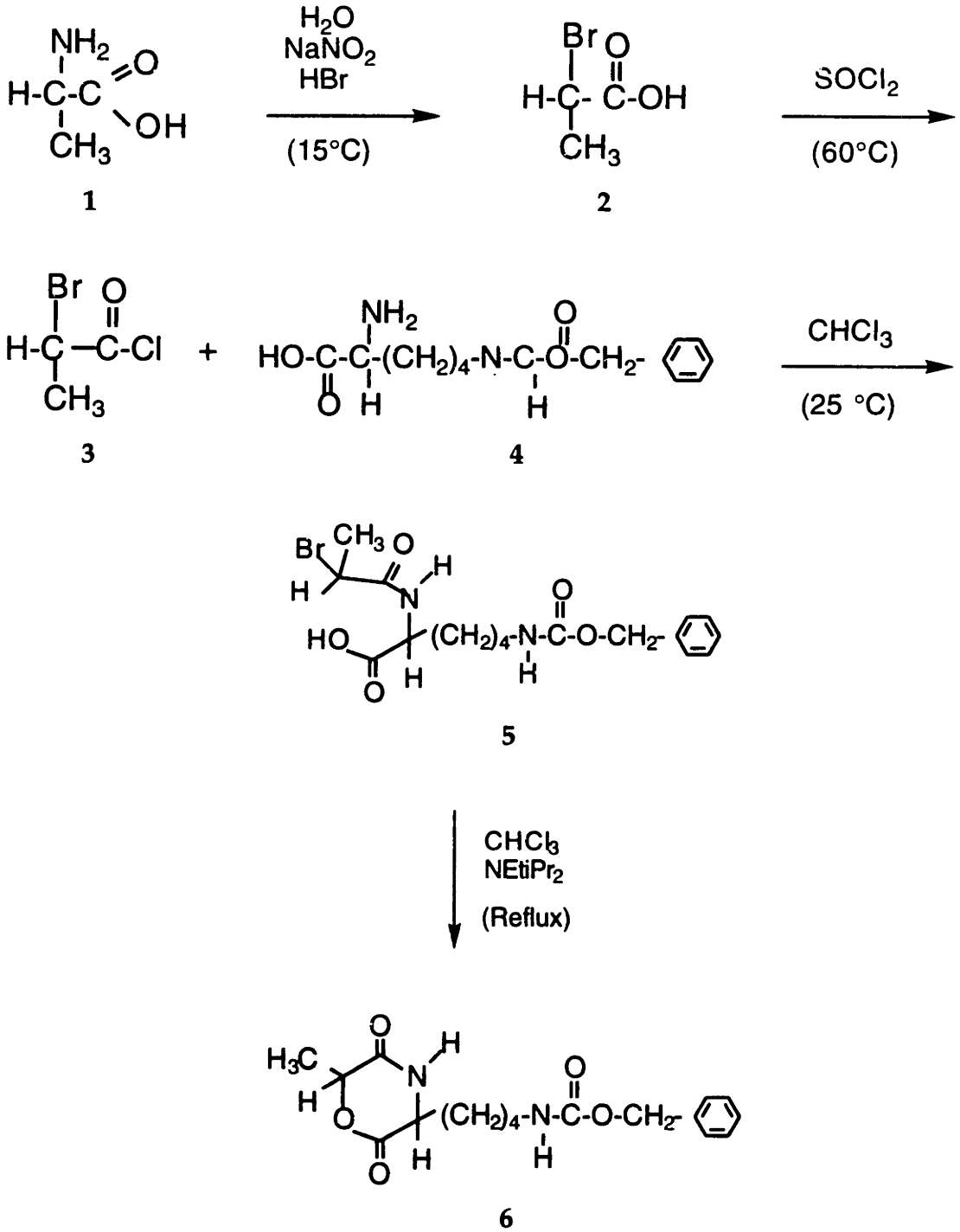

Figure 3.2: The synthesis scheme for creating the cyclic lysine-containing monomer. See text for description of the reaction steps.

3.1.2 NMR Results

Samples (20 mg) of each of the batches of monomer product (**6**) were submitted to Spectral Data Services (Champaign, Illinois) for ^1H NMR analysis, using DMF-d_7 as the solvent. Spectra were collected on a 360 MHz spectrometer and results were returned with integrations. By comparing the spectra to previous results it was observed in each case that the monomer product had been created. Figure 3.3 shows a typical spectrum. Table 3.3 is a sample analysis of the peak integrations showing that the correct number of peaks (corresponding to the 22 protons in the lysine-containing monomer) are present in approximately the correct height ratios. In every instance the difference between theoretical and actual peak areas was less than 15% except for peaks 5 and 12, which corresponded to only a small fraction (0.03) of a proton. In this case, a small difference in peak area (.04 vs .03) led to a high percent difference. This difference was diminished if the sum of peaks 5 and 6, and 11 and 12, respectively were compared to the theoretical sum of these two peaks.

3.1.3 FTIR Results

Samples of each of the monomer products were pressed on a Carver Press into potassium bromide (KBr) to make a disk that was analyzed by Fourier Transform Infrared Spectroscopy (FTIR). Spectra were obtained using a Nicolet 550 Magna FTIR spectrometer operated with Omnic software. A sample spectra is shown in Figure 3.4. By comparing this spectra to spectra taken previously (3), it was concluded that each batch of the monomer had the correct IR structure.

Figure 3.3
^{1}H NMR Spectra

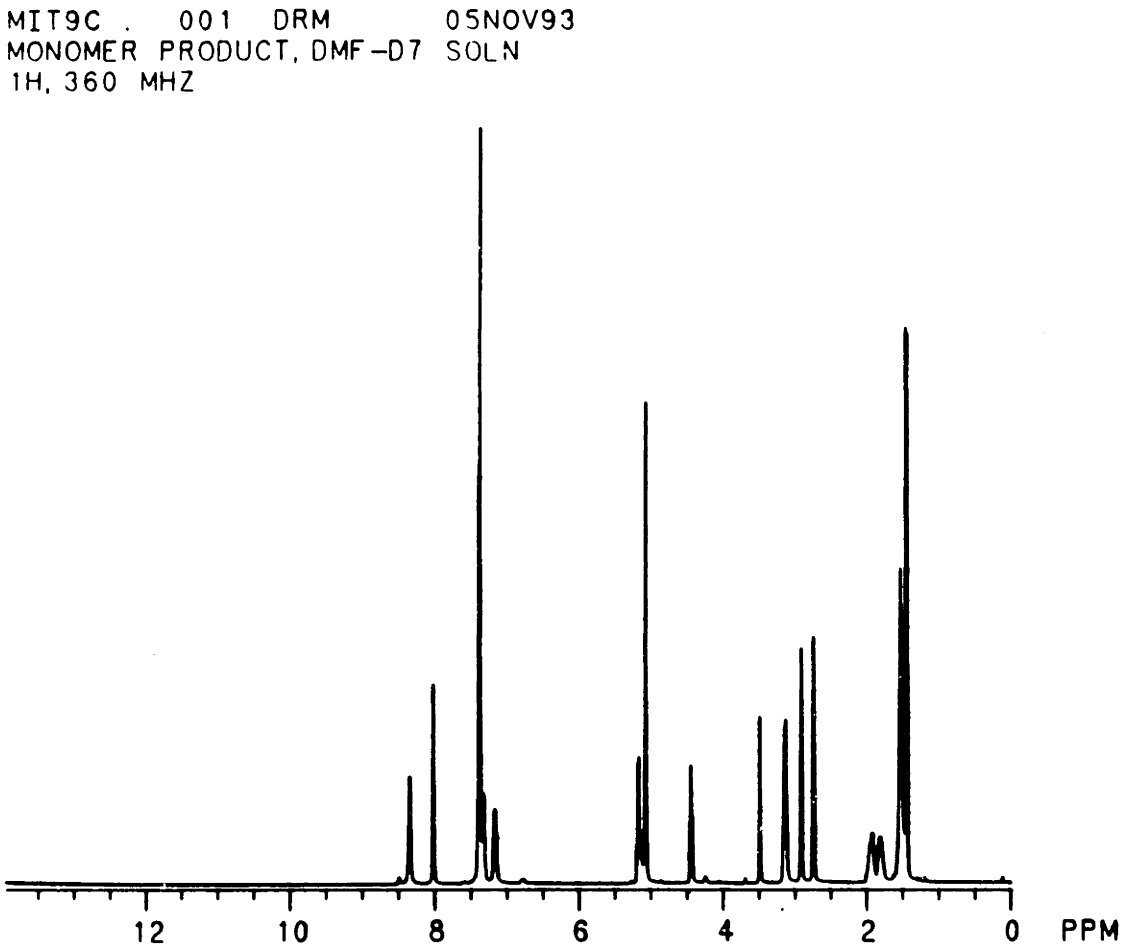

Figure 3.3: ^{1}H NMR spectra of the Lysine-containing monomer. Numbering of the peaks is from right to left, skipping peaks at $\delta = 2.7, 2.9, 3.5$ and 8.0, which can be attributed to DMF-d_7. There are 12 remaining peaks, corresponding to the 22 protons in the lysine-containing monomer. See Table 3.3 for analysis.

Table 3.3
Analysis of ^1H NMR Spectra

Peak #	δ	type	group	# H's	Integral	Ratioed to Peak 10	% Diff
1	1.43	d	CH_3	3	743.55	2.85	-5
2	1.51	m	CH_2 (2)	4	1091.30	4.18	5
3	1.7-2.0	m	CH_2 (1)	2	542.14	2.08	4
4	3.12	m	Carb. CH_2 (1)	2	555.99	2.13	7
5	4.25	td	$HNC\underline{H}CH_2$	0.03	10.07	0.04	29
6	4.44	t	$HNC\underline{H}CH_2$	0.97	255.99	0.98	1
7	5.06	s	CH_2Ph	2	491.65	1.91	-5
8	5.16	q	$OC\underline{H}CH_3$	1	301.42	1.15	15
9	7.19	t	Carb. NH	1	251.18	0.96	-4
10	7.2-7.4	m	aromatic	5	1304.03	5.00	0
11	8.38	s	amide NH	0.97	249.32	0.96	-2
12	8.52	s	amide NH	0.03	10.00	0.04	27

Table 3.3: Analysis of the ^1H NMR spectra of the lysine-containing monomer, comparing the theoretical number of hydrogen atoms (#H's) to the measured protons normalized to the protons from the phenyl group (Ratioed to Peak 10). Designations used to describe the types of peaks are: s=singlet, d=doublet, t=triplet, q=quartet, m=multiplet, td=triple doublet. The difference between the expected and measured hydrogens is shown in the last column.

Table 3.4
FTIR Analysis

Peak position	Group
3330	amide NH
3220	carbamate NH
3100-3000	aromatic
1750	CO-carboxylic acid
1685	CO-carbamate and amide type I
1530	amide type II from carbamate

Table 3.4: Peak assignments from the FTIR spectrum of the Lysine-containing monomer.

Figure 3.4
Sample FTIR Results

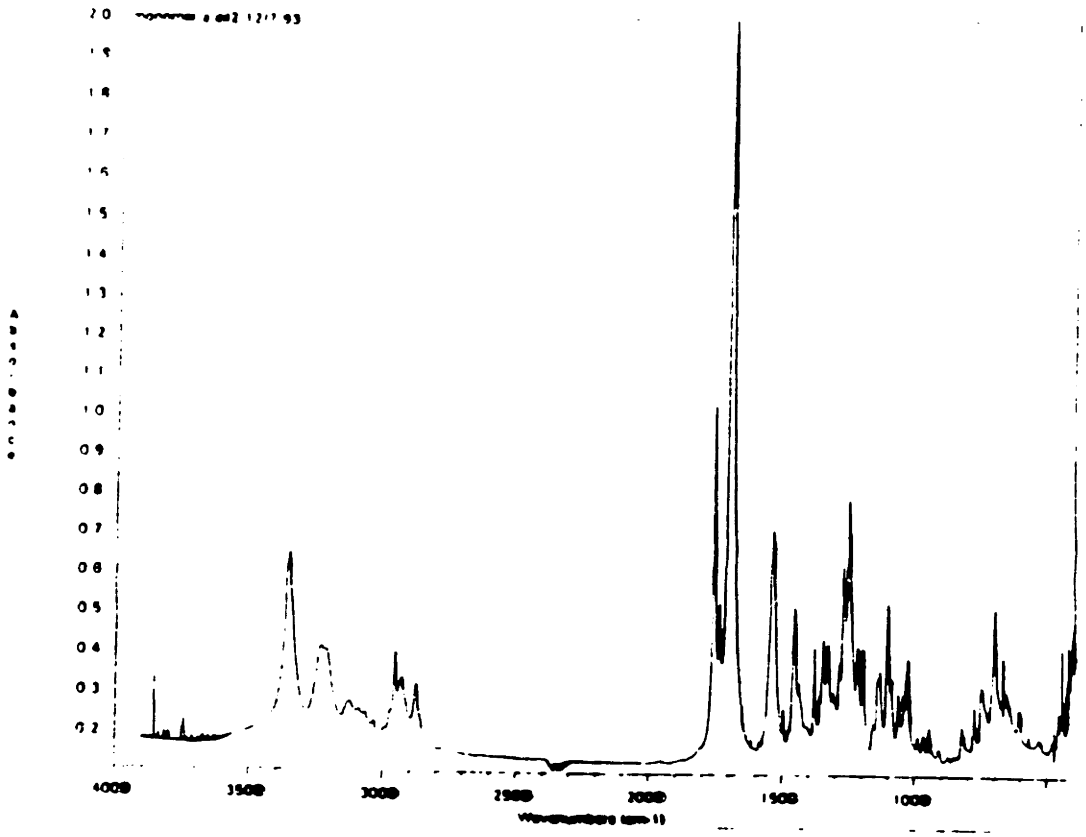

Figure 3.3: FTIR spectrum of the Lysine-containing monomer. See Table 3.4 for peak assignments.

3.1.4 DSC Results

Samples of each of the batches of monomer were analyzed on a Perkin Elmer Series 7 Differential Scanning Calorimeter (DSC) to determine the melting temperature (T_m) of the monomer product. Previous analysis had shown that the melting temperature of the monomer was T_m=137.2°C, onset = 135.3°C at 20°C/min and T_m =138.1°C, onset = 136.2°C at 5°C/min. A sample spectra is shown in Figure 3.5. Table 3.5 lists the results for each of the monomer samples completed to date.

Figure 3.5
DSC Results

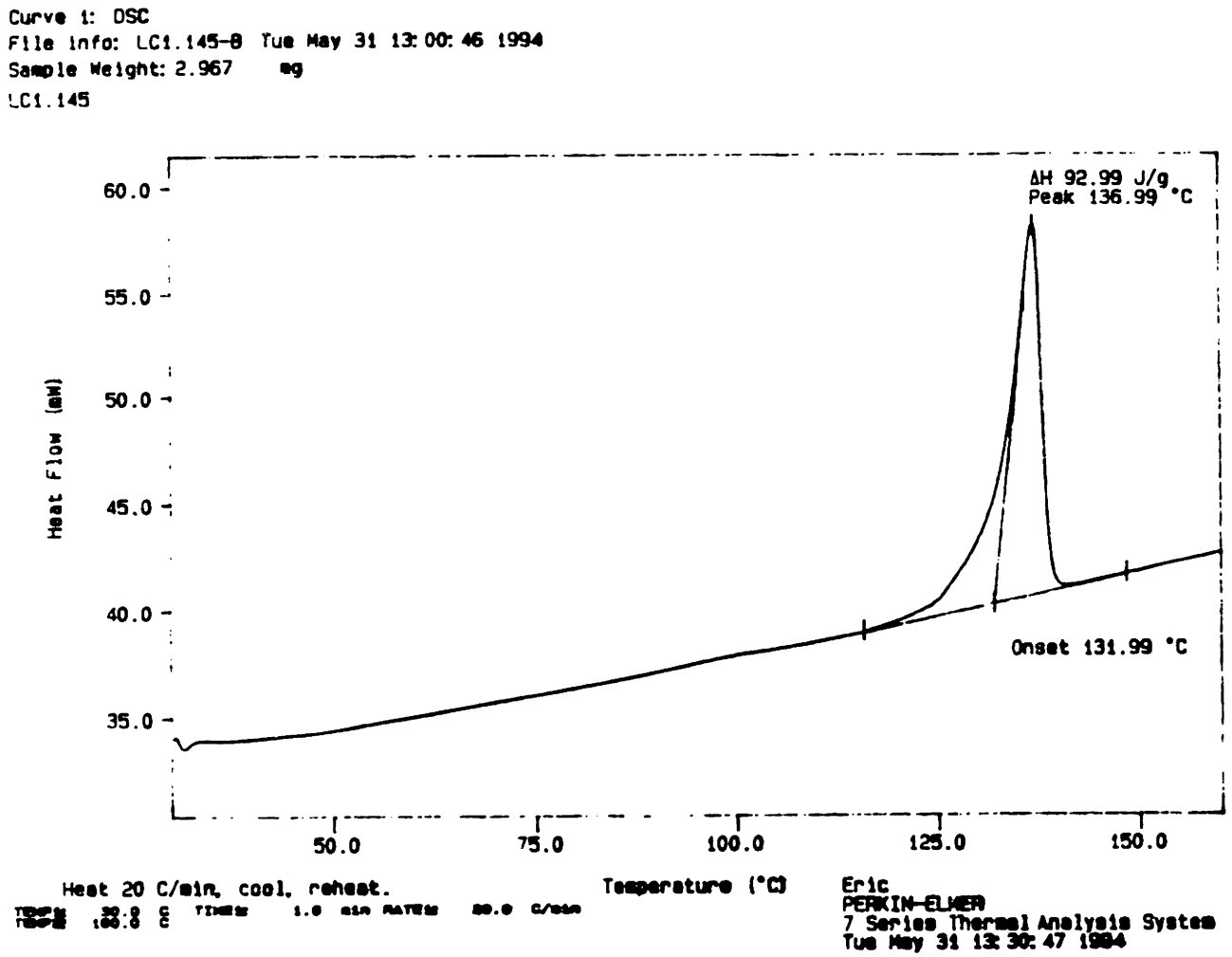

Figure 3.5: Differential Scanning Calorimetry (DSC) analysis of the lysine-containing monomer to determine the melting point (T_m).

Table 3.5
Melting Temperature Results

DSC Scan Rate:	20°C/min		5°C/min	
Monomer	**Peak**	**Onset**	**Peak**	**Onset**
Prior Analysis	137.2	135.3	138.1	136.2
LCM1	138.7	134.7	135.6	132.1
LCM2	137.6	132.8	133.6	129.1
LCM3A	137.5	135.5	134.2	133.4
LCM3B	n.d.	n.d.	n.d.	n.d.
LCM4A	136.0	133.6	133.5	131.8
LCM4B	134.6	130.9	132.7	129.1
LCM5A	133.6	130.4	129.1	126.4
LCM5B	134.7	131.9	138.3	136.2
LCM6A	138.9	135.9	135.6	134.0
LCM6B	133.5	130.5	130.5	125.7
LCM7A	138.0	134.2	133.8	131.2
LCM7B	140.3	138.0	136.9	135.0
LCM8A	133.7	131.4	130.6	127.0
LCM8B	135.8	132.9	132.8	128.7
LCM9	138.3	132.2	136.6	134.7
LCM10	140.4	136.2	137.8	135.9
LCM11	137.0	131.3	136.5	134.5

Table 3.5: Melting temperatures of the various batches of lysine-containing monomer, as determined by differential scanning calorimetry at two different scan speeds, 20°C/min and 5°C/min. (n.d. = not determined)

3.1.5 Elemental Analysis Results

A sample of approximately 20-50 mg of each of the monomer batches was submitted for elemental analysis to Galbraith Labs (Knoxville, TN). The theoretical elemental composition was calculated from the molecular structure. Results for each of the batches are shown in Table 3.6. The silicon content of the samples was analyzed and found to be present in all samples. Except for product LCM6, the silicon content was always less than 1%.

Table 3.6
Elemental Analysis Results

Monomer	C	H	N	O	Si	Total
Theoretical	61.10	6.60	8.40	23.90	0	100.0
LCM1	61.08	6.66	7.79	24.51	0.13	100.2
LCM2A	60.85	6.72	8.17	24.61	0.13	100.5
LCM2B	61.02	6.72	7.90	24.47	0.14	100.3
LCM3A	61.45	6.52	8.29	24.36	0.78	101.4
LCM3B	61.60	6.64	8.29	24.69	0.30	101.5
LCM4A	60.77	6.71	8.40	25.40	0.24	101.5
LCM4B	60.77	6.72	8.37	25.54	0.30	101.7
LCM5	60.16	6.70	8.16	24.36	0.49	99.9
LCM6A	60.57	6.63	8.41	25.19	3.81	104.6
LCM6B	59.73	6.46	8.22	25.13	1.51	101.1
LCM7A	59.80	6.55	8.22	n.d.	0.15	-
LCM7B	60.19	6.59	8.16	n.d.	0.19	-
LCM8A	60.57	6.74	8.46	n.d.	0.35	-
LCM8B	60.95	6.78	8.37	n.d.	0.21	-
LCM9	59.94	6.51	7.84	23.75	0.62	98.7
LCM10	60.80	6.64	7.61	24.35	0.20	99.6
LCM11	61.15	6.72	7.86	24.32	0.16	100.2

Table 3.6: Elemental Analysis results from Galbraith Labs of the various batches of lysine-containing monomer. (n.d. = not determined)

3.2 Copolymerization & Deprotection

The lysine-containing monomer (**6**) was co-polymerized with L,L-lactide (**7**) by a coordination ring-opening polymerization reaction at 100°C for 24 hrs. Stannous octoate was used as a catalyst. The L,L-lactide and lysine-containing monomer were first heated to produce a melt. The product (**8**) was purified by methanol precipitation and the lysine side groups were then deprotected (see Figure 3.6) using triethylsilane (Et_3SiH), methylene chloride (CH_2Cl_2), palladium chloride ($PdCl_2$) and triethylamine (Et_3N). Appendix 3B includes a complete protocol for the polymerization and deprotection reactions.

Figure 3.6
Copolymerization Scheme

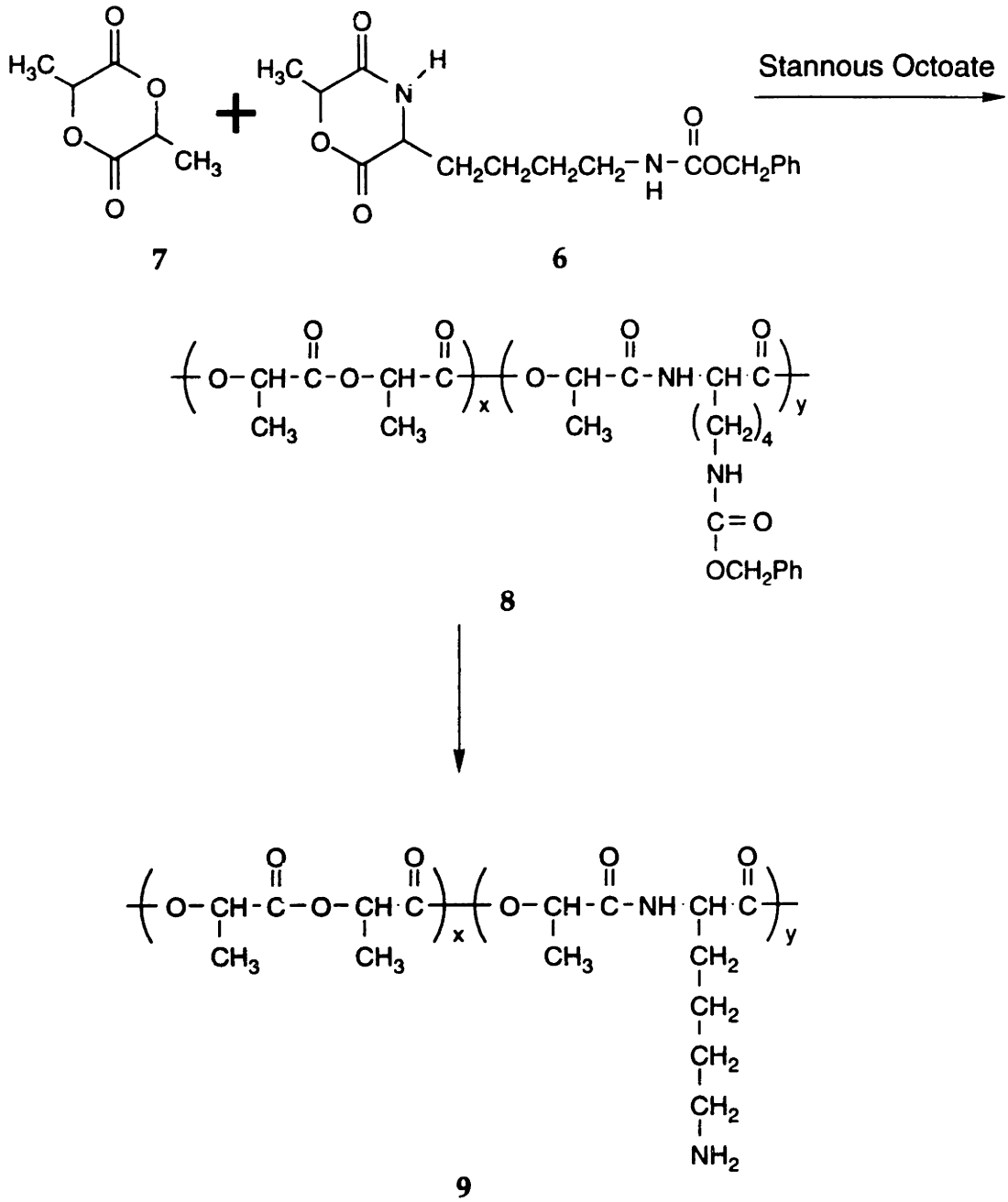

Poly (Lactic Acid-*co*-Lysine)

Several attempts were made to copolymerize the lysine-containing monomer with L,L-lactide. From previous work, it was determined that the optimal conditions were to run the reaction at 100°C for 24 hours, then deprotect the lysine group at room temperature for 5 days. It was observed that a molecular weight of 25,000 was necessary in order to process the polymer into solvent-cast films(1). The results of the co-polymerizations are shown in Table 3.7. The number average molecular weights (M_n) and the polydispersities (M_w/M_n) were determined by Gel Permeation Chromatography (GPC) using polystyrene standards. Each batch of polymer was deprotected. The results of these reactions are shown in Table 3.8.

Table 3.7
Copolymerization Results

Date	Monomer	Amt (g)	Lactide (g)	Polymer	Yield (g)	M_n	M_w/M_n
4/3/92	DB4. 225	2.77	10.85	DB4. 251	11.0	40,000	1.93
7/27/92	DB4. 225	2.66	8.36	DB5. 011	8.17	44,500	1.4
12/9/93	LC1. 216	1.33	4.22	JSH1. 021	4.18	20,000	1.55
12/14/93	LC1. 216	1.0	4.22	JSH1. 022	4.09	18,500	1.52
12/14/93	LC1. 216	0.67	4.22	JSH1. 023	3.87	27,800	1.81
9/9/94	ED1.105	1.5	9.8	JSH2. 087	8.0	-	-
11/4/94	JSH2. 097	0.25	1.6	JSH3. 007	1.2	4,600	1.3

Table 3.7: Monomer and Polymer Designations refer to the notebook pages of Denise Barrera (DB), Lon Cook (LC), Eric Dong (ED) or Jeff Hrkach (JSH). For example, DB4.225 refers to volume 4, page 225.

Table 3.8
Deprotection Results

Date	Polymer	Amt (g)	Deprotected	Yield (g)	M_n	M_w/M_n
8/6/92	DB5.011	8.048	DB5.022	7.373	27,200	1.5
1/11/94	JSH1.023	2.0	JSH1.027	1.73	28,500	1.7
4/8/94	JSH1.023	0.9	JSH1.050	0.6	25,000	1.6
6/9/94	DB4.251	1.4	JSH1.098	1.2	25,900	2.2
9/15/94	JSH2.087	6.0	JSH2.089	5.0	-	-
1/30/95	JSH2.093	6.0	JSH3.044	5.9	3,100	1.4

Table 3.8: Polymer designations refer to the notebook pages of Denise Barrera (DB) or Jeff Hrkach (JSH).

3.3 Processing Methods

In certain batches, the molecular weight of the resulting polymer was below the 25,000 g/mol value which was considered necessary to form the polymer into a solvent-cast film (1). In order to make use of the lower molecular weight polymer batches, other polymer processing techniques were investigated. This section describes the various polymer processing methods which were studied. The reason that the polymer sometimes did not result in high molecular weight material is most likely due to the relatively low relative reactivity of the lysine containing monomer as compared to lactide. The large side group on the lysine-containing monomer would act to limit the monomer's ability to effectively become incorporated into the polymer chain.

Table 3.9 and Figure 3.7 illustrate the effect of high initial concentrations of lysine-containing monomer on the molecular weight of the polymer. Table 3.9 is a list of polymerizations which were performed in an attempt to increase the lysine content of the polymer samples. The same data is plotted in Figure 3.7. As can be seen in Figure 3.7, the molecular weights (M_n) of the samples decreased as the percent of lysine-containing monomer was increased. (The lysine content was determined by ^{1}H NMR.) The compounds with molecular weights lower than 25,000 g/mol did not form films upon solvent casting. In addition, even though the incorporation of lysine units was linear, it was not in a 1:1 ratio to the amount of lysine-containing monomer added at the beginning, indicating that the reactivity of the L,L-lactide monomer is greater than the reactivity of the lysine-containing monomer. The ratio of incorporation was on the order of 2:5 monomer incorporated to monomer present and available for incorporation. Due to the differences in relative reactivities of the two monomers, the polymer chains that are formed initially consist of mostly lactic acid repeat units, and then once the lactide concentration is diminished, lysine-containing monomer units can be incorporated. These data are shown to illustrate the phenomenon which occurs upon copolymerization of the lysine-containing monomer with lactide. Altered reaction conditions produce different molecular weights, but the trends remain the same.

Table 3.9
Copolymerization Optimization Results

% Lys Monomer	M_n (g/mol)	M_w (g/mol)	Yield (%)	Lysine Content (%)
0.0	132,000	223,000	85	0.0
5.3	14,500	36,700	71	1.3
10.5	8,400	23,000	57	2.2
27.7	12,300	15,000	20	5.3
100.0	---	---	0	---

Table 3.9: The effect of increasing the amount of lysine-containing monomer on the molecular weight of the polymer. Reaction conditions: 136°C, 48 hrs. Source: Barrera, D. A., Ph. D. Thesis, MIT., p. 57 Reference (3).

Figure 3.7
Copolymerization Optimization (136°C, 48 hrs)

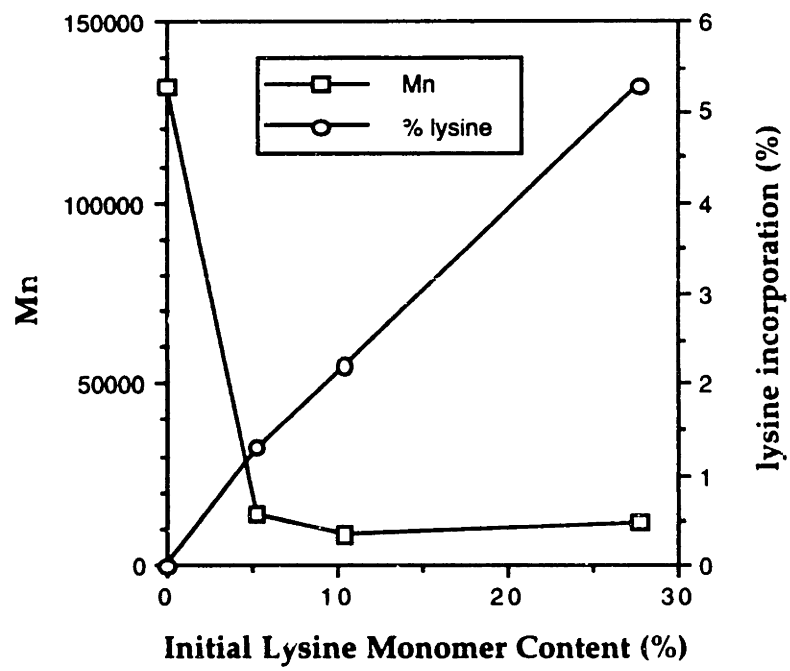

Figure 3.7: Effect of increasing the lysine-containing monomer content on the Molecular weight of the polymer. Under these reaction conditions (136°C, 48 hrs), no more than 1-2% of lysine was incorporated without significantly sacrificing molecular weight. Source: Barrera, D.A., Ph. D. Thesis, MIT., p. 57 Reference (3).

Five types of polymer films were used in the studies described below. Previously, samples were made by dissolving approximately 100 mg of polymer with bound peptides in 2 ml of chloroform in a clean 10 ml glass beaker and allowing the solvent to evaporate over 36-72 hours, followed by at least 24 hours under high vacuum to remove residual solvent. This process yielded samples that could be detached from the beaker in one piece and handled without breaking, but only when the molecular weight of the polymer was greater than 25,000 g/mol. In order to use batches of the polymer with molecular weight lower than 25,000, the polymer with bound peptides was dissolved in chloroform (500 mg in 10 ml) and a dental atomizer (Devilbus Corp.) was used to spray the polymer onto clean glass coverslips. In the case of poly(lactic acid) (PLA), which was used as a control in the experiments, this procedure yielded very thin films, which after drying, could be detached from the glass coverslips and handled without breaking. The low-molecular weight PLAL+GRGDY peptide films, however, were occassionally too brittle to be removed from the glass. The air-exposed side could be studied while still attached to the glass, but since it was necessary to investigate the nature of both sides of the samples, a second layer of high molecular weight PLA, which was sprayed onto the PLAL+GRGDY peptide samples before they were removed from the glass coverslips, was used to provide additional mechanical strength. For PLAL and PLAL+GRGDY, this technique yielded samples which could be removed from the glass without breaking. The third technique which was used to prepare samples was blending PLAL with PLA and solvent-casting the blends into films. In effect, this diluted the available NH_2 groups, but yielded samples which could be handled without breaking. The results given in the following chapters are identified as results from "solvent-cast", "sprayed" or "blended" films, corresponding to the method in which they were prepared. The following sections describe these processing methods in greater detail.

3.3.1 Solvent Casting

Polymer films were produced by dissolving 100 mg of the polymer in 2 ml of chloroform and allowing the solvent to evaporate slowly over 36 to 72 hrs. Glass beakers were cleaned before each use by soaking for at least twenty-four hours in a base bath consisting of potassium hydroxide (KOH) and ethanol (C_2H_5OH); soaked for at least twenty-four hours in a soap solution (RBS, Pierce); rinsed extensively with MilliQ water; and air dried. Immediately before use, the

beakers were immersed in $CHCl_3$ and blown dry by a stream of high pressure nitrogen gas. One hundred milligrams (100 mg) of polymer was placed in the beaker and dissolved in $CHCl_3$ by gently swirling the beaker by hand. The beakers were placed on a level tray in the chemical fume hood and covered with a glass recrystallization dish sealed to the bottom large petri dish by vacuum grease.

Analysis of the two sides of the samples by ESEM showed that the glass-contacting sides of the solvent-cast polymers were even and uniform, whereas the air-exposed sides were rough and porous (see Figure 3.8). The spherulite nature of PLA can be seen in Figure 3.8, which shows representative surfaces of the air-exposed sides (top) and glass-contacting sides (bottom) of solvent-cast PLA films without cells. There are some surface features which appear somewhat similar to spread cells, but the dimensions were larger (~50 μm) than cells (~10 to 20 μm), so with experience, the surface features could easily be distinguished from the cells.

An experiment was conducted to determine the smallest amount of polymer that was necessary to solvent-cast a film. Seven films of PLA were cast in different size beakers and then characterized. The standard size beaker was 10 ml, which produced films about 2 cm in diameter. Films cast in larger beakers were cut to produce samples the same size as those cast in the 10 ml beakers. This study used 50,000 MW PLA from Polysciences. The results are shown in Table 3.10.

Table 3.10
Casting Results

Beaker Size (ml)	# of Films	Ave. weight (mg)	Ave. Thickness (mm)	Held water	Clear
10	1	100	0.17 ± .02	Yes	No
10	1	50	0.09 ± .02	Yes	Yes
10	1	10	0.02 ± .008	No	Yes
50	5	20	0.05 ± .01	No	Yes
50	5	57	0.20 ± .02	Yes	No
100	7	60	0.29 ± .10	Yes	No
250	13	59	0.38 ± .14	No	No

Table 3.10: Various sizes of beakers and amounts of polymer were used to form solvent-cast films.

Figure 3.8
Top and Bottom of Solvent-cast PLA

A.

B.

Figure 3.8: A. Representative view of the top of solvent-cast PLA without cells. Notice the spherulite nature of the surface. B. Representative view of the bottom of solvent-cast PLA without cells. The spherulite nature of the surface can be seen, although the spherulites have joined together to form a fairly intact film layer. Some breaks in the surface can be seen, characterized by their spindle-like features.

The first conclusion from the solvent-casting study was that a film must contain at least 50 mg of polymer in order to hold water when placed in the teflon holder. It was also observed that transparent films were obtained when the thickness was less than 100 μm. In addition, there was no real advantage to casting the films in the larger beakers and then cutting them.

A follow-up study was performed with PLAL of approximately 40,000 g/mol molecular weight. Films of 20, 30, 40 and 50 mg were cast. The 40 and 50 mg films remained intact. The 20 and 30 mg films fell apart. From these observations, the minimum amount of polymer that was considered necessary for proper film formation by solvent-casting methods was 50 mg. Typically, 100 mg of polymer was used to guarantee that the material would hold water for the duration of the longest cell adhesion experiments (4 to 6 hours).

Another study was conducted to test the effect of casting the polymers at lower temperatures. Two films were placed in the refrigerator at 4°C and 2 films were placed in the fume hood at room temperature. The samples in the refrigerator were placed inside a large glass desiccator. The samples in the fume hood were placed underneath a recrystallization dish. The evaporation rate was reduced by lowering the temperature, but there was no apparent advantage to using lower temperatures, since all the samples formed good films.

3.3.2 *Spraying*

Glass cover slips were cleaned by scrubbing with soap (RBS, Pierce) and deionized (MilliQ) water, followed by dipping in $CHCl_3$ to remove all residual soap and any dust particles. Polymer solutions were dissolved at five per cent (5% w/v) in $CHCl_3$. A dental atomizer (Devilbus Corp.) was used, attached to a high pressure compressed gas tank (nitrogen or argon) to spray the polymer onto the glass cover slips. Twelve to twenty glass coverslips were sprayed from one batch of polymer. Control over the thickness and uniformity of the sprayed polymer was achieved by initially spraying to the side of the glass coverslips, and then smoothly spraying across a row of coverslips at a constant rate.

The films which resulted were cloudy, but were more transparent than the solvent-cast films, which were much thicker. The cross-sections of both solvent-cast and sprayed samples were measured using ESEM. Figure 3.9 shows representative cross-sections of the polymer films. The solvent-cast films measured approximately 200-300 μm in thickness. The sprayed films were 10-20 μm thick.

Figure 3.9
Cross-sections of Polymer Films

A.

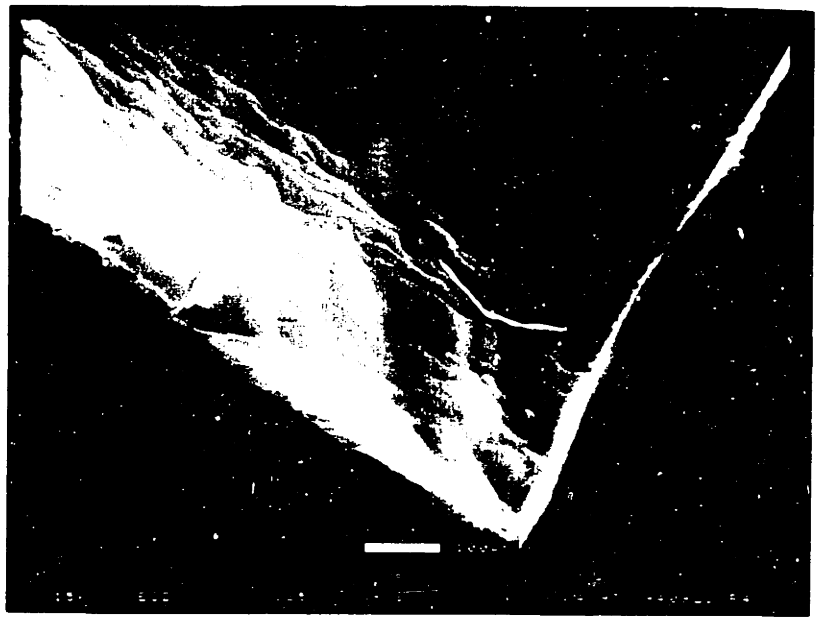

B.

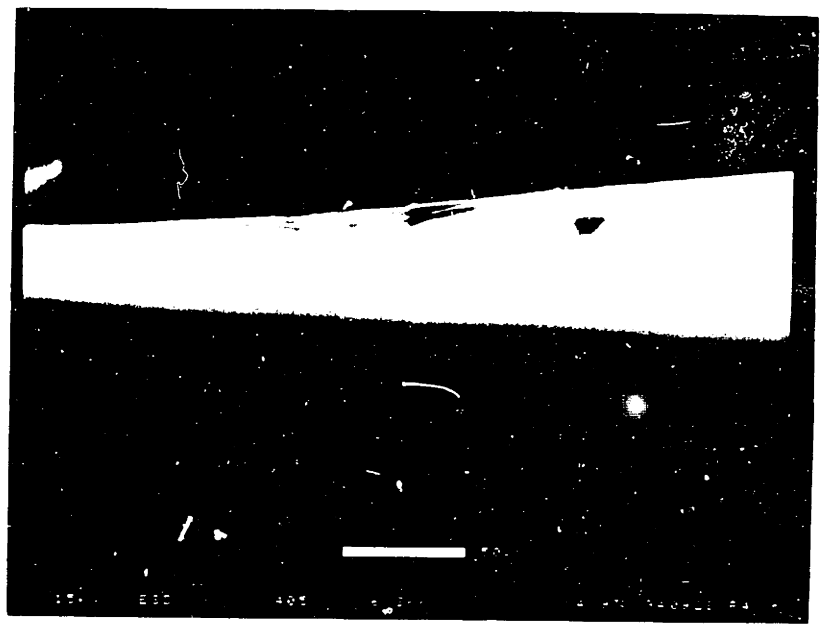

Figure 3.9 A. Cross-section of solvent-cast PLA. The thickness of these films was approximatley 200-300 μm. B. Cross-section of sprayed samples. The thickness of samples prepared by spraying was 10-20 μm.

Although the sprayed films resulted in surfaces which were able to be analyzed on one side (the top), they were not considered acceptable for complete characterization because of the difficulty in removing the film from the glass coverslip without tearing it. In addition, the film was too thin to be used as a scaffold for tissue engineering. To create thicker samples, a second or third layer of PLA was sprayed onto the PLAL+GRGDY polymer films. This resulted in films that could be removed from the glass coverslip and turned over to allow characterization of the glass-contacting side of the sample.

3.3.3 *Melt/quench*

Thermal processing of polymers eliminates the need for solvents. By heating polymers above their melting point, the polymers behave like liquids. In this state, they can be poured into molds or extruded. When the polymers cool, the polymers return to a solid-like state. If the cooling is rapid, and especially if the polymer is cooled to below its glass transition temperature, the polymer chains are unable to align into crystals. This process is called quenching, and results in amorphous materials. The properties of amorphous polymer samples can be very different than crystalline polymer samples.

To investigate the process of quenching as a possible method for preparing samples for exposure to cells, pieces of PLA solvent-cast films were placed on the top of clean glass microscope slides and heated in a vacuum oven to 120°C at -30 psig, then removed and placed in a stainless steel tray, which was previously cooled by placing it in a bucket of ice water. The contact of the bottom of the glass microscope slide with the cold metal tray quickly cooled the melted polymer on top of the slide to form a solid. Since this process prevents the formation of crystalline regions, the resulting samples were transparent. The film that formed bonded strongly to the underlying glass support. Due to the difficulty of removing the polymer from the glass slide, these samples were not investigated further for their ability to support cell adhesion and spreading.

3.3.4 *Annealing*

Amorphous polymer pieces which had previously been melt/quenched were heated at 70°C for up to 24 hrs. to allow crystalline regions to form. This technique produces a polymer which is opaque and tightly bonded to the glass substrate. The opaque appearance is a result of the crystalline nature of the material. There was no advantage to this processing technique for the purpose of

creating scaffolds for tissue engineering, so these samples were not analyzed further.

3.3.5 Blending

Various amounts of poly(lactic acid-*co*-lysine) with or without covalently attached peptides were mixed with PLA by combining the two types of material in the same 10 ml beaker. For example, for a sample containing 100 mg of material, a 10% blend was created by adding 10 mg of PLAL+GRGDY to 90 mg of PLA. Two ml of $CHCl_3$ were then added to the beaker and the polymers were dissolved by gently rotating the beaker by hand. The beakers were then placed on a level platform in the hood and covered with a recrystallization dish to slow down the rate of solvent evaporation. The solvent was allowed to evaporate for 48 to 72 hours. This technique produced samples which were very similar in nature to the solvent-cast films. The use of this technique to produce samples which would have a sufficient density of peptides on the surface was doubted at first, but surface characterization of the blends showed that the peptides preferentially migrated to the glass-contacting (bottom) side of the polymer film (see Chapter 5) and that there were sufficient densities of NH_2 groups and peptides to produce a biological response.

3.4 Bulk Characterization

Bulk characterization of the samples used in the studies was performed to ensure that the desirable physical properties of the material were not compromised by the modifications which were incorporated into the samples.

3.4.1 Lysine & Peptide contents from AAA

The bulk lysine and peptide contents of the films were measured by Amino Acid Analysis. A sample of the polymer to be analyzed was dissolved in methylene chloride at 1 mg/ml or 10 mg/ml. Approximately 5 to 10 mg of material was used. The polymer solution was submitted to the Biopolymers Lab, Howard Hughes Medical Institute at MIT, where the samples were analyzed on an Applied Biosystems Model 420/130 Derivitizer/Amino Acid Analyzer using phenylisothiocyanate (PITC) pre-column derivitization chemistry. Gas phase hydrolysis was performed using a Waters Pico Tag Hydrolysis Workstation with 6N HCl and 0.1% phenol at 150°C for 1 hr. Daily calibration of the Analyzer was performed using 500 pmol of each amino acid, except cystine, where 250 pmol

were used. Elution peak heights were ratioed to the standards to calculate the concentrations of amino acids in the polymer samples. An internal standard of normal leucine (Nleu) was included in both the daily standards and the unknowns. A correction factor based on the amount of Nleu expected to the amount measured was used to adjust the final concentrations. Table 3.11 and Figure 3.10 show the results for bulk characterization of 10 to 50 % blends of PLAL with PLA. Table 3.12 and Figure 3.11 show the results for bulk characterization of 10 to 50% blends of PLAL+GRGDY-I_2:PLA. The formula for converting the results of the AAA to pmol/µl of polymer is the following:

$$\text{Lysine conc.} = \frac{(\text{Lys Rec.})\dfrac{(\text{Nleu Exp.})}{(\text{Nleu Rec.})}}{\left(\dfrac{\text{Deriv.}}{\text{Recon.}}\right)(\text{Hydro.})}$$

The values in the numerator all have units of pmol. The values in the denominator all have units of µl. The numerator corrects for the variations in peak height from one analysis to the next. The amount of lysine recovered (Lys Rec.), which is calculated from the peak height, is multiplied by the ratio of Nleu which is expected (Exp.) to that which is recovered (Rec.). The average concentration of the five amino acids comprising the peptide is used to determine the peptide concentration. The denominator accounts for the dilutions that are made during sample preparation. An aliquot of the initial sample is first hydrolyzed (Hydro.) and dried to a powder, then reconstituted (Recon.) in a buffer containing the Nleu at a known concentration. An aliquot of this solution is then derivitized (Deriv.) and it is from this sample that the absolute quantity of amino acid is determined. To convert from pmol/µl to µmol/g is straightforward for samples with initial concentrations of 1 mg/ml:

$$\left(\frac{1\ \text{pmol}}{\mu\text{l}}\right)\left(\frac{\text{ml}}{1\ \text{mg}}\right)\left(\frac{1000\ \mu\text{l}}{\text{ml}}\right)\left(\frac{1000\ \text{mg}}{\text{g}}\right)\left(\frac{\mu\text{mol}}{10^6\ \text{pmol}}\right) = \frac{1\ \mu\text{mol}}{\text{g}}$$

For samples with initial concentrations of 10 mg/ml, 1 pmol/µl = 0.1 µmol/g.

Table 3.11
Bulk Lysine Content of PLAL:PLA Blends

% PLAL	Hydro. (µl)	Reconst. (µl)	Deriv. (µl)	Nleu Exp. (pmol)	Nleu Rec. (pmol)	Lys. Rec. (pmol)	Lysine (µmol/g)
Experiment 1:							
10	600	100	30	300	198	905	7.62
20	600	100	15	300	235	768	10.89
30	600	100	8	288	240	1003	25.08
40	600	100	5	300	212	1060	50.00
50	600	100	5	300	229	1194	52.14
Experiment 2:							
10	300	100	30	300	246	781	10.58
20	300	100	15	300	238	677	18.96
30	300	100	8	288	223	635	34.17
40	300	100	5	300	234	484	41.37
50	300	100	5	300	189	507	53.65
Combined Averages:							
		% PLAL		**Ave ± SD**			
		10		9.1 ± 2.1			
		20		14.93 ± 5.7			
		30		29.63 ± 6.4			
		40		45.69 ± 6.1			
		50		52.90 ± 1.1			

Table 3.11: The results of two experiments which were conducted to determine the bulk concentration of lysine in 10 to 50% blends of PLAL:PLA.

Figure 3.10
Bulk Lysine Content of PLAL:PLA Blends

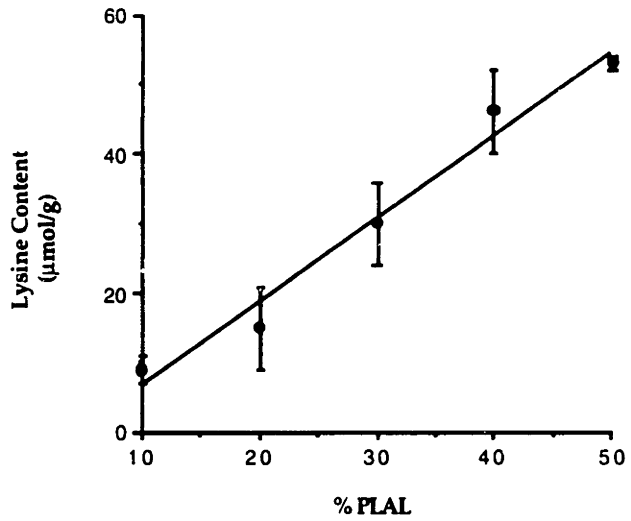

Figure 3.10: The average results of 2 Amino Acid Analysis experiments to determine the bulk lysine content of 10 to 50% PLAL·PLA blends. (Data are Ave. ± S.D., n=2 for each data point)

Figure 3.11
Bulk Peptide Content of PLAL+GRGDY-I_2:PLA Blends

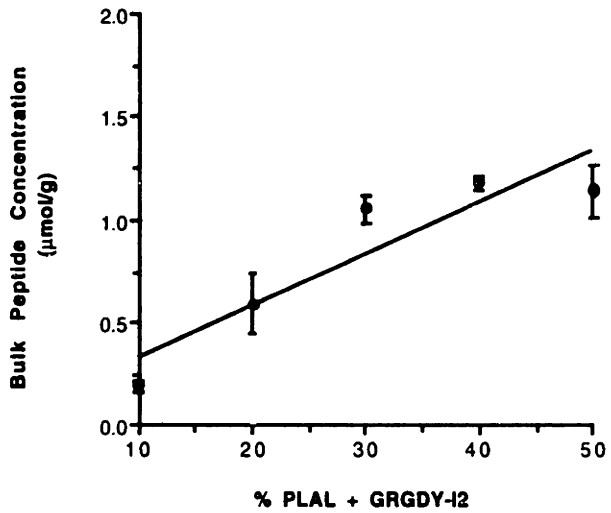

Figure 3.11: The average results of 3 Amino Acid Analysis experiments to determine the bulk peptide content of 10 to 50% PLAL+GRGDY-I_2:PLA blends. (Data are Ave. ± S.D., n=3 for each data point)

Table 3.12
Bulk Peptide Content of PLAL+GRGDY-I2:PLA Blends

% PLAL + RGD-I_2	Hydro. (µl)	Reconst. (µl)	Deriv. (µl)	Nleu Exp. (pmol)	Nleu Rec. (pmol)	Pep. Rec. (pmol)	Peptide (µmol/g)
Experiment 1:							
10	500	100	30	300	198	186.4	0.19
20	250	100	30	300	183	239.4	0.52
30	170	100	30	300	157	296.8	1.12
40	125	100	30	300	150	224.6	1.20
50	100	100	30	300	230	246.8	1.07
Experiment 2:							
10	500	100	30	300	169	185.8	0.22
20	250	100	30	300	189	230.2	0.49
30	170	100	30	300	171	288.2	0.99
40	125	100	30	300	156	223.0	1.14
50	100	100	30	300	228	242.6	1.06
Experiment 3:							
10	500	100	30	300	207	162.6	0.16
20	250	100	30	300	145	276.2	0.76
30	100	100	30	300	114	118.2	1.04
40	125	100	30	300	198	294.4	1.19
50	170	100	30	300	167	367.4	1.29
Combined Averages:							
		% PLAL		**Ave ± SD**			
		10		0.19 ± 0.03			
		20		0.59 ± 0.15			
		30		1.05 ± 0.07			
		40		1.18 ± 0.03			
		50		1.14 ± 0.13			

Table 3.12: The results of 3 experiments which were conducted to determine the bulk concentration of peptide in 10 to 50% blends of PLAL+GRGDY-I_2:PLA.

3.4.2 Degradation kinetics

Degradation studies were performed by immersing solvent-cast polymer films in phosphate buffered saline (PBS) at pH 7.2 and rotating them in an incubator at 37°C. The buffer was changed every week and analyzed for lactic acid. One film was removed every 2 weeks and analyzed for amino acid content and molecular weight decrease. Degradation studies demonstrated that by 4-6 weeks the weight average molecular weight $<M_W>$ is about one-half its original value (see Figure 3.12). Percent crystallinity increased with time, indicating that the amorphous regions were degraded first. Lactic acid was released at a constant rate after about 4 weeks. The results of these studies have been published (2). The PLAL and RGD polymer films did not totally dissolve after one year of soaking in buffered media, indicating that these materials are stable for long periods of time.

Figure 3.12

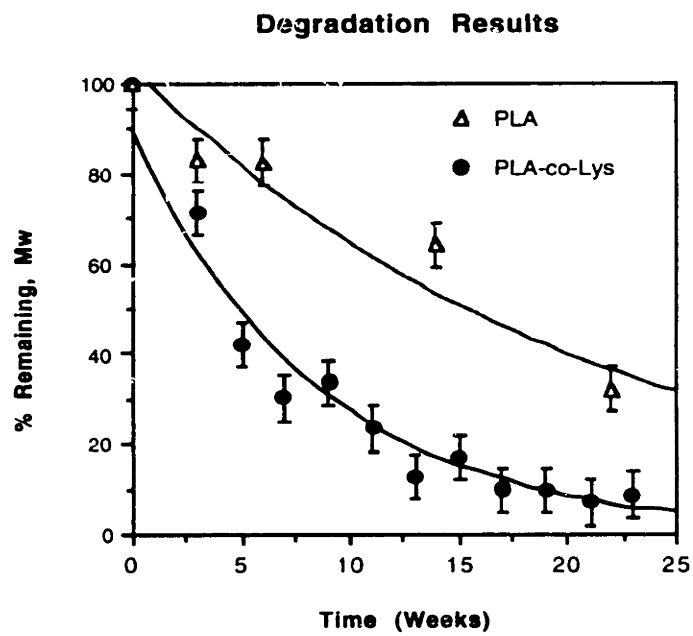

Figure 3.12: Comparison of degradation rates of PLA and PLAL. Source: Barrera, D.A., Ph.D. Thesis, MIT, (1993) and Ref. (2).

3.4.3 *Thermal Transitions and Crystallinity*

The melting temperature (T_m), glass transition temperature (T_g) and crystallinity were determined using differential scanning calorimetry (DSC). Typical values for the melting temperature (T_m) and glass transition temperature (T_g) were 158°C and 55° C respectively.

One of the issues that is often brought up in regards to blends is the phenomenon of phase separation of the various types of polymers during processing. Since PLAL is 99% poly(lactic acid), when the two are blended, no phase separation was expected and none was observed in samples up to 50% PLAL. Experiments using DSC were performed to confirm that no phase separation was occurring and to determine the effect of PLAL on the crystallinity. The semi-crystalline nature of the material imparts high strength and good processing capabilities to the polymer. Crystallinity was measured using a Perkin Elmer Series 7 Differential Scanning Calorimeter. The percent crystallinity was calculated from the enthalpy of melting as the ratio of the melting endotherm minus the crystallization exotherm of the sample to the theoretical enthalpy of melting of an ideal crystal, which has been calculated to be about 90 J/g (4, 5). Table 3.13 and Figure 3.13 show the results of the determination of the crystallinity of 10 to 50% blends of PLAL+ GRGDY-I_2 with PLA.

Table 3.13
Crystallinity of Blends

% PLAL+ GRGDY-I_2	T_m (°C)	ΔH_m (J/g)	T_c (°C)	ΔH_c (J/g)	% Cryst.
10	172.15	35.05	118.26	-0.785	38.07
20	173.31	33.71	118.26	-0.535	36.86
30	167.87	35.03	118.46	-0.536	38.33
40	169.74	39.35	118.28	-0.541	43.12
50	168.56	42.58	118.23	-0.252	47.03

Table 3.13: The crystallinity (% Cryst.) of the blends was calculated as the enthalpy of fusion (ΔH_m) minus the enthalpy of crystallization (ΔH_c) divided by 90 J/g.

Figure 3.13
Crystallinity of blends

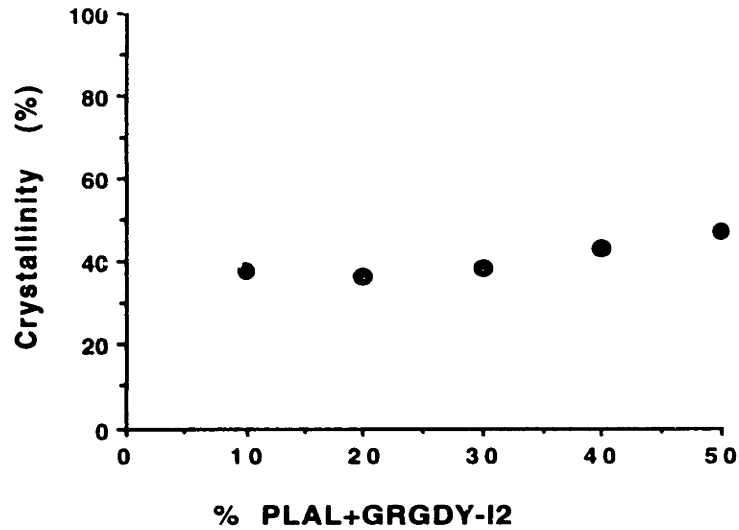

Figure 3.13: The crystallinity of the PLAL+GRGDY·I_2 blends was calculated from the enthalpy of fusion minus the enthalpy of crystallization divided by 90 J/g. See Table 3.13 for data. (n=1)

3.4.4 Density determination

The density of PLA was determined using a Helium Pycnometer. The density was determined to be 0.782 g/cm^3.

3.4.5 Molecular weight

Molecular weights were determined using gel permeation chromatography (GPC) and comparing the elution peaks to polystyrene standards. The synthesis of poly(lactic acid-*co*-lysine) has yielded polymer with molecular weights of approximately 80,000 g/mol. The molecular weight depends on the reaction time and temperature. After deprotection the molecular weight decreases to about 35,000 g/mol (2,3). Molecular weights for each batch of polymer are shown in Table 3.7 and 3.8.

3.5 References

1. Barrera, D.A., Zylstra, E., Lansbury, P. T., Langer, R., "Synthesis and RGD peptide modification of a new biodegradable copolymer: poly(lactic acid-*co*-lysine)", *J. Amer. Chem. Soc.*, **115** : 11010-11011, (1993).

2. Barrera, D.A., Zylstra, E., Lansbury, P. T., Langer, R., "Copolymerization and degradation of poly(lactic acid-*co*-lysine)", *Macromol.*, **28**(2): 425-432 (1995).

3. Barrera, D.A., "Synthesis and characterization of a novel biodegradable polymer-poly(lactic acid-*co*-lysine)", Ph.D. Thesis, MIT (1993)

4. Fischer, E. W., Sterzel, H. J., Wegner, G., "Investigation of the structure of solution grown crystals of lactide copolymers by means of chemical reactions", *Kolloid-Z. U. Z. Polymere*, **251**: 980-990 (1973).

5. Kalb, B., Pennings, A. J., "General crystallization behaviour of poly(L-lactic acid)", *Polymer*, **21**: 607-612 (1980).

Appendix 3A
Monomer Synthesis Protocol

Preparation

Two days toone week before beginning, make ice cubes from deionized (MilliQ) water. Use clean ice trays and cover them with saran wrap. Store the ice in a clean plastic bag until needed.

Stage 1

Purpose: Make D-alanine-bromo substituted

1. Dissolve 50 g of D-alanine in 580 ml of 48% HBr and 800 ml of water. Add ice made from deionized (MilliQ) water to bring the total volume up to 3400 ml.
2. Slowly add 104.5 g of $NaNO_2$ while stirring with a glass rod. This step takes about 20 min.
3. Add 700 g of Na_2SO_4, which takes about 10 min.
4. Stir the mixture with a motorized mechanical stirrer and Teflon wand until the temperature reaches 15°C. Use a 250°C thermometer. This takes about 2 hrs.
5. Decant liquid into two 2000 ml beakers.
6. Use ethyl ether-anhydrous to extract the product from the water phase. Divide the liquid into 3 batches of 1200 ml each (use a 2000 ml separatory funnel). Add 125 ml of ethyl ether 4 times.
7. Dry ethyl ether with Na_2SO_4. Use 200g per 900 ml in Erlenmeyer flasks for 1 hour. Use 400 g total. This takes 1 hr. Then dry over molecular sieves for 1 hour.
8. Filter with large diameter 0.45 μm filters.
9. Rotovap away the ethyl ether.

Stage 2

Repeat steps 1-9 from Stage 1.

Put the glassware for Stage 3 into the oven at 130°C. Need 3x250 ml round bottom flasks, 2x50 ml round bottom flasks, stopper, thermometer, distillation cow, adapter, cooling water attachment, all in a large glass dish.

Stage 3

Purpose: Distill the product from stages 1 and 2.

1. Assemble distillation apparatus: take the glassware out of the oven, set it aside to cool. Get a ring stand, lab jack, stir plate, oil bath and several ring stand clamps. Use the oil bath controller and a trap for the water aspirator in the hood. Attach the recirculating cooling water pump to the distillation column.
2. Place a few boiling chips in the large 1000 ml flask. Clamp it on the ring stand. Assemble the apparatus. The trap is needed so that the cold water faucet can be used as an aspirator without contaminating the system.
3. Heat the liquid slowly. Leave the controller set to 116°C for a while and watch the thermometer. It may stay at 65°C while a lot of clear liquid (30 ml) distills over. Collect this liquid in a 50 ml round bottom flask. After a while, put aluminum foil around the flask and oil bath to prevent heat loss and help the flask boil evenly.
4. When the temperature reaches 110°C, switch to the larger 250 ml flask and collect the product. The temperature will rise to 122°C and stay there for 30-45 min. The distillation is complete when the dripping slows down and there is only a thick orange liquid in the bottom of the 1000 ml flask. The product boils in the range of 110°C to 128°C. The oil bath temperature should be between 144°C and 164°C.
5. Remove the vacuum. Turn off the heat and cooling water. Set the product aside and rinse out the other round bottom flasks with acetone. Dump the waste into a small 500 ml waste container and leave the flasks and distillation apparatus in the hood to evaporate off the contamination overnight.
6. Weigh the product. Record the weight and calculate the yield.

Make NaOH bath (128 g/700 ml of water) and let dissolve at ice temp. overnight.

Stage 4

Purpose: Make 2-bromo propionyl chloride

1. Set up apparatus: Place a lab jack on a ring stand base. Place the stir plate and oil bath on top of the jack. Use a ring stand holder to suspend the round bottom flask with the product from Stage 3's distillation in the oil bath. Hook up the condenser with cooling water from the recirculating cooling water pump. Load the desiccant tube with glass wool and desiccant. Make sure the desiccant tube is properly connected to the NaOH sparger with the right size tubing and clamps.
2. Add 70 ml of $SOCl_2$ to 100 g of product from Stage 3's distillation.
3. Attach condenser and NaOH bubbler/purge.
4. Allow the reaction to proceed for 8 hrs. at 60°C.
5. Remove the sparger from the NaOH bath, then remove the reaction flask from the oil bath, cover loosely and leave overnight.

Place the following glassware in the oven at 130°C.

4 round bottom flasks: 1x250 ml, 2x50 ml, 1x25 ml

1 stopper

thermometer

4-way connector

distillation apparatus

large recrystallization dish

Stage 5

Purpose: Distill product from Stage 4 reaction

1. Remove the dry glassware from the oven and let it cool.
2. Set up the distillation apparatus: Ring stand, lab jack, stir plate, oil bath, ring clamps. Also need a cooling bath for the product collection flasks. Use an inverted recrystallization dish and a small lab jack and another recrystallization dish full of ice water.
3. Hook up the aspirator to provide a vacuum and set up the recirculating cooling water pump.
4. Heat the oil bath slowly. The liquid will begin to boil at about 30°C. Collect the distillation by-product (3 ml in 10 min). Then the temperature will start to rise.
5. At 31°C, switch to the large round bottom flask and collect the product. The oil bath will be at 45°C. The temperature will continue to increase and the liquid will boil faster. At 44°C, the temperature will become stable and stay there for 20 min. The distillate will be clear. Keep collecting until the bubbling stops and the liquid in the pot begins to turn a dark brown. The temperature may increase to 55 or 56°C before this happens.
6. Turn off the vacuum, the cooling water pump and the heat.
7. Calculate the yield.

Dry glassware for stage 6:

1 4000 ml Erlenmeyer flask

1 stir bar

1 500 ml beaker

5 pasteur pipettes

Put molecular sieves in a 4 L bottle of chloroform for Stage 6

Stage 6

Purpose: Combine lysine with acyl chloride product from stage 5

1. Add 96.6 g of Nε-CBZ-L-Lysine (Sigma) to 2000 ml of dry $CHCl_3$ in the 4000 ml erlenmeyer flask with stir bar. This takes about 20 min. Make sure all the big clumps are broken up. Put it on a stir plate and run argon gas into the flask.
2. Add 27.6 g of monomer product from Stage 5 to 200 ml of dry chloroform. Don't weigh out the product: estimate the density of the product by dividing its known weight by its approximate volume (=1.8 g/ml). So, actually transfer 15.3 ml with calibrated pasteur pipettes. Then add this 200 ml to the large erlenmeyer flask and fill the flask to 3400 ml.
3. Take TLC samples before adding the monomer, and at 0, 15 min, 1, 2, 4, and 6 hrs after adding the monomer. Use half of a TLC plate supported on plastic disks in the front of the hood. Use a piece of paper to mark the position of the plate. Place the alignment cover over the TLC plate. Tip the flask slightly to withdraw a sample. Hold the dropper with tweezers. Use another ring stand to hold the tubing and stopper while taking samples.
4. Turn the stirrer off after 6-7 hours and let the reaction proceed overnight.

Stage 7

Purpose: Filter the product of Stage 6

1. Take a 24 hr TLC sample and place the TLC plate in the chamber filled and equilibrated with 100 ml 93% $CHCl_3$/5% MeOH/2% Acetic Acid eluent. The eluent level should not touch the dots at the bottom of the TLC plate. Use the absorbent paper along the back wall of the chamber to equilibrate the environment.
2. When the eluent has migrated 80% up the TLC plate, remove it from the chamber, mark the position of the eluent height and let it dry for a few minutes. Use the UV lamp to light up the spots and circle them with a pencil.
3. The next day, after the plate has completely dried, cover it with Saran Wrap and make a photocopy at 65% reduction.
4. Begin filtering the product. Support the large Buchner funnel with a ring stand and clamp. Use the Whatman 113 filter papers. Connect the side arm flask to the house vacuum. Use the long teflon-coated rod to break up the gel and a stir rod to scrape the filter paper periodically. Place a large watch glass on top of the funnel to prevent evaporation.
5. Collect the product in a dry side-arm flask. Wash 4 times with chloroform.
6. Place the product in 2000 ml erlenmeyer flasks with molecular sieves for 1 hr.
7. Filter again through 0.45 μm filter paper to separate the product from molecular sieves. Filter into round bottom flasks. This requires another ring stand and holder, an adapter, another Buchner funnel, stir rod and watch glass. It is convenient to perform the second filtration in the hood in 318 and then move it directly to the rotovap.

Stage 8

1. Continue filtering the product and rotovapping off the solvent.
2. It takes about 6 L of chloroform to filter the product.

Stage 9

Purpose: Cyclization

1. Assemble the reflux apparatus: Use the large reflux labware that fits in the 24/40 1000 ml round bottom flask. Hook it up to the recirculating cooling water pump. Use a ring stand, a lab jack, a stir plate, the heating mantle and controller, and two ring stand holders to secure the flask and distillation piece.
2. Add boiling chips and a stir bar. Bring the volume up to 900 ml with chloroform. Add 24.2 ml (85 mol% of 2-bromo-propionyl chloride reagent added to make the gel) of base: N-N-diisopropylethylamine. To prevent white smoke, add the base to 50 ml of chloroform first, then add the base to the large round bottom flask.
3. Set the heating mantle to 3 on the blue controller. Leave the reaction overnight.
4. Take TLC samples by lowering the mantle with the lab jack and let the solution cool for a few minutes. Then lift the cooling apparatus off and remove a small sample to dot onto the TLC plate. Take samples at 0, 1, 2 4 hrs and then again the next day at 22 and 24 hrs.

Stage 10

1. Take the last two TLC samples. Stop the reaction.
2. Run the TLC plate, circle the resulting product spots under UV.
3. Use the Iodine chamber to show the by-products.
4. Rotovap the product to remove $CHCl_3$. Weigh a round bottom flask first. Place the product in chloroform into the round bottom flask and then weigh it again when only product remains. The product will turn to powder when all of the chloroform is gone.
5. Place the product under high vacuum for 1 hr. and then on the lyophilizer for 3 days.

Prepare seven 4 L bottles of chromatography eluent by removing 280 ml of $CHCl_3$ from each 4 L bottle and adding 200 ml of MeOH and 80 ml Acetic Acid to make a 93% $CHCl_3$, 5% MeOH and 2% Acetic Acid solution.

Soak 2500 ml of silica gel in the eluent. Use about 13 scoops per 2 L flask and make 2 flasks.

Stage 11
Chromatography

1. Use the eluent that was prepared in Stage 10: 93% $CHCl_3$, 5% MeOH and 2% Acetic acid solution.
2. Use the silica gel that was soaked in eluent in Stage 10.
3. Load the column 1 hr before starting. It takes about 3 tries to get the gel level to between 59 and 60 cm. Save the eluent to use as a rinse between samples later.
4. Drain the column until the top of the gel is just dry.
5. Add about 1 cm of sand, wash once by filling with eluent.
6. Add previously dissolved sample. About 17.5 g in 80 ml. Dissolve the sample slowly in eluent with stirring. Start with 40 ml and add 1 ml at a time while stirring. The solution turns brown once the monomer totally dissolves. It takes 45 min to an hour to dissolve.
7. Drain the sample into the gel.
8. Wash the sand with 5 pipette-fulls of eluent.
9. Add more sand. About 150 ml total.
10. Pour some eluent in and open the stopcock to start the column. A good speed to run the column is 100 ml in 3.5 min. This is the setting when the blue dot on the stopcock is straight up.
11. Drain the column slowly. Keep adding eluent to the collection flask on top. Add this flask very carefully. Use O-rings to seal the connections.
12. Collect samples. About 34x100 ml fractions in various erlenmeyer flasks. The by-product has some yellow color associated with it and comes down first. Then the color disappears for a while and reappears with the product.
13. Take a TLC sample from each flask.
14. Run the TLC.
15. Combine product flasks and rotovap off the eluent. It isn't necessary to rotovap the first day because then the product would be in a concentrated solution of acetic acid. Just rotovap the second and third days long enough to have room to add additional product.
16. After collecting all 4 fractions from the four days, combine and rotovap at 55-65°C to remove the acetic acid.
17. Let the concentrated solution cool by placing it on ice and then extract the rest of the acetic acid with petroleum ether. It may take 5 or 6 washes to turn the product to a solid.
18. Blow nitrogen over the sample for 20 mins. and then put the flask on the lyophilizer overnight.
19. If the monomer is not in powder form and is still yellow, recrystallize it by dissolving it in 150 ml of ethyl acetate by heating and stirring it in the round bottom flask for 30 min. It takes about 5

ml/g to dissolve. Let it reflux for 5 more min after all of it dissolves. Transfer the solution to a beaker and let it cool and recrystallize slowly. It takes about an hour.

20. Cold-filter the monomer by using a ground-glass frit filter and side arm flask hooked up to the house vacuum. Pour about 1/4 of the slurry in and drain it, then rinse with ethyl acetate that is cooled to liquid nitrogen temperature. Use a metal tray to hold the liquid nitrogen and a 60 ml beaker to hold the ethyl acetate.

21. Place the monomer on the lyophilizer overnight.

22. Weigh the product and determine the yield. About 7 g is normal.

Appendix 3B
Polymerization & Deprotection Protocols

Glassware preparation

1. Silanize clean glassware: Contact the surface with 10 vol% SurfaSil in dry toluene. Drain until mostly dry. Bake at 100°C for 30 min. Wash with deionized (MilliQ) water.
2. Dry glassware: Bake the glassware in the oven at 130°C overnight or at 140°C for 4 hrs. Cool under vacuum (put hot glassware into desiccator and attach to the vacuum). Release vacuum with argon. Be careful that the argon does not enter the desiccator too quickly, or the top will pop off. Transfer the glassware to the nitrogen environment inthe glove box. Prepare the glove box by attaching the vacuum pump and purging the box twice. Make sure there is P_2O_5 desiccant in the box.

Recrystallization

1. Dissolve the monomer in dry ethyl acetate by heating.
2. Hot filter lactide through 70-100 μm (B) glass frit filter.
3. Cool and allow the monomer to recrystallize.
4. Vacuum filter with 25-50 μm (C) glass frit filter.
5. Rinse with cold ethyl acetate (use liquid nitrogen as a coolant).
6. Transfer to a preweighed dry vial.
7. Complete solvent removal by vacuum overnight.

Note: The hot filtering is not necessary for the lysine monomer.

Transfer to Reaction Flask

1. Add lysine monomer (record weight).
2. Add lactide (record weight).
3. Make catalyst by first weighing it out on the bench or in the glove box if you want to be more careful, dissolve it in dry chloroform.
4. Calculate amount of catalyst solution needed.
5. Add catalyst solution.

Vacuum/Argon purging

1. Start pump on bench and pull vacuum on the polymer sample.
2. Flush with argon.
3. Repeat 5 times.

4. Pull final vacuum for 1 hour.
5. Heat for up to 30 min. with heating tape until the lactide starts to sublimate on the neck of the connector.
6. Seal under vacuum and put it in constant temperature oven at 100°C.

Deprotection

1. Dry glassware overnight in the oven at 130°C and coll under a nitrogen stream.
2. Dissolve 9.891 g of polymer in 225 ml of triethylsilane ($SiEt_3H$) and 225 ml of methylene chloride (CH_2Cl_2).
3. Add 1.8 g of palladium chloride ($PdCl_2$) and 2.1 ml of triethlyamine (Et_3N) with stirring.
4. Allow the reaction to proceed for 5 days, then filter to remove the $PdCl_2$.
5. Add 150 ml of methanol to stop the reaction.
6. After 10 min., pour the solution into 3000 ml of methanol to precipitate the polymer.
7. Filter by vacuum filtration to remove the methanol and collect the polymer.
8. Dry polymer under high vacuum.
9. Calculate yield.

Chapter 4

Peptide Attachment

This chapter describes the chemistries which were used to attach cell adhesion peptides to PLAL. The basis for this work was that others had created materials to increase cell attachment by immobilizing RGD-containing peptides to a variety of materials (1-8). However, none of these materials were degradable nor did they have the other desirable properties of the lactide/glycolide copolymers (*e.g.*: strength and processability). RGD was chosen because it had been identified as the cell adhesion site within fibronectin, a protein which is responsible for linking cells to their extracellular matrix *in vivo* (9).

4.1 Bulk Attachment

The bulk attachment chemistry which had been developed previously was used (10). GRGDY peptides were obtained from the MIT Biopolymers Lab. CDI was obtained from Aldrich. The reaction scheme is shown in Figure 4.1. In summary, under dry, inert conditions, PLAL was dissolved in equal amounts of methylene chloride (CH_2Cl_2) and dimethylsulfoxide (DMSO). The peptide was dissolved in DMSO and added to the PLAL solution. A solution of 1,1'-carbonyldiimadazole (CDI) in CH_2Cl_2 was prepared and added to the PLAL-peptide solution with stirring. After 4 hrs., the CH_2Cl_2 was removed by evaporation and water was added to the DMSO solution to precipitate the polymer. The precipitate was collected by vacuum filtration and dried under high vacuum. The results of the peptide coupling reactions are shown in Table 4.1.

4.2 Surface Attachment

As an alternative to conducting bulk peptide attachments and then processing the polymer into films for testing, one of the research objectives was to process the polymer into films and then covalently attach peptides to the surfaces that were formed. In order for this to be successful, it was necessary to choose a different attachment chemistry than the one used previously. The bulk

attachment chemistry used previously was conducted in a 50:50 mixture of methylene chloride and dimethyl sulfoxide, which dissolved the polymer, the

Figure 4.1
Reaction Scheme for Bulk Peptide Attachment

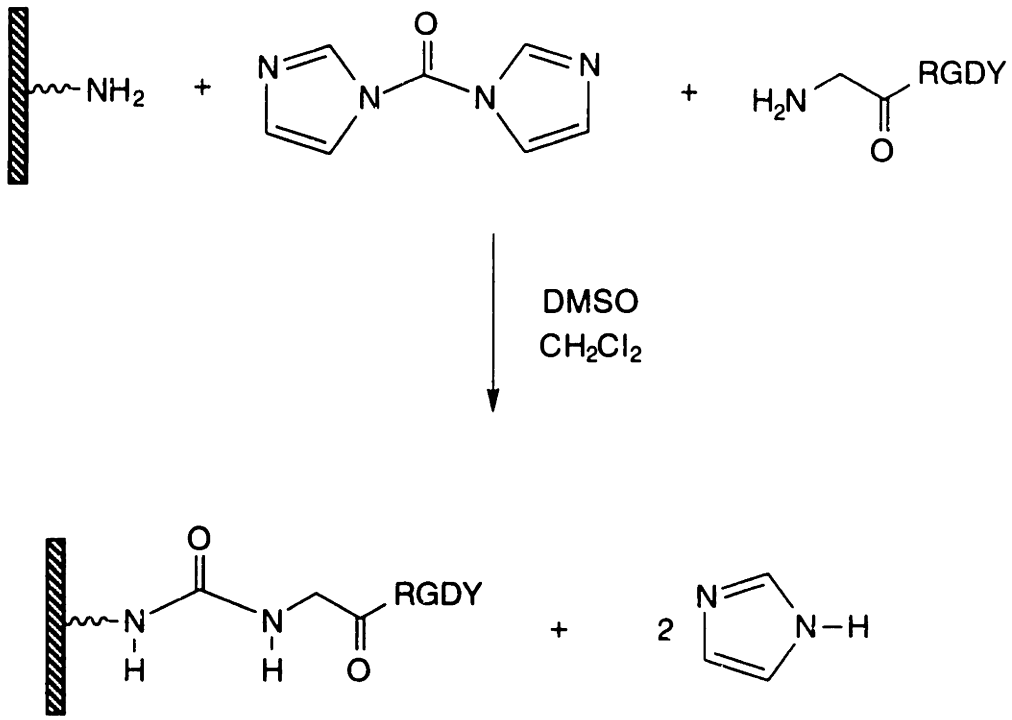

Figure 4.1: RGD-containing peptides were attached to PLAL in bulk using 1,1'-carbonyldiimidazole (CDI) as the linking agent. A 50:50 mixture of dimethylsulfoxide (DMSO) and methylene chloride (CH_2Cl_2) was used to dissolve the polymer, peptide and CDI in one reaction vessel. The polymer was purified by rinsing with water to remove the excess reagents and byproducts.

linking agent, and the peptide. For surface attachment reactions this chemistry was not feasible because the solvents would dissolve and deform the polymer. A simple solvent for conducting surface attachment chemistries is water, since the peptides are soluble in water, but the polymer is not. The water soluble reagents that were evaluated for use in surface attachment reactions are discussed in the next section.

Table 4.1
Bulk Peptide Attachment Results

Date	Polymer	Amt (g)	Peptide	Amt (g)	Yield (g)	Product	Peptide (μmol/g)
9/3/92	DB4.256	.0516	GRGDY	.001	0.050	DB5.055	1.53
9/29/92	DB4.256	.102	GRGDY	.001	0.063	DB5.058	3.09
10/8/92	DB5.022	.504	GRGDY	.005	0.422	DB5.069	1.72
11/5/92	DB5.022	.502	GRGDY	.010	0.418	LC1.124	-
5/14/93	DB5.022	1.50	GRGDY	.031	1.42	LC1.139	6.7
7/9/93	JSH1027	1.497	GRGDY	.030	0.652	LC1.171	0.9
7/9/93	JSH1027	1.007	GRGEY	.021	0.784	LC1.172	4.2
1/31/94	JSH1027	1.0	GRGDY	.025	0.8	JSH1030	0.6
4/26/94	JSH1050	0.6	GRGEY	.050	0.5	JSH1057	2.6
5/12/94	JSH1065	0.85	GRGDY	.045	0.80	JSH1070	1.6
5/12/94	JSH1065	0.85	GRGEY	.070	0.80	JSH1071	12.3
5/23/95	JSH3031	0.10	GRGDY-I_2	.010	0.076	JSH4028	6.35
7/5/95	JSH3031	0.20	GRGDY-I_2	.020	0.180	JSH4042	2.55
7/5/95	JSH3031	0.40	GRDGY	.025	0.347	JSH4046	2.52
7/29/95	JSH3031	2.00	GRGDY-I_2	.030	1.75	JSH4048	1.68
11/9/95	JSH3043	1.85	GRGDY-I_2	.030	-	SMC004.1	7.40
11/24/95	JSH3044	1.83	GRGDS	.030	-	SMC	12.87

4.2.1 Evaluation of Surface Attachment Chemistries

The reagents which were considered for use in conducting surface attachment reactions are shown in Table 4.2. Although it has been widely used as a surface immobilization reagent in the past, glutaraldehyde was eliminated based on the fact that glutaraldehyde crosslinks cells very readily. Any traces of glutaraldehyde left behind would be damaging to the cells. In addition, glutaraldehyde crosslinks many functional groups which may result in unwanted side reactions during coupling.

The Tosyl chloride (p-toluenesulfonyl chloride) and Tresyl chloride (2,2,2-Trifluoroethane-sulfonyl chloride) chemistries were eliminated because they have been observed to change the nature of the surface under investigation and it is very difficult to rinse away excess reagents (personal communication, Curtis Herbert).

Table 4.2
Surface Attachment Reagents

Reagent	Chemical Structure
Glutaraldehyde	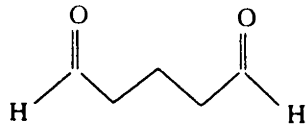
Tosyl Chloride	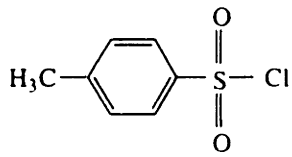
Tresyl Chloride	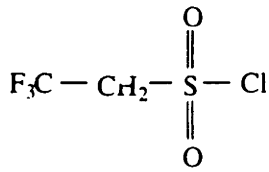
Bisoxirane	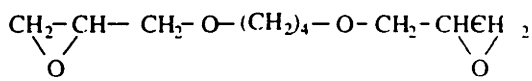
DMP	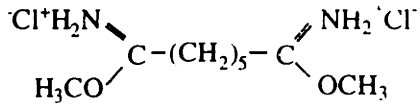
Sulfo-NHS	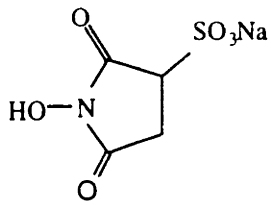
EDC	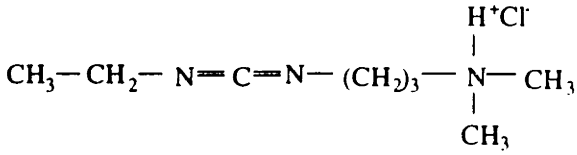

Bisoxirane was not considered based on poor performance of this reagent in studies conducted previously (personal communication, Denise Barrera).

DMP (Dimethylpimelimidate·HCl) was considered as a possible candidate for conducting surface immobilizations in one step. This reagent is recommended for use at alkaline pH's. Initial attempts to use this reagent did not result in any obvious advantages over the EDC/sulfo-NHS reagents, so further attempts were not undertaken to use it.

The EDC/Sulfo-NHS chemistry was chosen because it has proven to be useful in other peptide and protein immobilization systems (11). One of the main reasons for its usefulness is that it is highly soluble in water and rinses away very readily, so that competing reactions, such as crosslinking of the peptides, can be avoided. The reaction scheme for the EDC/Sulfo-NHS Chemistry is shown in Figure 4.2.

4.2.2 Materials and Methods

Optimization of the surface chemistry was performed using ^{125}I-radiolabeled peptides and alkylamine-derivitized polystyrene beads. The beads were obtained from the manufacturer (Pierce) with a relatively high density of primary amines (3 to 5 μmol/bead). Using these beads as a model surface allowed us to concentrate our efforts on optimizing the coupling reaction conditions without worrying about not knowing how many NH_2 groups were available on the PLAL samples. The use of radiolabeling is a standard technique for detecting molecules. The isotopes which are commonly used for labeling peptides are ^{125}I, ^{14}C, and ^{3}H. The advantages of ^{125}I isotopes are their high specific activity and due to their relatively short half-life, short-term storage before disposal. The disadvantages of ^{125}I are that only small amounts can be handled safely, labeling is labor intensive, and the size of the label may change the biological activity of the peptide. The advantages of using ^{3}H and ^{14}C are their long half-life (so material with a certain specific activity can be used for several months) and in the case of ^{3}H, the size of the label does not affect the properties of the peptide. Disadvantages of using ^{3}H include an initial higher cost and some radiolysis may occur over time, affecting the biological activity of the peptide.

Figure 4.2
EDC/Sulfo-NHS Reaction Scheme

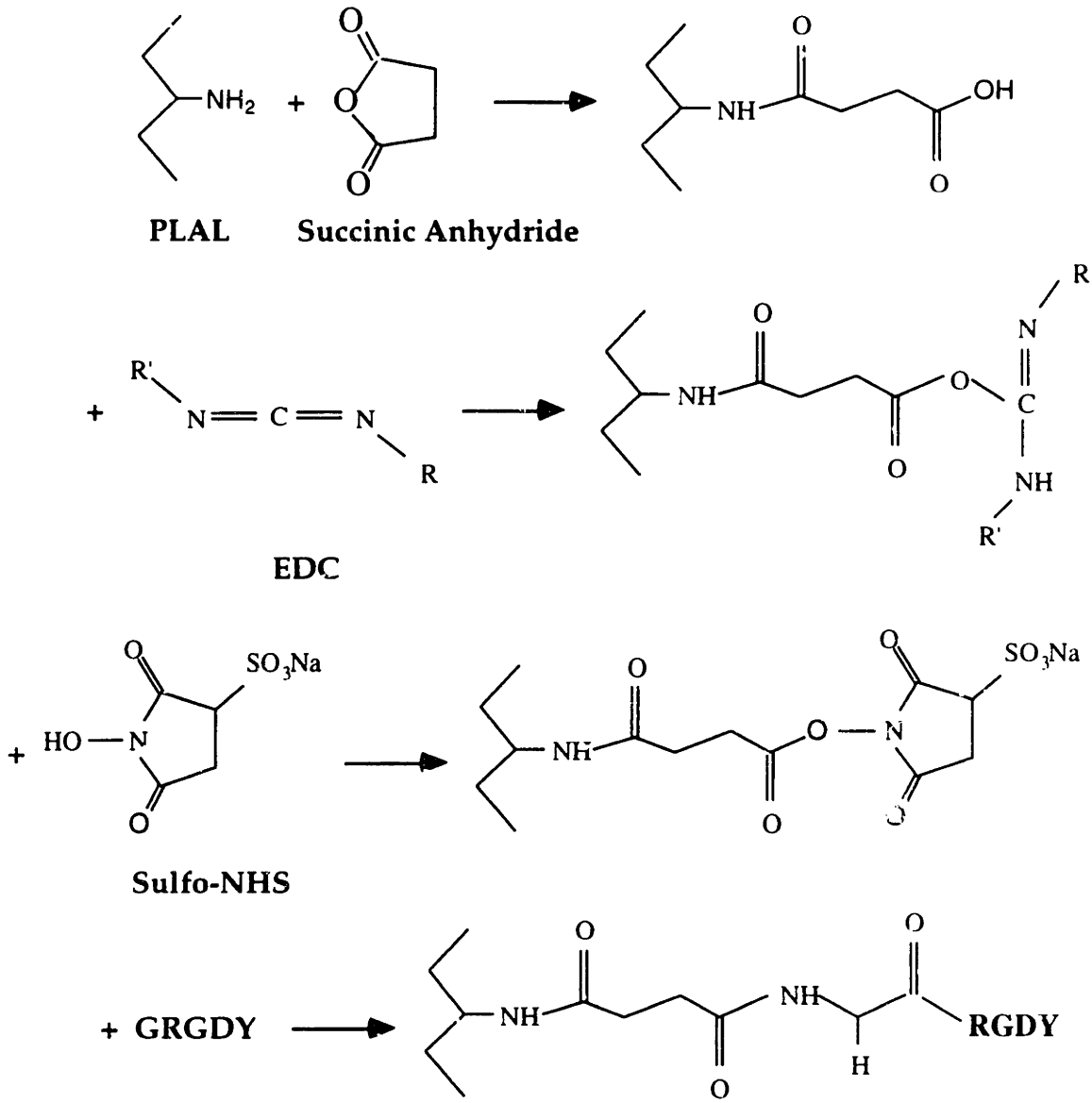

Massia and Hubbell used ^{125}I-labeled RGD-containing peptides attached to glycophase glass by tresyl chloride chemistry to determine the peptide loading required to support the attachment and spreading of fibroblasts (1). The specific activity of the peptides was approximately 44 mCi/mmol. This was high enough specific activity to detect as low as 2000 fmol (2 pmol) of peptide. In later work, Massia and Hubbell extended the sensitivity of their assay to detect

approximately 100 fmol of peptide (4). Due to the fact that the detection of peptide was linear in the range of 100-12,000 fmol, it was assumed that the linear relationship extended below the detectable limits and so reported surface concentrations for input dilutions of peptide used to obtain surface loadings below 100 fmol were extrapolated values.

In earlier work in our lab, we discovered that the traditional method of measuring peptide concentrations (by trace-labeling the peptide with radioactive iodine), was not successful in our case due to the low level of ^{125}I attached to the peptide and the high amount of non-specific adsorption of the radiolabeled peptide to PLA controls. The data in Table 4.3 show the results obtained using ^{125}I-labeled peptide radiolabeled by a traditional trace labeling method. The specific activity of the peptide used in this study was 64 mCi/mmol. The peptide was prepared using 2 mCi of $Na^{125}I$ and 2.06 mg of GRGDY peptide. 50 µl of 1M Acetic acid and 0.02 mM cold NaI were added to the mixture to stop the reaction. The peptide was purified by anion exchange chromatography using Dowex 1x8-50 anion exchange resin. Ten fractions were collected. Fraction 5 was used in this study. The concentration of peptide in each fraction was determined by Micro-BCA assay, using GRGDY peptide as a standard.

Table 4.3
Surface Attachments using Trace-labeled ^{125}I-GRGDY

Sample	Conditions	Peptide Density (pmol/cm^2)
Control A	1) Expose to ^{125}I-GRGDY only (No cold NaI, 0.1 M Acetic acid)	23.0
Control B	1) Activate with glutaraldehyde 2) React with cold glycine 3) Expose to ^{125}I-GRGDY	2.3
Sample	1) Activate with glutaraldehyde 2) Expose to ^{125}I-GRGDY	1.8

Table 4.3: Source: Barrera, Ph.D. Thesis, MIT, p. 140

The result of this experiment was that the non-specific attachment of the peptide to the controls was greater than to the PLAL sample.

For the radiolabeled peptide studies described hereafter, it was determined that there were two criteria which must be met for the peptide studies to be successful. The first requirement was that the peptides have a high enough specific activity that they could be detected at small densities (1 to 100 fmol/cm^2). To provide high specific activities, the stoichiometric radioiodination method of Tsomides was chosen (12). In addition to using larger quantities of $Na^{125}I$ (20 mCi for 2 mg of peptide), this method consists of adding 3 to 4 molar excess of "cold" $Na^{127}I$ to the reaction mixture to ensure that every peptide molecule undergoes iodination. Unlabeled peptide molecules are then separated by High Performance Liquid Chromatography (HPLC) from the peptides labeled with one iodine molecule and those containing two iodine molecules. By purifying the peptides on an HPLC column after labeling, the specific activity of the peptides is increased. The second requirement was that the surface attachment chemistry should be validated on surfaces which contained an excess of amino groups, so that the attachment chemistry would not be limited by the lack of available amino groups. To satisfy the second criteria, alkylamine-derivitized polystyrene beads were used. Each bead was 0.635 mm (1/4 in.) in diameter and contained 5 μmole of NH_2 groups.

The alkylamine-derivitized polystyrene beads, 1-ethyl-(3,3'-dimethylaminopropyl)-carbodiimide (EDC), and N-hydroxysulfosuccinimide (sulfo-NHS) were obtained from Pierce. Succinic anhydride was obtained from Sigma. In general, beads or blended polymer films were exposed to succinic anhydride for 15 hours, rinsed, activated with EDC, sulfo-NHS mixtures for 1.5 to 24 hours, rinsed, and then incubated in the presence of ^{125}I-GRGDY peptides under various conditions of time, temperature and pH.

Statistical analysis of the results was conducted using Student's t-test. This test compares the means and variances of two sets of data to determine the probability of the samples being equal. For sample sets in which less than 30 measurements are made, the customary assumptions that the variances are known and are equal cannot be used, so the proper test statistic (T') is defined as:

$$T' = \frac{(\bar{x}_1 - \bar{x}_2) - d_o}{\sqrt{\frac{s_1^2}{n_1} + \frac{s_2^2}{n_2}}}$$

with the degrees of freedom (v) defined as:

$$v = \frac{\left(s_1^2/n_1 + s_2^2/n_2\right)^2}{\frac{(s_1^2/n_1)^2}{n_1 - 1} + \frac{(s_2^2/n_2)^2}{n_2 - 1}}$$

where $\bar{x}_1$, s_1 and n_1 refer to the mean, standard deviation and number of measurements of data set 1. (The parameters for data set 2 are similarly defined.) The conditions for this test statistic are that $d_o = \mu_1 - \mu_2$ and $\sigma_1 \neq \sigma_2$, where μ_1 is the true mean of population 1 and s_1 is the true variance of population 1. For this test, the population means and variances are unknown. To analyze two data sets to show whether or not they are equal, the null hypothesis (H_o) is that $\mu_1 = \mu_2$, or $d_o = 0$. The alternative hypotheses (H_a) are $\mu_1 > \mu_2$, $\mu_1 < \mu_2$, or $\mu_1 \neq \mu_2$. The null hypothesis can be rejected if $T' > t_\alpha$ or $T' < -t_\alpha$ for one-tailed tests, or $T' < -t_{\alpha/2}$ and $T' > t_{\alpha/2}$ for a two-tailed test. The value of t_α is a function of v and α and can be determined from any standard t-Test table.

4.2.3 Results

The radioiodination of the GRGDY peptide was performed in a fully shielded and specially monitored glove box designated for radioactive studies. All steps were carried out at room temperature. Eight Iodo-Beads (Pierce) were washed twice with 0.1 M sodium phosphate, pH 7.0 and added to 0.3 ml of 0.1 M sodium phosphate buffer, pH 7.0 in a microcentrifuge tube. $Na^{125}I$ (20 mCi, NEN, DuPont) was mixed with 30 µl 0.1 M $Na^{127}I$ (Mallinckrodt) and added to the Iodo-Beads for 5 min. A color change to brown indicated active Iodo-Beads. Peptide dissolved in 0.5 ml PBS (Gibco/BRL), pH 7.4 was added to the oxidized iodide for 30 min. with occassional agitation. The mixture was transferred by syringe to a C18 Sep Pak cartridge (Waters) prepared according to manufacturer's instructions with methanol and PBS followed by 20 ml 0.1% TFA (HPLC solvent A). After the Sep Pak was loaded and washed with an additional 20 ml solvent A to remove free iodide, two fractions were eluted with 4 ml 50% solvent B/50% solvent A and 4 ml 100% solvent B (0.085% TFA in acetonitrile). These fractions were removed from the glove box for drying in a SpeedVac Concentrator (Savant). The fractions were resuspended in 1 ml solvent A, filtered through 0.45 µm filters (Millipore), and injected on a Beckman HPLC

system equipped with a C18 reverse-phase column (Vydac) and an on-line radioisotope detector. Figure 4.3 shows the results of the HPLC separation of the peptides. Peak 1 is mono-iodinated peptide, peak 2 is di-iodinated peptide. Each peak was collected, dried in a SpeedVac Concentrator, and taken up in water.

Figure 4.3
HPLC Separation of Radiolabeled Peptide Fractions

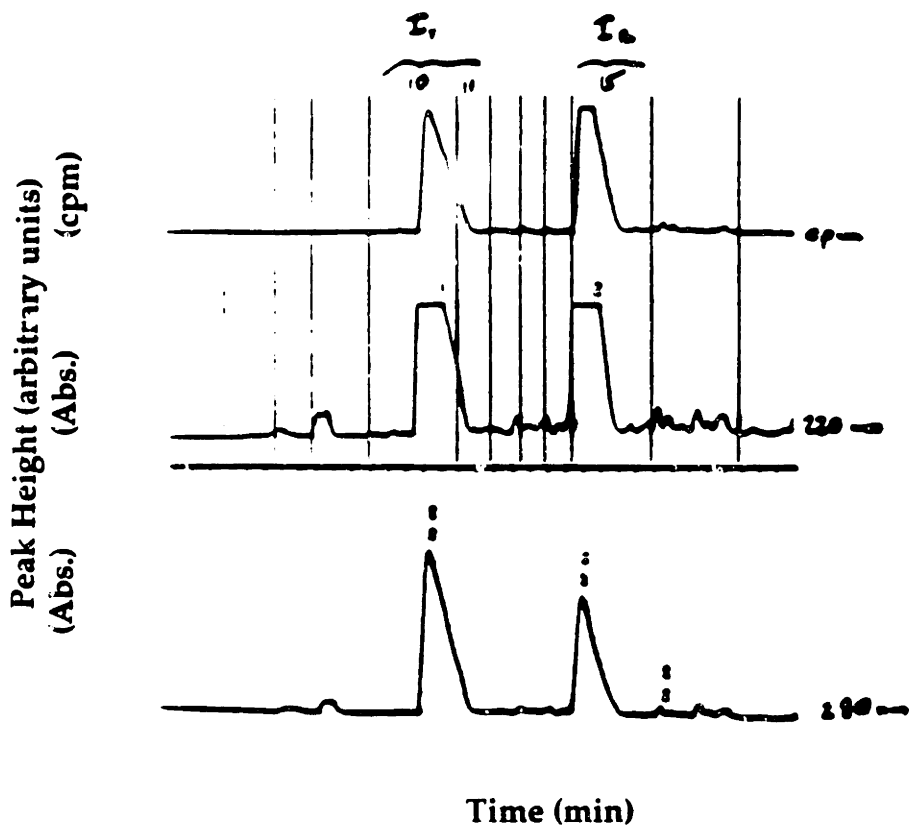

Figure 4.3: Replicas of the HPLC eluent traces, depicting the peak heights (arbitrary units) on the ordinate axis vs. eluent time (min.) on the abscissa. The top scan is from the on-line gamma counter and shows the position of the radioactive peaks. The second scan is from a U.V. detector set at 220 nm. The third scan is from a U.V. detector set at 280 nm. Dual U.V. measurements were made to provide semi-quantitative information.

The concentration of the peptide in each of the fractions was determined by Micro-BCA assay (Pierce), using bovine serum albumin (BSA, from ICN) as the standard. Figure 4.4 shows the standard curve used to calculate the radiolabeled peptide concentration. The use of BSA as a standard introduced some error into the determination of the concentrations of the radiolabeled peptides. The magnitude of this error was estimated by performing the Micro-BCA assay on a different day using BSA and "cold" GRGDY-I_2 to construct standard curves. Figure 4.5 is a comparison of the two standard curves which were constructed in order to determine the difference in the BSA and peptide calibration curves. The difference is probably due to the way in which the BCA reagents react with peptides vs. proteins. In addition, the tyrosine groups on the peptides are known to interfere with the assay.

The error from using BSA instead of GRGDY-I_2 peptide as the standard was determined to be a 40% underestimation of the concentration of the peptide. This factor was taken into account in subsequent calculations.

The initial specific activities of the two fractions were determined to be 610 mCi/mmol for I_1 and 1617 mCi/mmol for I_2. Figure 4.6 compares the specific activity of these radiolabeled peptides to the trace-labeled peptides of the earlier study described in section 4.2.2. The number shown above each bar in the graph represents the amount of peptide needed to produce 200 cpm, a level sufficiently above background to be considered reliable data. The experiments described below were all conducted with the I_2 fraction of the peptide, which meant that initially any level of attached peptide greater than 75 fmol was detectable.

The specific activity of the peptide was calculated for each day based on the following equation, which took into account radioactive decay:

$$A = A_o \exp(-t * \ln 2/t_{1/2})$$

where A = specific activity, A_o = initial specific activity, t = time (days), and $t_{1/2}$ = half-life (60 days for ^{125}I).

Figure 4.4
Micro-BCA Standard Curve for Radioiodination

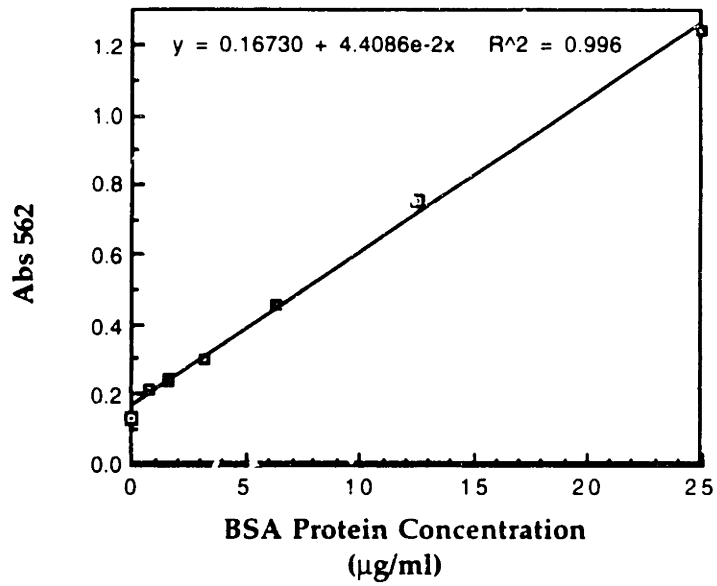

Figure 4.5
Micro-BCA Standard Curves of BSA vs. GRGDY-I_2 peptide

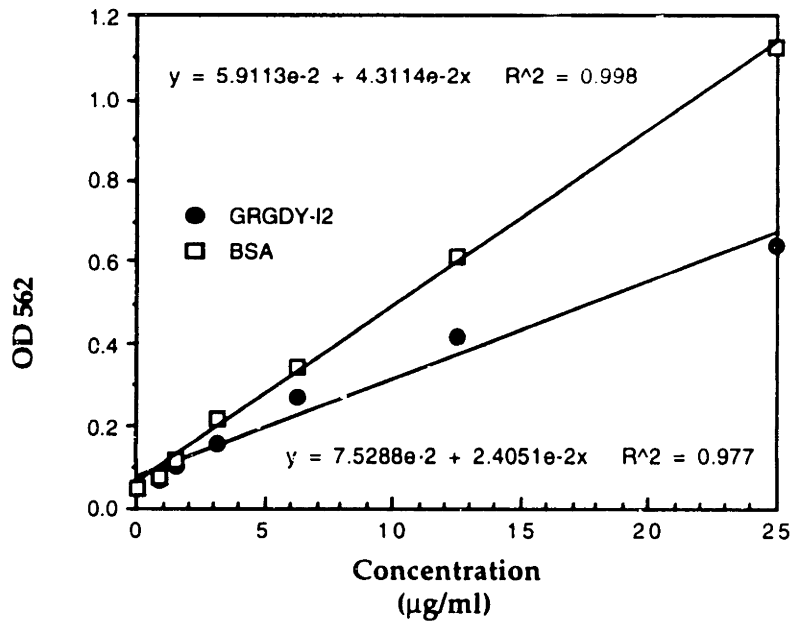

Figure 4.6
Comparison of Radioiodination R sults

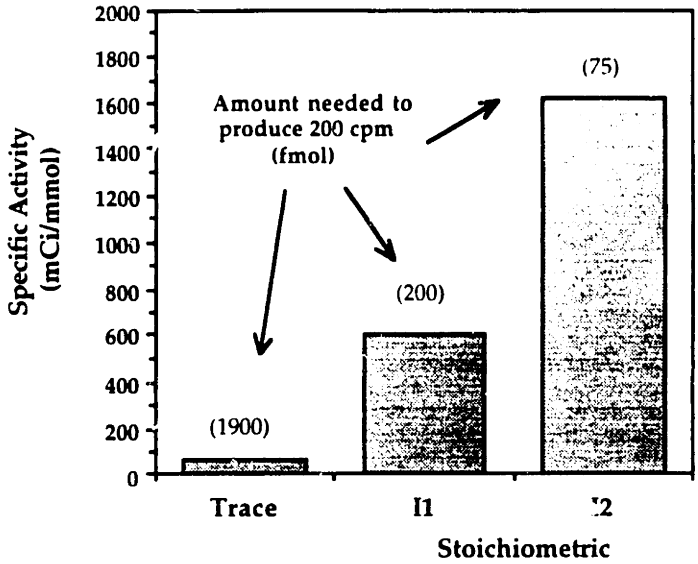

Figure 4.6: Stoichiometric vs. trace lableling of ^{125}I-labeled peptides. I1 indicates monoiodinated peptide fraction, I2 indicates diiodinated peptide fraction

Reaction Conditions

The water soluble carbodiimide (EDC) chemistry was optimized using the alkylamine beads. One of the reactions in the reaction scheme is the coupling of succinic anhydride to the amines to change the functional group from an amino to a carboxylic acid group. Another of the reactions involves sulfo-NHS as an agent to enhance the reaction. A set of experiments were conducted to determine the effect of succinic anhydride activation time and sulfo-NHS concentration on peptide attachment. The results of these experiments are summarized in Table 4.4 and presented graphically in Figure 4.7. All data are reported as Ave ± S.D.

Table 4.4
Optimization of Reaction Conditions

Activation Times	Sulfo-NHS Concentration (pmol/ml)	Peptide Bound (fmol/cm^2)	% Attachment
Reaction Set 1:			
Succinic Anhydride	5 (N=1, n=2)	7835 ± 552	57 ± 0.2
1.5 hrs.	50 (N=1, n=2)	6238 ± 915	43 ± 6
EDC/Sulfo-NHS	500 (N=1, n=2)	7839 ± 647	56 ± 4
10 min.	5000 (N=1, n=2)	7473 ± 401	51 ± 4
Reaction Set 2:			
Succinic Anhydride	5 (N=1, n=2)	14224 ± 2083	63 ± 7
20 hrs.	50 (N=1, n=2)	14248 ± 723	64 ± 6
EDC/Sulfo-NHS	500 (N=1, n=2)	13019 ± 1095	59 ± 4
2 hrs.	5000 (N=1, n=2)	15254 ± 548	64 ± 0.5

In the first set of reactions listed in Table 4.4, the alkylamine-derivitized beads were reacted with succinic anhydride (100 mg per bead in plastic test-tubes) for 1.5 hrs. The beads were then rinsed of excess succinic anhydride (1 wash of 2 ml of MilliQ H_20) and reacted with EDC/Sulfo-NHS for 10 min. at the various concentrations of sulfo-NHS shown in the Table. (The EDC concentration was 600 pmol/ml.) The beads were then rinsed of excess reagents (1 wash of 2 ml of MilliQ H_2O) and placed in 2 ml of a peptide solution containing approximately 10 pmol/ml (actual: 8.9 ± 0.4) of GRGDY-$^{125}I_2$ in PBS, pH 7.1 for 19 hrs. at 37°C with shaking. The beads were then washed (3 washes: MilliQ H_2O, then PBS, then MilliQ H_2O; 2 ml each) and counted. The third wash contained counts which were lower than 200 cpm and less than 1% of the total counts.

In the second set of reactions listed in Table 4.4, the alkylamine-derivitized beads were reacted with succinic anhydride for 20 hrs (100 mg per bead in plastic test-tubes, in PBS, pH 6.0). The beads were rinsed (1 wash of 2 ml of milliQ H_20) and then reacted with EDC/Sulfo-NHS for 2 hrs. (The EDC concentration was 150 pmol/ml.) The beads were rinsed (1 wash of 2 ml of MilliQ H_2O) and then

reacted with 2 ml of a peptide solution containing approximately 10 pmol/ml (actual: 14.3 ± 0.6) of GRGDY-$^{125}I_2$ in PBS, pH 7.1 for 18.5 hrs. at 37°C with shaking. The beads were then washed (3 washes: MilliQ H_2O, then PBS, then MilliQ H_2O; 2 ml each) and counted. The third wash contained counts which were lower than 200 cpm and less than 1% of the total counts.

Figure 4.7
Optimization of Reaction Conditions

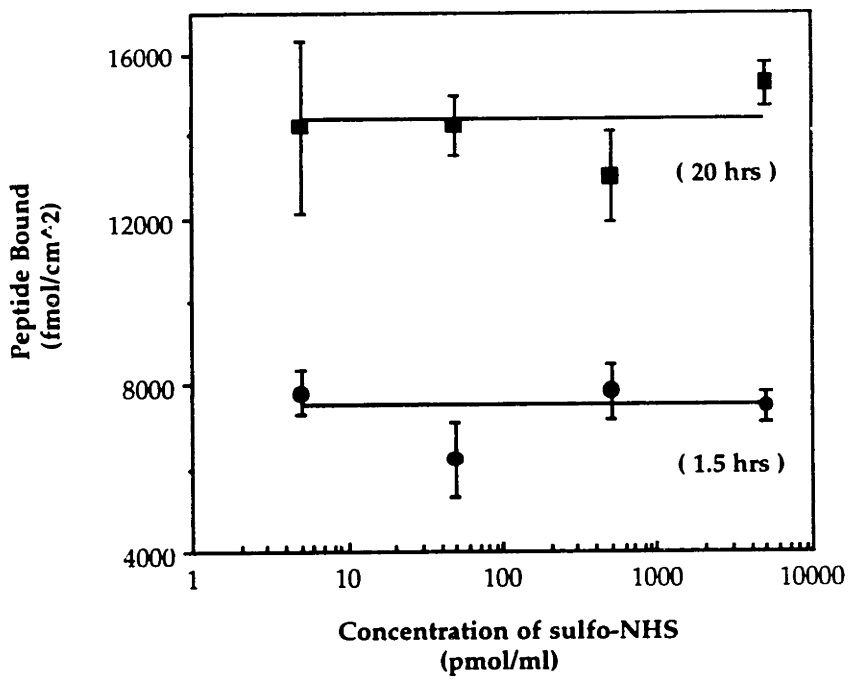

Figure 4.7: Two reaction conditions were tested in these experiments, the effect of incubation time with succinic anhydride and the concentration of Sulfo-NHS. (N=1, n=2 for each data point. Data are Ave ± S.D.)

Student's t test was used with the test statistic (T') and degrees of freedom (v) for population means which are unequal and unknown. A one-tailed test using alpha = 0.05 was performed. Neglecting the effect of sulfo-NHS concentration, calculating the average of all the data from the first set of reactions listed in Table 4.4, and comparing this to the average of all of the data from the second set of reactions showed that there was a significant difference (0.05 level of significance) due to reaction time. From this set of experiments it was

determined that longer reaction times with succinic anhydride were desired to improve the loading of peptide to the beads.

Incubation Time

In this set of reactions, the peptide incubation time was varied from 2 to 18 hrs. The results of these experiments are shown in Table 4.5 and shown graphically in Figure 4.8. All data are reported as Ave. ± S.D. These experiments were conducted in the presence of 1 mg/ml BSA (ICN, fraction V), which was added for 30 min. prior to adding the peptide in order to prevent non-specific association of the peptide to the incubation flask. No succinic anhydride was used and the controls were run without any EDC or sulfo-NHS.

Table 4.5
Effect of Time on Peptide Attachment

Time (hr)	Peptide Bound ($fmol/cm^2$)	% Attached
Controls		
2 (N=1, n=3)	1273 ± 188	10 ± 2
6 (N=1, n=3)	1961± 577	16 ± 5
18 (N=1, n=3)	3870 ± 212	30 ± 1
Samples		
2 (N=1, n=3)	1199 ± 90	10 ± 1
6 (N=1, n=3)	2343 ± 220	19 ± 2
18 (N=1, n=3)	4607 ± 243	36 ± 2

The 2 hr. and 18 hr. reactions were performed by incubating the beads in EDC/Sulfo-NHS for 10 min. The EDC concentration and the sulfo-NHS concentration were both 5000 pmol/ml. Excess reagents were removed by rinsing once with H_2O. The BSA was then added to the beads (1 ml) for 30 min. The peptide was then added to bring the total volume up to 2 ml. The final concentration of peptide was approximately 10 pmol/ml (actual: 7.9 ± 0.1) in PBS, pH 7.1. After 2 hrs the beads were washed (3 washes: MilliQ H_2O, then PBS, then MilliQ H_2O) and counted. The third wash contained counts which were lower than 200 cpm and less than 1% of the total counts.

The 6 hr reactions were performed on a different day. The only variation was the input concentration of peptide (actual: 7.8 ± 0.1 pmol/ml).

Figure 4.8
Effect of Time on Peptide Attachment

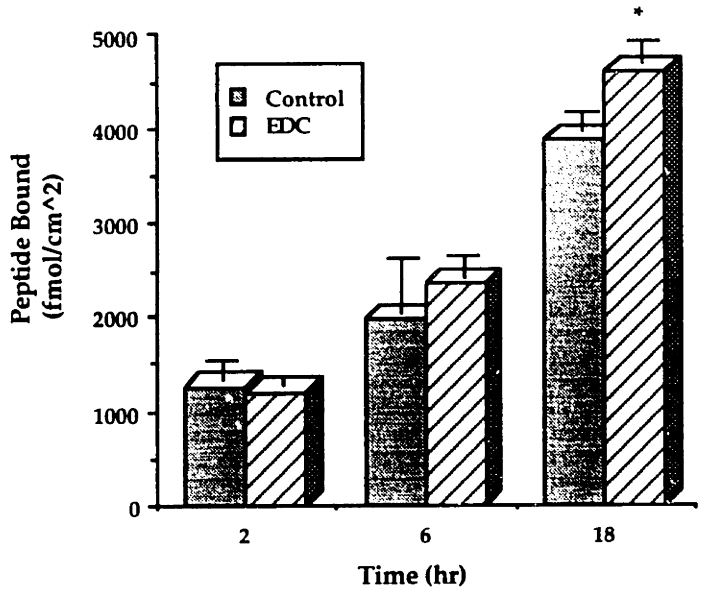

Figure 4.8: This experiment was performed to test the effect of peptide incubation time on final peptide loading. (N=1, n=3 for each bar. Data are Ave ± S. D. The asterisk indicates a significant difference between the sample and control at 18 hrs.)

Statistical analysis of the results demonstrated that there was a significant difference between the samples and controls at 18 hrs (0.05 level of significance). There was also a statistically significant effect of time (0.05 level of significance), but this was essentially the same for the controls as for the samples. In other words, both the specific attachment and the non-specific association of the peptide increased over time to roughly the same extent.

Effect of pH

In the next set of experiments, the pH of the peptide solution was varied from 5 to 8. The succinic anhydride activation (100 mg in 2 ml PBS per bead, pH 6.0) was performed for 19.5 hours, the beads were rinsed in 2 ml of MilliQ H_2O, the EDC/Sulfo-NHS reaction (2500 pmol/ml of each in 2 ml total volume) was performed for 3 hours. The samples were rinsed once with milliQ H_2O, then an aqueous solution of BSA (fraction V from ICN: 1.9 ml of 1 mg/ml) was added for 30 min., then 100 µl of peptide solution was added to produce a final concentration of approximately 10 pmol/ml (actual: 7.7 ± 1). The beads were incubated with peptide for 20 hrs. at 37°C with shaking. The beads were then washed (3 washes: MilliQ water, then PBS, then MilliQ water; 2 ml each) and counted. The third wash contained counts which were lower than 400 cpm and less than 2% of the total counts. The results of these experiments are shown in Table 4.6 and Figure 4.9. All data are Ave. ± S. D. Statistical analysis using Student's t-test as described previously showed that the effect of pH was significant at the 0.05 level of significance.

Table 4.6
Effect of pH on Peptide Attachment

pH	Peptide Bound ($fmol/cm^2$)	% Attachment
Control (N = 1 , n = 3)	5893 ± 801	48 ± 7
5 (N = 1 , n = 3)	9410 ± 435	77 ± 5
6 (N = 1 , n = 3)	9520 ± 577	79 ± 6
7 (N = 1 , n = 3)	8441 ± 333	67 ± 2
8 (N = 1 , n = 3)	7466 ± 806	61 ± 7

Figure 4.9
Effect of pH on Peptide Attachment

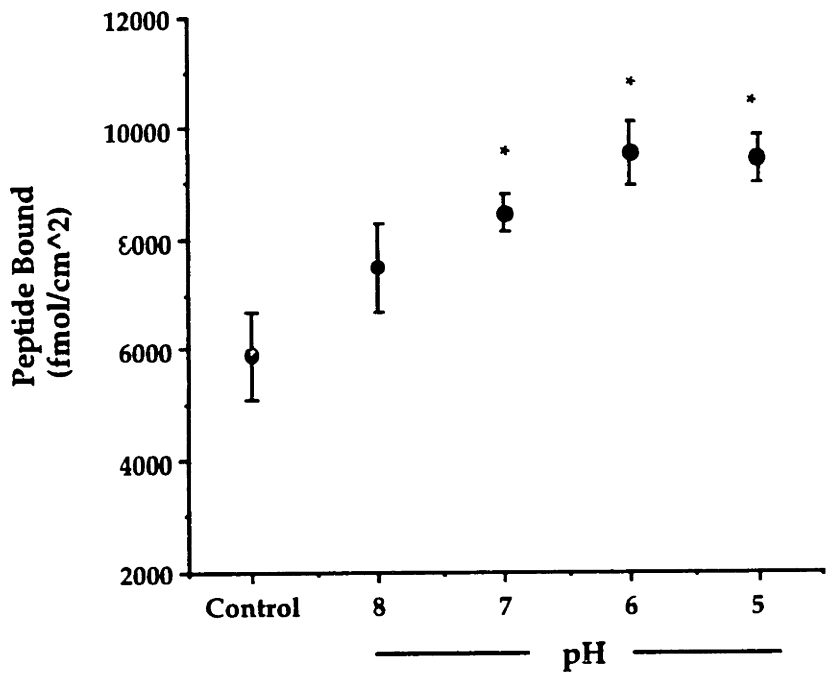

Figure 4.9: The effect of pH on peptide attachment to alkylamine derivitized polystyrene beads. (N=1, n=3, all data are Ave. ± S.D. The asterisks indicate data which are significantly different then the control.)

The effect of Input Concentration

The next experiment demonstrated that the amount of peptide bound to the beads was linearly related to the input concentration of peptide. These samples were incubated in succinic anhydride (100 mg per bead in 2 ml of PBS, pH 6.0) for 15 hrs, rinsed (1 wash of MilliQ water), followed by 2 hrs. in EDC/Sulfo-NHS (2500 pmol of each in 2 ml total volume). They were then rinsed (1 wash of MilliQ water) and incubated in peptide solutions (actual concentrations are shown in Table 11.5) in PBS, pH 7 for 22 hrs. The beads were then washed (3 washes: MilliQ water, then PBS, then MilliQ water; 2 ml each) and counted. The third wash contained counts which were lower than 2% of the total counts. The results are shown in Table 4.7 and Figure 4.10. All data are Ave. ± S.D.

Table 4.7
Effect of Input Concentration on Peptide Attachment

Input Concentration (pmol/ml)	Actual Conc. (pmol/ml)	Peptide Bound ($fmol/cm^2$)	% Attachment
Control (N = 1 , n = 3)	7.5 ± 0.08	8501 ± 509	71 ± 5
10 (N = 1 , n = 3)	8.0 ± 0.04	8978 ± 345	70 ± 2
20 (N = 1 , n = 3)	15.8 ± 0.13	18403 ± 698	73 ± 3
40 (N = 1 , n = 3)	34.1 ± 0.25	42269 ± 1358	78 ± 2
80 (N = 1 , n = 3)	69.2 ± 1.08	82590 ± 1309	75 ± 2

Figure 4.10
Effect of Input Concentration on Peptide Attachment

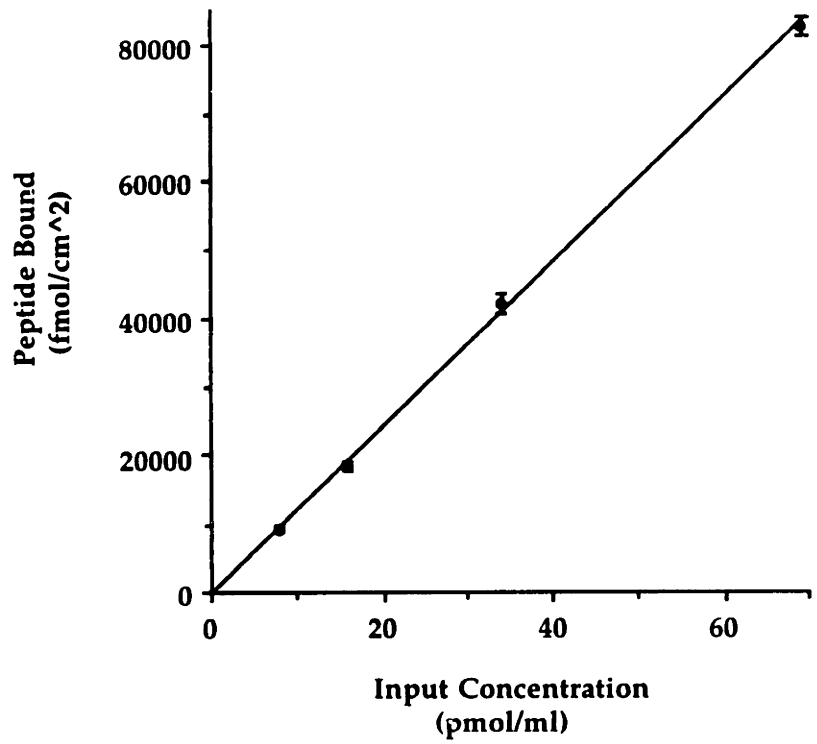

Figure 4.10: The effect of Input Concentration on peptide attachment to alkylamine-derivitized polystyrene beads. (N=1, n=3, data are Ave. ± S.D.)

Statistical analysis of the slope was performed to determine if there was a linear relationship between the amount of peptide bound to the beads and the input concentration of peptide. The null hypothesis in this test was that the slope of the line was equal to zero. The alternative hypothesis was that the slope was greater than zero. Student's t test was performed using the test statistic (T) and the degrees of freedom (v):

$$T = \frac{b_1 \sqrt{S_x}}{\sqrt{n\, s^2}} \qquad\qquad v = n - 2$$

A one-tailed test using $\alpha = 0.05$ was conducted on the average peptide bound at each input concentration. The results of this analysis were significant and therefore permit one to infer that there is a direct correlation (0.05 level of significance) between the amount of peptide that is attached to the beads and the input concentration of peptide.

4.2.4 Discussion

The radiolabeled peptide studies demonstrated that there is a substantial amount of non-specific association of peptides to the beads. Even after extensive rinsing, in which no detectable peptides were seen in the rinses, there still remained on the order of 5 to 10 pmol/cm^2 of peptide non-specifically attached to the control beads.

There were three types of peptide attachment. There was background, non-specific attachment that rinsed away, there was non-specific attachment that withstood washing, and there was specific attachment that could be blocked by the presence of excess BSA. Several attempts were made to determine the best way to wash the beads and polymer samples to eliminate the non-specific attachment. It was found that using as many as 9 washes did not eliminate the non-specifically bound peptides completely. The use of ethylene glycol was attempted unsuccessfully as well. It may be possible to find a combination of washes that does eliminate the non-specifically bound peptides. It may also be possible to rinse the polymers for several hours in various salts, or use sonication.

4.3 *Comparison of Bulk and Surface Attachment Chemistries*

This chapter has described two methods for attaching peptides to surfaces composed of NH_2 functionalities. In the remaining sections of the Thesis, the method of peptide attachment is referred to as either bulk attachment chemistry or surface attachment chemistry.

The two different methods of attaching the peptides to PLAL yielded surfaces with different densities of peptides. Results of bulk-attached peptide experiments and surface-attached peptide studies are shown in Table 4.8. The results of the bulk attachment experiments were obtained by Amino Acid Analysis. Assuming the surface concentrations of the lysine and peptides are the same as in the bulk, that the surface consists of the top 10 Å, and that the density of the polymer is 0.782 g/cm^3, then the surface density of lysine would be 17.3 pmol/cm^2 (Range: 3.4 to 103 pmol/cm^2) and the surface density of peptides would be 211 fmol/cm^2 (Range: 47 to 328 fmol/cm^2). (This analysis does not take into account the possibility of surface enrichment of lysine.)

The surface-attachment reaction consists of reacting the NH_2 groups with succinic anhydride to change the functional group to carboxylic acid, reacting the surface with EDC in water, then adding the peptides. The surface densities of lysine were obtained using the sulfo-SDTB assay, and the surface densities of peptides were acquired by using radiolabeled peptides. Results of these measurements indicate that the surface densities were approximately 720 pmol/cm^2 of lysine and 283 ± 21 fmol/cm^2 of peptides.

The first conclusion from this analysis is that the bulk-attachment method yields higher reaction efficiencies than the surface attachment method. A second conclusion is that the peptide densities measured on surfaces prepared with the surface-attachment method are within the same range as those surfaces which are prepared from polymer which has had peptide coupled by the bulk-attachment method. Another observation is that the lysine density is higher (by a factor of 30) than the average lysine content predicted by assuming the surface is only 10Å deep and the same as the bulk, as measured by amino acid analysis. This could indicate that there is surface enrichment of lysine during processing, or it could indicate that the sulfo-SDTB method overestimates the actual lysine densities.

Table 4.8
Comparison of Bulk- and Surface-Attachment Methods

Product Designation	Peptide Content* (μmol/g)	Lysine Content* (μmol/g)	Efficiency† (%)
Bulk-Attachment			
DB5.055	1.5	59	2.6
DB5.058	3.1	77	4.0
DB5.069	1.7	127	1.4
LC1.124	2.6	77	3.4
LC1.139	6.7	102	6.5
LC1.171	0.9	106	0.8
LC1.172	4.2	1311	0.3
JSH1030	0.6	87	0.7
JSH1057	2.6	43	6.0
Average ± S.D.:	2.7 ± 1.9	221 ± 410	2.9 ± 2.3
Surface-Attachment**	(fmol/cm^2)	(nmol/cm^2)	
Beads (Table 4.4)	15,254 ± 548	40.15 ± 3.3	0.04
Beads (Table 4.5)	4607 ± 243	40.15 ± 3.3	0.01
Beads (Table 4.6)	9520 ± 577	40.15 ± 3.3	0.02
Beads (Table 4.7)	82,590 ± 1309	40.15 ± 3.3	0.21
Average ± S. D.:			0.07 ± 0.09
Blends	283 ± 21	~ 0.72	0.04

Table 4.8: * For the Bulk-attachment studies, lysine and peptide contents were determined by Amino Acid Analysis
** For the Surface-attachment studies, lysine densities were determined by sulfo-SDTB colorimetric assays, peptide densities were determined by radiolabeled peptide measurements.
† Efficiency was defined as the amount of peptide attached divided by the amount of lysine available.

4.4 References

1. Massia, S.P., Hubbell, J. A., "Covalent surface immobilization of Arg-Gly-Asp- and Tyr-Ile-Gly-Ser-Arg- containing peptides to obtain well-defined cell-adhesive substrates", *Anal. Biochem.*, **187** : 292-301, (1990).

2. Massia, S.P., Hubbell, J. A., "Covalently attached GRGD on polymer surfaces promotes biospecific adhesion of mammaliam cells", *Ann. N. Y. Acad. Sci.*, **589** : 261-270, (1990).

3. Massia, S.P., Hubbell, J. A., "Human endothelial cell interactions with surface-coupled adhesion peptides on a nonadhesive glass substrate and two polymeric biomaterials", *J. Biom. Mat. Res.*, **25** : 223-242, (1991).

4. Massia, S.P., Hubbell, J. A., "RGD spacing of 440 nm is sufficient for integrin $\alpha_v\beta_3$-mediated fibroblast spreading and 140 nm for focal contact and stress fiber formation", *J. Cell Biol.*, **114** (5): 1089-1100, (1991).

5. Lin, H.B., Zhao, Z. C., Garcia-Echeverria, C., Rich, D. H., Cooper, S. L., "Synthesis of a novel polyurethane copolymer containing covalently attached RGD peptide", *J. Biomat. Sci.*, **3**:217-227 (1991).

6. Ito, Y., Kajihara, M., Imanishi, Y., "Materials for enhancing cell adhesion by immobilization of cell-adhesive peptide", *J. Biomed. Mat. Res.*, **25** : 1325-1337, (1991).

7. Hubbell, J.A., Massia, S. P., Drumheller, P. D., "Surface-grafted cell-binding peptides in tissue engineering of the vascular graft", *Ann. N. Y. Acad. Sci.*, **665** : 253-258, (1992).

8. Brandley, B.K., Schnaar, R. L., "Covalent attachment of an Arg-Gly-Asp sequence peptide to derivatizable polyacrylamide surfaces: support of fibroblast adhesion and long-term growth", *Anal. Biochem.*, **172** : 270-278, (1988).

9. Pierschbacher, M.D., Ruoslahti, E., "Cell attachment activity of fibronectin can be duplicated by small synthetic fragments of the molecule", *Nature*, **309** : 30-33, (1984).

10. Barrera, D.A., Zylstra, E., Lansbury, P. T., Langer, R., "Synthesis and RGD peptide modification of a new biodegradable copolymer: poly(lactic acid-*co*-lysine)", *J. Amer. Chem. Soc.*, **115** : 11010-11011, (1993).

11. Drumheller, P.D., Hubbell, J. A., "Surface immobilization of adhesion ligands for investigations of cell/substrate interactions", CRC Handbook of Biomedical Engineering, (1994)

12. Tsomides, T.J., Eisen, H. N., "Stoichiometric labeling of peptides by iodination on tyrosyl or histidyl residues", *Anal. Biochem.*, **210** : 129-135, (1993).

Chapter 5

Surface Characterization

5.1 Introduction

It has been well established that the evaluation of any biomaterial requires an extensive characterization of the surface of that material, because the interaction of any biological molecule or cell with a biomaterial occurs primarily at the surface (1). It has been further demonstrated that the surface is usually not representative of the bulk, but rather represents a history of exposure to past environments (1-4). It is particularly important to fully characterize the surfaces of biodegradable polymers because it would be expected that the surfaces of these materials undergo constant changes. The rate at which changes occur will have a profound impact on the ability of the polymer to carry out its desired function. Cell viability, local chemical concentrations, the strength of cell attachment, the presence of toxic chemical entities, and the attraction of scavenger cells are all influenced by changes occurring on the polymer surface. In addition, it should be remembered that cells which come in contact with biomaterial surfaces will react to many aspects of that surface besides the bulk polymer, such as contaminants, residual solvents, and surface structures which are formed as a result of processing steps.

There are numerous methods for investigating the chemical, physical and electrical characteristics of a biomaterial surface. Figure 5.1 lists some of the most common methods (1). Although there are many methods for analyzing surfaces, most of the techniques suffer from severe limitations and interpretation of the data is often subject to skeptical criticism. One must be aware that the data is influenced by the technique used to obtain that information. In reporting the results of a measurement, it is necessary to identify the technique used to make the measurement and the standards which were used to calibrate the equipment making the measurements. Often, the surface concentration of a particular entity as determined by one method will differ greatly from a measurement of the same entity made by another method.

Figure 5.1

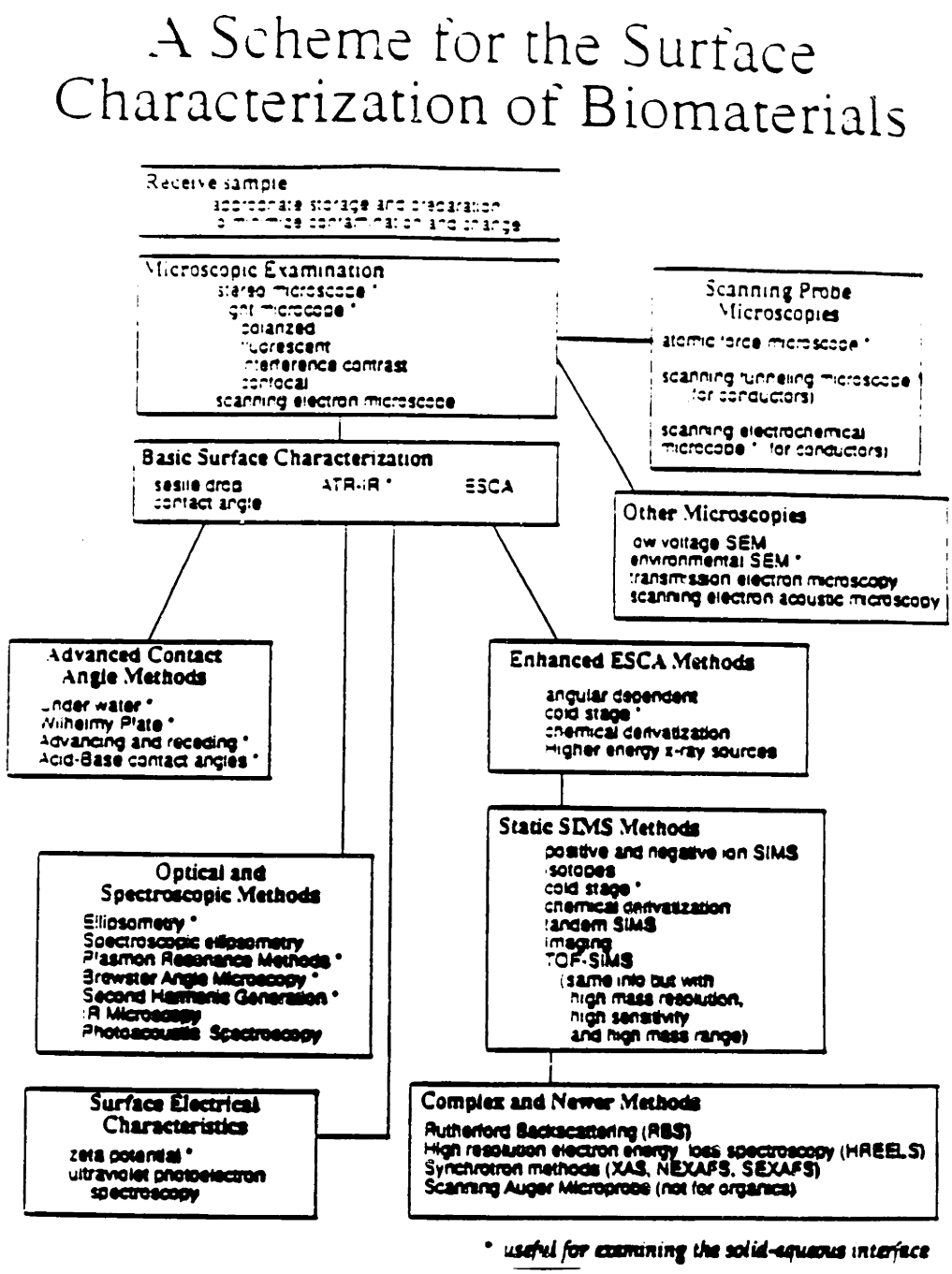

Figure 5.1: Common methods for characterizing biomaterials. Source: Ratner, B. D., *Cardio. Path.* 2(3) (Suppl.): 87S-100S (1993)

5.1.1 *Methods chosen to perform surface analysis*

In practice, many of the surface analysis techniques are complementary and so several techniques are often used to fully characterize a surface. One of the most important aspects of surface analysis is identifying a distinct, measurable entity for each method. The signal eminating from that entity must be strong enough to be resolved from background contributions. The surface analysis techniques which were investigated are listed in Table 5.1 along with the entity which each method measures.

Table 5.1
Methods for Characterizing PLAL and Bound Peptides

Method	Measured Entity
X-ray Photoelectron Spectroscopy	Elemental composition
Contact Angles	Surface Energy/Wettability
Secondary Ion Mass Spectroscopy	Molecular composition
Colorimetric Dyes	Amine groups
Fourier Transform Infrared Spectroscopy	Chemical bonds
Antibody Assays	Peptide availability
Radiolabeled Peptides	Peptide attachment
Fluorescent Labels	Peptide availability
Cell Adhesion Assays	Biocompatibility
Scanning Electron Microscopy	Morphology

The overall objective of this phase of the research was to systematically characterize the surfaces of poly(lactic acid-*co*-lysine) (PLAL) samples that were modified with cell adhesion peptides and relate the surface properties to cell behavior. The goal of evaluating the surface analytical techniques listed above was to develop methods to quantify three entities: the ε-amino groups of lysine present on the surface, peptides attached to the ε-amino groups, and the percentage of the peptide groups that were in the proper configuration to be accessible to endothelial cells. This thesis describes the way in which the available surface analysis tools were applied to studying this system. In applying these tools to this particular system, it was expected that some methods would become preferred over others due to differences in convenience and reliability of the results. Not all of the systems were expected to yield

information of the same caliber, but all of the methods were evaluated in order to fully characterize the system. The end product of these analyses was the determination of the factors which are most important in creating a biodegradable extracellular matrix which can support the attachment of a monolayer of endothelial cells.

The first level of information which was desired was a measurement of the amount of lysine that was present on the surfaces of PLAL samples in comparison to the bulk composition of the polymer. The effects of polymer processing on the surface concentration of lysine were determined. Various processing techniques were examined in order to optimize the availability of lysine on the surface. Bulk lysine concentrations were measured by amino acid analysis (see Section 3.4.1). The surface concentration of lysine was calculated from nitrogen contents measured by XPS and from surface reactions with colorimetric dyes that react with amino groups. In addition, XPS studies utilizing pentafluorobenzaldehyde (PFBA) were used to assess the reactivity of the lysine groups (see Section 5.2.2). Contact angle studies were performed in order to determine the effect of processing on the wettability of the samples (see Section 5.4.2). XPS and SIMS studies using frozen, hydrated samples were performed in order to measure the changes which occur due to degradation by hydrolysis (see Section 5.3.4).

The second level of information that was desired was the concentration, or surface density of the peptides present on the surface. Surface concentrations of peptide were measured with XPS (see Section 5.2.2), SIMS (see Section 5.5.3), colorimetric dyes (see Section 5.2.1), and radioactive peptides (see Section 4.2.3). Changes in surface wettability due to the presence of peptides were measured by contact angles (see Section 5.4.2).

The third level of information that was desired was whether or not the peptides were available for interaction with cells and whether or not they were biologically active. These studies were necessary because processing steps might damage the peptides or portions of the peptides which are necessary to elicit proper cell responses. In addition, the RGD segment of the peptide might not be accessible to the cells if processing of the polymer into films results in surface roughness that prevents cells from approaching the immobilized peptides. Bovine aortic endothelial cells were used to determine the accessibility of the peptides attached to the polymer surface. The biological activity of the peptides was measured by cell spreading assays (see Section 6.2.2).

5.1.2 Sensitivity Analysis

In order to maximize productivity and focus the research efforts on the surface analysis methods which would yield the most reliable data, a preliminary sensitivity analysis of the various techniques was conducted based on theoretical limits reported in the literature. Table 5.2 summarizes the information which was required to make the calculations which led to the results that are shown graphically in Figure 5.2.

Table 5.2
Sensitivity Data

Technique	Entity Detected	Moles Detectable	* Weight	† Area	† Depth	¥ Volume
^{1}H NMR	Protons from lysine	680 nmol	20 mg	N.A.	N.A.	0.5 ml
	Protons from peptides	176 nmol				
EA	Elements (i.e. iodine)	787 pmol	5 mg	N.A.	N.A.	N.A.
AAA	Amino acids	100 pmol	5 mg	N.A.	N.A.	5 ml
Antibodies	epitopes on the peptide	88 pmol	50 ng	N.A.	N.A.	0.01 ml
XPS	electrons	103 fmol	10 mg	.5 mm^2	30 Å	N.A.
Fluor.	light from Calcein	5 fmol	1 mg	N.A.	N.A.	0.5 ml
	light from CBQCA	13 µmol				
SIMS	ions, fragments, molecules	1.6 fmol	10 mg	.1 cm^2	10 Å	N.A.
Radiation: ^{125}I	g-rays from labeled peptides	4.5 fmol	3 pg	N.A.	N.A.	N.A.
Radiation: ^{3}H	b particles from labeled peptides	1.1 fmol	0.6 pg	N.A.	N.A.	N.A.
Color: Ninhydrin	absorbance due to molecule attached to amine	470 pmol	266 ng	N.A.	N.A.	0.5 ml
Color: Sulfo-SDTB	absorbance due to molecule attached to amine	802 pmol	450 ng	N.A.	N.A.	0.5 ml

Table 5.2: Sensitivity analysis of a variety of surface analytical techniques.
* Weight designates how much material is needed to conduct an analysis.
† Area and depth are the surface dimensions examined during analysis.
¥ Volume is the working volume if the test is done with the material in solution.
N.A. = Not applicable

Figure 5.2
Relative Sensitivities of the Detection Methods

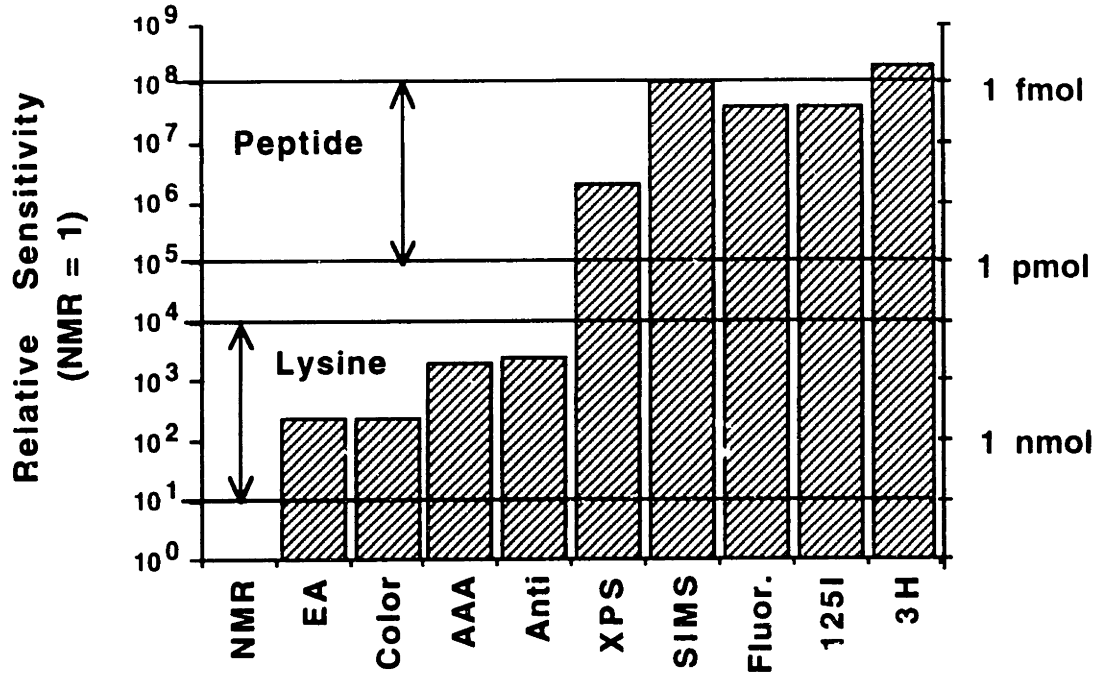

Figure 5.2. This figure shows the relative sensitivities of the various techniques that were considered for use in the surface characterization studies. On the left axis is the relative sensitivity of the technique scaled to ^{1}H-NMR. On the right axis is the actual amount of lysine or peptide that could be detected. The ranges of interest for lysine and peptides are shown on the graph.

This sensitivity analysis resulted in the submission of only the minimal number of samples to the least sensitive techniques, preserving most of the samples for the more sensitive techniques. Since the sensitivity of the various methods for detecting NH_2 groups and peptides was predicted to be critical to the success of the technique, this analysis also led to the development of ideas of how to modify the peptides to make the signals stronger, where necessary, in each of the techniques. Details of the sensitivity analysis for each method are given in the sections of this chapter.

^{1}H NMR

^{1}H NMR is one of the methods which has been routinely used to monitor the bulk composition of PLAL before and after deprotection of the ε-amino side group. When performing ^{1}H NMR, the polymer powder is dissolved in a

deuterated solvent, normally DMF-d_7. The relative peak heights of the benzene-ring protons to the methyne protons are used to calculate the lysine content. The accuracy of ^1H NMR for detecting lysine is limited by the fact that the peaks are relative to one another. The lower limit of detection for lysine units is 0.5% lysine as compared to lactic acid units. In absolute terms, because 20 mg of polymer is needed to properly characterize the lysine content, the sensitivity of this technique is on the order of 680 nmol for lysine or 176 nmol for the peptide.

Elemental Analysis

Determination of the carbon, nitrogen, and oxygen contents of an organic compound by the Kjedahl method requires that 5 mg of material be tested. Sensitivity of this technique is 0.5% of the total elemental composition. Other techniques (chemical methods) can be used to improve the sensitivity of elemental analysis to 0.1 ppm, but they require 1 g of material (personal communication, Galbraith Labs). For practical analysis, no more than 20 mg can be submitted, which limits the sensitivity to 20 ppm. This corresponds, in the case of iodine, to 787 pmol.

Amino Acid Analysis

This analysis is performed by dissolving a sample in methylene chloride, hydrolyzing a known concentration in 6N HCl for 24 hours, then determining the concentration of each amino acid by HPLC, using UV absorption to detect the various amino acids. Due to the chemical structure of the amino acids, each one is known to elute from the column at different time points. Standards containing 500 pmol of each amino acid are used to calibrate the instrument. Unknowns are quantified by comparing the peak height at the same elution time as the standards. Normally 5 mg of material is dissolved in 5 ml of solvent and delivered to the Biopolymers Lab. From this, 120 µl are withdrawn for analysis. The lower limit to the detection of peptides by this method is 100 pmol (personal communication, MIT Biopolymers Lab).

Antibodies

In typical experiments, no less than 50 ng of antigen are deposited (by physical adsorption from aqueous solution) into each well of a 96 well plate (Dr. Janaki Blum, personal communication). This corresponds to 88 pmol of peptide.

X-ray Photoelectron Spectroscopy

Normal XPS analysis yields information in which an element that is present at 1% is detectable (1), but the error in this value is ± 0.5%. The sensitivity of XPS can be increased by using chemical derivitization methods (1). Sensitivities of 0.1 atomic % can be obtained with these methods. In addition, the sensitivity of XPS can be increased by using angular-resolved methods (4). Calculating the amount of nitrogen that is needed to produce 0.1 atomic % gives 103 fmol as the lowest amount that could be detected.

Secondary Ion Mass Spectroscopy

The theoretical sensitivity of SIMS has been calculated to be 1×10^{10} atoms/cm^2 for magnesium as a contaminant on silicon wafers (5). The diameter of the spot analyzed during SIMS studies ranges from 500 Å to 1 μm. In static SIMS, the size of the sample to be analyzed can be 0.1 to 0.3 cm^2. Normal sensitivity for detection of peptides is low because some peptide fragments have the same mass as fragments of the polymer. The sensitivity of SIMS can be increased by incorporating a marker into the peptide. The marker used in the studies described in this report was iodine.

Fluorescence

In routine work on a spectrofluorometer (SPEX Fluorolog-2) in Jim Weaver's lab at MIT, calcein can be measured at concentrations as low as 10 pmol/L. Claims by the inventors of 3-(4-carboxy-benzoyl)-2-quinoline-carboxaldehyde (CBQCA) (6, 7), which is a compound that has been developed to detect amino acids at attomol (10^{-18} mol/L) quantities, led us to try the reaction with the available equipment. In our reaction, glycine was dissolved in water and the CBQCA reagents were added. The lowest concentration which produced a measurable signal was 1 mg/ml, which corresponded to 13.3 μmol in the 1 ml of sample, or if it is assumed that the signal came from only 10 μl of the sample, then 133 nmol were detected.

Colorimetric Assays

Two methods were investigated. The first involved the use of ninhydrin, which reacts with amines on surfaces. Reliable UV/VIS measurements were obtained for the standards down to 0.03 mg/ml. It may be possible to dilute the

standards a factor of 5 more and still obtain reliable results, which would make it possible to detect approximately 470 pmol of material.

The second method involved using sulfo-SDTB, which also reacts with amines on the surface. This reagent forms a compound which is then removed by perchloric acid to form a colored solution. The lowest level of detection of this compound was 100 pmol.

Radiolabeled peptides

The radiolabeling of peptides would be expected to yield the most sensitive detection. The choice is between ^{125}I and ^{3}H labels. These are described separately.

^{125}I-radiolabeled peptides

The theoretical specific activity of ^{125}I is 2000 Ci/mmol, but due to government regulations on the amount of exposure that a radiation worker can get, the practical limit is 10 Ci/mmol. Even this level of exposure poses significant risk to the worker because γ-rays have higher energies than other types of radiation.

At a specific activity of 10 Ci/mmol, 4.5 fmol of radiolabeled peptide would produce 100 cpm.

^{3}H-radiolabelled peptides

Using catalytic reductive tritiation of ^{127}I-labeled peptide to ^{3}H would allow a theoretical limit of 40 Ci/mmol. Routine tritiation procedures done at NEN, DuPont have produced 1 Ci/mmol specific activities. One fmol of tritiated peptide at 40 Ci/mmol would produce 100 dpm on the scintillation counter. If the specific activity is 1 Ci/mmol, then 40 fmol would be needed to produce a signal well above background.

Summary of Sensitivity Analysis

The sensitivity analysis was very helpful in focusing the research efforts on the most sensitive techniques. From the results of these initial calculations, XPS, ^{125}I-labeled peptides, and colorimetric dyes were chosen as the main techniques to characterize this system. Most of the samples which were prepared were analyzed by one of these three techniques. Comparatively few samples

were analyzed by contact angles, static SIMS, antibody tests, FTIR, amino acid analysis, fluorescent dyes, or elemental analysis.

5.2 *Measurement of Surface Amino Group Densities*

Two methods were used to measure surface amino group densities: colorimetric methods and X-ray photoelectron spectroscopy (XPS).

Many colorimetric reagents are available to probe surfaces for amino groups. One of the traditional methods consists of using ninhydrin. Recently, Ngo reported the use of Traut's and Ellman's reagents to react with amino groups and concurrently introduce free sulfhydryl groups, which are then colorimetrically titrated (8). Another relatively new technique was described by Gaur, who developed a method for using N-succinimidyl-4-O-(4,4'-dimethoxytrityl)-butyrate (sulfo-SDTB) to detect amines on surfaces of polymers (9). This reaction forms a new chemical entity on the surface. After removal of excess, non-reacted reagents, the leaving group is cleaved by perchloric acid. The amino groups that are detected by this method are those which are accessible to the reagents only.

X-ray Photoelectron Spectoscopy (XPS), which is also known as Electron Spectroscopy for Chemical Analysis (ESCA) uses X-rays to bombard a surface and a detector which measures the binding energies of the secondary electrons released from the surface. The binding energies of the electrons knocked out of the sample are characteristic of the elements from which they are released, and since the X-rays penetrate only 10-100 Å into the surface, the elemental composition of the surface can be determined.

Several review articles on the use of XPS for analyzing biomaterial polymers have been published in the last 5 years (10, 11). In general, recent studies seem to have focused on 3 areas of research: the changes that occur when samples are exposed to water, the correlation of surface properties with biological events, and the use of derivitization methods to enhance the information that is available from studying the surface. These subjects are dealt with in more detail in the next three sections. In addition, specific information on PLA was found in the literature. For example, Briggs reported that the C_{1s} binding energies of PLA are 285.0 for <u>C</u>Hx, 286.98 for <u>C</u>OC=O, and 289.06 for <u>C</u>(=O)O (12).

The use of XPS for studying polymers exposed to water

To prove that surfaces change after soaking, Wang, *et.al.* investigated the surface dynamics of poly(ethylene teraphthalate) (PET) upon heating samples in air and soaking samples in water for one hour (13). The angle-resolved XPS data showed that the surface concentrations of all the species dropped. These results support the hypothesis that fluorine-based functional groups in the surface region migrate mainly toward the bulk from the surface when exposed to water.

Lewis and Ratner developed a method to investigate the nature of biomaterial surfaces which are designed to be in contact with an aqueous environment (14). Their approach consisted of a seven step protocol in which the samples were 1. hydrated, 2. mounted in the first chamber while still wet, 3. frozen (3-8 min, -40 to -80°C), 4. dried for 1/2 to 2 hr., 5. transferred to the analysis chamber (-120°C analysis), 6. returned to the first chamber and warmed to room temperature, and 7. re-analyzed at -120°C. Several copolymers and PDMS contaminated polymers were examined using this protocol and it was found that measurable surface enrichment and decreases in PDMS due to hydrolysis were detectable.

Correlation of surface compositions with biological events

Sawada, *et. al.* studied the relationship between bulk hydroxyl and surface oxygen content and the effect of these chemical entities on interactions of serum with polymers (15). Serum interactions with various polymeric materials showed greater correlation with surface oxygen content than with bulk hydroxyl content, suggesting that it is the surface that determines the result of biological interactions with a biomaterial.

The XPS analysis of polyurethanes with covalently grafted RGD-peptides was performed by Lin, *et. al.* (16). In these studies, peptides were attached in bulk and then these modified polymers were coated onto glass coverslips for analysis. Although the elemental surface contents of the samples were always below the theoretical stoichiometric values, increases in peptide density reflected increases in the amount of grafted peptide.

The use of derivitization methods

Derivitization methods using trifluoroacetic anhydride (17) and pentafluorobenzaldehyde (18) have been described. The features of a good label have also been described. They are: the label must contain a unique atom, the

label must be specific to the functional group of interest and react quantitatively, and the labeling process should not disrupt the surface.

5.2.1 Colorimetric Methods

In these studies, PLAL:PLA blends were created using low molecular weight PLAL (3000 to 5000 g/mol) and PLA with molecular weights of approximately 50, 100, 200 and 300,000 g/mol. The blending method involved weighing out various amounts of PLAL (10 to 90 mg) in a 10 ml beaker, adding corresponding amounts of PLA for a final weight of 100 mg, and dissolving the polymers in 2 ml of chloroform ($CHCl_3$). The solvent was allowed to evaporate over the course of 24 to 72 hours on a level support in the chemical fume hood. During evaporation, the samples were covered with a recrystallization dish to prevent contamination and to slow down the evaporation rate. After the solvent was evaporated, the samples were transferred to clean vials, placed under high vacuum for a minimum of twenty-four hours to remove any residual solvent, and further analyzed for proper formation and stability. The blends were cut into four relatively equal pieces with a sterile scalpel blade. The surface areas of these four pieces were determined by tracing around the samples onto a piece of paper and using a ruler to measure the dimensions of the samples.

The purpose of these experiments was twofold: first, to prepare samples which varied in lysine content; and second, to measure in real numbers the available amine content of those surfaces. The sulfo-SDTB reaction was used to investigate the amine content of the PLAL blends. The effect of processing on the surface content of available amines was elucidated by this technique. Sulfo-SDTB was obtained from Pierce. Stock solution was prepared using 11.2 mg of sulfo-SDTB dissolved in 0.5 ml dimethylformamide (DMF, Aldrich) and 4 ml sodium bicarbonate buffer (420 mg sodium bicarbonate [molecular weight = 84.01 g/mol, Mallinckrodt] dissolved in 100 ml distilled water). From the stock solution, eight standards were prepared by serial dilution which produced a calibration curve for amino group concentration. In the first tube, 0.02 ml of stock solution was added to 2 ml of 35% perchloric acid solution (50 ml 70% perchloric acid and 50 ml distilled water). The final result was an amino group concentration of approximately 41 nmol/ml (4.1×10^{-8} mol/ml). Two ml of the solution in the first tube were then added to 2 ml of 35% perchloric acid (Mallinckrodt) solution in a second sterile tube, resulting in an amino group concentration of half the original first tube concentration (21 nmol/ml). In a

similar manner, dilutions were prepared up to 1/128 of the original concentration (0.33 nmol/ml). Absorbance readings were taken at a wavelength of 498 nm using a UV/Vis spectrophotometer (Perkin Elmer) zeroed with a cuvette containing 1 ml of 35% perchloric acid solution. All absorbance samples had a volume of 1 ml from an original reaction volume of 2 ml. For the PLAL:PLA blends, the blend quarters were soaked in stock solution for 10 min. The blends were then rinsed with 1 ml distilled water using a pipette and soaked in 10 ml distilled water for an additional ten minutes. At this point, the blends were placed in 2 ml of 35% perchloric acid solution for approximately 10 minutes, upon which an orange color developed, indicating the presence of amino groups. One ml of the sample was transferred to a cuvette, and the absorbance was read at 498 nm. This procedure was also performed on a 100% PLA sample and blends of protected PLAL:PLA as controls. Figure 5.3 summarizes the reaction scheme for these experiments.

Figure 5.3
Sulfo-SDTB Colorimetric Assay Reaction Scheme

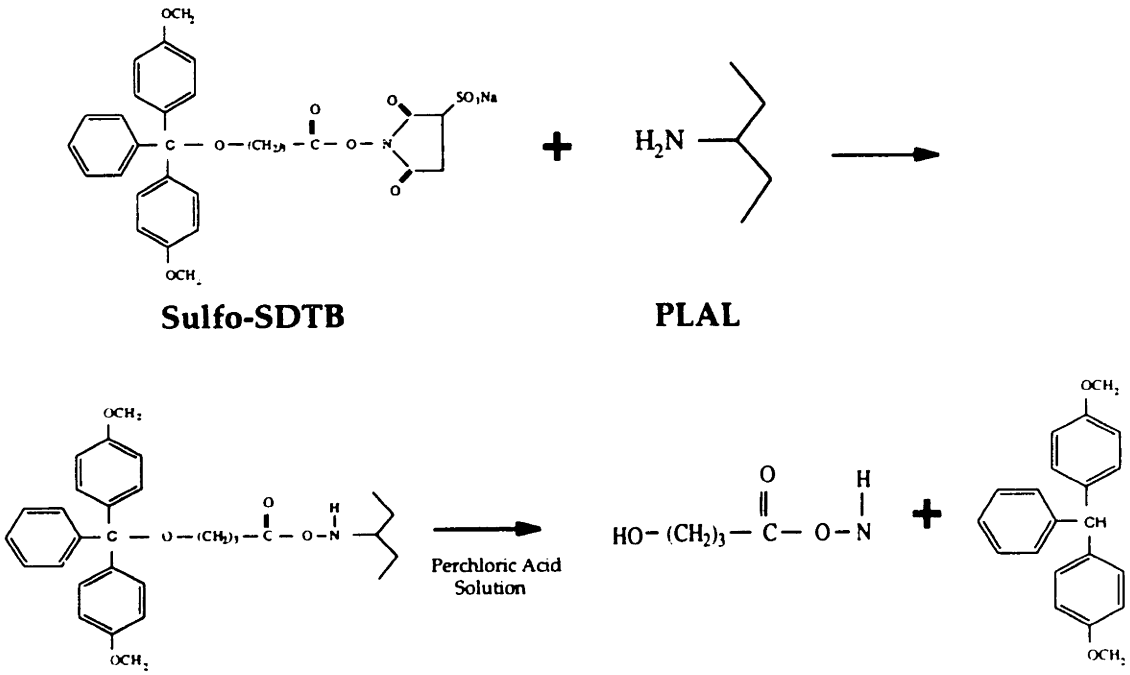

Figure 5.3: Sulfo-SDTB reacts with amino groups on PLAL to form a stable compound. Excess reagents are rinsed from the polymer, and a perchloric acid solution is used to release the dimethoxytrityl cation from the polymer, which is detected at 498 nm.

Figure 5.4 is a representative calibration curve. The detectable range of amino groups was from 0.33 to 41 nmol/cm^2. The apparent [NH_2] surface concentration in terms of nmol/cm^2 was calculated from the equation for the standard curve and the OD_{498} readings for the various PLAL/PLA blends. Variation in size of the blend quarters was taken into account and background PLA contributions were subtracted. Figure 5.5 is a representative plot of the relationship between apparent surface amine concentration and bulk PLAL content.

Greater concentrations of PLAL in the blends produced a corresponding increase in the amino group surface concentration, as hypothesized. This experiment was repeated 14 times and in each case the results were similar. Table 5.3 is a summary of the results on the different samples. PLAL was blended with PLA of higher and lower molecular weights in order to assess the possibility of extending the range of NH_2 surface concentrations and the strength of the resulting blends. Due to day to day variations in the colorimetric assay, and true variations in the surface content of the blends themselves, a distribution of surface contents was found.

Figure 5.4
Typical Standard Curve

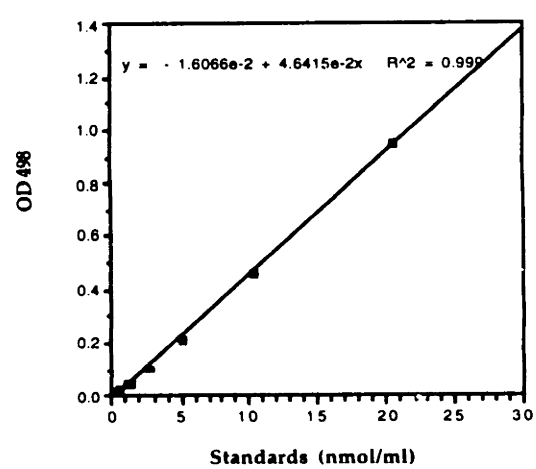

Figure 5.4: Standard curve for sulfo-SDTB reaction. (N=1, n=2, Data are Ave. ± S.D., Error bars are smaller than the symbols.)

Figure 5.6 is a plot of the average results for the PLAL:PLA 100 samples conducted over a 3 month period. The error bars represent the standard deviation of all the data for this time period. The large error bars can be attributed to variations in the actual surface concentrations of lysine and not to experimental error, since the standard deviations of the data within experiments were always similar to those shown in Figure 5.5.

Table 5.3
Summary of sulfo-SDTB Experiments

Sample	OD 498 (Mean ± S.D.)	Apparent [NH_2] ($nmol/cm^2$) (Mean ± S.D.)	App [NH_2] - PLA ($nmol/cm^2$) (Mean ± S.D.)
PLA (N=12, n=28)	0.118 ± 0.083	0.78 ± 0.55	-
PLAL Protected			
10:90 (N=4, n=8)	0.202 ± 0.109	1.25 ± 0.65	0.29 ± 0.70
20:80 (N=4, n=8)	0.182 ± 0.122	1.30 ± 0.77	0.34 ± 0.60
30:70 (N=4, n=8)	0.209 ± 0.091	1.36 ± 0.53	0.40 ± 0.40
40:60 (N=4, n=8)	0.248 ± 0.274	1.39 ± 1.03	0.43 ± 1.34
50:50 (N=3, n=6)	0.185 ± 0.116	1.53 ± 1.24	0.72 ± 1.01
PLAL:PLA Blends			
50,000 MW PLA			
10:90 (N=1, n=2)	0.320 ± 0.011	1.87 ± 0.02	0.47 ± 0.02
20:80 (N=1, n=2)	0.302 ± 0.037	1.88 ± 0.38	0.48 ± 0.38
30:70 (N=1, n=2)	0.224 ± 0.013	1.81 ± 0.29	0.41 ± 0.29
100,000 MW PLA			
10:90 (N=6, n=11)	0.136 ± 0.071	1.06 ± 0.50	0.23 ± 0.46
20:80 (N=6, n=11)	0.184 ± 0.085	1.40 ± 0.61	0.57 ± 0.47
30:70 (N=6, n=11)	0.227 ± 0.080	1.62 ± 0.70	0.78 ± 0.55
40:60 (N=6, n=11)	0.257 ± 0.107	1.94 ± 0.78	1.10 ± 0.66
50:50 (N=6, n=10)	0.283 ± 0.102	2.30 ± 1.02	1.45 ± 0.85
200,000 MW PLA			
10:90 (N=2, n=8)	0.199 ± 0.091	1.09 ± 0.49	0.50 ± 0.52
20:80 (N=2, n=8)	0.212 ± 0.071	1.24 ± 0.55	0.65 ± 0.60
30:70 (N=2, n=8)	0.277 ± 0.067	1.52 ± 0.38	0.92 ± .032
40:60 (N=2, n=7)	0.308 ± 0.036	1.69 ± 0.29	1.13 ± 0.23
60:40 (N=2, n=7)	0.243 ± 0.054	1.98 ± 0.44	1.41 ± 0.32
70:30 (N=1, n=2)	0.205 ± 0.006	2.49 ± 0.40	1.73 ± 0.40
300,000 MW PLA			
10:90 (N=1, n=3)	0.065 ± 0.008	0.56 ± 0.06	0.11 ± 0.06
20:80 (N=1, n=3)	0.076 ± 0.035	0.63 ± 0.23	0.18 ± 0.23
30:70 (N=1, n=3)	0.075 ± 0.006	0.66 ± 0.04	0.21 ± 0.04
40:60 (N=1, n=3)	0.106 ± 0.017	0.88 ± 0.15	0.43 ± 0.15
50:50 (N=1, n=3)	0.148 ± 0.033	1.23 ± 0.20	0.78 ± 0.20
60:40 (N=1, n=3)	0.153 ± 0.062	1.33 ± 0.53	0.88 ± 0.53
70:30 (N=1, n=1)	0.184	1.46	1.01

Figure 5.5
Representative Results of Sulfo-SDTB Assay

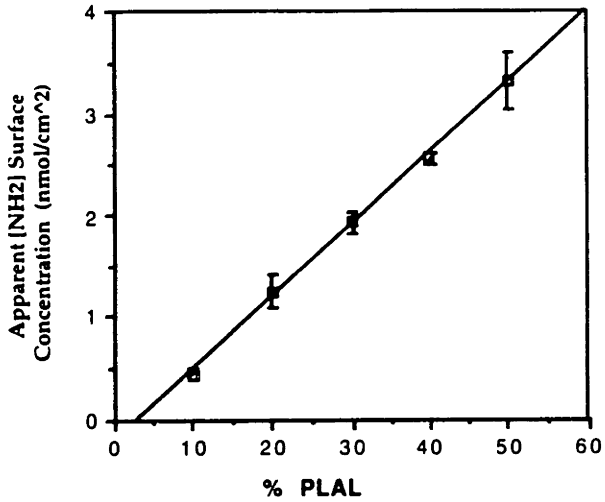

Figure 5.5: Results of the sulfo-SDTB assay. (N=1, n=2, data are Ave. ± S.D.)

Figure 5.6
Average Results of PLAL blends with 100,000 M.W. PLA

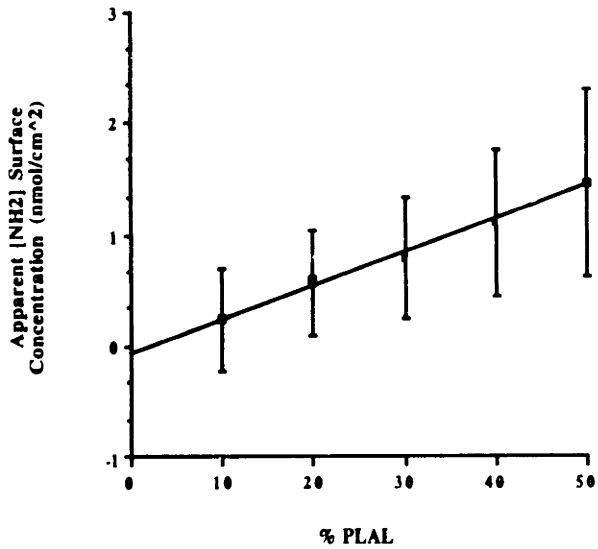

Figure 5.6: Average results of sulfo-SDTB assay on samples of PLAL:PLA. Data are Ave. ± S.D. (N=6, n=11)

In absolute terms, the surface content of amino groups that was determined by the sulfo-SDTB assay was higher than predicted by theoretical calculations based on the amount of lysine that was measured by ^{1}H-NMR in the PLAL copolymer. In order to determine if the excess was due to a competing reaction or simply due to non-specific adsorption of the reagent to the PLA surface, PLAL that had not been deprotected was blended with PLA. The results of these experiments are shown in Figure 5.7 compared to the results of the 100,000 MW PLA blends. Only the averages are shown, to illustrate that the slopes are different.

Figure 5.7
PLAL vs. Protected PLAL Blends

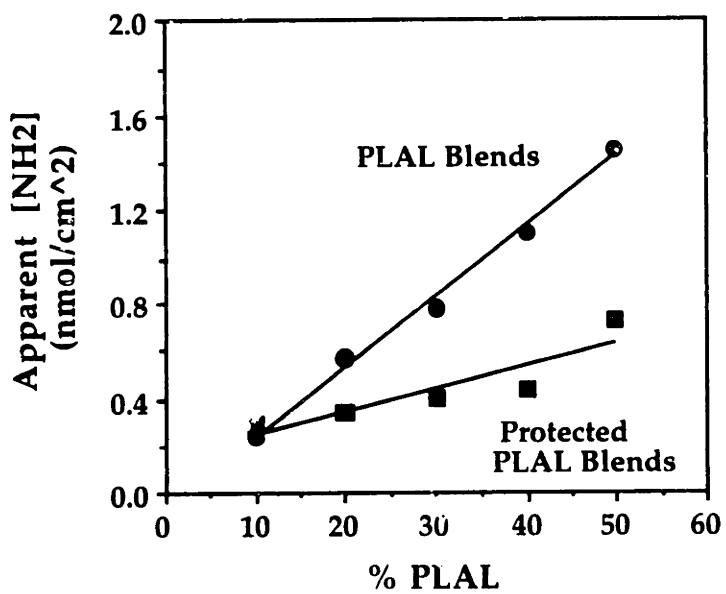

Two different types of analyses were performed on the data listed in Table 5.3. The first analysis was done to determine whether or not the data determined from the blends was statistically significant compared to the contribution from PLA controls. Student's t test was used with the test statistic (T') and degrees of freedom (n) for population means which are unequal and unknown. A one-tailed test using alpha = 0.05 was performed. The data in column 3 of Table 5.3 was used to conduct this analysis. The average and standard deviation of each type of sample was compared to the average and standard deviation of the PLA controls. The results of this analysis are shown in Table 5.4.

Table 5.4
Statistical Analysis of sulfo-SDTB Results

Sample	T'	ν	$-t_{0.05}$	Significant?
PLAL prot				
10	-1.86	10	-1.812	Yes
20	-1.78	9	-1.833	No
30	-2.71	11	-1.796	Yes
40	-1.61	8	-1.860	No
50	-1.45	5	-2.015	No
PLA 50				
10	-10.39	27	-1.703	Yes
20	-3.82	1	-6.314	No
30	-4.48	1	-6.314	No
PLA 100				
10	-1.53	20	-1.725	No
20	-2.93	16	-1.746	Yes
30	-3.57	15	-1.753	Yes
40	-4.51	14	-1.761	Yes
50	-4.49	10	-1.812	Yes
PLA 200				
10	-1.53	12	-1.782	No
20	-2.09	11	-1.796	Yes
30	-4.36	16	-1.746	Yes
40	-6.02	18	-1.734	Yes
60	-6.12	11	-1.796	Yes
70	-5.67	1	-6.314	No
PLA 300				
10	2.01	28	-1.701	No
20	0.89	5	-2.015	No
30	1.13	28	-1.701	No
40	-0.74	10	-1.812	No
50	-2.9	6	-1.943	Yes
60	-1.7	2	-2.920	No
70	N/A	N/A	N/A	N/A

Table 5.4: Results of statistical analysis of the data in Table 5.3, using Student's t-test. The last column indicates whether or not the average was significantly higher (0.05 level of significance) than PLA.

One can infer from the results shown in Table 5.4 that for those samples which are listed as "Yes" under the column heading "Significant", the apparent surface concentration of amino groups is significantly higher (0.05 level of significance) than on PLA controls. For the protected PLAL samples, 3 out 5 of the samples did not produce significantly higher amino group concentrations. On the PLA 100,000 and 200,000 blends, 8 out of 11 sample types did produce significantly higher amino group concentrations. Of the 3 types of samples that did not show a significant difference, 1 was a 10% PLAL blend, 1 was a 20% blend and the other was a 70% blend that only had 2 samples in the data set. On the PLA 50,000 and 300,000 blends, only 2 out of 10 sample types were significantly higher in amino groups, but this result can be attributed to the low number of samples tested. For the most part, this analysis supports the hypothesis that there was a significant difference in amino group concentration detected on the blends vs. the PLA controls.

The second test that was performed was a test of the slope of the least squares curve fit of each type of blends to determine if there was a linear relationship between the amount of PLAL incorporated into the sample and the amino group concentration as determined by the sulfo-SDTB reaction. The null hypothesis in this test was that the slope of the line was equal to zero. The alternative hypothesis was that the slope was greater than zero. Student's t test was performed using the test statistic (T) and the degrees of freedom (v):

$$T = \frac{b_1 \sqrt{S_x}}{\sqrt{n\, s^2}} \qquad\qquad v = n - 2$$

A one-tailed test using alpha = 0.05 was conducted on the averages shown in the third column of Table 5.3 vs. % PLAL from the first column. The results of this analysis are shown in Table 5.5. This analysis permits one to infer that there is a direct correlation (0.05 level of significance) between the amount of PLAL that is incorporated into the blends (except for the 50,000 MW blends) and the number of amino groups present on the surface.

Table 5.5
Analysis of Slopes

Sample	Slope	R^2	T	ν	$t_{0.05}$	Significant?
Prot.	.0095	.802	3.49	3	2.35	Yes
50	-.003	.628	-1.3	1	6.31	No
100	.0297	.994	22.49	3	2.35	Yes
200	.0199	.989	18.7	4	2.13	Yes
300	.0167	.944	9.19	5	2.02	Yes

Table 5.5: Statistical analysis of slopes. The last column indicates whether or not a significant linear relationship exists between the bulk amount of PLAL and the surface NH_2 concentration.

From the results of these colorimetric assays, two important conclusions can be drawn. First, it is possible to vary the lysine content of the surfaces of PLAL:PLA blends by varying the amount of PLAL used. Second, the surface concentrations of NH_2 groups can be measured and small differences between samples can be distinguished. This is an important measurement in order to explain the results of the reactions involved in attaching peptides to the polymer blends.

While the results show that the surface is directly influenced by the bulk, there are three different ways that the sulfo-SDTB reagents interact with the sample surface. Some of the sulfo-SDTB molecules interact non-specifically with PLA, some molecules react specifically to the free ε-amines of PLAL, and some of the molecules interact with PLAL that has the free ε-amines blocked from reacting further. After taking into account day-to-day variations in the reaction conditions and differences in sample size, the results for the sulfo-SDTB reaction are reported in terms of $nmol/cm^2$. The day-to-day variations were taken into account by using daily calibration curves. The differences in sample size were accounted for by measuring the dimensions of each film and adjusting for differences in surface area. These results are denoted as the apparent surface concentration of NH_2 groups because of the non-specific contributions described above. The expected surface concentrations of NH_2 groups are much lower based on calculations from bulk NMR and AAA data. Assuming that the PLAL polymer is 1% lysine, that the surface is representative of the bulk, and that the

sulfo-SDTB only can access the top 10 Å of the surface, then the expected surface concentrations of the blends are shown in column 3 of Table 5.6.

Table 5.6
Comparison of Expected and Measured NH_2 Concentration

PLAL Content (%)	Bulk Concentration (μmol/g)	Expected Surface NH_2 Concentration ($pmol/cm^2$)	Measured Surface NH_2 Concentration ($pmol/cm^2$)
10	13.8	1.4	230 ± 460
20	27.6	2.8	570 ± 470
30	41.4	4.1	780 ± 550
40	55.2	5.5	1100 ± 660
50	69	6.9	1450 ± 850

Table 5.6: The bulk concentration of PLAL is based on a 1% lysine polymer. The expected surface NH_2 concentration is calculated from the bulk concentration. This is compared to the measured surface concentration for the 100,000 MW samples from Table 5.3.

There are three possible explanations for the discrepancy between the expected surface concentrations and the measured surface concentrations of NH_2. The surface could be enriched in lysine, or the reaction could be overestimating the surface concentration due to cross-reaction with the PLA and PLAL, or the reagents could be penetrating much farther than 10 Å into the surface. It could also be possible that the act of blending disrupts the crystallinity of the film and that amorphous sections respond differently to the sulfo-SDTB and perchloric acid chemistry than crystalline regions. This was checked by determining the crystallinity of the blends by DSC (see Section 3.4.3). It was found that the incorporation of the PLAL+GRGDY-I2 polymer into the blends did not significantly alter the crystallinity.

A different reaction which could be conducted consists of using Dinitrofluorobenzene (DNFB). This reagent would form a bond with the amino groups of the lysine that upon exposure to slightly basic conditions would be more stable than the lactic acid-lysine bond of the polymer backbone. After hydrolysis, the products could be separated and quantified using HPLC and commercially available standards. The results of this analysis would allow one to distinguish between specifically bound DNFB and reacted DNFB because the

excess, non-reacted DNFB would be converted to dinitrophenol (DNP) upon exposure to NaOH. The DNP-Lysine product would be able to be separated from the lactic acid component and quantified using HPLC.

5.2.2 XPS Analysis

The majority of the XPS analysis which was conducted was on samples with iodine-labeled peptides attached. The information that was acquired was used to calculate the surface densities of both lysine and peptides. Those data are reported in section 5.3. The data that are reported here were preliminary data which were acquired prior to the use of the iodine-labeled peptide. These data demonstrated that nitrogen groups could be detected on the surface of PLAL samples.

Several samples were analyzed by XPS in order to characterize the surfaces of the PLAL films. XPS studies were conducted at the Spectroscopy Facilities of Harvard University using a Surface Sciences SSX-100 spectrometer and at the University of Washington in Seattle using a modified version of the same spectrometer. Elemental compositions of the polymer surfaces were calculated from the XPS data. Initial studies demonstrated a segregation of lysine and silicon-containing contaminants to the glass-contacting side (bottom) and air-exposed side (top) of the samples, respectively (see Table 5.8). The effect of soaking was investigated, as was the use of pentafluorobenzaldehyde (PFBA) to increase the sensitivity of the lysine measurements. The results are compared to the expected values, which were determined from theoretical stoichiometric ratios.

Preliminary study

A summary of the results of the first study is shown in Table 5.7. Percent nitrogen was based on a ratio of carbon to nitrogen within the sample, disregarding the other elements present. The best result from this analysis was that nitrogen was detected at the surface of the PLAL and peptide-containing polymers, indicating that there were lysine groups and/or peptides present within the top 30 Å of the surface. Nitrogen was not detected in the PLAL-GRGDY (sputtered) sample, which was presumably an attempt to measure the elemental composition between 30 and 100 Å. This observation was unexpected. From these measurements, it was not possible to distinguish the lysine from the peptides, since both contain nitrogen.

Table 5.7
XPS Results

Sample	Theoretical %N	Actual %N	Contaminant
PLA	0	0	-
PLAL	1.6	4	-
PLAL-GRGDY (air side)	2.5	1	Si
PLAL-GRGDY (glass side)	2.5	2	Si
PLAL-GRGDY (sputtered)	2.5	0	S, Cl
GRGDY (powder)	26	23	Si, F

Table 5.7: Preliminary evidence to demonstrate the feasibility of measuring nitrogen on the surfaces cf PLAL and PLAL+GRGDY samples.

Evidence for species segregation in PLAL

This set of XPS studies were performed at the University of Washington in Seattle. The results of these studies are shown in Table 5.8. In this study, it was found that the air-exposed side and the glass-contacting side of the thicker PLAL films produced surfaces which contained very different nitrogen contents. In addition, silicon contamination, which was presumed to be from vacuum grease (polydimethyl siloxane), was found in greater quantities on the side of the polymer exposed to air during casting than on the glass contacting side. One possible explanation for this is that during the long, slow solvent-casting process the bottom of the film which is in contact with the glass beaker attracts the hydrophilic lysine groups, while the chloroform, which is evaporating off the top pulls most of the vacuum grease with it to the top, air-exposed side of the film. As the solvent evaporates, it leaves the vacuum grease (polydimethyl siloxane) behind.

A follow-up study was conducted on the same batch of polymer to determine if this effect was reproducible. Table 5.9 contains the results of this study. This study was done at the University of Washington in Seattle and confirmed their earlier finding that the air-exposed and glass-contacting sides of the polymer film contained very different amounts of nitrogen and silicon grease contamination. The conclusion that can be drawn from these studies is that the method of processing greatly effects the resulting surface. PLAL is a material that apparently permits great variations in surface properties due to the environmental history of the material.

Table 5.8
Evidence for Species Segregation
(100 mg films cast on glass)

Sample	Side	PFBA	%C	%O	%N	%F	%Si
PLA							
Expected:			60	40	0	0	0
	Air	No	63.5	34.9	n.d.	n.d.	1.2
	Glass	No	64.8	34.6	n.d.	n.d.	0.6
Expected:			60	40	0	0	0
	Air	Yes	64.1	35.9	n.d.	n.d.	n.d.
	Glass	Yes	65.4	34.6	n.d.	n.d.	n.d.
PLAL							
Expected:			60	39	1	0	0
	Air	No	54.2	24.5	n.d.	n.d.	**21.4†**
	Glass	No	77.6	19.2	**2.2***	n.d.	1.1
Expected:			59.9	36.8	1	2.3	0
	Air	Yes	59.4	21.8	n.d.	**1.5‡**	**17.4†**
	Glass	Yes	62.9	33.6	**1.8***	**1.6‡**	n.d.

Table 5.8: Analysis of silicon-contaminated PLAL samples produced the first evidence of species segregation within the polymer. Source: Barrera, D. A., Ph. D. Thesis, MIT, p. 101, Data from University of Washington, Seattle., n.d. = not detected
* Nitrogen was only detected on the glass-contacting side
† Silicon was detected in high concentrations on the air-exposed side
‡ Fluorine was only detected after exposure to PFBA, and only on PLAL

Table 5.9
Evidence for Species Segregation: Follow-up Study
(PLAL sample, 56 mg cast on glass)

Surface	%C	%O	%N	%Si
Expected:	60.0	39.0	1.0	0
Air	55.4	27.0	n.d.	17.7
Glass	60.1	37.6	2.3	n.d.

Table 5.9: Confirming evidence of species segregation within the solvent-cast films of PLAL. Source: Winblade, N., "Varying silicon contamination of Poly(lactic acid-*co*-lysine)", Univ. of Wash., Seattle, pp. A5, A11

The effect of soaking on PLAL surfaces

Due to the biodegradable nature of PLA and PLAL, some studies were done to elucidate the effect of soaking on the nature of the surfaces. There were two kinds of measurements that were desired. First, we wanted to determine if changes in nitrogen could be detected, indicating a preferential decrease in surface lysine content of the PLAL samples. Second, could changes in silicon concentration be detected, indicating a disappearance of contaminants over time? The results of these studies are shown in Table 5.10. In this experiment the samples were prepared by spray-coating glass coverslips with a thin layer of the polymer samples. Two types of samples were examined: the first was PLAL with GRGDY peptides attached by bulk CDI chemistry, the second was PLAL with bulk-attached GRGEY control peptides. The samples were left attached to the glass coverslips and soaked in water for 0, 4, 29 and 124.5 hrs. In all but one instance, the films remained attached to the glass during soaking, so the air-side was examined by XPS. In one case, the glass-contacting side was examined. As can be seen from the data, nitrogen was detected in only 2 cases, which indicates that 1) either it was not present on most of the samples, or 2) it was present at less than 1% and couldn't be resolved from background. These data also demonstrate that apparently there was no measurable effect of soaking on silicon content.

Table 5.10
Effect of Soaking
(Air side, sprayed films)

	PLAL+GRGDY				PLAL+GRGEY			
Time (h)	% C	%O	% N	%Si	%C	%O	%N	%Si
Expected:	60.2	38.2	1.5	0	60.2	38.2	1.5	0
0	61.0	37.6	n.d.	1.4	61.5	38.5	n.d.	n.d.
4	61.3	37.4	n.d.	1.4	69.6	30.4	n.d.	n.d.
29	67.1	29.7	n.d.	3.2	68.8	28.2	3.07	n.d.
124.5	60.6*	36.1*	1.7*	1.6*	69.7	30.3	n.d.	n.d.

Table 5.10: Effect of soaking samples in water on the surface density of peptides. (*these data are from the glass side of the film)

The use of PFBA

The use of derivitization techniques was used to gain an understanding of the quantity of reactive groups present on the surfaces. One of the techniques which we used was to expose the samples to pentafluorobenzaldehyde (PFBA) to amplify the nitrogen signal. Figure 5.8 shows the structure of this molecule.

Figure 5.8
Pentafluorobenzaldehyde

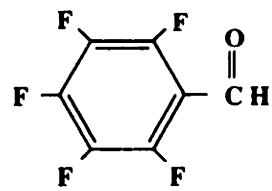

PFBA reacts with free amines, resulting in five fluorine atoms attached to each nitrogen. Since the polymer does not contain any fluorine, the presence of fluorine in the XPS spectra indicates that nitrogen groups are available for reaction at the surface.

In this study, which was performed at Harvard, it was found that nitrogen was not detectable on the air-contacting sides of the thin, sprayed films. The use of PFBA demonstrated in one case that fluorine was detectable at 2.2%, which would indicate that the nitrogen content was approximately 0.44%, since PFBA forms a complex with nitrogen in the ratio of five fluorine atoms to each nitrogen atom (see Table 5.11).

Table 5.11
The Use of PFBA to Detect Lysine
(Air side, solvent-cast & sprayed films)

Sample	%C	%O	%N	%F	%Si
PLA (expected):	60	40	0	0	0
Solvent-cast PLA (control)	60.1	39.9	n.d.	n.d.	n.d
Sprayed PLA (control)	58.8	37.0	n.d.	n.d.	4.2
PLAL+GRGDY (expected):	60.2	38.2	1.5	0	0
Sprayed PLAL+GRGDY	59.3	36.9	n.d.	n.d.	3.0
Sprayed PLAL+GRGEY	67.0	27.8	n.d.	**2.2**	3.1

Table 5.11: Pentafluorobenzaldehyde was used to detect nitrogen on the air-exposed side of sprayed samples. Fluorine was detected on one of the two samples.

An additional study, also performed at Harvard, demonstrated that soaking did not change the nitrogen, or PFBA-detectable nitrogen content of the glass-contacting side of the thin, sprayed samples (see Table 5.12). In this study, the thin, sprayed samples were sprayed a second time with high molecular weight PLA and then peeled off the glass and remounted on glass coverslips so the glass-contacting side could be studied. Samples were soaked in either water or PBS for 1 to 5 days. (The results of Day 1, soaking in PBS which shows 13.6 % F cannot be explained at this time. It is possible that this sample came in contact with a drop of PFBA or a piece of teflon tape which transferred fluorine to the surface of this film.) The lack of detectable nitrogen may indicate that the rapid formation of a film against glass after spraying does not produce the same surface as the slower solvent-casting method.

Table 5.12
Effect of Soaking
(Glass Side, PFBA)

PLAL	Time (d)	% C	% O	%N	%F	%Si
(Expected)		59.9	36.8	1.0	2.3	0
(Water)	1	59.2	35.7	n.d.	n.d.	5.2
	2	59.0	36.9	n.d.	1.3	2.8
	3	58.1	37.1	n.d.	n.d.	4.8
	4	59.7	35.8	n.d.	n.d.	4.5
	5	61.7	38.3	n.d.	n.d.	n.d.
PLAL	Time (d)	% C	% O	%N	%F	%Si
(PBS)	1*	47.1	25.9	n.d.	13.6	7.3
	2	59.9	34.7	n.d.	n.d.	5.4
	3	57.9	36.5	n.d.	n.d.	5.6
	4**	57.0	36.8	n.d.	n.d.	4.1
	5	59.2	35.1	n.d.	1.9	3.9

Table 5.12: The effect of soaking was examined, using PFBA as a probe for nitrogen groups. (*In addition to the elements listed above, 6.0 % Na was detected; ** 2.2 % Cl was detected. These contaminants were from the PBS.)

5.3 *Measurement of Surface Peptide Densities*

5.3.1 *Materials and Methods*

Peptide Synthesis

All peptides were synthesized at the MIT Center for Cancer Research-Howard Hughes Medical Institute, Biopolymers Laboratory on an ABI (Applied Biosystems, Inc.) Model 430A peptide synthesizer using NMP (N-methylpyrrolidone) - HOBT (hydroxybenzotriazole) - tBOC (tert-butyloxycarbonyl) chemistry. Operator manual instructions were followed for chain assembly with double coupling/capping for a 0.5 mMol cycle. All amino acids were obtained from Perkin Elmer-Applied Biosystems Div. with the exception of 3-5 di-iodo Tyrosine, which was obtained from Peninsula Labs. Side chains were protected with OBzl (benzyl) for Aspartate, 3-Br-Bzl (3-bromobenzyl) for 3-5 di-iodo Tyrosine, and Tos (tosyl) for Arginine. The starting resin was 1.0 meq. of p-methyl BHAR (benzhydrylamine resin) and was obtained from ABI. The peptides were cleaved from the resin simultaneously with the removal of side-chain protecting groups by treatment with HF-10% anisole for 30 min. at -10°C, followed by 30 min. at 0°C. The N-α-Boc group was removed prior to cleavage. The crude peptides were washed and precipitated with 3 x 20 ml treatments of -70°C diethyl ether with trace magnesium sulfate ($MgSO_4$) and extracted with 3 x 15 ml aliquots of 30% acetic acid prior to dilution and lyophilization. Amino acid analysis (see Section 3.4.1) and HPLC were used to ascertain homogeneity and concentration. For homogeneity, a Hewlett Packard 1090M HPLC was used, equipped with a reverse-phase C-18 column (0.01825 cm ID). The mobile phase was 0.1% TFA, the flow rate was 150 μl/min, and eluent peaks were detected by a U.V. detector set at 210 nm. Preparative reverse phase HPLC was used to purify the GRGDY-I_2 peptides before subsequent use. A reverse phase C-18 (0.21 cm ID) column was used for preparative HPLC.

Surface Peptide Attachment

GRGDY-I_2 peptides were attached to solvent cast blends of PLAL:PLA using water soluble carbodiimide (EDC) and sulfo-NHS chemistry, as described in Section 4.2.3.

Bulk Peptide Attachment

GRGDY-I_2 peptides were attached to PLAL using 1,1'-carbonyl-diimidazole (CDI) as a linking agent. The copolymer was dissolved in a 50:50 mixture of methylene chloride (CH_2Cl_2) and dimethyl sulfoxide (DMSO). The peptide was dissolved in DMSO and added to the copolymer solution. A solution of CDI in CH_2Cl_2 was added to the polymer/peptide solution with stirring. After 4 hours, the CH_2Cl_2 was removed by evaporation. Water was added to complete copolymer precipitation. The precipitate was collected by vacuum filtration using a Buchner funnel and dried under high vacuum on a lyophilizer system (<30 μmHg). Coupling yield (%) was determined from Amino acid analysis and was defined as the ratio of total peptide to total lysine.

Calculation of Lysine and Peptide Contents from XPS data

Based on the elemental composition of a sample and with the following assumptions about the species that are present in the sample, the molar ratios of the species on the surface can be estimated. Neglecting the presence of contaminants, so that the only species present are repeat units of lysine, peptides, and repeat units of lactic acid, then the molar ratios of lysine (x), peptides (y) and lactic acid (1-x-y) are calculated from the following expressions:

$$x = \frac{9\,y - 39\,y\,N - 5\,N}{4\,N - 2} \qquad [5.1]$$

$$y = \frac{10\,I}{4 - 8\,N - 42\,I} \qquad [5.2]$$

where I and N are the mass fractions of iodine and nitrogen determined from XPS ratios that include carbon, oxygen, iodine, and nitrogen.

The chemical formulas and molecular weights for each of the compounds used to calculate equations [5.1] and [5.2] are given in Table 5.13. A complete derivation of equations [5.1] and [5.2] are given in Appendix 5A, along with a compariosn of the results calculated by two other methods.

Table 5.13
Species in PLAL+GRGDY-I_2 Samples

Species	Chemical Formula	Molecular Weight
Lactic Acid	$C_3H_4O_2$	72 g/mol
Lysine	$C_6H_{11}N_2O$	127 g/mol
Peptide+EDC remnant	$C_{27}H_{36}O_{11}N_8I_2$	902 g/mol

Table 5.13: The surfaces of PLAL+GRGDY-I2:PLA blends are composed of three entities: molecules of lactic acid, lysine and peptides.

5.3.2 *Peptides detected when attached by surface chemistry*

In this study, which was conducted at the University of Washington, 24 samples were prepared and analyzed over a 3 month period. One purpose of this study was to test the modified peptide to see if the iodine incorporated into the peptide was detectable by XPS. Another purpose was to use the cold-stage to analyze the samples in a hydrated, frozen condition. The results of the first part of this study are shown in Table 5.14. The PLAL+GRGDY-I_2 samples D1 and D2 were prepared using EDC and sulfo-NHS chemistry to immobilize the GRGDY-I_2 peptide to the surface. The appearance of N and I on the PLAL-GRGDY-I_2 samples is evidence that there is peptide present on the surfaces of these samples. Although contaminants were present on the samples, they were not present in large quantities, and therefore do not present a major problem in interpreting these results. The sources of the contaminants can all be accounted for. The peptide coupling reaction was performed in Phosphate buffered saline (PBS), which accounts for the contaminants of sodium and chloride. The fluorine (from HF) and magnesium were present in the peptide as received. The sulfur comes from the sulfo-NHS reagent and also from trace $MgSO_4$ used in the peptide synthesis reaction.

These data are only from 2 of 24 samples sent to the University of Washington for analysis. These samples were examined before soaking. The other samples were soaked for 1 day, 1 week and >1 month to test the long-term effects of soaking on changes that may occur on the surface after peptides have been attached. The samples were analyzed by cold-stage XPS. The purpose of this approach was to capture any changes that soaking may have caused. After the samples undergo some degradation or exposure to water there may be detectable differences in the type of bonds that are present on the surfaces. These

differences will only be detectable if they are irreversible, or if they are trapped by freezing the samples before subjecting them to ultrahigh vacuum in the XPS spectrometer. If there are no changes in the chemical nature of the surfaces, which may occur if the samples simply "swell", or if the surface changes are minor, then XPS will not yield quantifiable data.

Table 5.14
The use of Iodine-labeled Peptides
Dry Samples before Soaking

Sample	T.O.A.	% C	% O	% N	% I	% Si	% F	% Mg	% Na	% Cl	% S
PLAL (Exp.):	-	60	39	1	0	0	0	0	0	0	0
PLAL	55	59.8	40.2	n.d.	n.d.	n.d.	n.d.	n.d.	n.d.	n.d.	n.d.
RGD (Exp.):	-	57.5	22.5	20	0	0	0	0	0	0	0
RGD	55	47.9	21.2	16.8	n.d.	n.d.	7.6	2.9	n.d.	n.d.	3.6
RGD-I2 (Exp.):	-	54.8	21.4	19	4.8	0	0	0	0	0	0
RGD-I2	55	49.9	23.3	12.8	1.9	n.d.	9.2	2.9	n.d.	n.d.	n.d.
D1, D2 (Exp.):	-	59.8	38.0	1.8	**0.4**	0	0	0	0	0	0
D1	72	60.3	29.1	6.7	**0.3**	n.d.	n.d.	n.d.	3.6	n.d.	n.d.
	0	58.2	31.9	3.5	**0.2**	2.0	n.d.	n.d.	2.5	1.8	n.d.
D2	72	62.8	28.1	4.6	**0.5**	4.0	n.d.	n.d.	n.d.	n.d.	n.d.
	0	60.9	32.6	3.5	**0.3**	1.6	0.5	n.d.	0.5	n.d.	n.d.

Table 5.14: Initial data from surface-attached peptide samples exposed to soaking conditions. (n.d. = not detected, T.O.A. = take off angle) Both of the samples produced measurable iodine contents at 2 different take off angles.

Based on the equations to calculate lysine and peptide surface densities, it was determined that samples D1 and D2 from Table 5.14 contained 12 ± 4.4 % lysine and 0.1 ± 0.04 % peptide. From these calculations it can be concluded that the surfaces were enriched in lysine (compared to 1% lysine from bulk ^{1}H-NMR measurements), and that the efficiency of the peptide attachment reaction was 0.8%. The calculation of attachment efficiency does not take into account the possibility of non-specific association of the peptides to the polymer.

5.3.3 Peptide detected when attached by bulk chemistry

Samples created by bulk attachment of peptides to PLAL and then blended with PLA were also analyzed by XPS to determine the surface densities of peptide and lysine. The results of these measurements are illustrated in Figure 5.9. Equations 5.1 and 5.2 were used to convert the data to surface densities of peptide.

Figure 5.9
Bulk Peptide Density Results

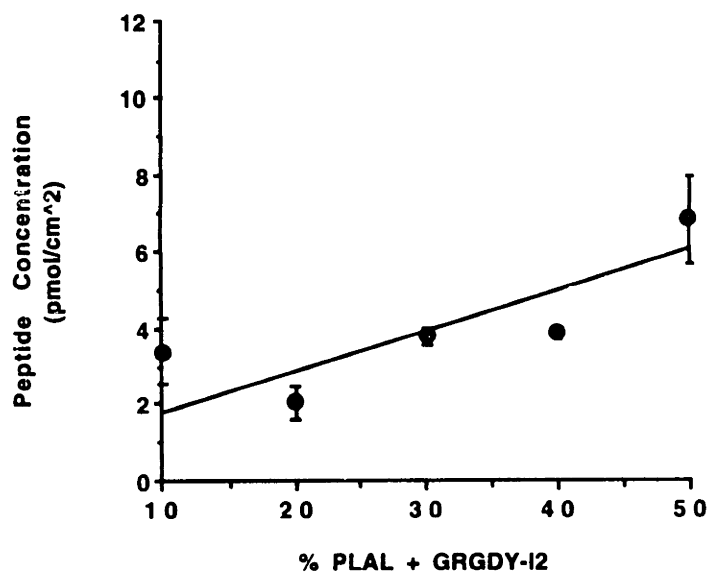

Figure 5.9: Analysis of 10 to 50% blends by XPS to measure the surface densities of the peptides. (Ave. ± S.D., N=3, n=3)

Statistical analysis of the slope of the line in Figure 5.9 was conducted using Student's t-test with the test statistic (T) and degrees of freedom (ν):

$$T = \frac{b_1 \sqrt{S_x}}{\sqrt{n\, s^2}} \qquad \nu = n - 2$$

The analysis demonstrated that there was a linear relationship between the amount of peptide on the surface and the bulk content of peptide.

5.3.4 *Peptide Stability/Cold Stage Studies*

In collaboration with Professor Buddy Ratner, preliminary XPS studies using a cold stage were conducted on samples soaked at 37°C for up to one month. The samples were left in a hydrated state and frozen in liquid nitrogen to preserve the surface during analysis. The reason these studies were performed was to avoid changes which could occur during high vacuum drying. The resulting surfaces after high vacuum drying would be different than the surfaces which cells would be exposed to. Iodine peaks were obtained on each of the samples, indicating a substantial amount (~pmol/cm^2) of peptide present even after one month of soaking.

It is often the practice for both SIMS and XPS studies to use very thin films of a material deposited onto gold, silver or aluminum foil to characterize the materials. This produces an analysis that is very different than studying the surfaces of constructs which are made for use as biomaterial implants. By using cold-stage in conjunction with biomaterial implants, one is able to obtain a more realistic sample of what the surface would be like in a hydrated environment *in vivo*.

5.3.5 *Discussion*

Poly(lactic acid) contains only carbon, hydrogen and oxygen. The lysine residue and the peptides contain nitrogen in addition to C, H and O. On an atomic percent scale, nitrogen should be present at approximately 1.0% throughout a sample of PLAL. After attaching peptides to the lysine residues, there should be 1.5% nitrogen. Due to this relatively small increase in nitrogen content after adding the peptides, XPS measurements of the nitrogen content of samples with peptides attached to them do not and will not reveal unmodified peptide content because the lysine residues also contribute to the total nitrogen content. Even if the lysine content of the polymer is increased, the measurement

of nitrogen contents would not be reliable enough to detect unmodified peptides. By using modified peptides containing non-radioactive iodine, however, the peptide content was able to be estimated. Iodine is not present in the polymer and had not been detected as a contaminant in previous studies. In spite of these promising results, this method does not distinguish between peptides which are covalently linked and those which are physically adsorbed. It was necessary to use radiolabeled peptides to distinguish between the number of peptides that were physically adsorbed and those which were covalently bound as a result of the EDC/sulfo-NHS chemistry.

5.4 Contact Angles

Contact angles of liquids on solid surfaces are used to determine the relative wettability of a surface. In order to study hydrated surfaces, it is common to invert and submerge a sample in a glass beaker and place bubbles of air or hydrocarbons underneath the sample. In studies performed by King, *et. al.* , captive bubbles of air and octane were used to determine the surface energies of hydrogels (19). Pettit, *et. al.* investigated the surface properties of polymers using XPS and underwater contact angle measurements (20). They found that the materials which would wet more easily (low captive air bubble contact angle) tended to be rich in oxygen. Fibronectin adsorption was higher on surfaces with higher captive air bubble contact angle (greater hydrophobicity).

The advancing contact angles of MilliQ water on amorphous (13 ± 2% crystallinity) and crystalline (approximately 67% crystallinity) samples of poly(L-lactic acid) (PLLA) were reported by Park and Cima to be the same (74° ± 3°), whereas the receding contact angles of amorphous and crystalline PLLA were different (64° ± 4° for amorphous and 61° ± 4° for crystalline, N=6, n=20 in each case) (21). The surface energy of these samples was calculated using an equation of state, to be approximately 50 dynes/cm.

5.4.1 Materials and Methods

A Ramé-Hart (model 100-00) goniometer was used to perform most of the sessile drop contact angle measurements. Advancing and receding angles were determined by adding or removing drops of water to the first sessile drop, and measuring the angle as a function of the number of drops present (drop size ranged from 0.5 μl to 1.5 μl). Underwater contact angle studies were performed using an optically clear chamber in which samples were immersed for testing.

Captive bubbles of air and octane (Aldrich) were used as the probe fluids. The octane and water were thoroughly mixed beforehand and then separated using a separatory funnel. Experiments were conducted using octane-saturated water and water-saturated octane. Surface energies were calculated using Young's equation for underwater sessile drops of air and octane. The harmonic mean equation was used to approximate the solid-liquid interfacial tensions (19). The derivation of the equations used to calculate the surface energy of hydrated samples from underwater contact angles and a sample calculation are given in Appendix 5B.

Additional contact angle measurements were made using a VCA2000 Contact Angle System. Samples were mounted on glass microscope slides using double-sided tape to ensure that they were flat.

5.4.2 Results

Studies which were performed include the characterization of PLA using sessile drop contact angles, the effect of soaking in PBS and water on the surface energy of PLAL using underwater contact angles, and the effect of incorporating PLAL+GRGDY-I_2 peptides into PLA in the form of solvent-cast blends.

The effect of soaking on PLA

In this study, the contact angle of water on PLA samples before and after soaking in PBS were obtained. After each sample was soaked for the predetermined time, the surfaces were blotted dry of all visible water and the contact angles were measured using sessile drops of water. Three measurements from three different drops were made within 1 minute after removing the polymer from water. Table 5.15 lists the data. Figure 5.10 shows the results of these experiments graphically. The effect was reversible, since approximately 1 hour after removing the samples from water, the contact angle returned to the original value.

Table 5.15
Effect of soaking on PLA

Soaking Time (hr)	Contact Angles (°)	Ave ± S.D. (°)
0	59,62,65,60,57,54	60±4
0.5	54,56,52	54±2
1	49,52,49	50±2
2	47,43,44	45±2
3	48,48,46	47±1
6	37,39,40	39±2
24	35,34,36	35±1
96	30	30
120	31,35,34	33±2

Figure 5.10
Effect of Soaking in PBS on the Contact Angle of PLA

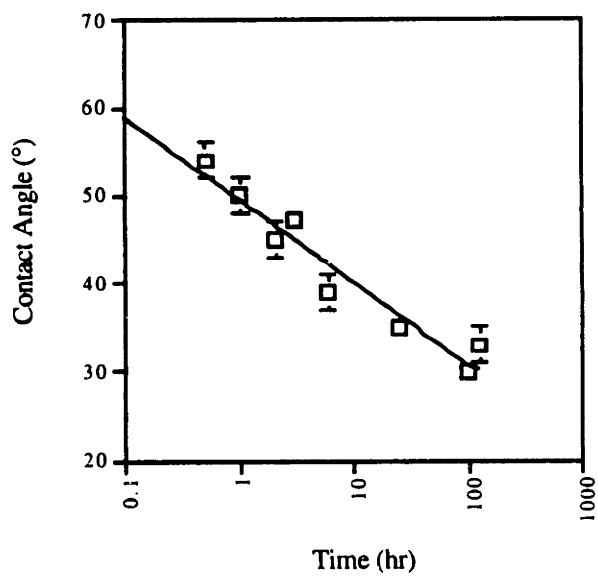

Figure 5.10: The contact angle of water is plotted vs. the soaking time. Measurements were made immediately after removing the sample from soaking in PBS and blotting the sample dry. Note the logarithmic scale on the abscissa. Data are Ave ± S.D. (N=1, n=3).

In a follow-up study, samples of PLA were soaked in MilliQ water for 1 to 12 days. Table 5.16 lists the data obtained in this study. Figure 5.11 shows the results graphically.

Table 5.16
The Effect of Soaking on PLA

	25°C		37°C	
Time (hr)	**Top**	**Bottom**	**Top**	**Bottom**
0.0	78±2 (6)	74±3 (6)	-	-
22.5	76±1 (6)	72±1 (2)	67±5 (6)	65±4 (2)
91.0	58±3 (6)	61±7 (6)	56±4 (6)	67±3 (6)
114.5	61±3 (6)	70±4 (6)	57±2 (6)	72±1 (6)
138.0	62±4 (6)	77±6 (6)	68 ±3 (6)	69±4 (6)
257.5	59±3 (6)	70±2 (6)	37±3 (6)	69±7 (6)
308.0	52±6 (6)	74±3 (6)	36±3 (6)	75±6 (6)

Table 5.16: Data are given as Ave ± S.D (number of measurements).

Figure 5.11
Effect of soaking in Water on the Contact Angle of PLA

A.

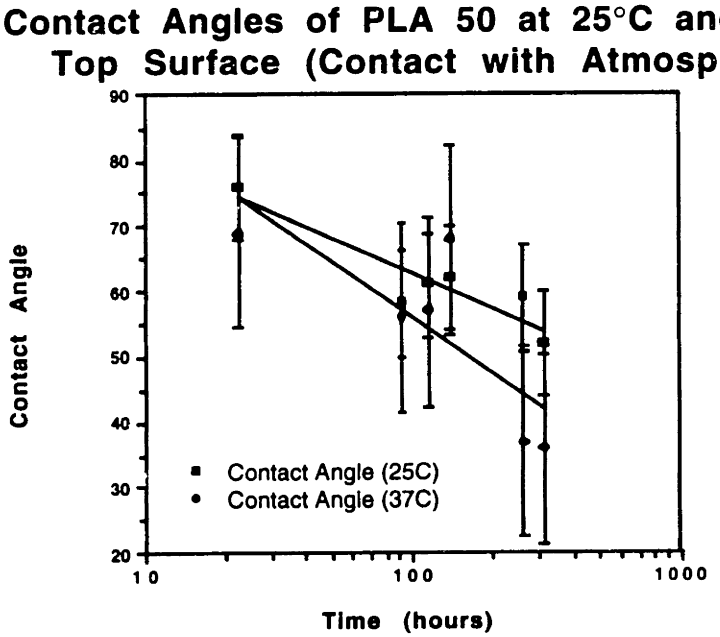

B.

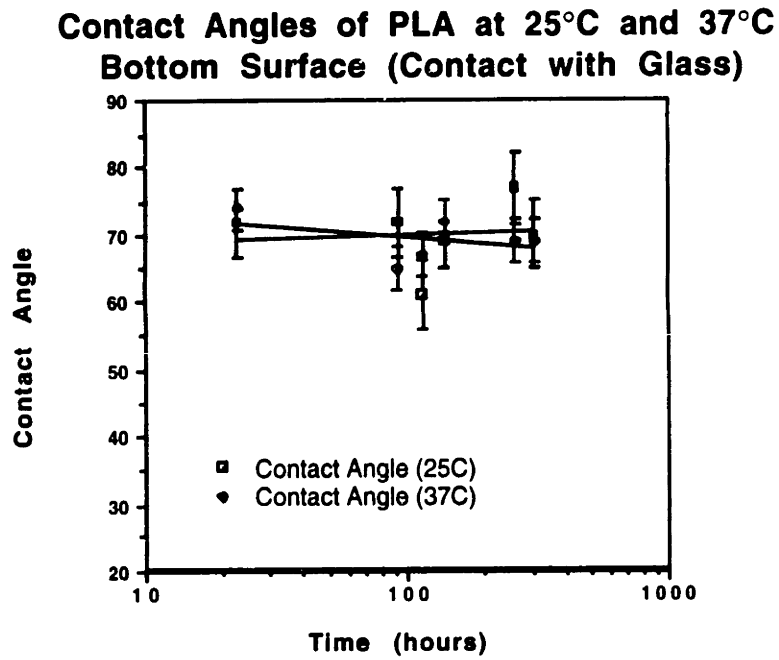

Figure 5.11: Comparison of the change that occurs on the top (A) and bottom (B) of PLA films when exposed to hydrolytic environments for up to 308 hrs. The top surfaces become more hydrophilic, whereas the bottom surfaces maintain their hydrophobic nature. Data are Ave ± S.D. (N=1, n=6).

The effect of soaking on the surface energy of PLAL

In these experiments, underwater contact angles of air and octane were measured on samples which were soaked for 1 to 5 days in either PBS or water. In addition, after the samples were removed from the soaking fluid, advancing and receding contact angle measurements were made as a function of drying time. These studies were done to determine the kinetics of surface restructuring after removal from the soaking fluid. All of the measurements were made on the glass-contacting side of PLAL. A summary of the underwater contact angle measurements and the calculated surface energies (γ_{SV}) is given in Table 5.17. The results are also shown graphically in Figure 5.12.

Table 5.17
Surface Energy of PLAL films

	Soaking Time (d)	θ_{oct} (°) n=24	θ_{air} (°) n=24	γ_{SV}^{p} (dyn/cm)	γ_{SV}^{d} (dyn/cm)	γ_{SV} (dyn/cm)
PBS	0	87±2	74±3	18.0	17.6	35.7
	1	84±4	66±3	19.3	24.2	43.5
	2	95±3	68±2	14.9	34.3	49.2
	3	91±5	67±2	16.4	30.6	47.1
	4	93±3	68±6	15.7	31.5	47.2
	5	86±4	67±4	18.4	24.9	43.3
Water	0	87±2	74±3	18.0	17.6	35.7
	1	85±3	67±3	18.8	23.9	42.7
	2	82±3	67±3	20.1	21.1	41.3
	3	89±5	66±3	17.2	29.7	47.0
	4	87±3	74±4	18.0	17.6	35.7
	5	81±3	73±3	20.5	14.6	35.1

Table 5.17: The measurement of the surface energy of PLAL films from underwater contact angles using octane and air. See appendix 5B for a sample calculation. Data are Ave. ± S.D. (n=24)

Figure 5.12

A.

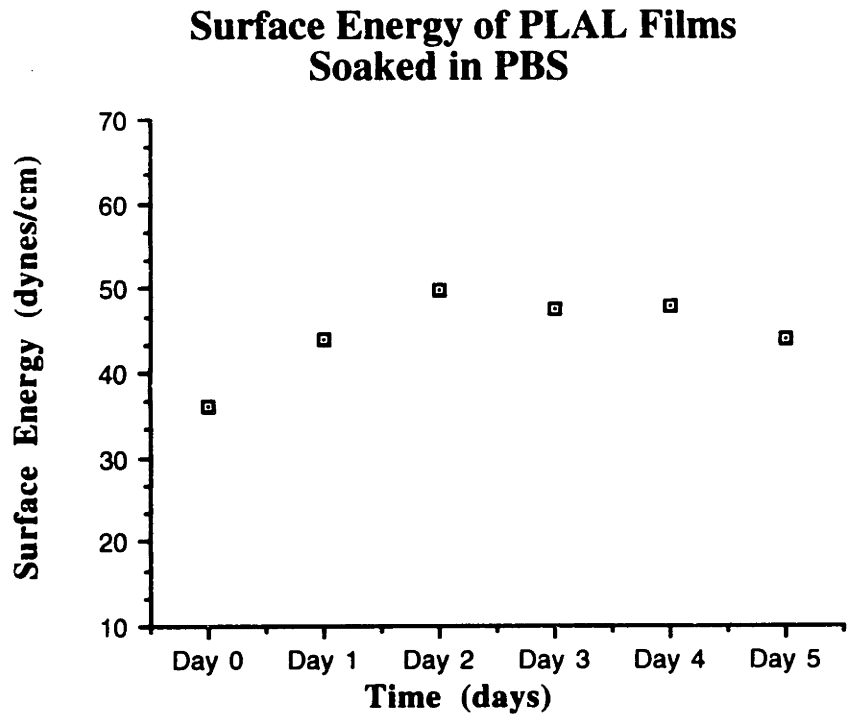

B.

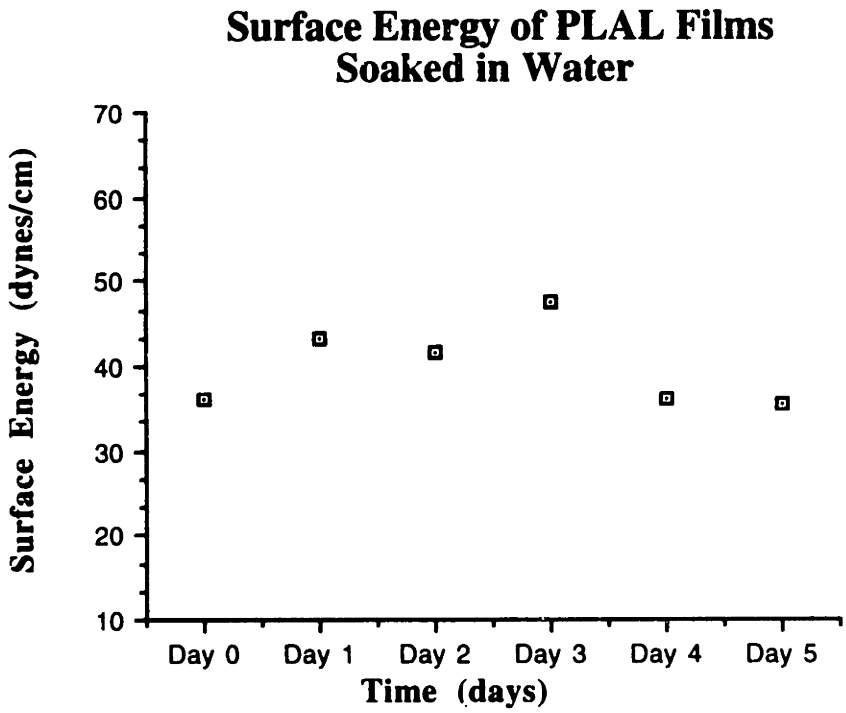

Figure 5.12: Data represent the calculated values for the surface energy of PLAL films vs. soaking time for PBS (A) and water (B).

The results of the surface energy calculations demonstrate the need to take into account the environmental history of the samples when reporting results. The results of the surface energy calculations are lower than the results reported by Park and Cima (21). These measurements were made with captive octane and air bubbles under water, whereas the measurements made by Park and Cima were advancing and receding contact angles of water in air.

On all of the samples described in Table 5.17, advancing and receding contact angle measurements were made after 5 min of air-drying, 1 hr of air-drying, 2 hrs of drying under vacuum, and 24 hrs of drying under vacuum. The typical hysteresis of contact angles on glass-contacting surfaces of PLAL is shown in Figure 5.13. (These data were obtained on dry PLAL.) There were no appreciable differences in advancing or receding contact angles as the polymers dried.

Figure 5.13
Contact Angle Hysteresis

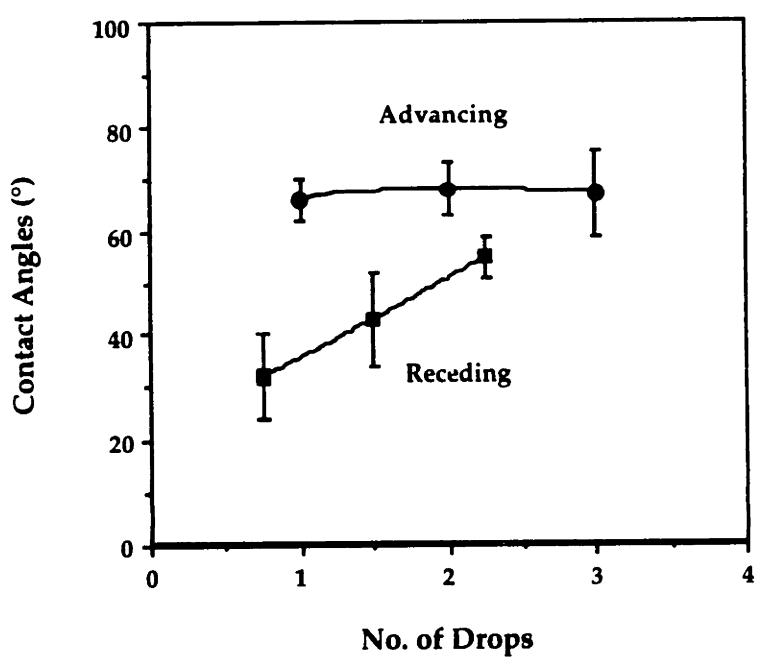

Figure 5.13: Advancing and receding contact angles were measured as a function of drying time after soaking in either PBS or water. The graph shown here is representative of all the data shown in Table 5.18. Data are Ave. ± S..D. (N=1, n=6)

The data for the contact angles measured as a function of drying time are shown in Table 5.18. These observations are consistent with the observations made earlier that the glass-contacting side of the polymer doesn't change as the polymers are soaked for longer times and that after drying, the contact angles revert to their initial values.

One of the issues involved in interpreting contact angles is that the results depend on the technique used to measure the angles and the environmental history of the samples. For this reason, it is difficult to compare results from experiment to experiment. Nevertheless, contact angles are useful for measuring changes in the wettability of polymers due to modifications that are made to the surface. Because PLA is a hydrophobic polymer and lysine is a hydrophilic amino acid, it has been suggested that part of the mechanism by which cell attachment and spreading may be increased is through changes in the wettability of the surface. Contact angle studies, therefore, are important to this project in order to determine possible variations in wettability due to the addition of lysine and peptides to the PLA samples and the effect of those variations on the extent of cell adhesion and spreading. Since the bottoms of solvent-cast films remain stable in regards to contact angles, it can be concluded that the observed increases in cell spreading were not due to variations in hydrophilicity over time.

The effect of peptides on wettability

Sessile drop contact angles were measured on samples of blends with 10 to 50% PLAL and 10 to 50% PLAL+GRGDY-I_2. The results are shown in Table 5.19 and Figure 5.14. There was no significant effect of the peptides or lysine groups on the wettability of the samples.

Table 5.18
Summary of Contact Angle Hysteresis Data

		Advancing Contact Angles						Receding Contact Angles					
	Drops	1		2		3		2.25		1.5		0.75	
Sample		Ave	± SD	Ave	± SD	Ave	± SD	Ave	± SD	Ave	± SD	Ave	± SD
Dry		68	± 3	68	± 5	67	± 5	55	± 4	43	± 9	32	± 3
Water	1x6												
1 day	Drop Time												
	5min	61	± 4	65	± 5	65	± 3	63	± 6	53	± 2	38	± 5
	1 hr	58	± 6	56	± 4	52	± 6	55	± 3	43	± 3	31	± 6
	2 hr	62	± 6	59	± 8	60	± 7	51	± 8	39	± 3	22	± 2
	24 hrs	64	± 2	63	± 6	66	± 5	58	± 6	47	± 9	30	± 5
2 days													
	5min	64	± 2	68	± 5	67	± 4	57	± 2	45	± 2	28	± 4
	1 hr	67	± 6	72	± 4	74	± 2	65	± 6	49	± 11	32	± 4
	2 hr	64	± 5	67	± 5	70	± 3	67	± 5	59	± 5	48	± 4
	24 hrs	73	± 2	72	± 2	71	± 3	53	± 7	39	± 5	20	± 3
3 days													
	5min	69	± 5	67	± 4	68	± 3	56	± 6	42	± 5	23	± 3
	1 hr	69	± 3	69	± 5	66	± 5	52	± 7	37	± 4	26	± 6
	2 hr	63	± 8	68	± 5	63	± 9	56	± 5	45	± 6	30	± 4
	24 hrs	63	± 4	70	± 3	67	± 5	58	± 2	44	± 5	26	± 3
4 days													
	5min	65	± 13	72	± 9	76	± 2	63	± 2	47	± 5	32	± 2
	1 hr	66	± 6	68	± 3	67	± 4	56	± 3	45	± 4	26	± 4
	2 hr	63	± 4	66	± 3	66	± 4	55	± 3	38	± 5	25	± 2
	24 hrs	70	± 5	71	± 3	65	± 3	58	± 5	40	± 4	23	± 5
5 days													
	5min	71	± 4	72	± 4	71	± 1	58	± 3	39	± 3	22	± 3
	1 hr	68	± 5	68	± 3	68	± 4	57	± 3	43	± 8	28	± 3
	2 hr	65	± 4	62	± 2	64	± 3	56	± 5	41	± 7	25	± 5
	24 hrs	61	± 3	65	± 4	65	± 4	56	± 3	39	± 4	27	± 2
PBS													
1 day													
	5min	62	± 5	61	± 4	66	± 4	56	± 3	48	± 4	35	± 4
	1 hr	64	± 2	63	± 2	65	± 3	58	± 3	49	± 4	36	± 6
	2 hr	52	± 2	53	± 1	53	± 2	47	± 3	40	± 2	30	± 3
	24 hrs	69	± 3	71	± 4	72	± 3	60	± 6	56	± 5	36	± 6
2 days													
	5min	59	± 7	60	± 6	62	± 4	56	± 7	45	± 9	29	± 4
	1 hr	69	± 4	72	± 2	70	± 4	64	± 5	51	± 4	37	± 3
	2 hr	68	± 6	68	± 4	69	± 6	58	± 6	49	± 3	35	± 5
	24 hrs	67	± 7	67	± 6	66	± 5	54	± 8	40	± 5	25	± 2
3 days													
	5min	68	± 4	68	± 3	72	± 3	63	± 5	46	± 3	25	± 2
	1 hr	73	± 4	72	± 8	70	± 8	60	± 9	40	± 11	25	± 9
	2 hr	68	± 4	72	± 2	71	± 1	61	± 3	44	± 4	32	± 2
	24 hrs	67	± 3	72	± 1	72	± 3	62	± 3	46	± 2	33	± 2
4 days													
	5min	64	± 9	67	± 8	71	± 4	60	± 3	44	± 2	29	± 2
	1 hr	71	± 6	71	± 5	71	± 4	60	± 5	45	± 3	33	± 2
	2 hr	67	± 5	68	± 5	68	± 4	52	± 3	41	± 2	25	± 2
	24 hrs	67	± 5	68	± 2	66	± 6	54	± 5	38	± 3	21	± 3
5 days													
	5min	73	± 7	72	± 4	76	± 5	61	± 5	46	± 2	26	± 5
	1 hr	67	± 4	74	± 6	72	± 4	60	± 6	45	± 6	30	± 6
	2 hr	67	± 6	68	± 6	70	± 4	59	± 4	44	± 6	28	± 4
	24 hrs	65	± 4	67	± 3	66	± 3	57	± 7	44	± 10	27	± 7

Figure 5.18: The data in this table were accumulated on samples which had been soaked in either water or PBS for up to 5 days. The advancing and receding contact angles were measured as a function of drying time.

Table 5.19
Effect of Lysine and Peptides on Surface Wettability

% PLAL	C. A. (Ave ± S.D.)	% PLAL + GRGDY-I_2	Adv. C.A. (Ave ± S.D.)	% PLAL + GRGDY-I_2	Rec. C.A. (Ave ± S.D.)
0 (N=2, n=12)	73±4	0 (N=5, n=30)	80±4	0 (N=1, n=10)	55±3
10 (N=2, n=12)	69±5	10 (N=2, n=20)	77±2	10 (N=1, n=10)	44±3
20 (N=2, n=12)	63±11	20 (N=2, n=20)	77±4	20 (N=1, n=10)	44±4
30 (N=2, n=12)	70±9	30 (N=2, n=20)	75±5	30 (N=1, n=10)	43±4
40 (N=2, n=12)	76±11	40 (N=2, n=20)	81±4	40 (N=1, n=10)	47±4
50 (N=2, n=12)	67±5	50 (N=2, n=20)	75±8	50 (N=1, n=10)	39±7

Table 5.19: The wettabilities of blends from 0 to 50% PLAL and PLAL+GRGDY-I_2 were measured by sessile drop contact angle. Both advancing (Adv. C. A.) and receding (Rec. C.A.) contact angles were measured on the samples containing peptides.

Figure 5.14
The Effect of Peptides on the Wettability of PLA

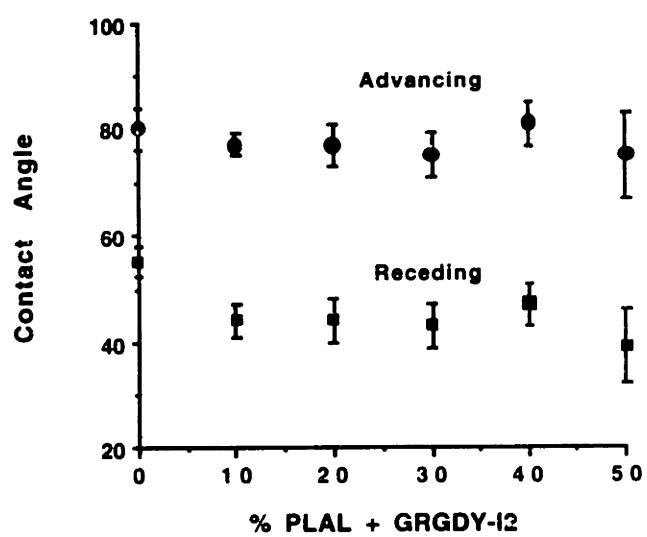

Figure 5.14: The effect of adding lysine or peptides to PLA on the wettability of the samples was tested. Data are Ave. ± S.D. (N=2, n=20 for advancing; N=1, n=10 for receding angles)

5.5 *Secondary Ion Mass Spectroscopy*

5.5.1 Background

The use of Static Secondary Ion Mass Spectroscopy (Static SIMS) for analyzing biomaterial surfaces is relatively new. Nonetheless, substantial work has been done recently to develop this technique. The surface is bombarded with ions and the kinetic energy of the ions is transferred to the surface under investigation, causing new ions to be formed. These secondary ions are analyzed by mass spectroscopy. The ions that are released are characteristic of the material under investigation. Because the primary ions do not penetrate very deeply (only 10 Å), the secondary ions are representative of the surface. SIMS data is very difficult to quantify, but it does give a relative idea of the molecules that are present, and it is considered one of the most sensitive techniques for studying surfaces. Chemical composition information that is complementary to XPS data can be obtained from static SIMS studies.

Mantus, *et. al.* used static SIMS to analyze adsorbed homopolymers of 16 amino acids, including polylysine (22). They identified peaks corresponding to molecular weight fragments of 30, 44, 56, 68 and 84 g/mol as characteristic peaks corresponding to polylysine. From their studies they were able to identify certain peaks within proteins that corresponded to amino acids.

Chilkoti, *et. al.* performed static SIMS analysis of poly(HEMA) in order to assess the effect of cross-linking on the surface mobility of the hydrogels (23). Changes in the peak intensities of atomic versus molecular secondary ions were observed in negative ion SIMS as a function of cross-linker concentration.

Brinen, *et. al.* studied the surfaces of copolymers of glycolide and trimethylene carbonate (TMC) by XPS and SIMS and found that whereas the XPS data was in agreement with the bulk composition data, SIMS indicated that the surfaces of the copolymers were enriched in the TMC component (24).

Davies, *et. al.* studied a copolymer of thioglycoside and methyl methacrylate (25). Using Time-of-Flight (TOF) SIMS they were able to detect galactose molecules on the surfaces of colloidal latex particles. The key to success in this study was the identification of a representative peak eminating from the galactose molecules which was distinct from peaks from the latex particles. The spectrum of galactose was obtained by depositing a layer of it onto aluminum foil.

In a study using TOF-SIMS, van Leyen, *et. al.* discovered that relatively low molecular weight oligomers (M_n = 1000) were desorbed with a higher

probability than polymer fragments of the same mass (26). In addition, it was concluded that the formation of cationized fragments and oligomers was strongly influenced by the substrate material and the surface coverage.

In an attempt to develop methods to quantify SIMS studies more accurately, Cornelio, *et. al.* used organic films produced from micropipette deposition and Langmuir-Blodgett techniques to develop calibration curves based on the integration of the protonated molecular ion to silver peak area ratio (27). Linear calibration curves were produced.

Davies, *et. al.* published the XPS and SIMS spectra of PLA and PGA (28). The positive SIMS peaks of PLA occur at 43, 55, 73, 83, 89, 99, 100, 101, 127, 128, 129, 143, 145, 199, 200, 201, 215, 217, 272, and 289. The negative SIMS peaks occur at 41, 43, 45, 71, 73, 87, 89, 143, 145, 159, and 161. Figure 5.14 shows the positive and negative SIMS peaks of PLA (from the paper by Davies).

Figure 5.15
Positive and Negative SIMS Spectra of PLA

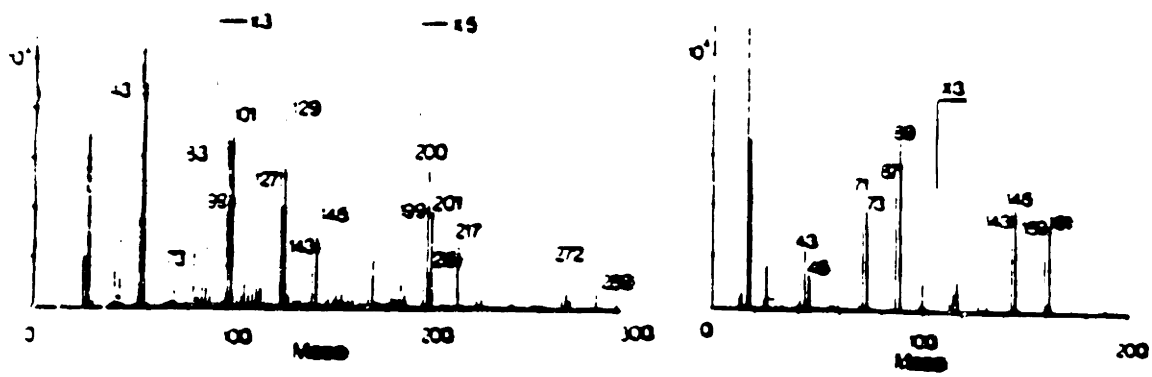

Positive SIMS spectra **Negative SIMS spectra**

Figure 5.15: The positive and negative static SIMS spectra of PLA. From Ref. 28.

Brown reviewed the use of SIMS for use in studying glass, polymer, catalysts and metals (29). Areas of frequent criticism were addressed and recommendations were made to handle those criticisms. The major problem which is often associated with SIMS is the inability to quantify the results. Proper calibration of the equipment has allowed some researchers to obtain

quantitative information. Another problem which is often brought up is the potential for destruction of the sample. In answer to this criticism, it was stated that as long as the experiments are conducted under static conditions, then no spot is hit more than once; surface annealing occurs in nanoseconds; and secondary ions are actually emitted from points very remote from the sites of primary ion impact.

Briggs identified the advantages of SIMS over XPS and described the complimentary nature of the two techniques (30).

5.5.2 *Materials and Methods*

Preliminary studies were conducted at MIT using a VG Ionex System 11006 Model# 1X70S SIMSLAB in order to become familiar with the techniques that are necessary to prepare samples most effectively. The paper by Davies, showing the results of SIMS analysis of poly(lactic acid) samples, was very useful in defining the conditions under which samples should be run (28). Later studies were performed at the University of Washington in Seattle on a PHI model 3700 static SIMS subsystem with a Balzers 511 quadrupole mass analyzer.

5.5.3 *Results*

Samples on Silicon

In the first set of studies, silicon wafers were used as the underlying support and PLAL with bulk-attached peptides was sprayed onto the wafers to form a thin layer of the polymer plus peptide. The sample was then coated with a thin layer of gold by thermal evaporation. Ion beams from two sources were used, gallium and xenon. Positive and negative ion beams and neutral molecules were used to create secondary ions and molecules, which were then detected and analyzed. Results of these studies are shown in Figures 5.16 and 5.17. These results are included to demonstrate that it was difficult to distinguish fragments from the peptide from fragments from the polymer. It was also difficult to replicate the results of Davies, *et al.* on the equipment at MIT.

Figure 5.16
Positive Static SIMS Spectra of PLAL+GRGDY on Silicon

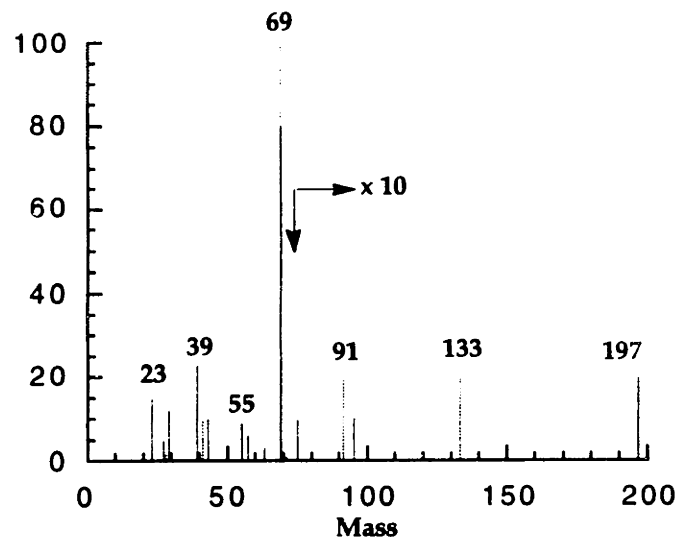

Figure 5.16: The positive static SIMS spectra of PLAL+GRGDY shows major peaks at 69, 91, 133 and 197.

Figure 5.17
Negative Static SIMS Spectra of PLAL + GRGDY on Silicon

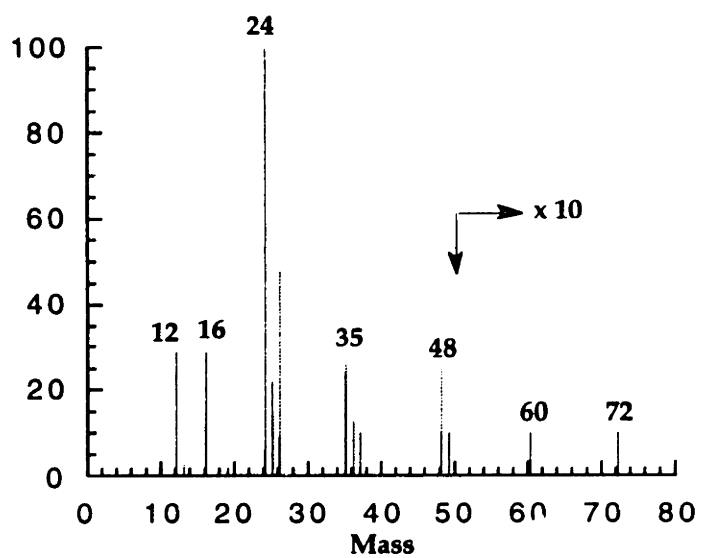

Figure 5.17: The negative static SIMS spectra of PLAL+GRGDY shows major peaks at 24, 35, 48, 60 and 72.

Samples on Gold

In the second set of studies, a high velocity nitrogen stream was used to spread a thin layer of PLAL with bound peptides onto a gold substrate. Results of the Negative SIMS analysis are shown in Figure 5.18. (Positive SIMS was not acquired in this manner.)

Figure 5.18
Negative Static SIMS of PLAL-GRGDY on Gold

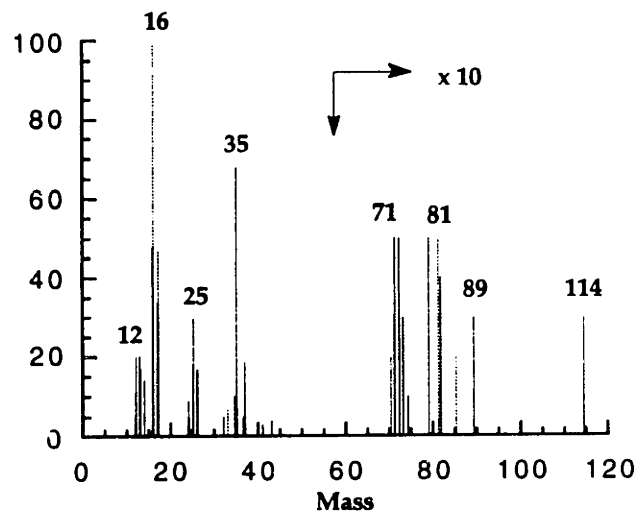

Figure 5.18: The negative static SIMS spectra of PLAL+GRGDY on Gold shows major peaks at 35, 71, 81, 89 and 114.

Frozen, hydrated samples

Static SIMS analysis of frozen, hydrated samples was performed at the University of Washingon in Seattle using a PHI model 3700 static SIMS subsystem with a Balzers 511 quadrupole mass analyzer. Polyethylene standards were used to calibrate the equipment. The samples which were examined included 100 mg films of solvent-cast PLA, blends of PLAL and PLA, and samples with iodine-labeled peptides attached by EDC surface chemistry to the PLAL:PLA blends. The peptides were labeled with non-radioactive ^{127}I to provide a distinguishing elemental marker that would be detectable by static SIMS. Representative spectra are shown in Figures 5.19 through 5.24.

Figure 5.19
Static SIMS Spectra of PLA: Top Surface

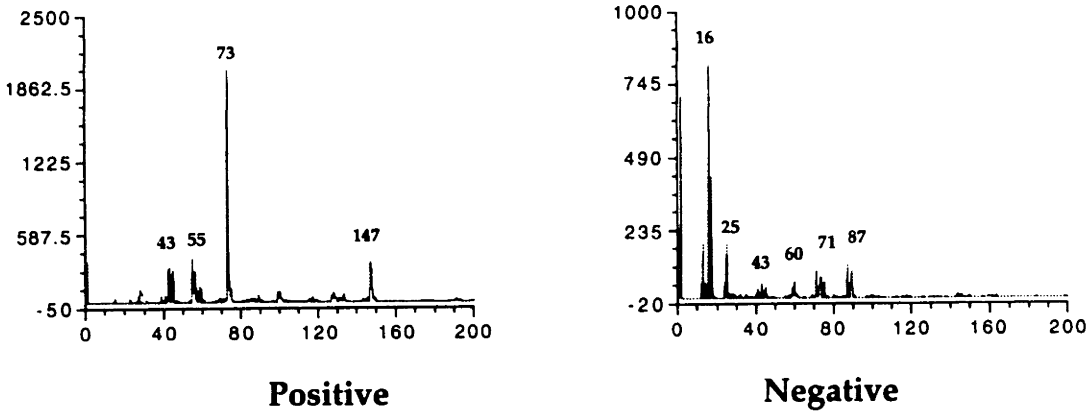

Figure 5.19: Positive and negative static SIMS spectra of the air exposed side of PLA.

Figure 5.20
Static SIMS Spectra of PLA: Bottom Surface

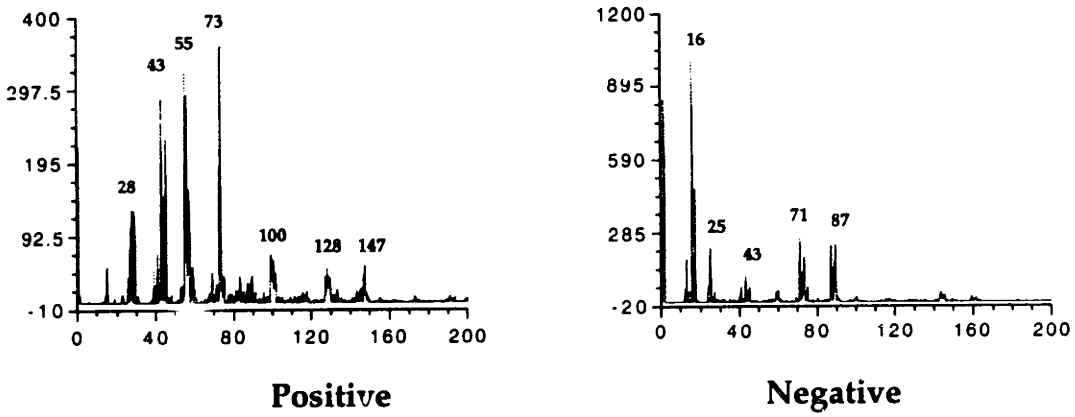

Figure 5.20: Positive and Negative static SIMS spectra of the bottom of a PLA sample.

Figure 5.21
Static SIMS Spectra of PLAL

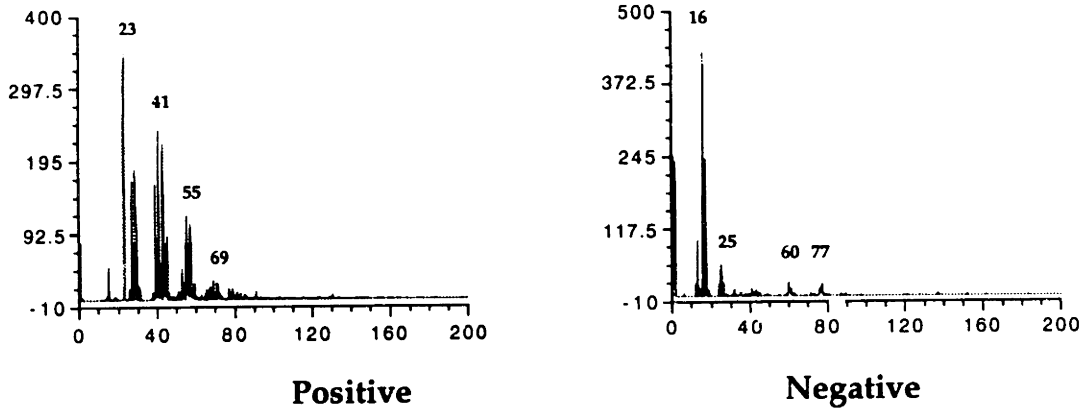

Figure 5.21: Positive and Negative static SIMS spectra of PLAL.

Figure 5.22
Static SIMS Spectra of GRGDY

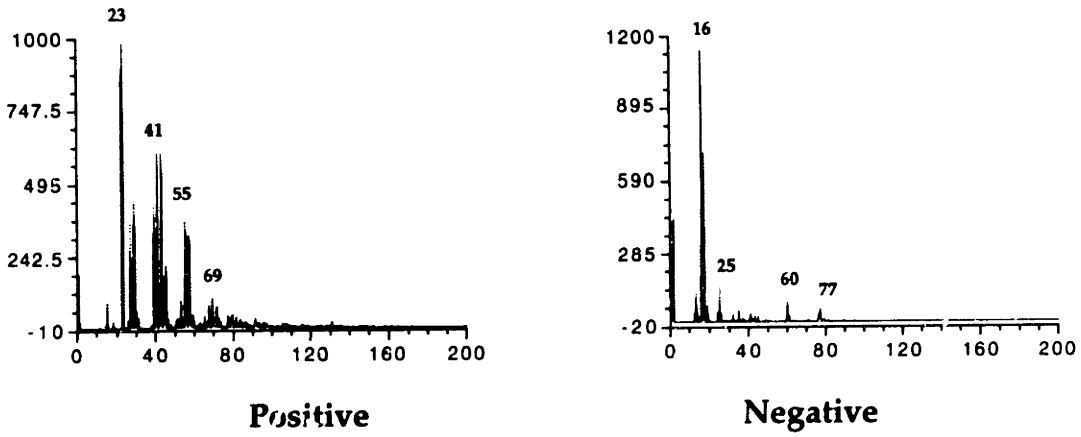

Figure 5.22: Positive and negative static SIMS spectra of GRGDY as a powder.

Figure 5.23
Static SIMS Spectra of GRGDY-I_2

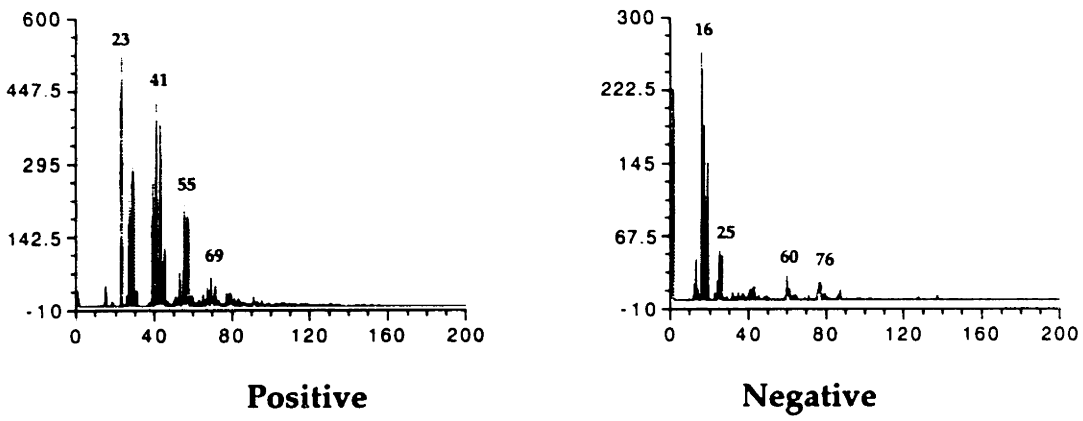

Figure 5.23: Positive and Negative Static SIMS of GRGDY-I_2 as a powder.

Figure 5.24
Static SIMS Spectra of PLAL+GRGDY-I_2

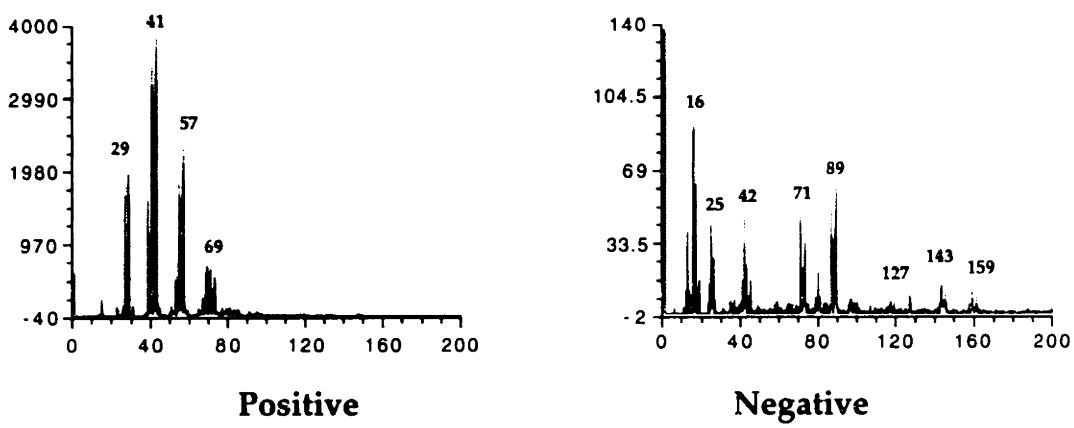

Figure 5.24: Positive and negative static SIMS spectra of PLAL+GRGDY-I_2.

5.5.4 Summary

Static SIMS is one technique in which the results depend greatly on the manner in which the samples are prepared for testing. By using thin films formed by spin-casting or spraying, information about surfaces of thin films formed quickly can be determined. More relevant information about the surfaces

that would be exposed to cells can be obtained by studying samples in the form which they will be used. Samples which are processed by solvent casting thick films have been shown by XPS and contact angles to produce very different surfaces depending on the environment in which the surface was formed. Table 5.20 summarizes the static SIMS information which was collected for PLA and compares this data to literature values. Data in the range from 0 to 40 mass weight were omitted. Table 5.21 lists the data for PLAL:PLA blends, GRGDY and GRGDY-I_2 peptides.

Table 5.20
Summary of Static SIMS Data for PLA on various substrates

Range	on Aluminum[1]	on Silicon[2]	on Gold[3]	Thick Samples[4]
Positive				
41-60	43, 55	41, 43, 55, 57		41, 43, 45, 55-57, 59
61-80	71, 73	63, 69, 71, 75	(data not	67, 69, 71, 73-75
81-100	83, 89, 99, 100	91, 95	taken)	83, 85, 87, 89, 99, 100
101-120	101			101, 115, 117, 119
121-140	127, 128, 129	133		127-129, 131, 133
141-160	143, 145			143, 145, 147, 155, 157, 159
161-180				173, 175, 177, 179
181-200	199, 200	197		187, 189, 191-193, 199, 200
201-220	201, 215, 217			
221-300	272, 273, 287, 289			
Negative				
41-60	41, 43, 45	48, 49, 60	41, 43	41, 43, 45, 55, 59, 60
61-80	71, 73	72	70-74, 79	69, 71, 73, 75, 80
81-100	87, 89		81, 85, 89	87, 89, 100
101-120			114	113, 115, 117, 119
121-140				125, 127, 129, 133, 135
141-160	143, 145, 159			141, 143, 145, 149, 159
161-180	161			161, 163

Table 5.20: Data for static SIMS studies
1. From Davies, et. al., *Surf. and Inter. Sci*, 14:115-120 (1989)
2. Conducted at MIT, using a SIMSLAB, Model # 1X70S (n=1)
3. Conducted at MIT, using a SIMSLAB, Model # 1X70S (n=1)
4. Conducted at UW, using a PHI static SIMS, Model # 3700 (n=4)

Table 5.21
Static SIMS Results for PLAL, GRGDY and GRGDY-I_2

Range	PLAL	GRGDY	GRGDY-I_2
Positive			
41-60	41, 43, 45, 53, 55, 57, 59	41, 43, 45, 53, 55-57	41-43, 45, 51, 53, 55, 57
61-80	67, 69, 71, 77, 79	65, 67, 69, 71, 73, 77, 79	65, 67, 69, 71, 77, 79
81-100	81, 83, 91	81, 83, 91	81, 83, 91, 93, 95
101-120		103, 105, 107, 109, 115, 117	102, 103, 105, 107, 112, 115
121-140	130	125, 128, 130, 135	130
141-160		151, 159	150
161-180			
181-200			
Negative			
41-60	60	41, 43, 45, 60	41-43, 60
61-80	61, 63, 71, 76, 77	61, 71, 73, 76, 77, 79	61, 76, 77, 79
81-100	87, 89	81, 87, 89, 95, 97	86, 87
101-120		119	113
121-140	137	127, 137	127, 137
141-160	152	145, 147, 160	
161-180			
181-200		197	

Table 5.21: Data for static SIMS studies

Table 5.22 lists the static SIMS results for PLAL:PLA 25:75 blends with covalently attached GRGDY-I_2 peptide which were analyzed dry (n=2) or after 1 day of soaking (n=1).

Table 5.22
Comparison of Dry and Soaked Samples

Range	Dry (Top)	Dry (Bottom)	Dry (Top)	Dry (Bottom)	Soaked (Top)	Soaked (Bottom)
Positive						
41-60	41, 43, 45, 55-57	41, 43, 45, 55-57, 59	41-45, 53, 55-57, 59	41, 43, 45, 55-57, 59	41, 43, 45, 55-60	41, 43, 45, 51, 53, 55, 57
61-80	73	69, 73	69, 73	69, 73	67, 69, 70, 73, 77, 79	65, 67, 69, 71, 73, 77, 79
81-100			99	100	81, 83, 87, 89, 91, 93, 99, 100	81, 83, 85, 91, 100
101-120	101	101, 115, 117, 119	101, 115	101, 115, 117, 119	101, 115	103, 105, 107, 109, 111, 112, 115, 117, 119
121-140	127-129, 131, 133, 135	127-129, 131, 133, 135	127, 129	128, 131, 133	127-129, 131, 133	125, 127, 131, 133
141-160	143, 145, 147	143, 145, 147	145, 147, 152	143, 145, 147, 155	143, 145, 147, 155	147
161-180		169, 173, 177	163, 178, 179	162, 169, 177, 179	171, 173	
181-200	191, 200	181, 189, 191, 193, 195	191	181, 191, 193	191, 193, 200	191
Negative						
41-60	59, 60	41-43, 59, 60	41-43, 45, 55, 59, 60	41-43, 59, 60	42, 59, 60	41-43, 45
61-80	69, 71, 73, 75, 79, 81	71, 73, 75, 79, 80, 81	71, 73, 75, 79	71, 73, 75, 80	71, 73, 75, 79, 80	71, 73, 79, 80
81-100	87, 89, 97	87, 89, 97	81, 87, 89, 100	87, 89	81, 87, 89, 97, 99	81, 87, 89, 97
101-120	117	115	117	117	117	117, 119
121-140	127	127	127	127	127	127
141-160	143, 145, 149, 159	143, 145, 159	143, 145, 159	143, 145, 149, 159	143, 145, 149, 159	143, 145, 155, 157, 159
161-180	161	161	161	161, 170	166, 188	161
181-200	182	187		193		

Table 5.22 Data for static SIMS studies before and after soaking of PLAL+GRGDY-I_2.

5.5.5 Discussion

Attempts to find differences in the static SIMS peaks of PLA, PLAL:PLA blends, the peptides, and the blends with bulk-attached peptides were unsuccessful. Occassional differences were seen, but they were not seen consistently. In some of the experiments, peaks which could be assigned to polydimethylsiloxane (PDMS) were seen. In positive SIMS, PDMS peaks occur at 73 and 147. In negative SIMS, PDMS peaks occur at 59, 60, 75 and 149. The occurrence of a peak at 127 on the samples with attached iodine-labeled GRGDY peptides may be indicative of the presence of iodine on these samples, but since many of the samples without iodine-labeled peptides also produced peaks at 127, more results are needed before this observation can be regarded as significant.

5. 6 References

1. Ratner, B.D., "Characterization of biomaterial surfaces", *Cardio. Path.*, **2** (3) (Suppl.): 87S-100S, (1993).

2. Lydon, M.J., Minett, T. W., Tighe, B. J., "Cellular interactions with synthetic polymer surfaces in culture", *Biomaterials*, **6**: 396-402, (1985).

3. Spector, M., Cease, C., Tong-Li, X., "The local tissue response to biomaterials", *Crit. Rev. Biocomp.*, **5** (3): 269-295, (1989).

4. Walls, J.M., "Methods of surface analysis", Methods of Surface Analysis, Walls, J.M., Ed., Cambridge University Press, Cambridge, U.K., (1989)

5. Biswas, S., Falster, R., Kelly, I. E., Littlewood, S. D., "Quantification of surface contamination on silicon wafers using polyencapsulation SIMS", Secondary Ion Mass Spectrometry (SIMS VII), 591-597, (1989)

6. Liu, J., Hsieh, Y.-Z., Wiesler, D., Novotny, M., "Design of 3-(4-carboxybenzoyl)-2-quinolinecarboxaldehyde as a reagent for ultrasensitive determination of primary amines by capillary electrophoresis using laser fluorescence detection", *Anal. Chem.*, **63**: 408-412, (1991).

7. Liu, J., Shirota, O., Wiesler, D., Novotny, M., "Ultrasensitive fluorometric detection of carbohydrates as derivatives in mixtures separated by capillary electrophoresis", *Proc. Natl. Acad. Sci. USA*, **88**: 2302-2306, (1991).

8. Ngo, T.T., "Colorimetric determination of reactive amino groups of a solid support using Traut's and Ellman's reagents", *Appl. Biochem. Biotech.*, **13**: 213-219, (1986).

9. Gaur, R.K., Gupta, K. C., "A spectrophotometric method for the estimation of amino groups on polymer supports", *Anal. Biochem.*, **180**: 253-258, (1989).

10. Christie, A.B., "X-ray photoelectron spectoscopy", Methods of Surface Analysis, Walls, J.M., ed., Cambridge Univ. Press, Cambridge, U. K., (1989)

11. Grant, J.T., "Methods for quantitative analysis in XPS and AES", *Surf. Inter. Anal.*, **14**: 271-283, (1989).

12. Briggs, D., Beamson, G., "Primary and secondary oxygen-induced C1s binding energy shifts in X-ray photoelectron spectroscoy of polymers", *Anal. Chem.*, **64**: 1729-1736, (1992).

13. Wang, J., Feng, D., Wang, H., Rembold, M., Thommen, F., "An XPS investigation of polymer surface dynamics. I. A study of surfaces modified by CF_4 and CF_4/CH_4 plasmas", *J. Appl. Poly. Sci.*, **50** : 585-599, (1993).

14. Lewis, K.B., Ratner, B. D., "Observation of surface rearrangement of polymers using ESCA", *J. Coll. Inter. Sci.*, **159**: 77-85, (1993).

15. Sawada, K., Shimoyama, T., Malchesky, P. S., Goldcamp, J. B., Omokawa, S., "Evaluation of a relationship between polymer bulk hydroxyl and surface oxygen content and *in vitro* serum-material interaction", *J. B. M. R.*, **27**: 547-555, (1993).

16. Lin, H.-B., Sun, W., Mosher, D. F., Garcia-Echeverria, C., Schaufelberger, K., Lelkes, P. I., Cooper, S. L., "Synthesis, surface, and cell-adhesion properties of polyurethanes containing covalently grafted RGD-peptides", *J. B. M. R.*, **28**: 329-342, (1994).

17. Ameen, A.P., Ward, R. J., Short, R. D., Beamson, G., Briggs, D., "A high-resolution X-ray photoelectron spectroscopy study of trifluoroacetic anhydride labelling of hydroxyl groups: demonstration of the b shift due to $-OC(O)CF_3$", *Polymer*, **34** (9): 1795-1799, (1993).

18. Barrera, D.A., "Synthesis and characterization of a novel biodegradable polymer-poly(lactic acid-*co*-lysine)", Ph.D. Thesis, M.I.T. (1993)

19. King, R.N., Andrade, J. I. Ma, S. M., Gregonis, D. E., Brostrom, L. R., "Interfacial tensions at acrylic hydrogel-water interfaces", *J. Coll. & Inter. Sci.*, **103** (1): 62-75, (1985).

20. Pettit, D.K., Horbett, T. A., Hoffman, A. S., "Influence of the substrate binding characteristics of fibronectin on corneal epithelial cell outgrowth", *J. Biomed. Mat. Res.*, **26**: 1259-1275, (1992).

21. Park, A., Cima, L. G., "In vitro cell response to differences in poly-L-lactide crystallinity", *J. B. M. R.*, (submitted): (1995).

22. Mantus, D. S., Ratner, B. D., Carlson, B. A., Moulder, J. F., "Static secondary ion mass spectrometry of adsorbed proteins", *Anal. Chem.*, **65**: 1431-1438, (1993).

23. Chilkoti, A., Lopez, G. P., Ratner, B. D., Hearn, M. J., Briggs, D., "Analysis of polymer surfaces by SIMS. 16. Investigation of surface cross-linking in polymer gels of 2-hydroxyethyl methacrylate", *Macromol.*, **26**: 4825-4832, (1993).

24. Brinen, J. S., Greenhouse, S., Jarrett, P. K., "XPS and SIMS studies of biodegradable suture materials", *Surf. Inter. Anal.*, **17**: 259-266, (1991).

25. Davies, M. C., Lynn, R. A. P., Davis, S. S., Hearn, J., Vickerman, J. C., Paul, A. J., "The application of time-of-flight SIMS for the surface characterization of polymer latex particles prepared with immobilized sugar residues", *J. Coll. Inter. Sci.*, **161**: 83-90, (1993).

26. van Leyen, D., Deimel, M., Hagenhoff, B., Benninghoven, A., "Secondary ion formation from polymer materials: a systematic investigation", Secondary Ion Mass Spectrometry (SIMS VII), 757-760, (1989)

27. Cornelio, P. A., Clark, M. B., Jr., Gardella, J. A., Jr., "Quantitation of organic molecular ions in static secondary ion mass spectrometry: can it be done?", Secondary Ion Mass Spectrometry (SIMS VII), 761-764, (1989)

28. Davies, M. C., Short, R. D., Khan, M. A., Watts, J. F., Brown, A., Eccles, A. J., Humphrey, P., Vickerman, J. C., Vert, M., "An XPS and SIMS analysis of biodegradable biomedical polyesters", *Surf. Inter. Sci.*, **14**: 115-120, (1989).

29. Brown, A., Vickerman, J. C., "Static SIMS for applied surface analysis", *Surf. and Inter. Analysis*, **6** (1): 1-14, (1984).

30. Briggs, D., "SIMS for the study of polymer surfaces: a review", *Surf. and Inter. Analysis*, **9**: 391-404, (1986).

Appendix 5A
Determination of Lysine and Peptide Surface Densities from XPS

In the samples analyzed by XPS within this polymer system, there are three entities in a stoichiometrically ideal surface:

Peptide (+ CO from CDI) : $C_{24}H_{33}O_9N_9I_2$ MW =845 g/mol

MW = Lysine: $C_6H_{11}N_2O$ MW = 127 g/mol

Lactic Acid: $C_3H_4O_2$ MW = 72 g/mol

For purposes of illustration, suppose the surface is characterized by XPS and found to contain the following mole fractions of C, O, N and I:

C: 0.6285, O: 0.3545, N: 0.0156, I: 0.0014

The question is, what are the mole fractions of the peptide, lysine and lactic acid repeat units on the surface of the polymer? Using as a basis 1 mole of atoms, then the mole fractions can be considered absolute numbers. Since the iodine is only found in the peptide, and there are 2 moles of iodine per peptide, then there are 0.0014/2 = 0.0007 moles of peptide. Since there are 9 moles of nitrogen per peptide, there are 0.0063 moles of N from the peptide, leaving 0.0156 - 0.0063 = 0.0093 moles of N from lysine. Since there are 2 moles of N per mole of lysine, then there are 0.0093/2 = 0.00465 moles of lysine. Using the amount of oxygen or carbon in the lysines and the peptides, one can then determine the amount of lactic acid. First, using the oxygen: there are 9 moles of oxygen per mole of peptide, so 9(.0007) = 0.0063 moles of oxygen from the peptide, and there is one mole of oxygen from the lysines, so there is 1(.00465) = 0.00465 moles of oxygen from the lysines. Subtracting the moles of oxygen contributed by the lysine and the peptides from the total moles of oxygen gives 0.3545 - .00465 - .0063 = 0.34355 moles of oxygen from lactic acid. Since there are 2 moles of oxygen per mole of lactic acid, then there are 0.34355/2 = 0.171775 moles of oxygen.

Adding up the 3 absolute values and dividing by the total gives the mole fraction of lysine, peptide and lactic acid in the sample.

	Absolute	Mole Fraction	Mole %
Peptide:	.0007	.00395	0.395
Lysine:	.00465	.02625	2.625
Lactic Acid	.171775	.969795	96.980
Total	.177125	1.000	100.00

A second calculation, using carbon gives similar results: there are 24 carbons from the peptide, so 24(.0007) = 0.0168 moles of carbon from the peptide. There are 6 carbons from the lysine, so 6(.00465) = 0.0279 moles of carbon from the lysine. Subtracting from the total carbon gives .6285 - 0.0186 - 0.0279 = 0.5838, which can be assigned to the lactic acid. Since there are 3 moles of carbon per mole of lactic acid, then there are 0.5838/3 = .1946 moles of lactic acid. Adding up the 3 absolute values and dividing by the total gives the mole fraction of lysine, peptide and lactic acid in the sample.

	Absolute	Mole Fraction	Mole %
Peptide	.0007	.0035	0.35
Lysine	.00465	.0233	2.33
Lactic Acid	.1946	.9732	97.32
Total	.19995	1.000	100.00

The differences in the two approaches could be a result of hydrocarbons or silicon grease contamination which contribute carbons or oxygens to the totals, but which are not accounted for in this calculation.

XPS Data is given in units of atomic percent. It is based on the ratio of the area under the curve of the electron binding energies for each of the elements. The units are number of electrons from a given element per total number of electrons from all the elements analyzed. For example:

% Iodine = 100 x (molecules of iodine)/(total molecules of iodine, carbon, nitrogen and oxygen)

The contribution to the total number of carbon atoms is from the lactic acid residues, the lysine residues, and the peptides. If we introduce a factor to account for the contributions of the 3 different species to the total atom count,

then we can calculate the percent of each entity by solving the equations for the new factors. For example:

Let x = mole fraction of lysine
Let y = mole fraction of peptide
Then 1-x-y = mole fraction of lactic acid

I = mole fraction of iodine (atomic % /100)
N = mole fraction of nitrogen (atomic % /100)
C = mole fraction of carbon (atomic % /100)
O = mole fraction of oxygen (atomic % /100)

Lysine = $C_6H_{11}N_2O$	9 atoms/mole (w/o hydrogen)
Lactic acid = $C_3H_4O_2$	5 atoms/mole (w/o hydrogen)
Peptide + CDI = $C_{24}H_{33}O_9N_9I_2$	44 atoms/mole (w/o hydrogen)

Each atom is counted equally in the following calculation because the XPS analysis has corrected for differences in electrons from different atoms by dividing by a sensitivity factor based on the cross-sectional area of the various atoms. The mole fractions of the lysine + lactic acid + peptide will equal 1. The mole fractions of the C, O, N and I will equal 1. From the stoichiometry of an ideal surface composed solely of residues of lactic acid, lysine and peptides, the following equation describes what the XPS is telling us:

I = [(2 moles iodine/mol peptide) . (y moles peptide/total moles)]/{(44 moles of atoms/mol peptide) . (y moles peptide/total moles) + (9 moles atoms/mol lysine). (x moles lysine/total moles) + (5 moles atoms/mol lactic acid) . (1-x-y moles lactic acid/total moles)}

Rewriting gives:
$I = 2y/(39y + 4x + 5)$

For the other elements:
$N = (9y + 2x)/(39y + 4x + 5)$
$C = (21y + 3x + 3)/(39y + 4x + 5)$
$O = (7y - x + 2)/(39y + 4x + 5)$

(Notice that the sum of I + N + C + O = 1.)

It is sufficient to pick only two equations to solve for expressions for y and x in terms of the elemental compositions. Let's use I and N.

From the I equation:

$$39\,y\,I + 4\,x\,I + 5\,I = 2\,y$$

$$y\,(39\,I - 2) = -4\,x\,I - 5\,I$$

$$y = (-4\,x\,I - 5\,I)/(39\,I - 2)$$

From the N equation:

$$39\,y\,N + 4\,x\,N + 5\,N = 9\,y + 2\,x$$

$$x\,(4\,N - 2) = 9\,y - 39\,y\,N - 5\,N$$

$$x = (9\,y - 39\,y\,N - 5\,N)/(4\,N - 2)$$

To solve for y alone, substitute x into y above.

$$y = \{-4\,[(9\,y - 39\,y\,N - 5\,N)/(4\,N - 2)]\,I - 5\,I\}/(39\,I - 2)$$

$$y = \{[(-36\,y\,I + 156\,y\,N\,I + 20\,N\,I)/(4\,N - 2)] - 5\,I\}/(39\,I - 2)$$

$$y(39\,I - 2) + 5\,I = (-36\,y\,I + 156\,y\,N\,I + 20\,N\,I)/(4\,N - 2)$$

$$(39\,y\,I - 2\,y + 5\,I)\,.\,(4\,N - 2) = (-36\,y\,I + 156\,y\,N\,I + 20\,N\,I)$$

$$156\,y\,N\,I - 8\,N\,y + 20\,N\,I - 78\,y\,I + 4\,y - 10\,I = 156\,y\,N\,I - 36\,y\,I + 20\,N\,I$$

$$-8\,N\,y + (-78 + 36)\,y\,I + 4\,y - 10\,I = 0$$

$$y\,(-8\,N - 42\,I + 4) = 10\,I$$

$$y = 10\,I/(4 - 8\,N - 42\,I)$$

To calculate peptide, lysine and lactic acid, use the same example from above:

$$C: 0.6285, \quad O: 0.3545, \quad N: 0.0156, \quad I: 0.0014$$

$$y = 10\,(.0014)/[4 - 8(.0156) - 42\,(.0014)] = 0.003668$$

$$x = [9\,(.003668) - 39\,(0.003668)\,(0.0156) - 5\,(0.0156)]/[4(0.0156) - 2] = 0.02437$$

$$1\text{-}x\text{-}y = 1 - 0.02437 - 0.003668 = .97196$$

Comparing these results to the results obtained in the first method gives:

	Mole % (using O)	Mole % (using C)	Mole % (Equations)
Peptide	0.40	0.35	0.37
Lysine	2.63	2.33	2.44
Lactic Acid	96.98	97.32	97.20

The equations are the easiest and most straight forward, so they were used to calculate the surface densities of peptides and lysine. They give an average value. From the mole fractions, we make some assumptions about our surfaces in order to calculate the surface densities.

Assumptions:

The surface is homogeneous and continuous (no pores or cracks)

The surface is defined as the top 10 Å

The density of the polymer is 1 g/cm^3

The distribution of the peptides in the top 10 Å is the same as in the top 30 to 100 Å, where the XPS data is taken.

The average molecular weight of the entities is that of lactic acid repeat unit (72 g/mol)

The calculation is as follows:

The total amount of peptide is found from the geometry of the volume which is examined:

Volume = (area) · (depth)

Area = $1.7\,x^2\,\pi/4$, where x = spot size (1000, 600, 300 or 150 μm)

Depth = 100 Å for TOA = 0°
50 Å for TOA = 35°
40 Å for TOA = 70°

Peptide = (Volume) (Density) (mole fraction peptide)/(MW)

For example, if a 1000 μm spot size is used and 0° TOA, then the area is

$$1.7\ (1000\ \mu m)^2\ \pi/4\ (10{,}000\ \mu m/cm)^2 = .01335\ cm^2$$

$$\text{Volume} = (0.01335\ cm^2)\ (100\ Å)\ (1\ cm/10^8\ Å) = 1.335 \times 10^{-8}\ cm^3$$

$$\text{Moles of Peptide} = \frac{(1.335 \times 10^{-8}\ cm^3)\ (1g/cm3)\ (10^{15}\ fmol/mol)\ (0.0037)}{(72g/mol)}$$

= 686 fmol in the top 100 Å

There should be only 1/10th in the top 10 Å, so that is 68.6 fmol.

Then the peptide density would be 68.6 fmol/.01335 cm^2 = 5139 fmol/cm^2

Appendix 5B
Sample Calculation of Surface Energy

Using underwater sessile drops of air, Young's equation can be written as:

$$\gamma^*_{SV} = \gamma_{SW} + \gamma_{WV} \cos \theta_{air} \qquad [5B.1]$$

where γ^*_{SV} denotes the fully water-equilibrated-solid surface tension, S denotes the solid surface, V denotes water-vapor and W denotes water. Using underwater sessile drops of octane, a second equation can be written:

$$\gamma^*_{SO} = \gamma_{SW} + \gamma_{WO} \cos \theta_{Octane} \qquad [5B.2]$$

where γ^*_{SO} designates the fully water-equilibrated-solid surface tension as measured with octane (O).

There are two unknowns in each of the underwater forms of Young's equation: γ^*_{SV} and γ_{SW} in equation [5B.1] and γ^*_{SO} and γ_{SW} in equation [5B.2], but since γ_{SW} is the same in each equation, then there are just three unknowns. The system of two equations cannot be solved, so additional relationships are needed. Each of the surface energies can be divided into polar and dispersive components. For example, the solid-water vapor surface energy is defined as:

$$\gamma^*_{SV} = \gamma^p_{SV} + \gamma^d_{SV} \qquad [5B.3]$$

When these substitutions are made, each unknown is replaced by two unknowns. The harmonic mean equation can be used to approximate the solid-liquid interfacial tensions as weighted averages of the effects of the surface-water vapor and liquid-vapor interfacial tensions. These approximations are shown in equations [5B.4] and [5B.5].

$$\gamma^*_{SO} \approx \gamma^*_{SV} + \gamma_{OV} - 4\left(\frac{\gamma^d_{SV}\gamma^d_{OV}}{\gamma^d_{SV} + \gamma^d_{OV}}\right) - 4\left(\frac{\gamma^p_{SV}\gamma^p_{OV}}{\gamma^p_{SV} + \gamma^p_{OV}}\right) \qquad [5B.4]$$

$$\gamma_{SW} \approx \gamma_{SV}^{*} + \gamma_{WV} - 4\left(\frac{\gamma_{SV}^{d}\gamma_{WV}^{d}}{\gamma_{SV}^{d} + \gamma_{WV}^{d}}\right) - 4\left(\frac{\gamma_{SV}^{p}\gamma_{WV}^{p}}{\gamma_{SV}^{p} + \gamma_{WV}^{p}}\right) \qquad [5B.5]$$

By introducing the harmonic mean equations, additional relationships between the known quantities and unknown variables are created, giving us more equations. The system now consists of 4 equations and 4 unknowns. The unknowns, are γ_{SO}^{*}, γ_{SV}^{d}, γ_{SV}^{p}, and γ_{SW}. If the contact angles of two liquids (with known γ_{LV}^{d} and γ_{LV}^{p}) are measured on the same surface, one has a system of equations which can be solved for γ_{SV}^{d} and γ_{SV}^{p}. For example, the surface energies of stable hydrophilic surfaces such as hydrogels were determined with underwater captive bubbles of air and a hydrocarbon (19).

Substituting equations [5B.4] and [5B.5] into equation [5B.2], rearranging, solving for γ_{SV}^{p} and simplifying for the special case of octane and water, in which the following statements hold, yields equation [5B.6].

$$\gamma_{OV}^{d} = 21.6 \text{ dyne/cm at } 25°C$$
$$\gamma_{OV}^{p} = 0 \text{ dyne/cm at } 25°C$$
$$\gamma_{WV}^{d} = 21.6 \text{ dyne/cm at } 25°C$$
$$\gamma_{WV}^{p} = 50.5 \text{ dyne/cm at } 25°C = \gamma_{OW}$$

(The second half of the last equation is true if one assumes that the spreading pressure of water vapor on liquid octane is zero, since this requires that the polar component of water and the octane-water interfacial tension be equal.)

$$\gamma_{SV}^{p} = 50.5 \frac{K_{octane}}{50.5 - K_{octane}} \qquad [5B.6]$$

where $K_{octane} = 50.5\,(1 + \cos\theta_{octane})\,/\,4$.

Repeating the substitution, rearrangement, solving for γ_{SV}^{d} and simplification for the case of captive air bubbles, in which the following relations hold, yields equation [5B.7].

$$\gamma^d_{LV} = 0$$
$$\gamma^p_{LV} = 0$$
$$\gamma_{WV} = 72$$
$$\gamma^d_{WV} = 21.6 \text{ dyne/cm at } 25°C$$
$$\gamma^p_{WV} = 50.5 \text{ dyne/cm at } 25°C = \gamma_{OW}$$

$$\gamma^d_{SV} = \frac{21.6\, K_{air} - \gamma^p_{SV}\left\{\frac{(21.6)\,(50.5)}{\gamma^p_{SV} + 50.5}\right\}}{21.6 - K_{air} + \gamma^p_{SV}\left\{\frac{(50.5)}{\gamma^p_{SV} + 50.5}\right\}} \qquad [5B.7]$$

where $K_{air} = 72.1(1 + \cos\theta_{air}) / 4$, θ_{octane} and θ_{air} are in degrees, and γ_{SV} is the hydrated solid surface energy. From measurements of θ_{air} and θ_{octane}, these equations were solved to yield the values for surface energy of the PLAL samples shown in Table 5.17 and Figure 5.12.

Chapter 6

Cell Interactions

6.1 Introduction

The hypothesis of this research project was that immobilized cell adhesion molecules such as those containing the Arginine-Glycine-Aspartic Acic (RGD) sequence would interact with cells to produce alterations in cell behavior. This chapter describes the experiments which were conducted to examine this hypothesis. The effect of immobilized RGD peptides on the adhesion and spreading behavior of bovine aortic endothelial (BAE) cells was evaluated. In addition, the viability of cells in contact with the various substrates was measured. BAE cells were used in all of the experiments due to the potential application of endothelial cells in the development of tissue engineered blood vessels and because they are relatively easily handled. This model system illustrates only one way in which this polymer system can be utilized. Other potential applications (*e.g.*, the promotion of proliferation through the attachment of growth factors) were not investigated, although there are many possible uses for this system (1-14).

6.1.1 Cell Adhesion Assays

The most common method of measuring cell adhesion is to allow cells to settle onto a substrate, incubate them for a specified amount of time, and then remove the nonadherent cells by gentle washing. Results are reported as the fraction of the original quantity of cells that adhered. The main argument against these types of experiments is that the force of adhesion is not determined accurately. Efforts have therefore been made to develop assays for measuring the strength of cellular adhesion. For example, DiMilla, *et.al.* , have developed a method to measure cell adhesion and migration using an axisymmetric radial flow detachment assay (RFDA). Using this method they were able to measure the strength of the cell-substratum adhesive bond for human smooth muscle cells (1). Gryte has developed a method to measure cell adhesion using a quartz crystal microbalance (QCM) (2). This method uses the piezoelectrically active area of a QCM to monitor changes in the resonant frequency caused by cells

spreading on a metal surface connected to the QCM. The goal of the investigators is to use this technology to develop an automated adhesion detection system.

Cell adhesion to RGD-containing peptides and proteins

There have been numerous studies of cell adhesion to surfaces coated with RGD-containing peptides. For example, Mooney measured hepatocyte adhesion to RGD-coated polystyrene after 48 hours incubation at 37°C and at increasing concentrations of synthetic RGD (3). These studies showed that hepatocytes adhere to RGD-coated polystyrene dishes independently of the RGD density. In addition, Massia and Hubbell (4-10) have characterized RGD on glass and other polymers and shown that cell adhesion is enhanced on these surfaces. Likewise, Lin and Cooper have attached RGD-containing peptides to polyurethane (11). The peptide-grafted surfaces supported the adhesion and spreading of human umbilical vein endothelial cells (HUVEC) even without serum in the culture medium (12). Quantification of adherent cells was performed visually after 4 hours incubation and a gentle rinse to remove loose cells. Fifty percent of the cells adhered to RGDV-grafted surfaces, 23% adhered to RGDS-grafted surfaces, and 5% to controls. In other studies, Matsuda attached RGD-containing peptides to PVA and measured cell adhesion (13) and Brandley attached a nonapeptide containing the RGD sequence to previously nonadherent polyacrylamide and showed that fibroblasts grew at a rate comparable to that on tissue culture plastic (14).

6.1.2 Cell Detachment Assays

Hubbe published a classic review in 1981 describing the types of cell detachment assays that can be performed (15). Most of the described methods were developed in order to measure the forces required for detachment of cells. These methods include: micromanipulation, centrifugation, and hydrodynamic shear. In order to measure detaching forces of lesser magnitude, methods such as detachment by gravity, elution through packed columns, deposition on a prepared surface followed by a gentle rinse, or intercellular aggregation can be used. Temperature is a key parameter in cellular adhesion--it affects rates of metabolism, rates of other chemical reactions, conformations of proteins, adsorption at the cell surface, and the fluidity of the cell membrane. Processes of detachment and attachment are fundamentally different and not just the reverse

of each other. It is often observed in cell detachment assays that cellular material is left behind, indicating that it is the failure of the cell membrane and not the receptor-ligand bond that results in detachment. The main objection against these cell detachment assays is the lack of evidence that the forces measured are due to the specific interactions of the substrate and the integrin molecules within the cell membranes. The cell membranes are often disrupted by the applied forces before the cell adhesion molecules are loosened, indicating that the strength of the cell membrane may be below that of the integrin/receptor bond.

6.1.3 Spreading Assays

One of the first events that occurs after the attachment of cells to surfaces is the enlargement of the cell surface area through the formation of polymerized actin filaments and the assembly of microtubule bundles. This phenomenon is termed cell spreading and is characterized by the protrusion of pseudopods or filapodia from the cell outward. Endothelial cells spread on many surfaces, and the rate of cell spreading on fibronectin surfaces is well characterized (25). Spreading assays consist of measuring the initial cell surface area and following the increase in cell area over time, usually through the use of video microscopy. Images of the cells are captured, digitized and analyzed by computer.

6.2 Adhesion and Spreading Experiments

6.2.1 Materials and Methods

Samples of PLAL with attached peptides were prepared for adhesion and spreading experiments by sterilization under U.V. lamp for 10 minutes on each side and then by soaking in sterile phosphate buffered saline (PBS, pH 7.2, supplemented with 0.5% Penicillin, 0.5% streptomycin, and 1% L-glutamine) for at least 24 hours prior to seeding with cells. The samples were placed in a 24 well plate so that the side which contacted glass during casting was exposed to the cells. The samples were fixed to the bottom of the wells with sterile vacuum grease.

Bovine aortic endothelial (BAE) cells were maintained in Dulbecco's Modified Eagle Medium (DMEM) with 1000 mg/L glucose (low glucose) supplemented with 10% calf serum, 0.5% penicillin, 0.5% streptomycin, and 1% L-glutamine at sub-confluency between passages 5 and 9. Fresh media was supplied every 3 to 4 days. Every 6 to 8 days the cells were removed from the tissue culture dishes by removing the old media, rinsing with 10 ml of phosphate

buffered saline (PBS) without Ca^{++} or Mg^{++}, and adding 2 ml of 0.05% trypsin in 0.53 mM EDTA in Hank's buffered salt solution (HBSS). The cells were then incubated in trypsin at 37°C for 2-5 min., suspended, and transferred to new dishes containing fresh media. The cells were incubated at 37°C in a humidified incubator with 5% CO_2.

The BAE cells were a generous gift of Dr. Elazar Edelman. Dulbecco's modified Eagle medium (DMEM) with low glucose, Trypsin/EDTA, Penicillin, Streptomycin, L-Glutamine, and Phosphate buffered saline (PBS) were obtained from GIBCO/BRL. Soy Bean Trypsin Inhibitor (SBTI) was obtained from Sigma. Bovine Serum Albumin (Fraction V) was obtained from ICN. Calf serum was obtained from Hyclone.

Immediately prior to cell seeding, the samples were rinsed three times with sterile PBS. The cells were harvested using trypsin/EDTA, which was quenched by SBTI, then centrifuged and resuspended in DMEM without serum. Approximately 10,000 cells/cm^2 were placed on each sample. A complete protocol for these experiments is included in Appendix 6A.

Electron photomicrographs of polymer samples and cells attached to polymer samples were taken with an ElectroScan Environmental SEM located in the Electron Microscopy Facility at MIT. Polymer samples were prepared by mounting the samples on aluminum stubs using double-sided conducting tape. Polymer samples with cells attached to the surface were prepared by fixing the samples in a 1% glutaraldehyde solution for >10 min., rinsing in PBS, then rinsing in a graded series of ethanol solutions (50, 70, 90, and 100%), and allowing the samples to air dry before mounting the samples on aluminum stubs. Samples were analyzed at 10 or 15 keV.

6.2.2 Results

Spreading on samples of PLAL+GRGDY

In the first set of experiments, PLA was compared to PLAL+GRGDY samples. Table 6.1 shows the results of these experiments. Figure 6.1 gives a visual comparison of cell attachment to PLA and to PLAL+GRGDY after 2 hours. Data was accumulated from the SEM photographs by tracing the projected cell area using NIH Image software, version 1.56 . Figure 6.2 shows the distribution of cell areas which resulted from incubation on PLA vs. PLAL+GRGDY for 2 hours.

Table 6.1
Results of Spreading Experiments

	PLA Samples			
Sample	A (#19)*	B (#20)	C (#24)	D (#34)
Cell Area (μm^2)				
< 199	36	27	10	49
200-399	0	0	5	31
# of cells	36	27	15	80
Ave ± SD	95 ± 33	63 ± 27	208 ± 66	182 ± 75

	PLAL + GRGDY Samples	
Sample	A (#32)	B (#43)
Cell Area (μm^2)		
< 199	0	4
200-399	7	1
400-599	7	7
600-799	5	7
800-999	1	3
1000-1199	0	2
1200-1399	0	5
1400-1599	0	1
1600-1799	0	1
1800-1999	0	1
2000-2199	0	0
2200-2399	0	0
2400-2599	0	0
2600-2799	0	1
# of cells	20	33
Ave ± SD	506 ± 176	845 ± 558

Table 6.1: Results of initial cell spreading experiments comparing PLA to PLAL+GRGDY. Data are reported as projected cell areas and are grouped within 200 μm^2 ranges to illustrate the distribution of cell areas. (*Numbers in parentheses ae lab inventory numbers)

Figure 6.1
BAE Cell Behavior on PLA vs. PLAL+GRGDY

PLA

PLAL + GRGDY

Figure 6.1: SEM photomicrographs showing the visual appearance of BAE cells after 2 hrs. on PLA vs. PLAL+GRGDY.

Figure 6.2
Comparison of Spread Cell Area on PLA and PLAL + GRGDY

PLA

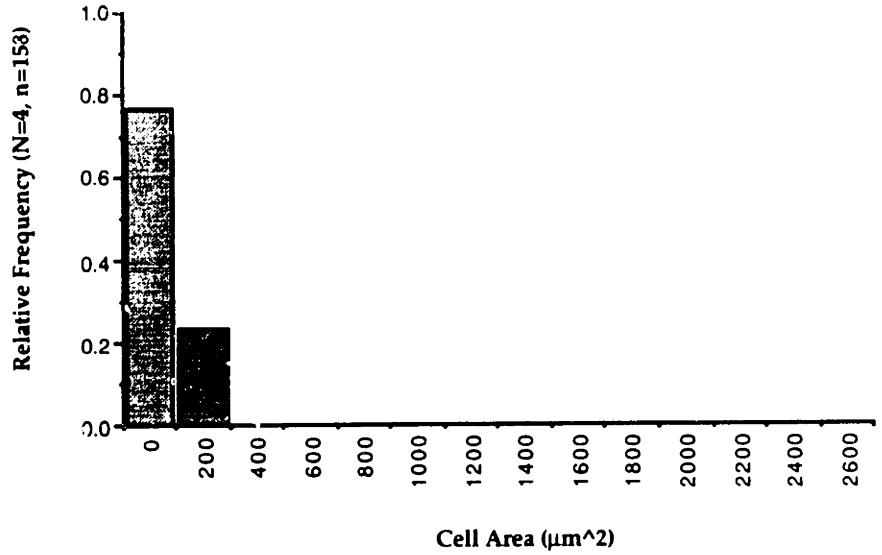

PLAL + GRGDY

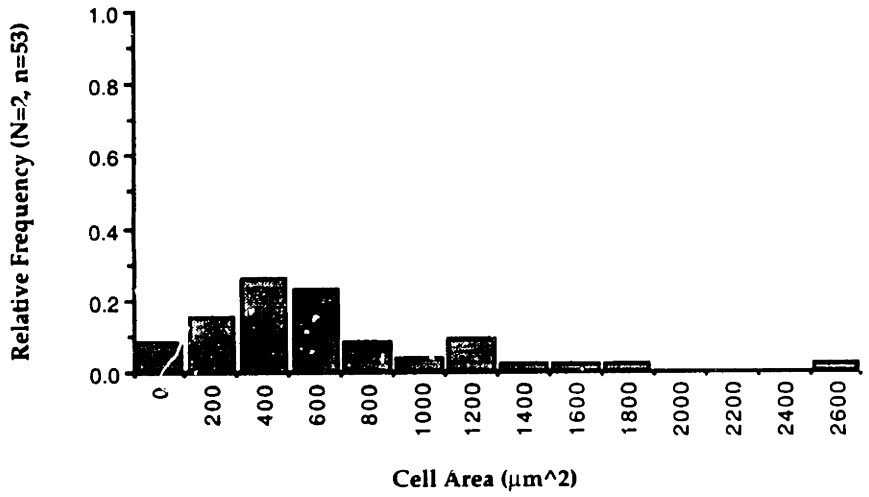

Figure 6.2: Histograms showing the distibution of cells on PLA and PLAL+GRGDY after 2 hrs. The abscissa values represent hte lowest value in the 200 μm2 range, for example: 0-199, 200-399, etc.

Spreading on blends of PLAL+GRGDS:PLA

In the second set of experiments, 40% blends of PLAL+GRGDS with PLA were used to create samples for testing. The control surfaces were PLA, 40% blends of PLAL+GRDGY with PLA, and 40% blends of PLAL with PLA. Positive and negative controls of tissue culture polystyrene with serum (PS + serum) and without serum (PS) were also included in each experiment. In this set of experiments, samples were incubated for 0, 0.5, 1, 1.5, 2 and 4 hours. Figure 6.3 shows the results of the cell spreading measurements for the 4 hour time points from one experiment. The data for all of the time points are shown in Table 6.2.

Figure 6.3
Spreading Measurements on 40% Blends

A.

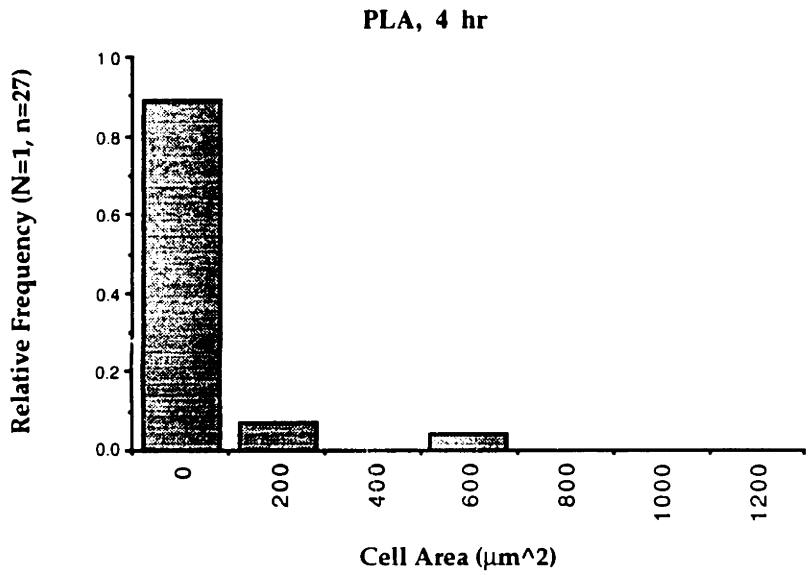

B.

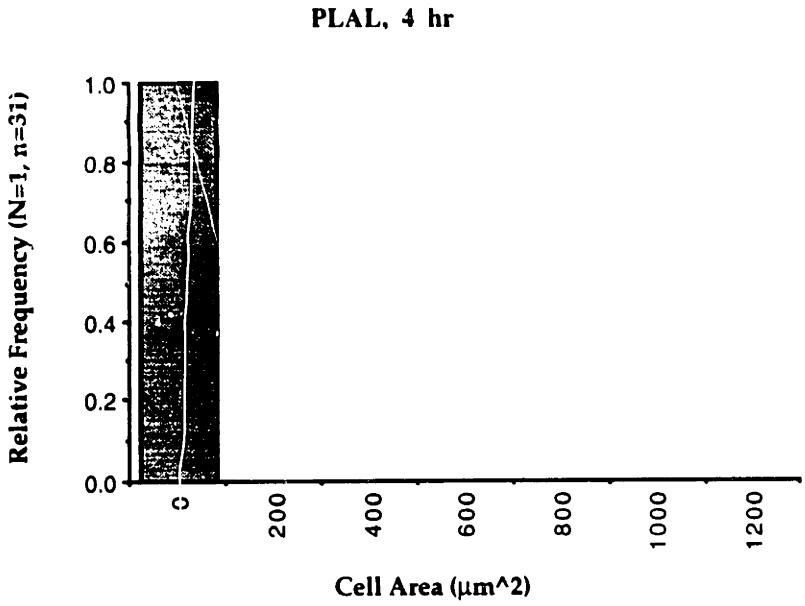
PLAL, 4 hr
Relative Frequency (N=1, n=31)
1.0
0.8
0.6
0.4
0.2
0.0
0
200
400
600
800
1000
1200
Cell Area (µm^2)

C.

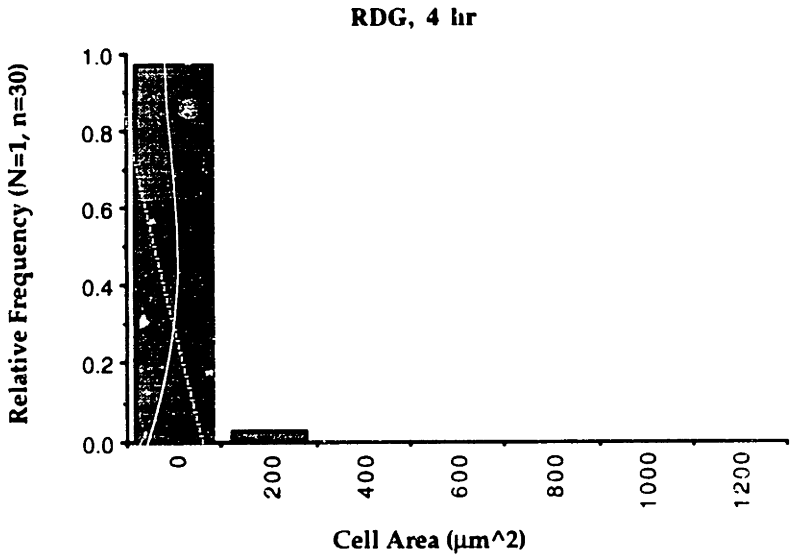
RDG, 4 hr
Relative Frequency (N=1, n=30)
1.0
0.8
0.6
0.4
0.2
0.0
0
200
400
600
800
1000
1200
Cell Area (µm^2)

D.

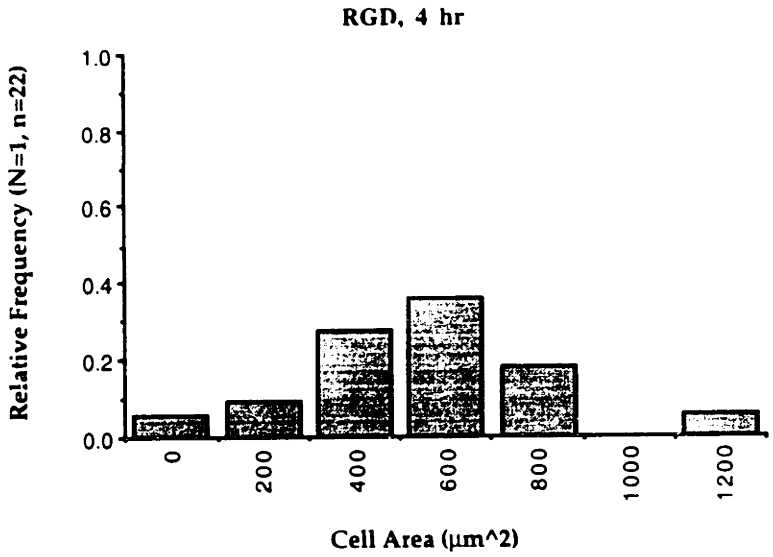
RGD, 4 hr
Relative Frequency (N=1, n=22)
1.0
0.8
0.6
0.4
0.2
0.0
0
200
400
600
800
1000
1200
Cell Area (μm^2)

E.

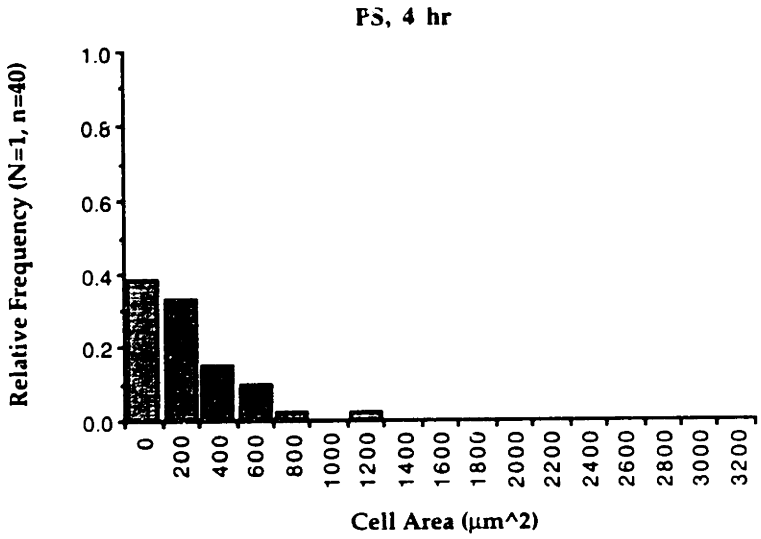
FS, 4 hr
Relative Frequency (N=1, n=40)
1.0
0.8
0.6
0.4
0.2
0.0
0
200
400
600
800
1000
1200
1400
1600
1800
2000
2200
2400
2600
2800
3000
3200
Cell Area (μm^2)

F.

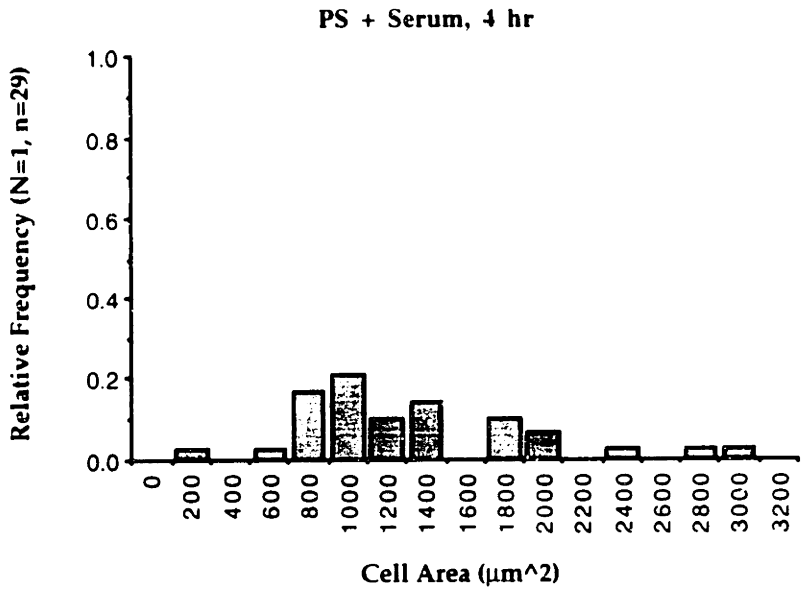

Figure 6.3: Histograms showing the distribution of BAE cells on (A) PLA, (B) 40% blends of PLAL, (C) 40% blends of PLAL+GRDGY, (D) 40% blends of PLAL+GRGDS, (E) PS and (F) PS+serum after 4 hrs.

Table 6.2
Spreading of BAE cells on 40% blends

PLA			RGD		
Time (hr)	n	Area (μm^2)	Time (hr)	n	Area (μm^2)
0	76	107 ± 6	0	53	77 ± 2
0.5	71	87 ± 6	0.5	78	191 ± 15
1	54	78 ± 4	1	83	167 ± 13
1.5	68	91 ± 6	1.5	68	231 ± 18
2	50	121 ± 8	2	103	257 ± 13
4	80	116 ± 11	4	72	405 ± 29
PLAL			**PS**		
0	46	93 ± 5	0	73	103 ± 4
0.5	61	120 ± 4	0.5	82	125 ± 10
1	47	103 ± 4	1	87	165 ± 11
1.5	66	108 ± 6	1.5	75	182 ± 9
2	60	81 ± 3	2	66	186 ± 16
4	62	87 ± 4	4	72	320 ± 27
RDG			**PS + Serum**		
0	49	98 ± 5	0	56	123 ± 6
0.5	82	86 ± 3	0.5	80	617 ± 35
1	70	77 ± 3	1	71	857 ± 41
1.5	67	73 ± 3	1.5	78	915 ± 46
2	57	83 ± 4	2	71	1148 ± 66
4	82	105 ± 4	4	69	1466 ± 77

Table 6.2: Cell Spreading results of 2 experiments (N=2) of BAE cells on PLA, 40% blends of PLAL, 40% blends of PLAL+GRDGY, 40% blends of PLAL+GRGDS, PS , and PS+serum. Data are Ave. ± S.E.M. The number of cells which were measured are indicated in the column under heading "n".

The results shown in Table 6.2 are the combined totals from experiments conducted on two separate days (N=2, n indicates the total number of cells which were measured). The averages for each sample are plotted in Figure 6.4 and 6.5.

Figure 6.4
Spreading of BAE cells on RGD vs. Polymer Controls

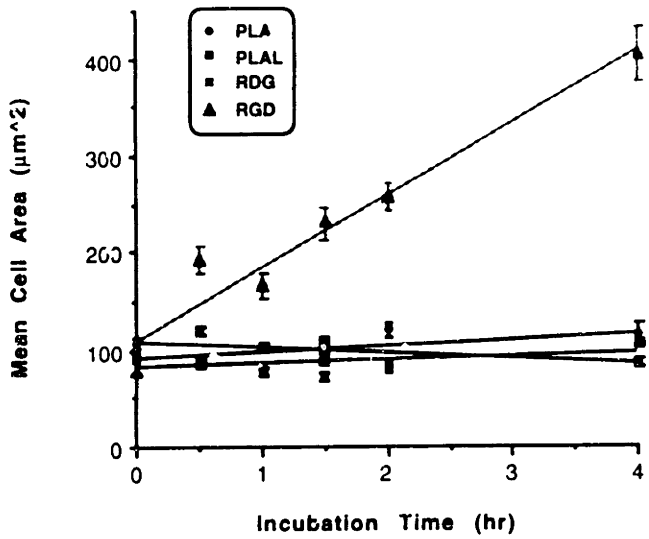

Figure 6.4: The spreading behavior of BAE cells vs. time is shown on PLA, PLAL, PLAL+GRDGY and PLAL+GRGDS. Data are Ave. ± S.E.M. from 2 full experiments (N=2). The number of cells measured at each time point (n) is shown in Table 6.2.

Figure 6.5
Spreading of BAE cells on PS and PS with Serum

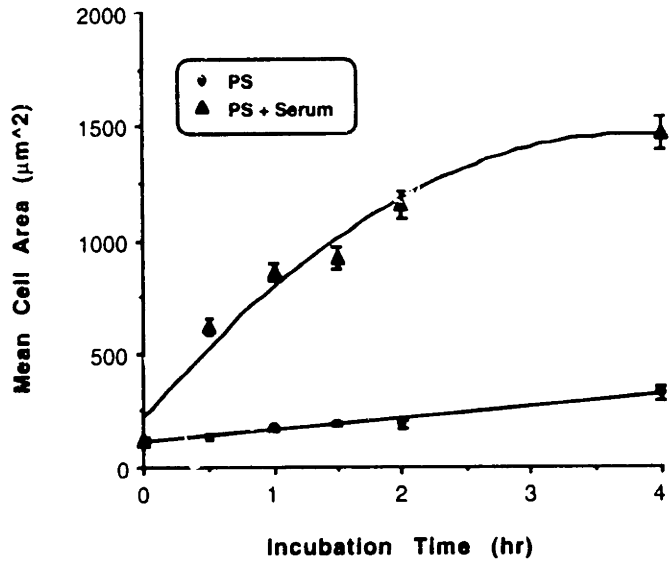

Figure 6.5: Spreading behavior of BAE cells vs. time on PS and PS+serum. Data are Ave. ± S.E.M. for 2 experiments (N=2). The number of data points at each time point (n) are shown in Table 6.2.

6.2.3 *Discussion*

The results obtained in the spreading experiments indicate that the RGD peptides are interacting with the BAE cells to produce an increase in cell area. No spreading was observed on the polymer controls. Statistical analysis of the 4 hour data in Figure 6.4 was conducted using Student's t-test for population means which are unequal and unknown. For this test, the standard deviations of the data were used instead of the standard error of the mean (S.E.M.). A one-tailed test using α=0.05 was performed to compare the average cell area on PLAL, RDG and RGD surfaces to the PLA surfaces. The null hypothesis was that the average cell area on each of the test samples (μ_2) was the same as the average cell area on PLA (μ_1). The alternative hypothesis was that the average cell area on the test samples was greater than on PLA. In order to accept the alternative hypothesis, the test statistic (T') must be less than $-t_\alpha$. The results are shown in Table 6.3. This analysis demonstrated that after 4 hours of incubation, the average cell area on RGD-containing surfaces was significantly higher than on any of the other surfaces. The behavior of the cells on RGD-containing surfaces is similar to the behavior of cells on serum-coated polystyrene. This indicates that the RGD sequence is mimicking the function of serum proteins.

Table 6.3
Statistical Analysis of 4 hr. Spreading Data

Sample	T'	ν	$-t_{0.05}$	Significant?
PLAL	2.54	99	-1.645	No
GRDGY	0.99	82	-1.645	No
GRGDS	-9.20	90	-1.645	Yes

Table 6.3: Student's t-test was used to compare the average spread cell area on PLAL, PLAL+GRDGY and PLAL+GRGDS surfaces to PLA. T' is the value of the test statistic, ν is the degrees of freedom, $-t_{0.05}$ is the value of the t-distribution for α=0.05. A significant difference in area is indicated in the last column for GRGDS-containing surfaces compared to PLA.

A second statistical analysis of this data was conducted on the slopes. For this test, the following test statistic (T) and degrees of freedom (ν)were used:

$$T = \frac{b_1 \sqrt{S_x}}{\sqrt{n\, s^2}} \qquad \nu = n - 2$$

This analysis tested the slopes of the lines to determine if there was a linear relationship between the cell area and incubation time. The results are shown in Table 6.4.

Table 6.4
Statistical Analysis of Slopes from Spreading Experiments

Sample	Slope	R^2	T	ν	$t_{0.05}$	Significant?
PLA	6.43	0.274	1.23	4	2.132	No
PLAL	-5.16	0.255	-1.17	4	2.132	No
GRDGY	3.19	0.133	0.78	4	2.132	No
GRGDS	75.01	0.942	8.06	4	2.132	Yes

Table 6.4: This analysis of slopes of the data in Figure 6.4 was performed to test whether or not there was a significant relationship between the cell area and incubation time.

From the test of the slopes, it was determined that only the RGD-containing polymer sample promoted cell spreading. The slope of the line is equal to the rate at which the BAE cells spread. This was determined to be 75 μm^2/hour. By comparison, the spreading rate on tissue-culture treated polystyrene (PS) was 53 μm^2/hr in the absence of serum and 301 μm^2/hr in the presence of serum proteins. The latter spreading rate compares very well to the rate of cell spreading of 312 μm^2/hr calculated from data gathered by Olivier and Truskey for BAE cells on fibronectin-coated microscope slides (25).

6.3 Viability Experiments

6.3.1 Materials and Methods

The Live/Dead® Viability/Cytotoxicity kit was obtained from Molecular Probes. The kit contained a 4mM solution of calcein AM in DMSO (Solution 1), and a 2mM solution of ethidium homodimer-1 (EthD-1) in 1:4 DMSO/H_2O (Solution 2). A working solution was prepared by mixing 5 µl of Solution 1 and 20 µl of Solution 2 in 10 ml of PBS to create a 2 µM solution of calcein AM and a 4µM solution of EthD-1. The Live/Dead® assay was performed on cells which

were exposed to samples of PLA, PLAL, PLAL+GRGEY, and PLAL+GRGDY, where the peptides were covalently attached by bulk chemistry and all of the samples were prepared by spraying the polymer from solution onto clean glass coverslips using a dental atomizer. BAE cells were seeded onto the samples and incubated for 2 hrs. at 37°C in DMEM without serum. The cell media was removed and 200 µl of the working solution was added to each well. After 30 min., the samples were viewed through a fluorescent microscope equipped with a long pass fluorescent filter and photomicrographs were taken using Fujicolor 1600 color film. Nonadherent cells were washed off and another set of photographs were taken. Data was accumulated by counting the number of live and dead cells before and after washing. Viability results were determined from the visual counts by dividing the total number of live cells by the sum of the live and dead cells.

6.3.2 Results

The results of the Live/Dead® Assay are shown in Table 6.5 and Figure 6.6. Statistical analysis of the data in Table 6.5 was performed using Student's t test for sample populations with unequal and unknown means. In each experiment the average % viability for PLA before washing was compared with the average % viability for the other three samples. Separate comparisons between PLA and the other three samples were made for the data after washing the samples. In all cases, there was no statistically significant difference (0.05 level of significance) between PLA and any of the other samples. Based on this analysis, the data were normalized by dividing each result by the average % viability for PLA within each data set. The resulting values were averaged, and are those presented as the combined data in Table 6.5 and Figure 6.6.

Table 6.5
Live/Dead Assay Results

Sample	% Viability Before Washing	Ave ± S. D.	% Viability After Washing	Ave ± S.D.
Experiment 1				
PLA	67, 63, 75, 60	66 ± 7	82, 91, 89, 94	89 ± 5
PLAL	87, 72, 56	72 ± 16	78, 90, 69	79 ± 11
RGD	60, 60, 63	61 ± 2	90, 46, 68	68 ± 22
RGE	62, 57, 67	62 ± 5	60, 78	69 ± 13
Experiment 2				
PLA	60, 47, 46	51 ± 8	22, 70, 89, 33	54 ± 35
PLAL	42, 58, 50	50 ± 8	85, 84, 56	75 ± 16
RGD	57, 42, 42	47 ± 9	41, 46, 61	49 ± 10
RGE	47, 47, 60	51 ± 8	72, 42, 22	45 ± 25

	% Viability (Ave ± S.D.)
Combined Data	Normalized to PLA = 1
PLA (N=2, n=15)	1.00 ± 0.28
PLAL (N=2, n=12)	1.09 ± 0.27
RGD (N=2, n=12)	0.88 ± 0.17
RGE (N=2, n=11)	0.90 ± 0.24

Table 6.5: The results of the Live/Dead Assay to determine the relative toxicities of the PLA, PLAL, and PLAL with attached peptides. Data are Ave ± S.D.

Figure 6.6
Live/Dead Assay Results

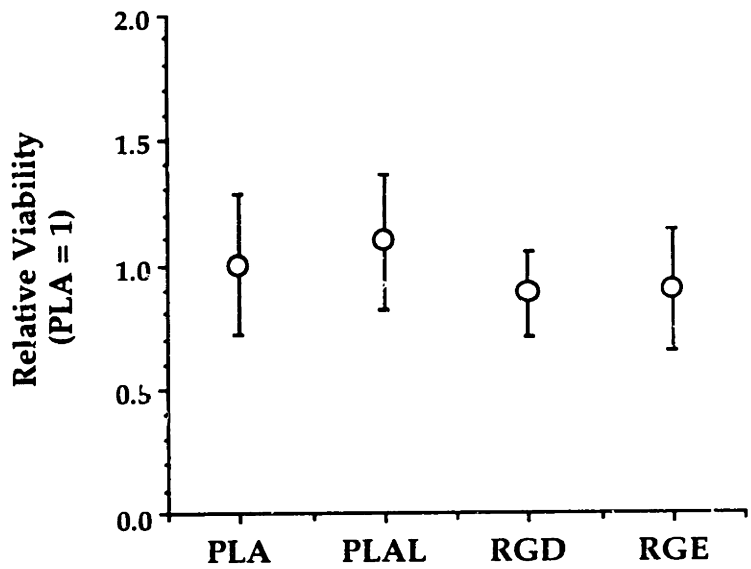

Figure 6.6: The results of the Live/Dead assay to determine the relative toxicities of PLA, PLAL, PLAL+GRGDY, and PLAL+GRGEY. Data are Ave. ± S. D. normalized to PLA = 1 within each experiment (N=2, n ≥ 11).

6.3.3 Discussion

The results of the Live/Dead® assay indicate that this is a reasonable method to assess the cytotoxicity of the polymer and peptide samples. The Live/Dead® assay is easy to perform, the reagents are non-toxic, and the cells can be removed and counted electronically, or allowed to proliferate after addition of the reagents. In theory, a transparent surface is not needed, so this assay could be conducted on thicker polymers, but the thicker samples which we created were unsatisfactory for this assay because they diffused the fluorescent light so that clear photographs were not obtainable. The results which were obtained were on samples prepared by spraying the polymers onto glass coverslips. The use of an epifluorescenct microscope system would enable one to obtain results on blends or solvent-cast films.

6.4 Theoretical Predictions

The mathematical description of the processes of cell adhesion and cell spreading have been shown to be useful in understanding the relative importance of the factors which contribute to the behavior of cells on various surfaces (16, 17). The first part of this section describes models of cell adhesion, while the second section describes cell spreading. The mathematical models of cell adhesion and spreading are described in order to provide a conceptual understanding of the processes which occur when a cell comes into contact with a surface. These models are based on the observation that cells interact with ligands for which the cells have specific receptors. Due to the fact that the PLAL+GRGDY samples which were developed and evaluated herein contain a measurable density of peptide ligands which are known to interact with a variety of integrin proteins found within endothelial cells, the parameters which are relevant to the design of scaffolds for tissue engineering were collected.

There are two principle ways to model cell adhesion: as an equilibrium phenomenon or as a dynamic process. The model that is chosen to describe the process of adhesion should reflect the experiments that are performed.

Equilibrium models

Two approaches have been taken to model cell attachment as an equilibrium phenomenon: as a thermodynamic equilibrium and as a mechanical equilibrium. One of the first attempts to explain cell adhesion mathematically was a thermodynamic equilibrium model developed by Bell (18, 19). The interaction of cells with surfaces was described as a competition between the formation of specific macromolecular bridges (integrin-receptor bonds) and non-specific repulsions. The minimization of the Gibb's free energy associated with the interactions of the receptors on the cell and the ligands on the surface was used to determine whether or not cells would attach. The mechanical equilibrium approach has been used by Evans (20), and more recently by Ward and Hammer (21).

Dynamic models

The first attempt to model cell adhesion as a dynamic phenomenon was made by Hammer, who extended Bell's mathematical model to sum the forces between the cell and surface, including fluid forces, gravity, and receptor-ligand bonds (16, 17). At the time Hammer developed his model, there was essentially

no experimental evidence to compare with his model. In an attempt to generate experimental data, Cozens-Roberts performed studies using a Radial-Flow Detachment Assay and measured the critical shear stress necessary to remove receptor-coated latex beads from ligand-coated glass surfaces (22). She also developed expressions to describe the total force exerted by the flowing fluid on an adherent particle and the number of bonds required for adhesion at the critical radius. Dembo, *et. al.* created a model to describe the reaction-limited kinetics of cell adhesion to surfaces (23). Kuo and Lauffenburger measured the adhesion strength of receptor ligand bonds and confirmed the prediction of the model developed by Dembo that adhesion strength varies with the logarithm of the binding affinity (24). Olivier and Truskey developed a model to describe the attachment and spreading of bovine aortic endothelial (BAE) cells under the influence of a laminar flow in a parallel plate flow chamber (25). Hammer's most recent work has consisted of computer-aided simulations of cells as they approach a surface and begin to form bonds (26).

The use of mathematical models to describe the attachment of BAE cells to ligand-containing surfaces is illustrated below by showing calculations from two of the existing models applied to PLAL+GRGDY peptides.

6.4.1 Point Attachment Model

The first model developed by Hammer and Lauffenburger to describe receptor/ligand mediated cell adhesion has become known as the "point attachment" model. It is a deterministic model which allows one to predict whether or not a cell which comes into contact with a surface will attach to that surface. Figure 6.7 is a representation of the physical events that occur when a cell comes into close contact with a surface.

Figure 6.7
Point Attachment Model of Cell Adhesion

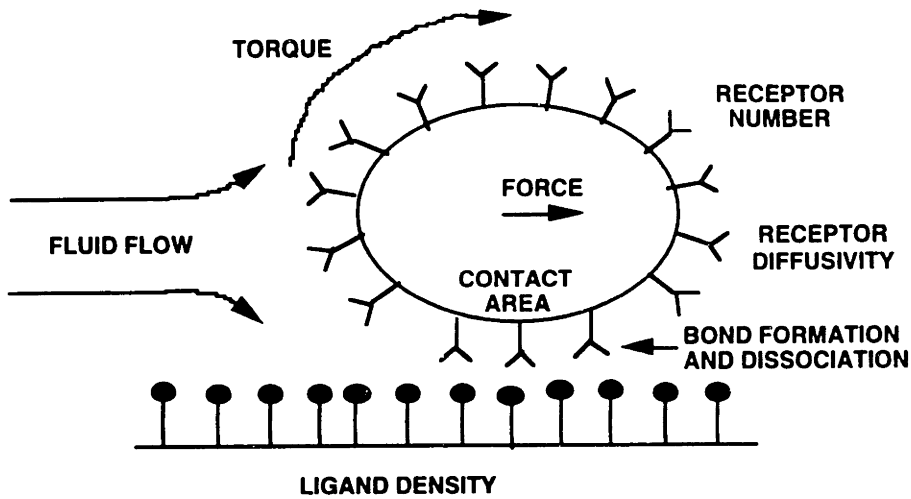

Figure 6.7: The point attachment model assumes that the cell possesses one receptor class of number R_T available for binding. The ligand density on the substrate is N_{lo}. Bond formation and dissociation occur according to characteristic rate constants k_f and k_r, respectively. The contact area is assumed to be a disk of radius a. Receptors have an intrinsic diffusional mobility in the plane of the membrane, D. As the cell approaches the surface, a hydrodynamic pressure builds between the cell and the substrate, causing a flattening of the cell, which becomes the contact area A_C. During a short contact time, T_C, bonds form between the cell and the surface unstressed. Source: Hammer, D. A., Lauffenburger, D. A., *Cell Biophysics*, **14**:139-173 (1989)

One example of the type of information that can be obtained from this model is the relationship between the number of receptors needed for adhesion and the dissociation constant at different bond formation rates. The model predicts that fewer receptors are required for adhesion as the bond formation rate increases at a fixed dimensionless dissociation constant. Another example is the dependence of the shear rate on the number of receptors. The model predicts that as the receptor number increases at a fixed dissociation constant, the permissible shear rate goes up.

The equations and initial conditions which are used to describe cell attachment at equilibrium are:

$$\frac{dN_b}{dt} = k_f N_{l_o} N_a - k_r N_b \qquad [6.1]$$

$$\frac{dN_a}{dt} = -k_f N_{l_o} N_a + k_r N_b + \Delta(N_{c_o} - N_a) \qquad [6.2]$$

at t = 0:

$$N_b = 0 \qquad [6.3]$$

$$N_a = \frac{R_T}{4\pi R_c^2} \qquad [6.4]$$

where N_a = the density of free receptors on the cell surface (molecules/cm^2)

N_b = the density of bonds (molecules/cm^2)

N_{co} = the initial density of receptors (molecules/cm^2)

N_{lo} = the initial density of ligands on the surface (molecules/cm^2)

k_f = the forward rate constant [bond formation] (cm^2/molecules · s)

k_r = the reverse rate constant [bond dissociation] (1/s)

Δ = accumulation coefficient to account for diffusion of free receptors into the contact area [mass transfer rate constant] (1/s)

R_T = Total number of receptors on the cell (molecules)

R_c = cell radius (cm)

N_a and N_b are functions of time, N_{co} and N_{lo} are constants, and theoretically, k_f and k_r can be determined from the equations:

$$k_f = \frac{k_+ k_{+1}}{k_{+1} + k_-} \qquad [6.5]$$

$$k_r = \frac{k_{-1} k_-}{k_{+1} + k_-} \qquad [6.6]$$

where the constants k_+, k_{+1}, k_-, and k_{-1} are descriptive of the rates at which bonds (B) are formed between receptors (R) and ligands (L) through an intermediate receptor-ligand complex (RL^*):

$$R + L \underset{k_-}{\overset{k_+}{\rightleftharpoons}} RL^* \underset{k_{-1}}{\overset{k_{+1}}{\rightleftharpoons}} B \qquad [6.7]$$

The constants k_+ and k_- describe forward and reverse rates of transport of the receptors and ligands into close enough proximity to form the intermediate complex. The constants k_{+1} and k_{-1} describe the forward and reverse rates of stable bond formation. (These constants can be calculated from thermodynamic equations, however, the more common practice is to use values for k_f and k_r^o measured experimentally.)

The reverse rate constant k_r has two forms. During initial contact of the cell with the surface ($t \leq T_c$), the bonds are unstressed and k_r takes its base value, k_r^o; after a short time ($t > T_c$), the bonds are stressed and their lifetime is decreased. The constant k_r then becomes:

$$k_r = k_r^o \exp\left(\frac{\gamma F_b}{k_b T}\right) \qquad [6.8]$$

where γ = the characteristic breakage length of a solid bond (cm)

F_b = the Force per bond under stressed conditions (dyn/cm^2)

k_b = Boltzmann's constant (J/K · molecule)

T = absolute temperature (K).

T_c is calculated as the sum of T_1 and T_2, where

T_1 = the time from which the cell first comes into contact with the surface until the first bond is formed, and

T_2 = the time from when the first bond is formed until the bonds become stressed.

Expressions for T_1 and T_2 are:

$$T_1 = \frac{1}{k_f N_{l_o}} \ln\left(1 - \frac{1}{A_c N_{c_o}}\right)^{-1} \qquad [6.9]$$

$$T_2 = \frac{a}{V} \qquad [6.10]$$

where A_c = the area of the contact region (μm^2)

a = the radius of the contact region (μm)

V = the translational velocity of the cell (μm/s).

The translational velocity (V) is a function of the shear rate (SR) and is calculated from the following equation:

$$V = SR \cdot R_c \frac{\frac{1}{2} F^t \tau^s - \left(1 + \frac{h}{R_c}\right) F^s \tau^r}{F^t \tau^r - F^r \tau^t} \qquad [6.11]$$

where F denotes force, τ denotes torque, the superscripts s, r, ant t denote shear, rotation, and translation, and h is the separation distance (μm). Values for the last term in the equation for V have been tabulated as a function of h/R_c.

F_b is time-dependent (since N_b is a function of time) and is calculated from the equation:

$$F_b = \frac{F_t}{\pi a^2 N_b} \qquad [6.12]$$

where F_t is the total force acting on the bonds (dynes), and is given by the expression:

$$F_t = 6\pi\mu\left(\frac{h}{R_c}\right) R_c^2 \cdot SR \cdot \sqrt{\left(1 + \frac{h}{R_c}\right)^2 F^{s^2}\left(1 + \frac{9\pi^2 R_c^2}{16a^2}\right) + \left(1 + \frac{h}{R_c}\right) F^s \tau^s \frac{3\pi^2 R_c^2}{4a^2} + \frac{(\pi R_c)^2}{4a^2} \tau^{s^2}} \qquad [6.13]$$

Values for the last term in the equation above have been tabulated as a function of h/R_c.

The mass transport rate constant, D, is calculated from the expression

$$\Delta = \frac{2D}{a^2} + \frac{2\Omega R_c}{\pi a} \qquad [6.14]$$

when the cell is rotating and the bonds are unstressed ($t \leq T_c$). When the bonds are stressed ($t > T_c$) and the cells aren't rotating, $\Omega = 0$, and D becomes:

$$\Delta = \frac{2D}{a^2} \qquad [6.15]$$

where D = the diffusivity of the receptors in the plane of the cell membrane ($\mu m^2/s$)

Ω = the angular velocity of the cell ($\mu m/s$)

The angular velocity is calculated from the equation:

$$\Omega = SR \cdot \frac{\left(1 + \frac{h}{R_c}\right)\tau^t F^s - \frac{1}{2}F^t\tau^s}{F^t\tau^r - F^r\tau^t} \qquad [6.16]$$

The last term in the equation has been tabulated as a function of h/R_c.

The equations can be non-dimensionalized by introducing the following terms:

$$\tau = \frac{t}{T_c} \qquad \eta_a = \frac{N_a}{N_{c_o}} \qquad \eta_b = \frac{N_b}{N_{c_o}} \qquad \theta = k_f N_{l_o} T_c \qquad [6.17a\text{-}d]$$

$$\beta = \frac{1}{4}\left(\frac{a}{R_c}\right)^2 \qquad \kappa = \frac{k_r^o}{k_f N_{l_o}} \qquad \alpha = \frac{\gamma F_t}{k_b T} \qquad \delta = \frac{\Delta}{k_f N_{l_o}} \qquad [6.17e\text{-}h]$$

where the physical meaning of these dimensionless parameters are shown in Table 6.6 with a range of values which they can possess and the values chosen for the sample calculation described below.

Table 6.6
Dimensionless Parameters of the Point Attachment Model

Parameter	Physical Meaning	Range	Sample Calc.
t	time	$0 - \infty$	1
η_a	free receptor density	0 - 1	-
η_b	bond density	0 - 1	-
θ	bond formation rate	10^{-4} - 10	0.0064
β	contact area	10^{-4} - 10^{-2}	0.00154
κ	dissociation constant	10^{-8} - 10^{2}	0.001
α	energy which bonds must withstand scaled to thermal energy	0 - 1000	0 for $t \leq 1$ 25 for $t > 1$
δ	transport of free receptors scaled to forward reaction rate	10^{-2} - 10^{2}	67.44 for $t \leq 1$ 3.08 for $t > 1$
$1/\kappa$	affinity	10^{-2} - 10^{8}	1000

The resulting equations and initial conditions in dimensionless form are:

$$\frac{d\eta_b}{d\tau} = \theta\left(\eta_a - \kappa\eta_b \exp\left(\frac{\alpha}{\beta R_T \eta_b}\right)\right) \qquad [6.18]$$

$$\frac{d\eta_a}{d\tau} = \theta\left(-\eta_a + \kappa\eta_b \exp\left(\frac{\alpha}{\beta R_T \eta_b}\right) + \delta(1-\eta_a)\right) \qquad [6.19]$$

at t = 0:

$$\eta_a = 1 \qquad [6.20]$$

$$\eta_b = 0 \qquad [6.21]$$

For short times ($t \leq T_c$), the case in which the bonds are unstressed, the energy and free receptor transport terms can be written as:

$$t \leq 1 \qquad \alpha = 0 \qquad \delta = \frac{2D}{k_f N_{l_o} a^2} + \frac{2\Omega R_c}{\pi\, a\, k_f N_{l_o}} \qquad [6.22]$$

For long times (t > Tc), the case in which the bonds are stressed, the energy and free receptor transport terms can be written as:

$$t > 1 \qquad \alpha = \frac{\gamma F_t}{k_b T} \qquad \delta = \frac{2D}{k_f N_{l_o} a^2} \qquad [6.23]$$

This set of equations has been solved using phase-plane techniques. Figure 6.8 illustrates the nature of the solutions that are obtained. The results obtained under various conditions were used to construct charts to show how the various parameters are inter-related. Figure 6.9 shows the relationship between the number of receptors required for adhesion and the dimensionless dissociation constant (κ) as a function of the dimensionless bond formation rate (θ).

Figure 6.8
Typical Results of the Point Attachment Model

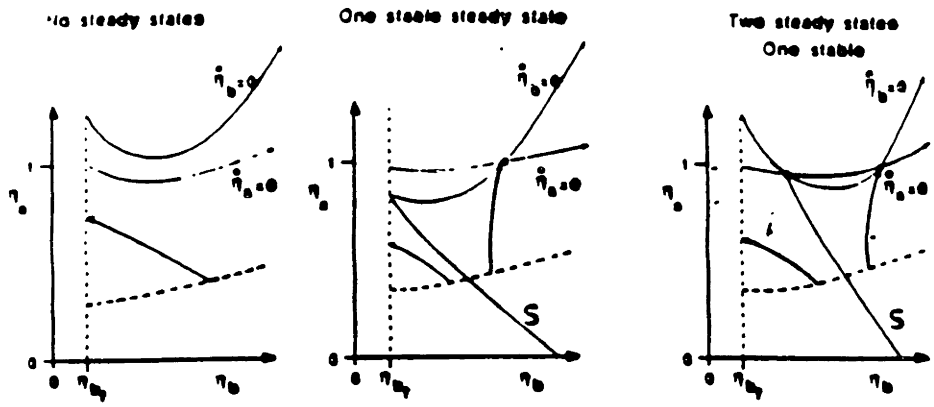

Figure 6.8: Typical solutions to the equations of the point attachment model are depicted. Source: Hammer, Ph. D. Thesis, p. 213

Figure 6.9 demonstrates that the results predicted by this model are characterized by two asymptotic regions. On the left side of the figure (at high affinity, low κ), the curves reach a horizontal asymptote which represents a rate-controlled regime. The number of receptors required is independent of κ and depends only on the mean time necessary to form a single bond:

$$R_T = \frac{1}{\beta\left(1 - e^{-\theta}\right)} \qquad [6.24]$$

On the right side of the figure (at low affinity, high κ), the curves reach a slanting asymptote which represents an affinity-controlled regime. The number of receptors is proportional to κ and is characteristic of an equilibrium controlled situation. This asymptote is given by:

$$R_T = \frac{\alpha \kappa e}{\beta} \qquad [6.25]$$

where e is the base for natural logarithms (e = 2.71828...).

Figure 6.9
Receptor Number vs. Bond Dissociation Rate

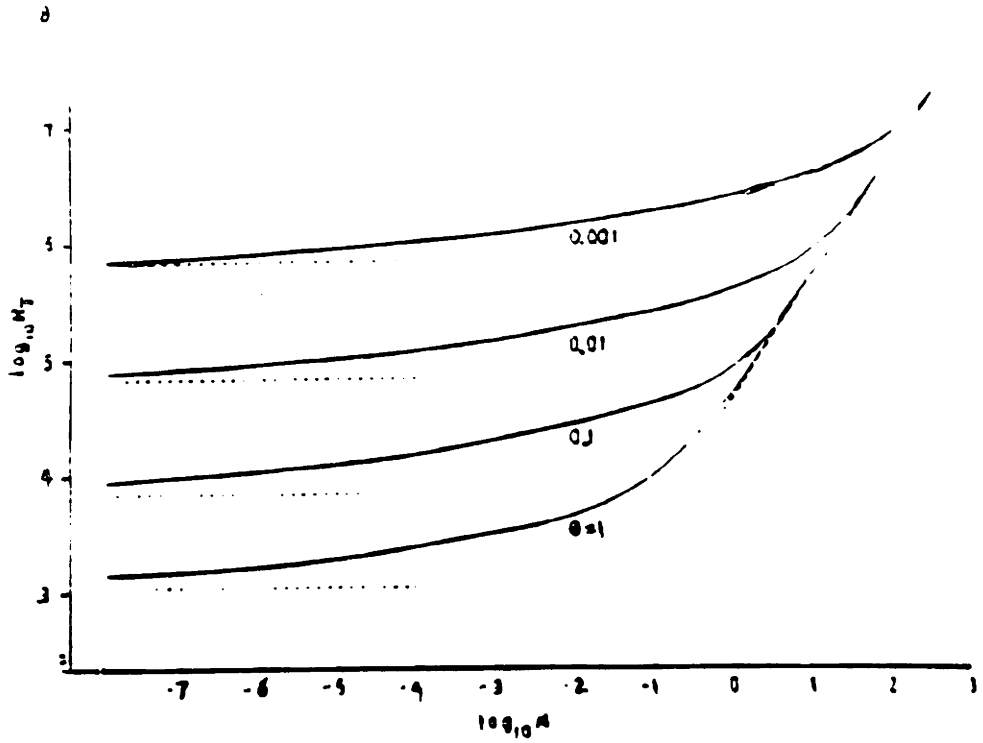

Figure 6.9: The receptor number is dependent on the bond dissociation rate. The horizonal asymptotes represent rate-controlled regimes. The slanting asymptote on the right side of the graph represents an affinity controlled regime. Source: Hammer, D. A., Lauffenburger, D. A, *Biophys. J.*, 52:475-487 (1987)

As an example of how this model is used, the following calculation was performed:

Suppose that a BAE cell with 500,000 receptors (R_T) flows past a surface with 100 fmol/cm^2 of peptide ligands (N_{lo}) under the influence of a shear rate (SR) of 7.4 s^{-1}. Will the cell attach to the surface? The parameters describing this situation are shown in Table 6.7.

Table 6.7
Parameter Values for Sample Calculation

Parameter	Physical Meaning	Value
N_{lo}	Ligand density	100 fmol/cm^2
k_f	Forward rate constant	4.14×10^{-12} cm^2/molecule/s
k_r^o	Reverse rate constant	2.49×10^{-4} s^{-1}
D	Diffusivity of the receptors	1×10^{-9} cm^2/s
R_T	Total number of receptors	5×10^5
R_c	Cell radius	6.5 μm
N_{co}	Initial receptor density	942/μm^2
T_1	Time until first bond is formed	0.0052 s
T_2	Time from first bond until bonds are stressed	0.0204 s
T_c	Contact time for bonds to form unstressed	0.0256 s
γ	Characteristic breakage length for a solid bond	5×10^{-8} cm
k_b	Boltzmann constant	1.38×10^{-23} J/K
T	Temperature	310 K
A_c	Area of the contact region	0.82 μm^2
a	Radius of the contact region	0.51 μm
V	Translational velocity of the cell	25 μm/s
Ω	Rotational velocity of the cell	1.98 s^{-1}
SR	Shear rate	7.4 s^{-1}
F_t	Total force on the cell	2.14×10^{-5} dynes
μ	Viscosity	0.7 cP
h	Separation distance	0.05 μm
Factor 1	Term used in calculating F_t	2.6644
Factor 2	Term used in calculating V	0.5186
Factor 3	Term used in calculating Ω	0.2672

The values chosen for this calculation represent the best estimates that could be found to describe a situation in which BAE cells are seeded onto RGD-containing samples at a flow rate that is within the reported range for venous flow. The question which was considered was whether or not the model would predict that a single cell would attach to the surface given a chance to contact the surface. The time required to form the first bond (T_1) was calculated to be 5.2 milliseconds. The time from T_1 until the bonds become stressed (T_2) was determined to be 20.4 milliseconds, and thus, the critical time (T_c) was 25.6 milliseconds. The asymptotic limits are tabulated in Table 6.8. A plot of the number of receptors (R_T) vs. the dimensionless dissociation constant (κ) is shown in Figure 6.10 along with the asymptotes for $\theta = 0.0064$, which is the dimensionless bond formation rate for the sample calculation.

Table 6.8
Asymptotic Limits for Sample Calculation

κ	$\log_{10} \kappa$	R_T	$\log_{10} R_T$
High Affinity			
1×10^{-8}	-8	1.02×10^5	5.01
1×10^{-7}	-7	1.02×10^5	5.01
1×10^{-6}	-6	1.02×10^5	5.01
1×10^{-5}	-5	1.02×10^5	5.01
Low Affinity			
1	0	4.4×10^4	4.65
10	1	4.4×10^5	5.65
100	2	4.4×10^6	6.65
1000	3	4.4×10^7	7.65

Figure 6.10
Sample Calculation Plot of log R_T vs log κ

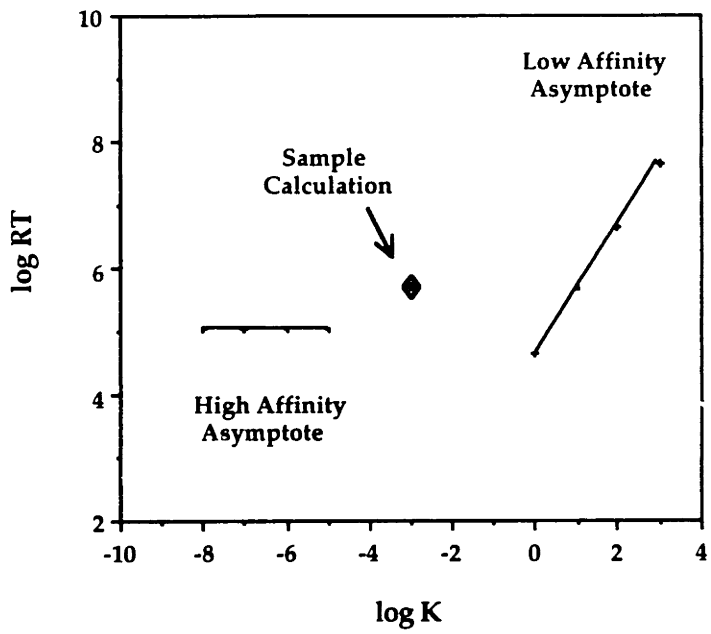

The implication of the sample calculation is that because the value of $\log_{10}R_T$ vs. $\log_{10}\kappa$ falls above the region defined by the high affinity asymptote and the low affinity asymptote, the model predicts that adhesion will occur.

Extending the model to other conditions allows one to test the sensitivity of the model predictions to slight perturbations in the parameters. For example, the effect of shear rate on the total force on the cell and on α are shown in Table 6.9.

Table 6.9
Determination of α

SR (s^{-1}) [Shear Rate]	F_t (μdyn) [Total Force on the Cell]	α [Dimensionless Energy]
1	3	3
5	14	17
7.4	21	25
10	29	34
50	144	169
100	288	337

The physiologically relevant values for shear stress have been reported to be approximately 4 dyn/cm^2 for venous flow and 15 to 25 dyn/cm^2 for arterial flow (27). Shear rate (SR) and shear stress (τ_w) are related by the viscosity (μ) of the fluid:

$$SR = \frac{1}{\mu}\tau_w \qquad [6.26]$$

The corresponding values for shear rate, using μ = 0.7 cP for water at 37°C, are 5.7 s^{-1} for venous flow and 21 to 35 s^{-1} for arterial flow.

Many of the parameters depended strongly on the value of N_{lo} which was chosen. Table 6.10 shows the effect that increasing N_{lo} has on the values of T_c, θ, κ, and δ.

Table 6.10
Effect of Increasing Ligand Density

N_{lo} (fmol/cm^2)	N_{lo} (molec./cm^2)	T_c (ms)	θ	κ	δ
1	6×10^8	540	0.0014	1×10^{-1}	6.7×10^3
10	6×10^9	72	0.0018	1×10^{-2}	6.7×10^2
10^2	6×10^{10}	26	0.0064	1×10^{-3}	6.7×10^1
10^3	6×10^{11}	21	0.0522	1×10^{-4}	6.7
10^4	6×10^{12}	21	0.510	1×10^{-5}	6.7×10^{-1}
10^5	6×10^{13}	20	5.090	1×10^{-6}	6.7×10^{-2}
10^6	6×10^{14}	20	50.90	1×10^{-7}	6.7×10^{-3}

Plots similar to that of Figure 6.10 can be constructed at each of these values of κ and θ. Table 6.11 lists the high affinity asymptote values for such plots (the low affinity asymptote is the same as in Figure 6.10).

Table 6.11
High Affinity Asymptotes Compared to Model Value
(for $R_T = 5 \times 10^5$)

High Affinity Asymptote Values			Model Value	
N_{lo}	θ	$\log_{10} R_T$	$\log_{10} \kappa$	$\log_{10} R_T$
1	1.35×10^{-3}	5.68	-1	5.7
10	1.8×10^{-3}	5.56	-2	5.7
10^2	6.38×10^{-3}	5.01	-3	5.7
10^3	5.22×10^{-2}	4.11	-4	5.7
10^4	5.1×10^{-1}	3.21	-5	5.7
10^5	5.09	2.82	-6	5.7
10^6	50.9	2.81	-7	5.7

Because the high affinity asymptote value for $\log_{10}R_T$ is less than the model value of $\log_{10}R_T$ (5.7 for $R_T = 5\times10^5$), the model predicts that adhesion will occur for all values of N_{lo} over 1 fmol/cm^2. In applying this to the PLAL+RGD system, all of the samples containing RGD peptides which were evaluated during the course of this project had surface peptide densities which were on the order of 4 pmol/cm^2, approximately 3 orders of magnitude above the required density. The value of this exercise was the definition of the minimally required peptide densities based on the current understanding of the mechanism of cell attachment. Further efforts to design an tissue-engineered blood vessel would require the measurement of the behavior of cells under the influence of a shear stress. This could be accomplished using a laminar flow chamber and image analysis system (24).

6.4.2 Spreading Model

The model developed by Olivier and Truskey can be used to describe the effect that adhesion and spreading have on the resistance of the cell to detachment due to fluid forces. The model consists of an equilibrium balance between the forces acting on the cell and the forces generated by the bonds that are formed between the cell and the surface. The fluid forces acting on the cell were calculated by finite element modeling for four different stages of cell spreading, as illustrated in Figure 6.11.

Stage 1 represents a cell just touching the surface. The dimensions for stages 2, 3, and 4 were calculated from measurements from SEM photomicrographs of BAE cells seeded onto fibronectin-coated glass slides. The drag force (F) and torque (T) acting on the cell in each of the four stages was found to be linearly related to the shear stress at the wall (τ_w). The regression slopes are shown in Table 6.12.

Figure 6.11
Stages of Cell Spreading

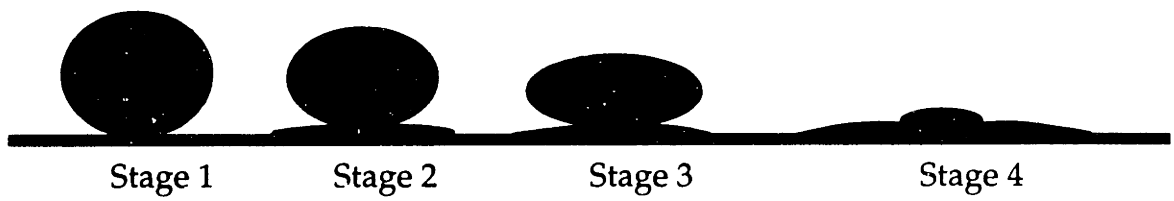

Figure 6.11: Four stages of cell spreading are depicted. BAE cells move from a round shape (Stage 1) while in suspension to a flattened conformation (Stage 2). Source: Olivier and Truskey, *Biotech. Bioengin.*, **42**: 963-973 (1993).

Table 6.12
Regression Slopes for Spreading Model

Stage of Spreading	M (cm)	N (cm^2)
Stage 1	8.07×10^{-3}	7.03×10^{-6}
Stage 2	8.61×10^{-3}	7.56×10^{-6}
Stage 3	6.85×10^{-3}	4.53×10^{-6}
Stage 4	4.58×10^{-3}	3.11×10^{-7}

To calculate the force and torque acting on the cell at each of the stages of spreading, the following equations are used:

$$F = M\,\tau_w \qquad [6.27]$$

$$T = N\,\tau_w \qquad [6.28]$$

The forces on the bonds were calculated for two extreme cases: the uniform stress model, and the peeling model. The uniform stress model assumes that all of the bonds break at the same time once the total force has exceeded the critical force necessary to withstand detachment. The peeling model is based on the assumption that the force acting on the cells first acts to break bonds on the perimeter of the cell. Once one bond is broken, the rest of the bonds are susceptible to the same forces and eventually all bonds are broken. The equations describing the force per bond (f) for each model are:

Uniform Stress model:

$$f = \frac{1}{2\,a^2\,N_b}\left(a^2\,F_{xs}^2 + 4\,T_{zs}^2\right)^{1/2} \qquad [6.29]$$

Peeling model:

$$f = \frac{1}{2\,N_b}\left(\frac{F_{xs}^2}{a^2} + \frac{T_{zs}^2}{\left[a\delta - \delta^2\left(1 - e^{-a/\delta}\right)\right]^2}\right)^{1/2} \qquad [6.30]$$

where δ is given by:

$$\delta = \left(2\;B\,\frac{l_b^2}{\gamma}\right)^{1/4} \qquad [6.31]$$

and γ is defined as:

$$\gamma = \frac{N_b\,f_{max}\,l_b}{2} \qquad [6.32]$$

Table 6.13 defines the parameters involved in solving these equations and the values used for the sample calculations described below.

Table 6.13
Parameters for Spreading Model

Parameter	Physical Meaning	Value for Calculation
N_b	Bond density	1.61×10^{10} bonds/cm^2
f_{max}	Maximum force per bond before breakage	1×10^{-6} dyn/bond
τ_w	Shear stress at the wall	4 dyn/cm^2
F_{xs}	Horizontal fluid force on cell	0.0323 dyn/cm
T_{zs}	Torque on cell	2.8×10^{-5} dyn
a	Radius of the contact region	0.51 μm
A_c	Area of the contact region	0.82 μm^2
A_p	Projected area	130 μm^2
δ	Characteristic decay length	1.49×10^{-5}
B	Bending elastic modulus	2×10^{-9} dyn · cm
l_b	Maximum bond displacement	1×10^{-7} cm
γ	Free energy of adhesion	8.05×10^{-4} dyn/cm

Figure 6.12 describes the results of this model, in terms of the net force per bond (f) as a function of wall shear stress (τ_w). In Figure 6.12 the equations of the lines which are shown can be expressed as linear relationships. For cells in stage 1, the equations are:

<u>Uniform Stress Model:</u>

$$f = 1.68 \times 10^{-7}\, \tau_w \qquad [6.33]$$

<u>Peeling Model:</u>

$$f = 4.0 \times 10^{-7}\, \tau_w \qquad [6.34]$$

Figure 6.12
Forces on Bonds for Uniform Stress Model and Peeling Model

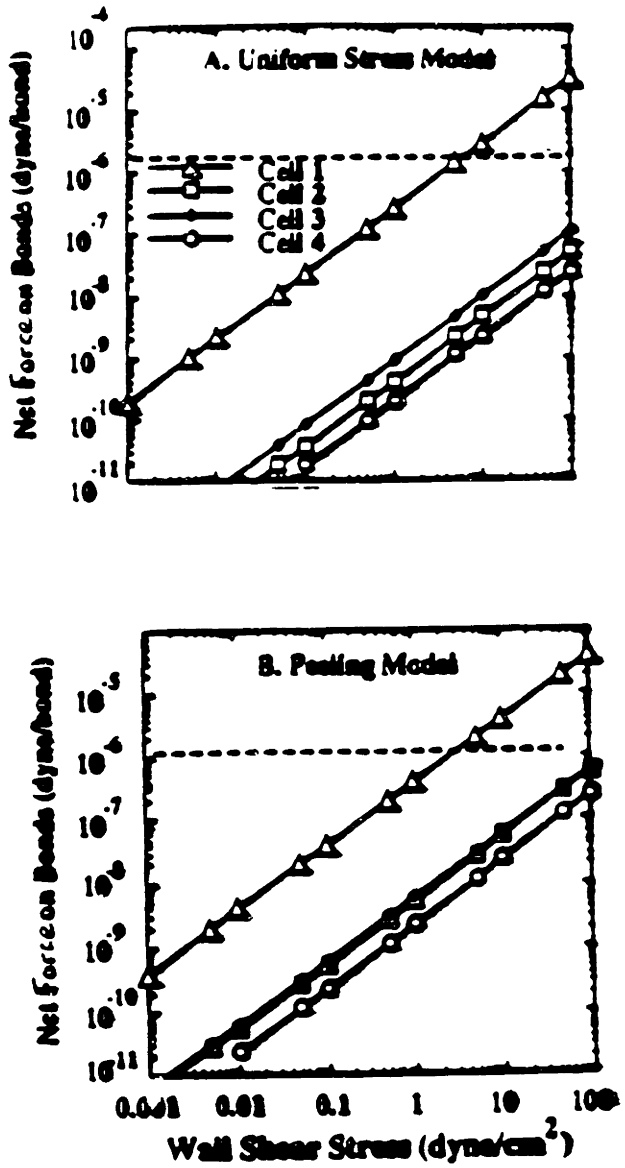

Figure 6.12: Plotting the net force on the bonds as a function of wall shear stress demonstrates a linear relationship. Source: Olivier and Truskey, *Biotech. Bioeng.* 42:963-973 (1993).

For the sample calculation that was performed to apply this model to the PLAL+GRGDY system, the question that was considered was: How many bonds must form before attachment is strong enough to withstand the forces exerted by the fluid on the cell? The limiting case of the cell in stage 1 was used with the equations of the peeling model (representing the worse case scenario). Results from this calculation indicated that at a wall shear stress of 4.0 dyn/cm^2, 232 bonds (2.8 x 10^{10} bonds/cm^2, 47 fmol of receptors/cm^2) must form to provide enough force to withstand the fluid forces. Table 6.14 shows this result and similar results obtained for other flow rates (see Figure 6.13 also).

Table 6.14
Number of Bonds Required to Withstand Fluid Forces

Shear Stress (dynes/cm^2)	Uniform Stress model (Bonds/cell)	Peeling model (Bonds/cell)
0.1	2	3
1	22	45
2.5	55	132
4 (venous)	89	232
5.95	132	376
10	222	713
20 (arterial)	443	1695
40	887	4075
80	1774	9901

Table 6.14: The number of bonds which are required to maintain a cell attached to a surface increase in proportion to the shear stress of the fluid.

The results of this analysis demonstrate that in the worst case, a density of 100 fmol/cm^2 would be sufficient (by a factor of 2) to provide enough bonds for a cell to withstand 4 dyn/cm^2 of shear stress. As more bonds form, greater shear stresses would be able to be withstood. The predictions of this model can be tested by creating samples with well-defined ligand densities, seeding the cells onto these surfaces, and after waiting a short time for bonds to form, exposing the cells to various shear flows.

Figure 6.13
Effect of Shear Stress on Bonds Required

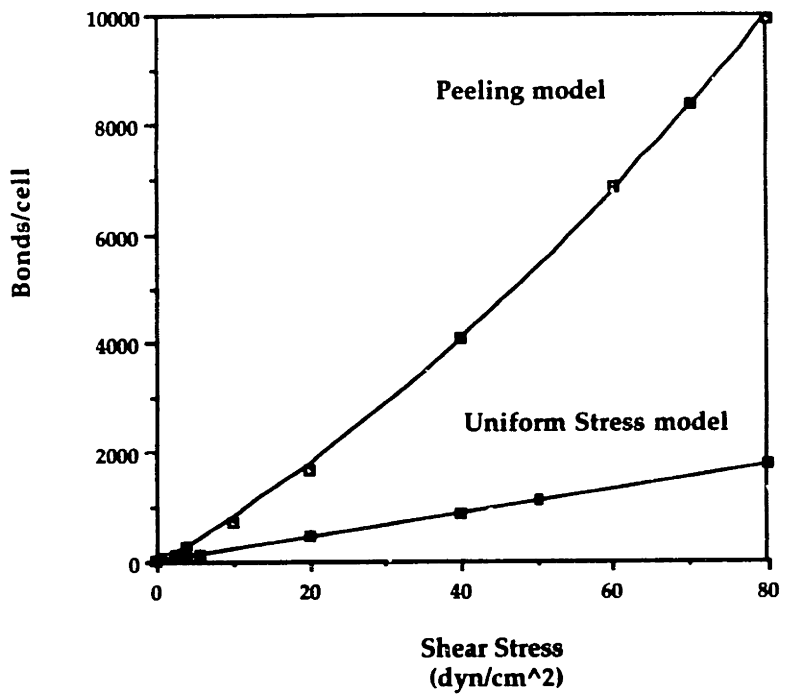

Figure 6.13: This graph depicts the minimum number of bonds which are required to maintain cell attachment to a surface, for two models: the peeling model and the uniform stress model.

Both of the models described above predict that 100 fmol/cm^2 is a sufficient density of peptide ligands to support attachment of BAE cells under the influence of a shear flow. This evaluation indicates that at the present loading of approximately 4 pmol/cm^2, the 40% blends of PLAL+GRGDS peptide would be a good candidate for incorporation into devices such as tissue engineered blood vessels in which endothelial cells are exposed to fluid flow. The models establish the theoretical basis for accepting the PLAL+GRGDS blends for use in applications to promote the adhesion and spreading of endothelial cells. Experimental evidence also suggests that only 1 to 10 fmol/cm^2 of peptides are needed to promote cell adhesion and focal contact formation (8).

6.6 References

1. DiMilla, P.A., Stone, J. A., Albelda, S. M., Lauffenburger, D. A., Quinn, J. A., "Measurement of cell adhesion and migration on protein-coated surfaces", (1993).

2. Gryte, D.M., Ward, M. D., Hu, W.-S., "Real-time measurement of anchorage-dependent cell adhesion using a quartz crystal microbalance", *Biotechnol. Prog.*, **9** : 105-108, (1993).

3. Mooney, D.J., Langer, R., Hansen, L. K., Vacanti, J. P., Ingber, D. E., "Induction of hepatocyte differentiation by the extracellular matrix and an RGD-containing synthetic peptide", in Cima, L.G., Ron, E.S. (eds.) Tissue Inducing Biomaterials. Materials Research Society Symposium Proceedings, **252**:199, Pittsburgh, PA, Materials Research Society (1992).

4. Desai, N.P., Hubbell, J. A., "Surface modifications of polymeric biomaterials for reduced thrombogenicity", *Poly. Mat. Sci. Eng.*, **62** : 731-735, (1990).

5. Massia, S.P., Hubbell, J. A., "Covalent surface immobilization of Arg-Gly-Asp- and Tyr-Ile-Gly-Ser-Arg- containing peptides to obtain well-defined cell-adhesive substrates", *Anal. Biochem.*, **187** : 292-301, (1990).

6. Massia, S.P., Hubbell, J. A., "Covalently attached GRGD on polymer surfaces promotes biospecific adhesion of mammaliam cells", *Ann. N. Y. Acad. Sci.*, **589** : 261-270, (1990).

7. Massia, S.P., Hubbell, J. A., "Human endothelial cell interactions with surface-coupled adhesion peptides on a nonadhesive glass substrate and two polymeric biomaterials", *J. Biom. Mat. Res.*, **25** : 223-242, (1991).

8. Massia, S.P., Hubbell, J. A., "RGD spacing of 440 nm is sufficient for integrin $\alpha_v\beta_3$-mediated fibroblast spreading and 140 nm for focal contact and stress fiber formation", *J. Cell Biol.*, **114** (5): 1089-1100, (1991).

9. Hubbell, J.A., McIntire, L. V., "*In vitro* visualization of thrombosis on polyurethane and collagen", Artificial Organs, Andrade, J.D., Brophy, J. J., Detmer, D. E., Kim, S. W., Normann, R. A., Olsen, D. B., Stephen, R. L., ed., VCH Publishers, Inc., New York, (1987)

10. Hubbell, J.A., Massia, S. P., Drumheller, P. D., "Surface-grafted cell-binding peptides in tissue engineering of the vascular graft", *Ann. N. Y. Acad. Sci.*, **665** : 253-258, (1992).

11. Lin, H.B., Zhao, Z. C., Garcia-Echeverria, C., Rich, D. H., Cooper, S. L., "Synthesis of a novel polyurethane copolymer containing covalently attached RGD peptide", *J. Biomat. Sci.*, (In press): (1991).

12. Lin, H.-B., Garcia-Echeverria, C., Asakura, S., Sun, W., Mosher, D. F., Cooper, S. L., "Endothelial cell adhesion on polyurethanes containing covalently attached RGD-peptides", *Biomat.*, **13** (13): 905-914, (1992).

13. Matsuda, T., Kondo, A., Makino, K., Akutsu, T., "Development of a novel artificial matrix with cell adhesion peptides for cell culture and artificial and hybrid organs", *ASAIO Trans.*, **35** : 677-679, (1989).

14. Brandley, B.K., Schnarr, R. L., "Covalent attachment of an Arg-Gly-Asp sequence peptide to derivatizable polyacrylamide surfaces: Support of fibroblast adhesion and long-term growth", *Anal. Biochem.*, **172** : 270-278, (1988).

15. Hubbe, M.A., "Adhesion and detachment of biological cells in vitro", *Prog. Surf. Sci.*, **11** : 65-138, (1981).

16. Hammer, D.A., Lauffenburger, D. A., "A dynamical model for receptor-mediated cell adhesion to surfaces in viscous shear flow", *Cell Biophysics*, **14** : 139-173, (1989).

17. Hammer, D.A., Lauffenburger, D. A., "A dynamical model for receptor-mediated cell adhesion to surfaces", *Biophys. J.*, **52** : 475-487, (1987).

18. Bell, G.I., Dembo, M., Bongrand, P., "Cell adhesion. Competition between nonspecific repulsion and specific bonding", *Biophys. J.*, **45** : 1051-1064, (1984).

19. Bell, G.I., "Models for the specific adhesion of cells to cells", *Science*, **200** : 618-627, (1978).

20. Evans, E.A., *Biophys. J.*, **48** : 175, (1985).

21. Ward, M.D., Hammer, D. A., "A theoretical analysis for the effect of focal contact formation on cell-substrate attachment strength", *Biophys. J.*, **64** : 936-959, (1993).

22. Cozens-Roberts, C., Quinn, J. A., Lauffenburger, D. A., "Receptor-mediated adhesion phenomena. Model studies with the radial-flow detachment assay", *Biophys. J.*, **58** : 107-125, (1990).

23. Dembo, M., Torney, D. C., Saxman, K., Hammer, D., "The reaction-limited kinetics of membrane-to-surface adhesion and detachment", *Proc. R. Soc. Lond. Ser. B*, **234** : 55-83, (1988).

24. Kuo, S.C., Lauffenburger, D. A., "Relationship between receptor/ligand binding affinity and adhesion strength", *Biophys. J.*, **65** : 2191-2200, (1993).

25. Olivier, L.A., Truskey, G. A., "A numerical analysis of forces exerted by laminar flow on spreading cells in a parallel plate flow chamber assay", *Biotech. Bioengin.*, **42** : 963-973, (1993).

26. Hammer, D.A., Apte, S. M., "Simulation of cell rolling and adhesion on surfaces in shear flow: general results and analysis of selectin-mediated neutrophil adhesion", *Biophys. J.*, **63** : 35-57, (1992).

27. Diamond, S.L., Eskin, S. G., McIntire, L. V., "Fluid flow stimulates tissue plasminogen activator secretion by cultured human endothelial cells", *Science*, **243** : 1483-1485, (1989).

Appendix 6A
Cell Spreading Protocol

Purpose: To test the interaction of cells with the RGD peptide in comparison to PLA, PLAL and RDG controls. Specific endpoint: cell spreading as a function of time.

Pre-wetting:
At least one day prior to the study, prepare the films and allow them to soak in PBS with 0.5% Penicillin, 0.5% Streptomycin and 1% L-Glutamine in the following manner:

1. Use 1 film each of PLA, PLAL, RGD and RDG. Record the inventory number of the sample.
2. In the sterile laminar hood, cut each film into 6 pieces, leaving the lip on. Use an open petri dish or lid to support each film.
3. Sterilize the top side of each film for 10 min. under the U.V. lamp.
4. One by one, holding each sample with sterile forceps, cut off the lip from each sample, keeping track of the top side. Place a small amount of sterile silicon grease on the top and then place the sample in one well of a 24 well plate so that the bottom of the film is facing up.
5. Place the films in the plate in the following manner:
   A1-6 PLA
   B1-6 PLAL
   C1-6 RGD
   D1-6 RDG
6. Sterilize the bottom sides of the films by U.V. for 10 min.
7. Add PBS without Ca^{2+} or Mg^{2+}, supplemented with 0.5% Penicillin, 0.5% Streptomycin, and 1% L-glutamine.
8. Place films in the incubator for 24 hours.

Pre-conditioning:
On the day of the experiment, remove the PBS and rinse each film three times with PBS to remove any soluble particles, peptides, degradation products or debris. Then add DMEM w/o serum with Penicillin, Streptomycin and L-Glutamine for at least one hour prior to adding cells. This also gives you a chance to check to make sure the films are securely attached to the 24 well plate and will remain attached during rinsing. Set up a control plate. Negative control is PS without serum. Positive control is PS with normal media containing serum.

Plate 2:
A1-6 PS
B1-6 PS + serum

Cell Preparation:

On the day of the experiment, prepare a solution of cells in DMEM without serum with Penicillin, Streptomycin and L-Glutamine at 50,000 cells/ml concentration in the following manner:

1. Prepare a 1 mg/ml solution of Soy Bean Trypsin Inhibitor using 10 mg in 10 ml of DMEM without serum. Use a 15 ml tube.
2. Sterilize the SBTI solution using a syringe filter into a new 15 ml tube.
3. Rinse the cells with PBS without Ca^{2+} or Mg^{2+}
4. Add 5 ml of trypsin/EDTA to remove the cells from the flask.
5. Incubate 2-5 min until the cells are freely floating.
6. Add sterile SBTI, 10 ml
7. Transfer cell suspension to a 50 ml centrifuge tube
8. Centrifuge the cells into a pellet
9. Resuspend in 2 ml of DMEM without serum with P/S/G
10. Use 100 µl into 19.9 ml of sterile Isoton II to count cells electronically
11. Determine conc., and required media to make 50,000 cell/ml solution: Divide by 0.5 ml, multiply by 20 ml, divide by .1 ml, multiply by 1.9 ml, divide by 50,000 cells/ml, subtract 1.9 ml.
12. Add the required amount of serum-free media to make a suspension at 50,000 cells/ml. Need at least 19 ml total.
13. Add 0.5 ml of cells to each of the samples, and count 0.5 ml of cells electronically. Each surface will have approximately 10,000 cells/cm^2.
14. Allow the cells approximately 10 min to settle undisturbed onto the samples.
15. In the first well of each row, carefully remove the media by suction, moving down from the top of the liquid to the bottom along the side of the well, away from the polymer sample. Add 0.5 ml of 2% glutaraldehyde in PBS without Ca^{2+} or Mg^{2+}.
16. Incubate the whole plate for 30 min.
17. Remove the glutaraldehyde from the first column, add 0.5 ml of PBS.
18. Remove the media from the next column, add glutaraldehyde.
19. Repeat procedure at 1 hr, 1.5 hrs, 2 hrs. and 4 hrs.
20. After all the samples have been fixed in glutaraldehyde for 30 min. and rinsed with PBS, use a series of ethanol solutions to dry the samples. Add 50% , 70%, 90% and 100% ethanol for at least one minute on each surface.
21. Remove the 100% ethanol and let the samples air dry, covered, overnight.
22. Transfer samples to SEM stubs
23. Take SEM photomicrographs at 10 keV, with a +20° tilt.
24. Scan SEM photomicrographs into the computer using the DeskScan II software, and settings for Sharp Black and White Photographs.
25. Analyze cells by tracing them using NIH Image software
26. Calculate mean cell area vs. time for the different samples.

Chapter 7

Conclusions

7.1 Summary

The field of tissue engineering has as its principle objective the controlled proliferation of cells to regenerate lost tissues and organs, such as occurs during embryonic formation of tissues and as also occurs during wound healing. Although there exists a considerable amount of knowledge concerning the molecules, signals and pathways involved in neomorphogenesis, the key limitation to making this approach a versatile clinical tool is a lack of control over this process. In order to duplicate the body's ability to regenerate lost structures and replace lost functions, methods must be developed to control the process of tissue regeneration. The goal of this research was to gain a better understanding of the interactions of cells with synthetic resorbable polymers in order to provide a means to control those interactions.

The approach towards tissue engineering which has been used previously has been to create scaffolds out of resorbable polymers, incubate cells with those scaffolds *in vitro* to initiate the creation of new extracellular matrix proteins, then transplant the resulting constructs (composed of cells, partially degraded polymers and newly formed extracellular matrix) into an *in vivo* environment. The scaffolds provide physical support for the cells to maintain the desired shape during the initial stages of transplantation, but the scaffolds that are presently used (PGA non-woven meshes) do not interact with the cells.

The goal of this research was to create a resorbable polymer which could also interact with cells. The polymer which was formed is a copolymer of poly(lactic acid) and lysine, which combines two naturally-occurring molecules into a material which takes advantages of the properties of both components. The poly(lactic acid) provides good mechanical properties and processing capabilities, whereas the lysine groups provide functional engraftment sites to which a variety of naturally occurring signaling molecules can be attached.

The three objectives of the studies described herein were: 1) to attach RGD-containing peptides to poly(lactic acid-*co*-lysine) (PLAL) in sufficient

quantities to promote cell attachment and spreading, 2) to develop methods to measure the surface concentrations of lysine and peptides (which can vary with the processing method which is chosen), and 3) to correlate the number of peptides with the cell response. There were three phases to this research project: product development, surface characterization and cell interactions.

The processing steps to create samples for testing included monomer synthesis, copolymerization, deprotection, polymer processing, and peptide attachment. The samples were then sterilized and cells were seeded on them. The experimental system which was chosen to study consisted of bovine aortic endothelial cells, which contain integrins that interact with RGD-containing peptides. The peptides were covalently linked to surfaces of poly(lactic acid-*co*-lysine) samples.

The monomer synthesis consisted of a four step process. In the first step, D-Alanine was reacted with an aqueous solution of hydrobromic acid and sodium nitrite at 15°C to produce bromo-substituted D-Alanine. The product was purified by distillation. The second step was to react the product of the first reaction, bromo-substituted D-Alanine with thionyl chloride at 60°C to produce D-α-bromopropionyl chloride, which was also purified by distillation. The third step was to react D-α-bromopropionyl chloride with L-lysine whose terminal amino group was protected by CBZ (carbonylbenzoxy) protecting group. This reaction was performed in chloroform at room temperature to form (2-bromo-1-oxopropyl)-phenylmethoxy carbonyl -L-lysine. In step four, the previous molecule was closed into a ring to form the lysine-containing monomer. This was accomplished using diisopropylethylamine in chloroform at 62°C for 24 hours. The product was separated and purified using silica gel chromatography and characterized by FTIR, ^{1}H-NMR and elemental analysis. The purity of the monomer was also tested by measuring variations in the melting point by differential scanning calorimetry (DSC) (section 3.1).

The newly created monomer was reacted with L,L-lactide in a ring-opening polymerization reaction to form the copolymer of lactic acid and lysine. This reaction was carried out at 100°C for 24 hours under a nitrogen atmosphere using stannous octoate as a catalyst. The propagation steps proceed by a nonionic coordination insertion reaction. The protecting group on the ε-amino group of lysine was removed by reaction with palladium chloride as the catalyst in a reagent system consisting of methylene chloride, triethylamine, and triethylsilane. This reaction was carried out at room temperature (section 3.2).

Polymer processing was performed by a variety of methods, but the one that was used in the majority of the work involved solution casting from chloroform to produce flat molded films on the order of 100 to 200 μm thick The films were semicrystalline, rigid, yet pliable in that they could bend without breaking. They could also be cut with scissors to any desired shape (section 3.3). Bulk characterization of the polymer was conducted to determine lysine content, degradation kinetics, crystallinity, density and molecular weight (section 3.4).

Peptide attachment consisted of two approaches. The first approach was the attachment of the peptides in solution (bulk attachment) and then the creation of samples from the resulting bulk-attached polymer-peptide combination. In this reaction, the polymer, peptide and linking agents were all dissolved in a mixture of 50% methylene chloride and 50% dimethylsulfoxide in a single reaction step. The final product was precipitated and rinsed extensively in water to produce a purified polymer-peptide coupled compound (section 4.1). The second approach was the creation of polymer films, then the surface attachment of peptides in a reaction which preserved the physical integrity of the polymer sample. To attach the RGD-containing peptides to the surfaces using the available NH_2 groups, water soluble carbodiimide chemistry was used. This chemistry consisted of a 4 step reaction in which the NH_2 group was first converted to a carboxylic acid using succinic anhydride. The next step was to couple the EDC molecule to the polymer and then remove the excess reagents. Sulfo-NHS was then used to replace the EDC molecule and form a larger leaving group. The peptide was then added and the resulting film was rinsed clear of excess peptides. In this chemistry all of the reactions were carried out in aqueous buffer (section 4.2).

There were several challenges which were overcome in the course of this research project. The first was the time and expense required to produce the polymer films used in the cell adhesion studies. A team of students and scientists was organized to assist in the production of samples. The second challenge was determining methods to measure very small surface densities of peptides and amino groups. This challenge was met by adapting the components of this system to match the requirements of existing technologies. Specificaly, the incorporation of non-radioactive iodine into the RGD-containing peptide made possible the detection of the peptide by XPS (section 5.3.3). A third challenge was determining a method to quantify the interaction of cells with the surfaces of these materials. This was accomplished using computerized image

analysis to measure the area of spread cells (section 6.2). The final result of this work was the identification of methods to completely characterize samples containing PLAL + RGD. Table 7.1 summarizes the characterization questions which were asked and lists the methods used to provide the data.

Table 7.1
Characterization Questions and Techniques

Characterization Question	Technique
1. How many free NH_2 groups are present at the surface of PLAL films as a result of various processing steps?	Colorimetric assays XPS
2. How many peptides are attached?	^{125}I-labeled peptides XPS with ^{127}I-labeled peptides
3. Are the peptides accessible to cells?	Cell Spreading Assays
4. How does soaking change the surface?	Contact Angles XPS with cold stage
5. How do buffers, media and proteins change the way cells interact with the surface?	Contact Angles Cell Spreading Assays

The various techniques which were applied to studying the samples tested in the experiments described in this report produced results that were dependent on the way in which the samples were prepared and the method used to analyze the samples. The tools which were used to characterize the surfaces of these samples were X-ray photoelectron spectroscopy (XPS), colorimetric assays, contact angles and environmental scanning electron microscopy (ESEM). XPS provided an elemental analysis of the top 10-50 Å depending on the take-off-angle which was used. Colorimetric assays using sulfo-SDTB gave a nice visual result and results were quantified using a standard UV/Vis spectrophotometer. Contact angles provided information about the wettability of the surfaces.

Environmental SEM permitted the analysis of samples without extensive preparations which could potentially damage the morphological features of the samples and the cells. The use of surface analysis techniques was important because the quantification of the peptide densities on the surfaces of these samples was critical to the interpretation of the observed cell responses. The following sections describe the methods which were evaluated for analyzing surfaces and discuss the predicted usefulness of these techniques in characterizing similar samples produced in the future.

7.1.1 X-ray Photoelectron Spectroscopy

The XPS results demonstrated that on the bottom, glass-contacting side of the PLAL+GRGDY-I_2:PLA blends, there were levels of peptide (1 to 5 pmol/cm^2) available which exceeded the reported minimum level of peptide necessary to promote cell interactions (1 to 10 fmol/cm^2). The results obtained by XPS were considered the most reliable measurements of the nature of the surfaces. XPS proved to be very useful for characterizing PLA and PLAL samples, but was not sensitive enough to detect peptides when this project was begun. The difficulties encountered with measuring peptides attached to the polymer were twofold: the relatively small densities of peptides produced a signal which was too low to be detected, and the signal from the nitrogen within the peptides was camouflaged by the signal from the nitrogen within the lysine of the PLAL. The use of iodine-labeled peptides provided a way to tag the peptides so they could be measured separately from the lysine. The iodine-containing peptides were prepared by de-novo synthesis using diiodotyrosine in the peptide synthesis. The peptide was purified by HPLC. The XPS data also indicated the level of amino groups that were present on the surface, determined from the nitrogen content of the surface. The use of cold-stage studies and variable take-off angle techniques, along with high resolution scans were also used to provide a very detailed portrait of the surfaces that were created (section 5.2, 5.3).

7.1.2 Contact Angles

The use of contact angles to characterize the various surfaces that were created was necessary to rule out the possibility that changes in hydrophobicity was the cause for increased cell adhesion and spreading. For example, one of the main effects of treating polystyrene by radio-frequency-glow-discharge to create Tissue Culture grade plastic is an increase in hydrophilicity of the surface, which

allows proteins to adsorb more readily and in conformations which are conducive to cell adhesion and spreading. Contact angle measurements were used to show that surfaces were being created which were not only more wettable, but also contained specific chemical groups with which cells could interact. The effect of the incorporation of the lysine molecules and the peptides into the samples on the wettability of the samples was measured using advancing water contact angles. The results showed that there was a minimal effect on wettability due to the incorporation of peptides at this level (section 5.4).

7.1.3 Colorimetric Dyes

The first goal of the characterization studies was to measure the available NH_2 content of the surfaces. The assay which was used for quantification was the sulfo-SDTB assay, in which the reagent was combined with Poly(lactic acid-*co*-lysine) for 10 min., excess reagent was rinsed away, then perchloric acid was used to cleave off the reacted compound yielding a colored compound. The concentration of the resulting compound was measured by UV/Vis spectrophotometry, compared to standards and divided by the surface area of the sample to obtain the results in apparent NH_2 concentration per cm^2 of surface area. The colorimetric dyes were very useful for determining the lysine content of the surfaces of the blends.

7.1.4 Radiolabeled Peptides

In all of the peptide coupling optimization reactions, ^{125}I-radiolabeled peptides were used. The peptides were radiolabeled using a stoichiometric labeling technique to provide higher specific activity than is achievable through traditional trace labeling techniques (section 4.2). The benefits associated with using radiolabeled peptides provided more than enough justification for using this technique to determine the concentrations of peptides immobilized onto the surfaces of PLAL samples.

7.1.5 Scanning Electron Microscopy

SEM photomicrographs provided an unequaled assessment of the effectiveness of the modifications made to the surfaces on the behavior of cells. An environmental SEM allowed samples to be minimally prepared. All of the spreading data was obtained from digitized SEM images.

7.1.6 Cell Spreading Assays

When bovine aortic endothelial (BAE) cells were placed in contact with control surfaces, such as poly(lactic acid) in the absence of serum proteins, very few adhered, they remained rounded and did not spread. When the cells were placed on surfaces containing RGD peptides, the cells attached and spread out on the surface, indicating that they were interacting with the peptides on the surface. The extent of spreading was measured using image analysis of the projected area per cell, and it was found that after 4 hours on PLA, PLAL and PLAL+GRDGY over 90% of the cells remained round, with a mean cell area of approximately 100 μm^2, whereas on RGD, all of the cells increased their cell area to a mean area of approximately 405 μm^2.

7.2 Future Directions

Many other experiments could be conducted with this polymer system. The issues which remain to be addressed before this polymer can be used as a biomaterial include details about the nature of the degradation products of the polymer and the effect of those degradation products on cells, the stability of the structures during tissue formation, and the impact of the polymer on the interaction of cells with other cells. These issues can be addressed through *in vivo* animal testing and toxicological studies. Degradation studies which were reported herein were conducted *in vitro*. In the *in vivo* environment, enzymatic degradation can also occur, which may influence the way in which cells interact with the polymer. In addition, it is desirable to know how strongly the cells are attached to the polymer and whether or not there are variations in cell response due to slight changes in the length or sequence of the peptide. Strengths of adhesion could be measured using a Helé-Shaw flow system, which allows for a variation of shear stresses within each experiment. (The current limitation to performing these studies is the opaque nature of the solvent-cast blends.) The effect of spacers could be tested by using the following peptides (whose sequences correspond to the natural sequence of fibronectin), immobilized by either surface or bulk attachment chemistries: GRGDS, TGRGDS, VTGRGDS, and AVTGRGDS.

Variations in RGD-containing peptides have been reported. It may be possible to use peptides from various sources to find one which produces a more pronounced biological effect. For example, Cheng reported the synthesis of a cyclic RGD-containing peptide, which possessed higher potency than previous

peptides (1). RGD-containing peptides may not be the optimal peptides. Many cells are known to posess integrins which interact with the RGD sequence, including smooth muscle cells, platelets, and fibroblasts. The use of other peptide sequences, such as the REDV peptide, which has been shown to selectively interact with endothelial cells, but not with platelets, fibroblasts or smooth muscle cells, would be particulary useful for the application of an engineered blood vessel (2).

Another peptide which may be useful in some applications is the YIGSR peptide, which is derived from laminan, a major protein component of the basement membrane of many tissues.

The effect of individual serum proteins adsorbed onto PLAL+GRGDS surfaces could be studied to determine if there is any synergistic effect of the physically adsorbed proteins and the covalently bound peptides. The effect of adding soluble growth factors, protein synthesis inhibitors, or elements such as manganese could also be studied to determine their individual or combined effects on the adhesion and spreading of cells.

In addition to the methods described above, there are many other ways to process the polymer. These include spin casting, compression molding, extrusion, melting/quenching, salt casting (sponges), and molding (tubes). The use of different processing techniques could result in new applications for this material. In order to be processed by other methods than blending, the molecular weight of the PLAL polymer would have to be increased. As one example, in order for PLAL to be extruded into fibers, the minimal requirements would be 50 g of polymer at no less than 50,000 molecular weight (personal communication, Peter Ma). Attempts to extrude blends would most likely result in phase separation of the two polymers.

In order to produce higher molecular weight material, different reaction conditions could be explored. The current protocol consists of a reaction temperature of 100°C for 24 hrs. using stannous octoate as a catalyst. Previous work indicated that at lower polymerization temperatures, the molecular weight increased (3). Other temperatures, other catalyst concentrations and different catalysts could be tested. In addition, another aspect of the monomer synthesis which could be explored is the relative reactivity of the lysine-containing monomer to L,L-Lactide.

To quantify cell spreading, other visualization techniques could be explored, such as epifluorescence. Another method which could be used would

be to videotape the scanning electron microscope images, and then use a frame grabber to capture images off of the video tape onto the computer for image analysis.

During the course of the cell spreading experiments, it was observed that the GRGDY-I_2 peptides did not produce as great a response as the GRGDY and GRGDS peptides. The hypothesis for this is that the two iodine molecules sterically hinder the cells from interacting with the peptides. Experiments to verify this effect could be performed by testing the two materials at the same time.

7.3 References

1. Cheng, S., Craig, W. S., Mullen, D., Tschopp, J. F., Dixon, D., Pierschbacher, M. D., "Design and synthesis of novel cyclic RGD-containing peptides as highly potent and selective integrin $\alpha_{IIb}\beta_3$ antagonists", *J. Med. Chem.*, **37** (1): 1-8, (1994).

2. Massia, S.P., Hubbell, J. A., "Vascular endothelial cell adhesion and spreading promoted by the peptide REDV of the IIICS region of plasma fibronectin is mediated by integrin $\alpha_4\beta_1$", J. *Biol. Chem.*, **267** (20): 14019-14026, (1992).

3. Barrera, D.A., "Synthesis and characterization of a novel biodegradable polymer-poly(lactic acid-*co*-lysine)", Ph.D. Thesis, MIT (1993)